Western Iowa Missouri River Flooding—Geo-Infrastructure Damage Assessment, Repair, and Mitigation Strategies

SEPTEMBER 2013

Final Report

CENTER FOR
CEER
EARTHWORKS ENGINEERING
RESEARCH

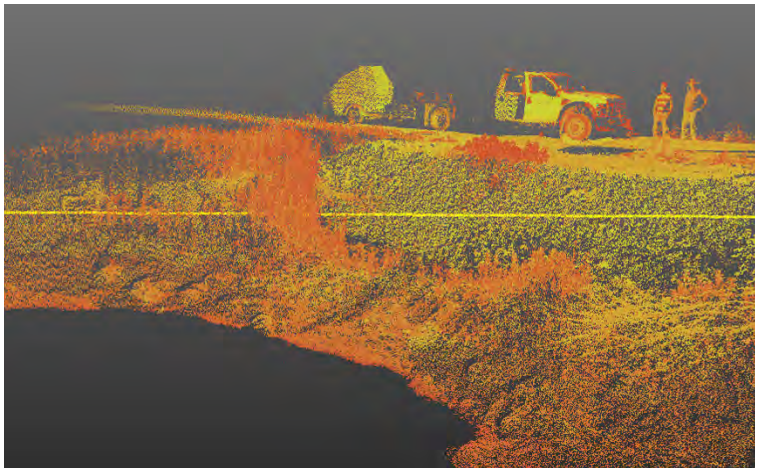



IOWA STATE UNIVERSITY
Institute for Transportation

Sponsored by
Federal Highway Administration
Iowa Highway Research Board
(IHRB Project TR-638)
Iowa Department of Transportation
(InTrans Project 11-419)

About the Center for Earthworks Engineering Research

The mission of the Center for Earthworks Engineering Research (CEER) at Iowa State University is to be the nation's premier institution for developing fundamental knowledge of earth mechanics, and creating innovative technologies, sensors, and systems to enable rapid, high quality, environmentally friendly, and economical construction of roadways, aviation runways, railroad embankments, dams, structural foundations, fortifications constructed from earth materials, and related geotechnical applications.

Disclaimer Notice

The contents of this report reflect the views of the authors, who are responsible for the facts and the accuracy of the information presented herein. The opinions, findings and conclusions expressed in this publication are those of the authors and not necessarily those of the sponsors.

The sponsors assume no liability for the contents or use of the information contained in this document. This report does not constitute a standard, specification, or regulation.

The sponsors do not endorse products or manufacturers. Trademarks or manufacturers' names appear in this report only because they are considered essential to the objective of the document.

Non-Discrimination Statement

Iowa State University does not discriminate on the basis of race, color, age, religion, national origin, sexual orientation, gender identity, genetic information, sex, marital status, disability, or status as a U.S. veteran. Inquiries can be directed to the Director of Equal Opportunity and Compliance, 3280 Beardshear Hall, (515) 294-7612.

Iowa Department of Transportation Statements

Federal and state laws prohibit employment and/or public accommodation discrimination on the basis of age, color, creed, disability, gender identity, national origin, pregnancy, race, religion, sex, sexual orientation or veteran's status. If you believe you have been discriminated against, please contact the Iowa Civil Rights Commission at 800-457-4416 or the Iowa Department of Transportation affirmative action officer. If you need accommodations because of a disability to access the Iowa Department of Transportation's services, contact the agency's affirmative action officer at 800-262-0003.

The preparation of this report was financed in part through funds provided by the Iowa Department of Transportation through its "Second Revised Agreement for the Management of Research Conducted by Iowa State University for the Iowa Department of Transportation," and its amendments.

The opinions, findings, and conclusions expressed in this publication are those of the authors and not necessarily those of the Iowa Department of Transportation or the U.S. Department of Transportation Federal Highway Administration.

Technical Report Documentation Page

1. Report No.	2. Government Accession No.	3. Recipient's Catalog No.
IHRB Project TR-638		

4. Title and Subtitle	5. Report Date
Western Iowa Missouri River Flooding — Geo-Infrastructure Damage Assessment, Repair and Mitigation Strategies	September 2013
	6. Performing Organization Code

7. Author(s)	8. Performing Organization Report No.
Pavana Vennapusa, David White, Kelly Miller	InTrans Project 11-419

9. Performing Organization Name and Address	10. Work Unit No. (TRAIS)
Center for Earthworks Engineering Research Iowa State University 2711 South Loop Drive, Suite 4600 Ames, IA 50010-8664	**11. Contract or Grant No.**

12. Sponsoring Organization Name and Address		13. Type of Report and Period Covered
Iowa Highway Research Board Iowa Department of Transportation 800 Lincoln Way Ames, IA 50010	Federal Highway Administration U.S. Department of Transportation 1200 New Jersey Avenue SE Washington, DC 20590	Final Report
		14. Sponsoring Agency Code SPR RB18-012

15. Supplementary Notes

Visit www.ceer.iastate.edu for color pdfs of this and other research reports.

16. Abstract

The 2011 Missouri River flooding caused significant damage to many geo-infrastructure systems including levees, bridge abutments/foundations, paved and unpaved roadways, culverts, and embankment slopes in western Iowa. The flooding resulted in closures of several interchanges along Interstate 29 and of more than 100 miles of secondary roads in western Iowa, causing severe inconvenience to residents and losses to local businesses. The main goals of this research project were to assist county and city engineers by deploying and using advanced technologies to rapidly assess the damage to geo-infrastructure and develop effective repair and mitigation strategies and solutions for use during future flood events in Iowa.

The research team visited selected sites in western Iowa to conduct field reconnaissance, in situ testing on bridge abutment backfills that were affected by floods, flooded and non-flooded secondary roadways, and culverts. In situ testing was conducted shortly after the flood waters receded, and several months after flooding to evaluate recovery and performance. Tests included falling weight deflectometer, dynamic cone penetrometer, three-dimensional (3D) laser scanning, ground penetrating radar, and hand auger soil sampling.

Field results indicated significant differences in roadway support characteristics between flooded and non-flooded areas. Support characteristics in some flooded areas recovered over time, while others did not. Voids were detected in culvert and bridge abutment backfill materials shortly after flooding and several months after flooding. A catalog of field assessment techniques and 20 potential repair/mitigation solutions are provided in this report. A flow chart relating the damages observed, assessment techniques, and potential repair/mitigation solutions is provided. These options are discussed for paved/unpaved roads, culverts, and bridge abutments, and are applicable for both primary and secondary roadways.

17. Key Words	18. Distribution Statement
falling weight deflectometer—flood damage—gravel roads—ground penetrating radar—in situ testing—soil stabilization	No restrictions.

19. Security Classification (of this report)	20. Security Classification (of this page)	21. No. of Pages	22. Price
Unclassified.	Unclassified.	267	NA

Form DOT F 1700.7 (8-72) **Reproduction of completed page authorized**

WESTERN IOWA MISSOURI RIVER FLOODING — GEO-INFRASTRUCTURE DAMAGE ASSESSMENT, REPAIR AND MITIGATION STRATEGIES

Final Report
September 2013

Principal Investigator
David J. White, PhD
Associate Professor and Director of CEER

Co-Principal Investigators
Pavana K. R. Vennapusa, PhD
Research Assistant Professor and Assistant Director of CEER

D. Kelly Miller
Assistant Scientist, CEER

Authors
Pavana Vennapusa, David White, Kelly Miller

Sponsored by
the Iowa Department of Transportation
Iowa Highway Research Board
(IHRB Project TR-638)
and the Federal Highway Administration
State Planning and Research Funding
(SPR RB18-012)

Preparation of this report was financed in part
through funds provided by the Iowa Department of Transportation
through its Research Management Agreement with the
Institute for Transportation and the Center for Earthworks Engineering Research.
(InTrans Project 11-419)

A report from
Center for Earthworks Engineering Research (CEER)
Iowa State University
2711 South Loop Drive, Suite 4600
Ames, IA 50010-8664
Phone: 515-294-7910 Fax: 515-294-0467
www.ceer.iastate.edu

TABLE OF CONTENTS

ACKNOWLEDGMENTS xix

EXECUTIVE SUMMARY xxi

Project Overview xxi
Summary of Flood Damages to Secondary Roadways and Repair Measures xxii
In Situ Test Results and Statistical Analysis xxiii
Gravel Roads and Culvert Crossings xxiii
HMA Pavement xxiv
PCC Pavement xxiv
Bridge Abutments xxv
Post-Flood Geo-Infrastructure Assessment Techniques and Repair/Mitigation Solutions xxv

CHAPTER 1: INTRODUCTION 1

Problem Statement 1
Goals and Research Objectives 1
Research Approach 2

CHAPTER 2: BACKGROUND 3

2011 Missouri River Flooding 3
Description of the Missouri River Basin and Causes of 2011 Flooding 3
Significant Events During and After Flooding 7
Previous Studies on Assessment of Flood Damaged Roadway 17
Pavement Structures Damage after Hurricane Katrina Flooding, New Orleans, Louisiana (2005) 17
HMA Pavement on State Highway 24 in McClain County, Oklahoma (2007) 17
Evaluating "Unseen" Pavement Damage by Flooding after Hurricane Sandy (2012) and Katrina (2005) 17
Investigation of Galveston Airport Pavements after Hurricane Ike, Galveston, Texas (2008) 18
Iowa DOT Primary Roads Evaluation after 2011 Missouri River Flooding (2011) 18

CHAPTER 3: LOW VOLUME ROAD FOUNDATION LAYER DESIGN INPUTS 19

CHAPTER 4: TESTING METHODS AND STATISTICAL DATA ANALYSIS 23

In Situ Testing 23
Dynamic Cone Penetrometer 23
Falling Weight Deflectometer 24
Hand Auger Soil Sampling 29
Ground Penetrating Radar 29
Laser Scanning 31
Laboratory Testing 31
Soil Classification 31
Moisture Content 31
Statistical Data Analysis 32

CHAPTER 5: EMERGENCY OPERATIONS AND REPAIR OF FLOOD-DAMAGED GEO-INFRASTRUCTURE....34
Reported Costs of Emergency Operations and Repair Measures....34
Geo-Infrastructure Damages and Repair Measures....34
Primary Roadways....35
Secondary Roadways....38
CHAPTER 6: FIELD EVALUATION OF GEO-INFRASTRUCTURE ON SECONDARY ROADWAYS....62
Pottawattamie County....62
TS1 – Old Mormon Bridge Road (HMA)....65
TS2 – Old Mormon Bridge Road (PCC)....70
TS3 – 110th Street (Gravel)....77
TS4 – Desoto Avenue East (Emulsified Oil-Stabilized Base)....85
TS5 – 145th Street (Gravel)....90
TS5 – Laser Scanning of a Breach next to 145th Street....98
TS6 – River Road North (Gravel)....105
TS7 – Desoto Avenue West (Oil Stabilized Base)....113
Fremont County....121
TS 1 – 260th Street (Gravel)....124
TS 2 – 285th Street (Gravel)....136
TS 3 – 185th Avenue (Gravel)....145
TS 4 – 220th Street (Chipseal Surfacing over Gravel)....152
Statistical Analysis....157
Comparison between Flooded and Non-Flooded Areas....157
Correlations between DCP-CBR and FWD Measurements....161
CHAPTER 7: KEY FINDINGS FROM FIELD TESTING AND OBSERVATIONS....167
Summary of Flood Damages to Secondary Roadways and Repair Measures....167
In Situ Test Results and Statistical Analysis....168
Gravel Roads and Culvert Crossings....168
HMA Pavement....169
PCC Pavement....169
Bridge Abutments....170
CHAPTER 8: GUIDANCE FOR GEO-INFRASTRUCTURE DAMAGE ASSESSMENT AND SELECTION OF REPAIR AND MITIGATION SOLUTIONS....171
REFERENCES....175
APPENDIX A: SUMMARY OF DAMAGES, EMERGENCY OPERATIONS, AND DAMAGE COSTS REPORTED BY THE IOWA DOT....181
APPENDIX B. TIME-LAPSED GRAPHICAL DEPICTION OF FLOODWATER BOUNDARIES NEAR I-29 AND I-680....187
APPENDIX C. GROUND TEMPERATURE DATA FROM MOVILLE, IOWA....197

APPENDIX D: DESCRIPTION OF DAMAGE ASSESSMENT TEQHNIQUES AND REAPAIR/MITIGATION SOLUTIONS 199

Flood Damage Evaluation Procedures 202
Aerial and LiDAR Imagery Review 202
Visual On-Ground Inspection 208
Dynamic Plate Load Tests 208
Penetration Tests 209
Roller-Integrated Compaction Monitoring 211
Ground Penetrating Radar (GPR) 213
Surface Laser Scanning 218
Underwater Sonar Scanning and Culvert Inspection 220
Potential Damage Repair and Mitigation Solutions 221
Roadways 222
Bridge Abutments 232
Culverts 241

LIST OF FIGURES

Figure 1. Missouri river basin map with USACE operated dam locations (USACE 2012a) 4
Figure 2. Missouri river main stem system watershed with Civil Works boundary and USACE operated dam locations (McMahon and Farhat 2012) 4
Figure 3. Missouri river basin annual runoff upstream of Sioux City, Iowa from 1898 to 2012 (Grode 2012) 5
Figure 4. Main components of runoff (Latka 2012) 5
Figure 5. Moderate resolution imaging spectroradiometer (MODIS) images from NASA's Aqua satellite captured on (a) June 29, 2010, and (b) June 30, 2011 during flooding (Images Courtesy of MODIS Rapid Response Team, NASA's Goddard Space Flight Center, Greenbelt, Maryland) 6
Figure 6. Landsat 5 image showing Missouri river flooding on Interstate 29 at Iowa/Nebraska border on July 6, 2011 (Images Courtesy of NASA's Goddard Space Flight Center, Greenbelt, Maryland) 7
Figure 7. Aerial photo taken over Sioux City, Iowa on June 1, 2011 (Image Courtesy of Tim Hynds, AP Photos/Sioux City Journal) 11
Figure 8. Aerial photo of the Hamilton Blvd exit of I-29 (Exit 149) on June 3, 2011 (Image Courtesy of Mercy Aircare, Sioux City, Iowa) 12
Figure 9. Gavin's Point dam releases 150,000 ft^3/s of runoff volume on June 14, 2011 (Image Courtesy of Jay Woods, USACE) 12
Figure 10. Aerial photo of the flooding on I-29 between Council Bluffs and Hamburg, Iowa on June 16, 2011 (Image Courtesy of Rodney White, The Register) 13
Figure 11. Aerial photo of the full breach at Federal levee 575 near Hamburg, Iowa, on June 14, 2011 (Image Courtesy of USACEhttp://www.flickr.com/photos/usacehq/5837117182/in/photostream/) 13
Figure 12. Aerial photo of the flooding near the Fort Calhoun nuclear power plant near Blair, Nebraska on June 17, 2011 (Image Courtesy of Omaha Public Power District) 14
Figure 13. Aerial photo of the overtopping of Federal levee 550 near Highway 136 in Atchison County, Missouri, on June 19, 2011 (Image Courtesy of USACE http://www.flickr.com/photos/usacehq/5849817627/in/photostream/) 14
Figure 14. Timeline of daily average release of runoff from Gavins Point dam and significant events related to Iowa Transportation occurred during between 05/27/11 and 08/29/11 (Image Courtesy of Bonnie Castillo, Disaster Operations Manager, Iowa DOT State Emergency Operations) 15
Figure 15. Timeline of daily average release of runoff from Gavins Point dam and significant events related to Iowa Transportation occurred during between 08/29/11 and 11/15/11 (Image Courtesy of Bonnie Castillo, Disaster Operations Manager, Iowa DOT State Emergency Operations) 16
Figure 16. Six climatic regions in the United States (AASHTO 1993) 20
Figure 17. Dynamic cone penetrometer (DCP) 23
Figure 18. Ilustration of weighted average CBR calculation 24
Figure 19. KUAB falling weight deflectometer (FWD) 26
Figure 20. FWD plate and sensor setup (top), and typical deflection basin (bottom) 26
Figure 21. Interpretation of E_{SG} from FWD deflection basin results 27
Figure 22. Determination of $k_{FWD\text{-}dynamic}$ using the AREA method (AASHTO 1993) 28

Figure 23. Void detection using load-deflection data from FWD test....28
Figure 24. Extracting soil samples using a hand auger equiped with a Dutch auger head....29
Figure 25. Ground penetrating radar scanning using GSSI SIR-20 data acquisition system....30
Figure 26. Trimble CX 3D laser scanner....31
Figure 27. Pictures taken near I-29 and I-680 intersection north of Council Bluffs on 9/21/2013....36
Figure 28. Aerial infrared imagery showing extent of Missouri River in Summer 2010 (left) and Summer 2011 (right) in western Iowa....41
Figure 29. Aerial infrared imagery showing extent of Missouri River in Summer 2010 (left) and Summer 2011 (right) in Woodbury County....42
Figure 30. Aerial infrared imagery showing extent of Missouri River in Summer 2010 (left) and Summer 2011 (right) in Monona County....43
Figure 31. Aerial infrared imagery showing extent of Missouri River in Summer 2010 (left) and Summer 2011 (right) in Harrison County....44
Figure 32. Aerial infrared imagery showing extent of Missouri River in Summer 2010 (left) and Summer 2011 (right) in Pottawattamie County....45
Figure 33. Aerial infrared imagery showing extent of Missouri River in Summer 2010 (left) and Summer 2011 (right) in Mills County....46
Figure 34. Aerial infrared imagery showing extent of Missouri River in Summer 2010 (left) and Summer 2011 (right) in Fremont County....47
Figure 35. Levee breach in north part of Fremont County (images updated on 6/9/10 and 8/11/11)....48
Figure 36. Levee breach in southern part of Fremont County (images updated on 6/9/10, 7/17/11, and 8/11/11)....49
Figure 37. Flood water coverage maps north of Council Bluffs from 6/4/11 to 6/11/11 – Pottawattamie County....50
Figure 38. Flood water coverage maps north of Council Bluffs from 6/14/11 to 8/31/11 – Pottawattamie County....51
Figure 39. Fremont county map with flood affected areas showing sites funded by FEMA for damage repair....52
Figure 40. Delaminated HMA overlay over PCC pavement and eroded shoulders refilled with crushed limestone – Old Mormon Road (looking east), Pottawatamie County (Photos taken on 9/21/11)....53
Figure 41. Eroded shoulder next to PCC pavement being reconstructed on 9/21/11 – Old Mormon Road (looking west towards I-680 and I-29 intersection), Pottawatamie County (Photos taken on 9/21/11)....53
Figure 42. Water overtopping a thin chipseal coat surfaced road underlain by oil stabilized granular base on 9/21/11 showing delamination of chipseal and rolled asphalt at the surface – Desoto Avenue, Pottawattamie County (Photos taken on 9/21/11)....54
Figure 43. Clogged culvert inlets due to scouring and erosion of embankment material beneath chipseal coat surfaced road on 9/21/11 – Desoto Avenue, Pottawatamie County (Photos taken on 9/21/11)....54
Figure 44. Scouring and erosion of bridge backfill material around a timber abutment supporting a concrete bridge deck – Pottawatamie County (Photos taken on 9/21/11)....55
Figure 45. Full breach of about 150 m (500 ft) long unsurfaced access road – Pottawatamie County (Photo taken on 9/21/11)....55

Figure 46. Potholes (with about 0.5 m (1.5 ft) diameter) under gravel road due to erosion of backfill material around a culvert located beneath the road – Pottawatamie County (Photos taken on 9/21/11 and 9/23/11) 56
Figure 47. Weep holes detected under a gravel road – Meadowlark Loop Road, Pottawatamie County (Photos taken on 9/22/11) 57
Figure 48. Rutting along right wheel path on chipseal surfaced gravel road and erosion of granular shoulder during flooding – 220th Street, Fremont County (Photo taken 10/26/11) 58
Figure 49. Erosion of shoulder and roadbed on a chip seal surfaced gravel road – Fremont County (Photo taken on 10/26/11) 58
Figure 50. Delaminated or stripped chipseal surfacing – Fremont County (Photo taken on 10/26/11) 59
Figure 51. Full breach of a gravel road (about 100 m (330 ft) long) – Fremont County (Photo taken on 10/26/11) 59
Figure 52. Gravel road segments washed away during floods – Fremont County (Photo taken on 10/26/11) 60
Figure 53. Reconstruction of a gravel road washed away during floods and deposited with silt and sand– Fremont County (Photo taken on 10/26/11) 60
Figure 54. Erosion of backfill material around timber back wall supporting a timber bridge crossing a creek – Fremont County (Photos taken on 10/26/11) 61
Figure 55. Locations of test sections – Pottawattamie County (Image updated on 6/28/2010) 65
Figure 56. Aerial imagery showing pre-flood (left from 6/28/10) and during flood (right from 7/17/11) conditions on TS1 – Pottawattamie County 67
Figure 57. FWD testing on HMA pavement on TS1 (Photo taken on 9/21/11) – Pottawattamie County 68
Figure 58. Surface modulus and subgrade E_{SG} at three different times after flooding on TS1 – Pottawattamie County 68
Figure 59. DCP-CBR profiles at two test locations at two different times after flooding on TS1 – Pottawattamie County 69
Figure 60. Box plots of subgrade modulus values in flooded and non-flooded zones in comparison with relative quality ratings on TS1 – Pottawattamie County 69
Figure 61. Comparison of subgrade CBR values in flooded and non-flooded zones with relative quality ratings on TS1 – Pottawattamie County 70
Figure 62. Aerial imagery showing pre-flood (top from 6/28/10) and during flood (bottom from 7/17/11) conditions on TS2 – Pottawattamie County 72
Figure 63. Eroded base material and voids under PCC pavement filled with cement grout – TS2 [Note: Cement grout was placed two days prior to taking these photos] (Photos taken on 9/21/11) – Pottawattamie County 73
Figure 64. Longitudinal cracks on PCC pavement with undermined base material on TS2 (Photo taken on 9/21/11) – Pottawattamie County 73
Figure 65. FWD results from three different testing times after flooding on TS2 – Pottawattamie County 74
Figure 66. DCP-CBR profiles at one test locations at two different times after flooding on TS2 – Pottawattamie County 75
Figure 67. GPR scanning setup with 400 MHz antenna along the south side of the east bound lane on TS2 – Pottawattamie County 75

Figure 68. GPR scan using 400 MHz antenna along the north side of the east bound lane on TS2 (note 0 ft on the figure represents the 38 m station and the 100 ft on the figure represents the 68 m station of the TS) – areas circled in red denote rebars in pavement – Pottawattamie County 76
Figure 69. GPR scan using 400 MHz antenna along the middle of the east bound lane on TS2 (note 0 ft on the figure represents the 38 m station and the 100 ft on the figure represents the 68 m station of the TS) – Pottawattamie County 76
Figure 70. GPR scan using 400 MHz antenna along the south side of the east bound lane on TS2 (note 0 ft on the figure represents the 38 m station and the 100 ft on the figure represents the 68 m station of the TS) – area circled in red denote a potential void zone beneath pavement – Pottawattamie County 77
Figure 71. Aerial imagery showing pre-flood (left from 6/28/10) and during flood (right from 7/17/11) conditions on TS3 – Pottawattamie County 79
Figure 72. New gravel placed at the middle of the segment following flooding on TS3 (Photo taken on 9/21/2011) – Pottawattamie County 80
Figure 73. Weep holes near culvert on TS3 (Photo taken on 10/25/2011) – Pottawattamie County 80
Figure 74. Soil moisture content profile with depth to water table at G-14 on 9/22/11 – Pottawattamie County 81
Figure 75. Surface FWD modulus and subgrade modulus at four different times after flooding on TS3 – Pottawattamie County 81
Figure 76. DCP-CBR profiles at four test locations from four different testing times on TS3 – Pottawattamie County 82
Figure 77. Box plots of subgrade modulus values in flooded and non-flooded zones in comparison with relative quality ratings on TS3 – Pottawattamie County 83
Figure 78. Comparison of subgrade CBR values in flooded and non-flooded zones with relative quality ratings on TS3 – Pottawattamie County 83
Figure 79. GPR scans using 200 and 400 MHz antennas on TS3 (note 0 ft on the figure represents the 130 m station of the TS) – Pottawattamie County 84
Figure 80. GPR scan using 200 MHz antenna on TS3 (note that 560 ft on the figure represents the 310 m station (at culvert) of the TS) – Pottawattamie County 85
Figure 81. Aerial imagery showing pre-flood (left from 6/28/10) and during flood (right from 7/17/11) conditions on TS4 – Pottawattamie County 87
Figure 82. Rutting observed near the east end of the test segment (near test location D-38) (photo taken on 9/23/11) on TS4 – Pottawattamie County 88
Figure 83. Surface FWD modulus and subgrade modulus at four different times after flooding on TS4 (highlighted in color are drainage, flooding, and home lot features observed from aerial maps) – Pottawattamie County 88
Figure 84. DCP-CBR profiles at four test locations from two different testing times on TS4 – Pottawattamie County 89
Figure 85. Box plots of subgrade modulus values in flooded and non-flooded zones in comparison with relative quality ratings on TS4 – Pottawattamie County 89
Figure 86. Comparison of subgrade CBR values in flooded and non-flooded zones with relative quality ratings on TS4 – Pottawattamie County 90
Figure 87. Aerial imagery showing pre-flood (from 6/28/10) conditions and test locations on TS5 – Pottawattamie County 92

Figure 88. Aerial imagery showing during flood (from 7/17/11) conditions and test locations on TS5 – Pottawattamie County 93
Figure 89. Potholes (with about 0.5 m (1.5 ft) diameter) under gravel road due to erosion of backfill material around a culvert located beneath the road TS 5 (Photos taken on 9/21/11 and 9/23/11) – Pottawatamie County 94
Figure 90. FWD testing on TS5 with floodwater up to the edge of the road (Photo taken 9/23/11) – Pottawattamie County 95
Figure 91. Weep holes (20+) around the culvert observed after flood waters receded on TS5 (Photo taken on 10/25/11) – Pottawattamie County 95
Figure 92. Loose backfill material around culvert replaced after flood waters receded on TS5 (Photo taken on 4/5/12) – Pottawattamie County 96
Figure 93. Surface FWD modulus and subgrade modulus at four different times after flooding on TS5 – Pottawattamie County 96
Figure 94. DCP-CBR profiles from three different testing times and soil moisture content profile at B14 from 9/23/11 on TS5 – Pottawattamie County 97
Figure 95. Box plots of subgrade modulus values in comparison with relative quality ratings on TS5 – Pottawattamie County 97
Figure 96. Subgrade CBR values at different testing times with relative quality ratings on TS5 – Pottawattamie County 98
Figure 97. Aerial imagery of the breach site located next to TS5 145th St. (Google image from 3/7/12) – Pottawattamie County 99
Figure 98. 3D laser scan setup at the levee breach site on TS5 145th St. – Pottawattamie County 100
Figure 99. Raw point cloud data showing intensity contrast – TS5 Pottawattamie County 101
Figure 100. Overhead view of scanned point cloud – TS5 Pottawattamie County 101
Figure 101. Contour map of site used for volumetric calculations – TS5 Pottawattamie County 102
Figure 102. Meshed surface used for volumetric calculations – TS5 Pottawattamie County 102
Figure 103. Meshed surface with photo overlay to show colored mesh surface – TS5 Pottawattamie County 103
Figure 104. Colored mesh surface with 0.6 m (2 ft) contour lines – TS5 Pottawattamie County 103
Figure 105. Colored point cloud data – TS5 Pottawattamie County 104
Figure 106. Merged point cloud with colored surface from photo – TS5 Pottawattamie County 104
Figure 107. Rendering of volume calculations – TS5 Pottawattamie County 105
Figure 108. Aerial imagery showing pre-flood (from 6/28/10) conditions and test locations on TS6 – Pottawattamie County 107
Figure 109. Aerial imagery showing during flood (from 7/17/11) conditions and test locations on TS6 – Pottawattamie County 108
Figure 113. Location of newly placed gravel on TS6 over a metal pipe culvert (Picture taken on 9/23/11) – Pottawattamie County 110
Figure 114. Surface FWD modulus and subgrade modulus at four different times after flooding on TS6 – Pottawattamie County 111
Figure 115. DCP-CBR profiles from two different testing times at C-6 test location on TS6 – Pottawattamie County 111

Figure 116. Box plots of subgrade modulus values in comparison with relative quality ratings on TS6 – Pottawattamie County 112
Figure 117. Subgrade CBR values at different testing times with relative quality ratings on TS6 – Pottawattamie County 112
Figure 118. Aerial imagery before flooding (from 6/28/10) and during flooding (from 7/17/11) on TS7 – Pottawattamie County....114
Figure 119. Aerial imagery before flooding (from 6/28/10) and during flooding (from 7/17/11) showing road scour and culvert locations on TS7 – Pottawattamie County....115
Figure 120. Water overtopping Desoto Avenue on 9/21/11 and delamination of chipseal coat at the surface (Pictures taken on 9/21/11) – Pottawattamie County 116
Figure 121. Delaminated surface chipseal on Desoto Avenue due to flood waters overtopping the roadway (Pictures taken on 10/25/11) – Pottawattamie County 117
Figure 122. Weep holes around culvert inlets on TS7 (Picture taken on 10/25/11) – Pottawattamie County....118
Figure 123. Surface FWD modulus and subgrade modulus at three different times after flooding on TS7 (entire TS was flooded and pre-flood ponding zones identified from aerial maps) – Pottawattamie County 118
Figure 124. Box plots of subgrade modulus values in comparison with relative quality ratings on TS7 – Pottawattamie County 119
Figure 125. GPR scan using 400 MHz antennas on TS7 showing location of culvert (at station 724 m) – Pottawattamie County....120
Figure 126. GPR scan using 900 MHz antenna on TS7 showing potential weep holes in the subgrade (between 720 m and 750 m stations on east bound lane) – Pottawattamie County....120
Figure 127. GPR scan using 900 MHz antenna on TS7 showing potential weep holes in the subgrade (between 1550 m and 1580 m stations on east bound lane) – Pottawattamie County....121
Figure 128. Location of all test segments – Fremont County (Image updated on 8/11/2011) 123
Figure 129. Aerial imagery before flooding on left (from 10/28/10) and during flooding on right (from 8/11/11) on TS1 – Fremont County 126
Figure 130. New bridge approach backfill material placed along the east approach on TS1 (Picture taken on 10/26/11) – Fremont County 127
Figure 131. *Erosion of embankment material along the west bank on TS1* (Picture taken on 10/26/11) – Fremont County....127
Figure 132. Erosion of embankment material along the west bank near abutment wing walls on TS1 (Picture taken on 10/26/11) – Fremont County....128
Figure 133. Erosion of backfill material behind the wing wall on TS1 (Picture taken on 10/26/11) – Fremont County....128
Figure 134. Bridge conditions on TS1 on 4/4/12 – Fremont County 129
Figure 135. Bridge conditions on TS1 on 6/9/12 – Fremont County 130
Figure 136. Surface FWD modulus at three different times after flooding on TS1 – Fremont County....131
Figure 137. Subgrade modulus measurements at three different times after flooding on TS1 – Fremont County....131
Figure 138. DCP-CBR profiles from two different testing times at five test locations on TS1 – Fremont County....132

Figure 139. Box plots of subgrade modulus values in flooded and non-flooded zones in comparison with relative quality ratings on TS1 – Fremont County....133
Figure 140. Comparison of subgrade CBR values in flooded and non-flooded zones with relative quality ratings on TS1 – Fremont County....133
Figure 141. GPR scans using 200 MHz antenna on TS1 longitudinally along the west bridge approach backfill at 0.6 to 2.4 m away from the north and south edges of the bridge (note: 0 ft mark on the horizontal scale represents about 6.7 m (22 ft) away from the west abutment) – Fremont County....134
Figure 142. GPR scans using 200 MHz antenna on TS1 longitudinally along the east bridge approach backfill at 0.6 m to 2.4 m away from the north and south edges of the bridge (note: 0 ft mark on the horizontal scale represents about 6.7 m (22 ft) away from the west abutment – Fremont County....135
Figure 143. Aerial imagery before flooding on left (from 10/28/10) and during flooding on right (from 8/11/11) on TS2 – Fremont County....138
Figure 144. Gravel surface on TS2 at the time of testing (Picture taken on 10/26/11)....139
Figure 145. Bridge approach on TS2 (Picture taken 10/26/11)....139
Figure 146. Void behind the west abutment wall due to erosion of backfill material at TS2 bridge (Pictures taken on 10/26/11) – Fremont County....140
Figure 147. West and east abutments on TS2 bridge (Pictures taken on 4/4/11) – Fremont County....141
Figure 148. Surface FWD modulus at three different times after flooding on TS2 – Fremont County....142
Figure 149. Subgrade modulus measurements at three different times after flooding on TS2 – Fremont County....142
Figure 150. TS2 bridge approach: (a) Bridge deck plan view showing DCP test locations on the approach backfill, and (b) cross-sectional view showing thickness of gravel base and void beneath the gravel layer across the bridge (tests conducted on 10/25/11) – Fremont County....143
Figure 151. DCP-CBR profiles from three different testing times on TS2 – Fremont County....144
Figure 152. Box plots of subgrade modulus values in flooded and non-flooded zones in comparison with relative quality ratings on TS2 – Fremont County....144
Figure 153. GPR scans using 200 MHz antenna on TS2 longitudinally along the west bridge approach backfill at 1.2 to 3.0 m away from the north edge of the bridge (note: 0 ft mark on the horizontal scale represents about 6.7 m (22 ft) away from the west abutment) – Fremont County....145
Figure 154. Aerial imagery before flooding on left (from 10/28/10) and during flooding on right (from 8/11/11) on TS3 – Fremont County....147
Figure 155. Newly placed gravel near a culvert at about 4700 m station on TS2 (Picture taken 10/27/11)....148
Figure 156. Rutting observed near 3000 m station on TS2 (Picture taken 4/4/12)....148
Figure 157. Surface FWD modulus (top) and subgrade modulus (bottom) at three different times after flooding on TS3 – Fremont County....149
Figure 158. DCP-CBR profiles at three different times after flooding at six test locations on TS3 – Fremont County....150
Figure 159. Box plots of subgrade modulus values in comparison with relative quality ratings on TS3 – Fremont County....151

Figure 160. Comparison of subgrade CBR values with relative quality ratings on TS3 – Fremont County 151
Figure 161. Aerial imagery before flooding on left (from 10/28/10) and during flooding on right (from 8/11/11) on TS4 – Fremont County 153
Figure 162. Rutting observed on the surface and washed out shoulders during flooding on TS4 – Fremont County (Picture taken 10/28/11) 154
Figure 163. Surface patch repair over a culvert on TS4 – Fremont County (Picture taken 10/28/11) 155
Figure 164. Surface FWD modulus (top) and subgrade modulus (bottom) at three different times after flooding on TS4 – Fremont County 155
Figure 165. DCP-CBR profiles at two test locations from two different testing times on TS4 – Fremont County 156
Figure 166. Box plots of subgrade modulus values in flooded and non-flooded zones in comparison with relative quality ratings on TS4 – Fremont County 156
Figure 167. Box plots of (a) E_{FWD} and (b) E_{SG} obtained shortly after flooding (about 20 to 30 days) from all test segments in flooded and non-flooded zones 158
Figure 168. Box plots of (a) E_{FWD} and (b) E_{SG} obtained about 7 to 8 months after flooding from all test segments in flooded and non-flooded zones 159
Figure 169. Regression analysis between: (a) CBR of Gravel and E_{FWD}, (b) CBR of subgrade and E_{FWD}, (c) CBR of subgrade and E_{SG}, and (d) E_{SG} and E_{FWD} 163
Figure 170. Results of multivariate regression analysis to predict E_{FWD} from CBR of gravel and CBR of subgrade 164
Figure 171. Chart to estimate FWD or LWD surface modulus from CBR of subgrade and gravel layers overlaid with in situ test measurements and AASHTO (1993) subgrade relative quality ratings 165
Figure 172. Chart showing relationship between CBR, rut depth, and FWD and LWD modulus, and typical range of CBR values observed after spring-thaw in Iowa (White et al. 2013b) for different stabilization methods 166
Figure 173. Flow chart to select assessment techniques and repair/mitigation solutions 173
Figure C1. Temperature data at different depths from Moville, Iowa (Based on data collected from Iowa Environmental Mesonet http://mesonet.agron.iastate.edu/request/rwis/soil.phtml) 197
Figure D1. Flow chart to select assessment techniques and repair/mitigation solutions 201
Figure D2. Aerial imagery showing during flood and after flood conditions, and FWD test results in flooded and non-flooded areas (imagery from Google Earth) 203
Figure D3. LiDAR 0.6 m (2 ft) contours from 2010 overlaid on Pottawattamie County map in ArcGIS 204
Figure D4. Demonstration of ArcGIS query feature to select areas with elevations higher than flood water levels using LiDAR data from 2010 205
Figure D5. Flood water depth map overlaid on Pottawattamie County map in ArcGIS 206
Figure D6. LiDAR contour lines from 2010 overlaid on aerial imagery for Fremont County in ArcGIS 207
Figure D7. Dynamic plate load tests: (a) FWD, (b) LWD, and (c) Clegg hammer 209
Figure D8. Hand push T-bar to inspect weep hole 210
Figure D9. Dynamic cone penetrometer testing (left) and an example plot comparing DCP-CBR profiles in flooded and non-flooded areas 210

Figure D10. Chart showing relationship between CBR, rut depth, and FWD and LWD modulus, and typical range of CBR values observed after spring-thaw in Iowa (White et al. 2013b) for different stabilization methods 211
Figure D11. Pictures of various roller manufacturers, roller configurations, and display software's with RICM technology (note that this does not represent a complete list) 212
Figure D12. Example RICM spatial map of compaction measurements obtained using CS74 smooth drum vibratory roller after spring-thaw on test sections in Boone constructed using different stabilization methods (White et al. 2013b) 213
Figure D13. GPR scanning using ground-coupled antennas 215
Figure D14. GPR scans using 200 MHz antenna on bridge approach backfill materials at several locations from the edge of the bridge identifying possible erosion/voids beneath surface 215
Figure D15. GPR scanning using air-borne (horn) antenna 216
Figure D16. FHWA step-frequency GPR (Courtesy of Jim Grove, FHWA) 216
Figure D17. GPR scan map showing voids under composite pavement (Yu 2012) 217
Figure D18. 3D visualization of SF-GPR data (Yu 2012) 217
Figure D19. Trimble CX 3D laser scanner 218
Figure D20. Contour map of site used for volumetric calculations 218
Figure D21. Meshed surface used for volumetric calculations 219
Figure D22. Colored mesh surface with 0.6 m (2 ft) contour lines 219
Figure D23. 3D imagery under water using BV5000 3D mechanical imaging sonar (sonar shown in insert) (Courtesy of Blue View Technologies, Inc., Seattle, Washington) 220
Figure D24. 2D imagery from sonar scanning in low visibility conditions in a culvert using P900 series sonar (sonar shown in insert) (Courtesy of Blue View Technologies, Inc., Seattle, Washington) 220
Figure D25. Starfish 990F side scanning acoustic sonar (Courtesy of Starfish Seabed Imaging Systems, Aberdeen, UK) 221
Figure D26. Versatrax 100™ for pipe/culvert inspection (Courtesy of Inuktun Services Ltd., British Columbia, Canada) 221
Figure D27. Chart for selection of stabilizer (Chu et al. 1955) 224
Figure D28. Chart for selection of stabilizer (Terrel et al. 1979) 225
Figure D29. Guide to selecting stabilization method (Austroads 1998) 225
Figure D30. Photos showing typical chemical stabilization process 226
Figure D31. Pictures showing soaking test results of different specimens after: (a) five minutes, (b) one hour, (c) four hours, and (d) one day (Gopalakrishnan et al. 2010) 227
Figure D32. Blending granular material with subgrade using a soil pulverizer 228
Figure D33. Woven geotextile (left) and non-woven geotextile (right) placed at subgrade/aggregate layer interface 230
Figure D34. Triaxial (left) and biaxial (right) polymer geogrids placed on the subgrade 231
Figure D35. High energy impact roller (equipment by Impact Roller Technology, Plattsmouth, Nebraska) 231
Figure D36. Cross-section of sheet pile abutment foundation system at a bridge site in Boone (Evans et al. 2012) 233
Figure D37. Pictures of a bridge site in Boone constructed with sheet pile abutments with geogrid-reinforced backfill material (Evans et al. 2012) 234

Figure D38. Schematic of GRS bridge abutment with geosynthetic wrapped sheets flexible facing at a bridge site in Buchanan County (Olympic Ave.) (Vennapusa et al. 2012)....236
Figure D39. Pictures of a bridge site in Buchanan County (Olympic Ave.) during construction of GRS fill in bridge abutments, placement of riprap and grout cover for erosion protection, and the finished bridge in 2011 (Vennapusa et al. 2012) 237
Figure D40. Pictures of a bridge site in Buchanan County (250th Street) during construction of GRS fill in bridge abutments, placement of rail road flat cars for superstructure, and after final placing the final gravel surface in 2011 (Vennapusa et al. 2012) 238
Figure D41. Pictures of a bridge site in Buchanan County (Olympic Ave.) after flash flooding occurred in May 2013.....239
Figure D42. Pictures of a bridge site in Buchanan County (250th Street) after flash flooding occurred in May 2013 240
Figure D43. Iowa DOT granular backfill gradation requirement compared with the range of most erodible soils 241

LIST OF TABLES

Table 1. Chronology of significant events in Western Iowa during and after the 2011 Missouri River flooding 8
Table 2. Seasonal lengths for different climatic regions (AASHTO 1993) 20
Table 3. Suggested seasonal subgrade soil resilient moduli as a function of the relative quality of the material (AASHTO 1993) 21
Table 4. Recommended gravel layer thickness (in mm) for different climatic regions, relative qualities of roadbed soil, and three levels of traffic (AASHTO 1993) 21
Table 5. Seasonal subgrade CBR values as a function of the relative quality of the material 22
Table 6. Summary of depth ranges for different frequency GPR antenna's (Geophysical Survey Systems, Inc. 2009) 30
Table 7. Reported costs for emergency operations and repair under the FHWA ER and FEMA PA programs in Iowa 34
Table 8. Geo-infrastructure damages and associated repair measures followed on primary roadways 37
Table 9. Geo-infrastructure damages and associated repair measures followed on secondary roadways 40
Table 10. Summary of field test segments — Pottawattamie County 63
Table 11. Fremont County - Summary of field testing 122
Table 12. Summary of statistical t-test results comparing flooded and non-flooded areas on each test segment – Pottawatamie County 160
Table 13. Summary of statistical t-test results comparing flooded and non-flooded areas on each test segment – Fremont County 161
Table 14. Summary of potential flood damage evaluation techniques and repair/mitigation solutions 172
Table A1. Summary of damages, emergency operations, and damage costs on primary roads in Iowa (information obtained from Bonie Castillo, Iowa DOT) 181
Table A2. Summary of damages, emergency operations, and damage costs on secondary roads in Iowa (Courtesy of Bonie Castillo, Iowa DOT) 185
Table D1. Summary of potential flood damage evaluation techniques and repair/mitigation solutions 200
Table D2. Summary of depth ranges for different frequency GPR antenna's (ground-coupled) and potential applications (Geophysical Survey Systems, Inc. 2009) 214
Table D3. Summary of repair/mitigation solutions and their applications 222
Table D4. Summary of cost information for different stabilization method 223
Table D5. Recommended cement contents for different soil types (Portland Cement Association 1995, Fang 1990) 226
Table D6. Construction costs of a bridge constructed with GRS backfill and rail road flat cars in Buchanan County (Vennapusa et al. 2012) 240

ACKNOWLEDGMENTS

The authors would like to thank the Federal Highway Administration for state planning and research (SPR) funding for this project and the Iowa Department of Transportation (DOT) and Iowa Highway Research Board (IHRB) for sponsoring this research (IHRB project TR-638).

The authors would also like to acknowledge the support of the Pottawattamie County Engineer John Rasmussen, PE, and Fremont County Engineer Dan Davis, PE, for touring the damaged areas with the research team, providing helpful insights, and assisting with traffic control during the course of this project. Iowa DOT staff members—Mark Dunn, Sandra Larson, Nicole Fox, Vanessa Geotz, and Thomas Samson—provided assistance with state and county coordination and graphical information system (GIS) imagery. Pottawattamie County staff, David Bayer and Jamie Petersen, provided aerial imagery of the flooded area and John Hanson and his associates provided traffic control during field testing.

David Eisenmann with the Center for Nondestructive Evaluation at Iowa State University (ISU) conducted ground-penetrating radar testing and provided a memo report with a summary of key findings. ISU Center for Earthworks Engineering Research (CEER) students Alex Johnson, Dustin Wheatley, and Simon Wang assisted with field and laboratory testing. All their help is greatly appreciated.

EXECUTIVE SUMMARY

Project Overview

In 2011, the Missouri River flooding caused significant damage to many geo-infrastructure systems including levees, bridge abutments/foundations, paved and unpaved roadways, culverts, and embankment slopes along the Missouri River basin extending from Montana to Missouri. The Iowa counties that were affected by this flood event included Woodbury, Monona, Harrison, Pottawattamie, Mills, and Freemont. The flooding resulted in closures of several interchanges along Interstate 29 (I-29) and of more than 100 miles of secondary roads in these counties, causing severe inconvenience to residents and losses to local businesses (Iowa HSEMD 2011).

The total reported direct cost to repair flood damage to the transportation infrastructure on primary and secondary roadways in these counties was about $63.5 million. The extent of damage was in some cases directly observable, i.e., where segments of the roadway were washed away, but in many cases was undetermined, i.e., where the damage was below the pavement surface or around bridges.

The main goals of this research project were to assist county and city engineers by deploying and using advanced technologies to rapidly assess the damage to geo-infrastructure and develop guidance for repair and mitigation strategies and solutions for use during future flood events in Iowa. Very limited studies have been documented on this topic (e.g., post-Katrina hurricane evaluation in Louisiana) and to the authors' knowledge, there are no documented studies to-date on post-flood assessment of secondary unpaved roadways.

The research team visited selected sites in Pottawattamie and Fremont counties in western Iowa to conduct field reconnaissance. Testing was conducted on bridge abutment backfills that were affected by floods, flooded and non-flooded secondary roadways, and culverts. In situ testing was conducted shortly after the flood waters receded (in September and October 2011), and several months after flooding (in April, May, and June 2012) to evaluate recovery and performance.

Road test segments were selected with an objective to monitor performance of the flooded versus non-flooded areas by evaluating their subsurface foundation layer characteristics over time. The research team compared measurements obtained in non-flooded areas to measurements in flooded areas to assess the damage or strength loss that occurred under roadways.

In situ testing involved conducting falling weight deflectometer (FWD), dynamic cone penetrometer (DCP), and ground-penetrating radar (GPR) testing, three-dimensional (3D) laser scanning, and hand auger soil borings. In situ testing was conducted on about 30 km (18.6 miles) of roadway, where the test segments varied in length from about 150 m (500 ft) to 7.0 km (4.3 miles). The test segments varied by flood condition (fully or partially flooded), and type of surfacing (gravel, chip seal surface over stabilized or unstabilized gravel base, portland cement concrete (PCC), and hot-mix asphalt (HMA)).

Summary of Flood Damages to Secondary Roadways and Repair Measures

Based on field reconnaissance of the flood-damaged areas by the research team, review of the damage inspection reports submitted to the Iowa Department of Transportation (DOT), and interviews with county engineers, the damages observed on secondary roadway geo-infrastructure are broadly categorized as follows:

A. Paved Roadways:
    1. Voids at shallow depths (< 150 mm (6 in.)) due to erosion of underlying base material
    2. Voids at deeper depths (> 150 mm (6 in.)) due to erosion of subsurface material
    3. Partial to complete erosion of PCC and HMA pavements and underlying base material
    4. Erosion of granular shoulders
B. Bridges:
    1. Erosion of bridge approach backfill material
    2. Erosion of embankment foreslopes
C. Culverts:
    1. Erosion of culvert backfill
    2. Separation of culverts
    3. Water outflow blockage
D. Unpaved Roadways:
    1. Erosion of gravel surface
    2. Rutting under traffic loading (on gravel roads and other detoured roadways due to excessive loading, although not flooded)
    3. Full breach of roadway embankments

Repairs on secondary roadways generally involved clearing damaged areas by removal of debris and re-construction by replacing damaged areas with new material to achieve targeted pre-flood condition. In some instances, flowable mortar grouting was used to fill voids beneath pavements, and emulsified-oil (bitumen) stabilization was used to stabilize the gravel layer. The total reported cost of flood damage to the transportation infrastructure on secondary roadways in western Iowa was about $12.6 million.

Field evaluation of damage by the county engineers and Federal Emergency Management Agency (FEMA) personnel was based primarily on visual inspection. A push T-bar was used in some cases to detect weep holes under gravel roads during the visual inspection.

Field evaluation of damage by the county engineers and Federal Emergency Management Agency (FEMA) personnel was based primarily on visual inspection. A push T-bar was used in some cases to detect weep holes under gravel roads during the visual inspection. The visual assessment approach worked well where the damage was obvious, i.e., where segments of roadway were washed away, but was not effective in detecting subsurface damage that was not immediately visible at the surface (due to erosion of subsurface materials). The research team found two areas that posed significant safety concerns to traffic due to subsurface damage that was not apparent at the surface. One of those areas resulted in deep potholes on a gravel road due

to eroded backfill around a culvert and the other resulted in deep voids beneath the roadway due to eroded backfill around a bridge abutment. Use of in situ DCP tests and GPR scanning was effective in identifying these areas and are discussed below.

In Situ Test Results and Statistical Analysis

The research team visited selected sites in Pottawattamie and Fremont Counties in western Iowa to conduct in situ testing shortly after the flood waters receded (in September and October 2011) and 7 to 8 months after flooding (in April, May, and June 2012) to evaluate performance. Road test segments were selected with an objective to monitor performance of the flooded versus non-flooded areas over time.

In situ testing involved conducting FWD, DCP, and GPR testing and performing hand auger soil borings. Testing was conducted on about 30 km (18.6 miles) of roadway, where the test segments varied in length from about 150 m (500 ft) to 7.0 km (4.3 miles). The test segments varied by flood condition (fully or partially flooded) and type of surfacing (gravel, chip seal surface over stabilized or unstabilized gravel base, PCC, and HMA). Key findings from in situ testing and observations on test segments with gravel roads (treated and untreated) with and without chipseal surfacing, HMA pavement, PCC pavement, and bridge abutments are as follows.

Gravel Roads and Culvert Crossings

- Comparison of in situ FWD test measurements obtained in flooded and non-flooded areas shortly after flooding revealed statistically significant differences in five out of the six test segments. All test segments showed recovery over time. Testing conducted several months after flooding revealed that in three test segments, the differences between flooded and non-flooded areas became statistically insignificant, while in three other test segments the differences remained statistically significant. This finding emphasizes the need for in situ testing to characterize the often complex field conditions that result from flooding.
- Statistical analysis between CBR of subgrade and gravel layers and FWD modulus indicated that the subgrade layer had about 86% of influence on the FWD measurements while the gravel layer had about 14% influence. This finding has practical importance because it indicates that the response to dynamic traffic loading at the surface will be more dependent on the quality of the subgrade layer.
- Weep holes were observed at several culvert locations directly beneath the gravel layer, indicating erosion of backfill material around the culvert. Most of the weep holes were not noticeable until the flood waters receded. On one test segment, erosion of culvert backfill materials resulted in formation of about 0.5 m (1.5 ft) diameter potholes on the middle of roadway. These potholes were undetected until they were formed and posed a significant safety concern to traffic.
- Significant rutting (up to 125 mm (4.9 in.) deep) was observed under wheel paths at several locations along a test segment (TS3) in Fremont County. DCP tests in some of those areas showed layers with CBR < 2 in the subgrade, which likely contributed to the rutting.

- GPR scanning using 200 and 400 MHz antennas identified changes in gravel layer thicknesses, culvert locations, and weep holes.

HMA Pavement

Only one pavement segment with 360 mm (14 in.) thick HMA underlain by 300 mm (12 in.) thick base and natural subgrade was tested as part of this study. Some key findings from this test segment were as follows:

- No structural failures were observed on the pavement. However, granular shoulder erosion was evident in areas close to the high water line.
- E_{FWD} and E_{SG} values were on average about 1.3 to 1.4 times higher in the non-flooded zone than in the flooded zone at all times of testing. FWD results obtained about 6 months after flooding were on average higher in the non-flooded zone and the results obtained about 9 months after flooding were on average similar in both flooded and non-flooded zones when compared to the results obtained shortly after flooding.
- The CBR of the base layer was about the same in both flooded and non-flooded zones (> 50), but the CBR of subgrade was on average about 10 times higher in the non-flooded zone than in the flooded zone. No significant difference was noted in the measurements obtained shortly after flooding and about 9 months after flooding.

PCC Pavement

Only one pavement segment with about 250 mm (9.8 in.) thick PCC, which was originally (before flooding) underlain by 150 mm (6 in.) thick subbase and natural subgrade, was tested as part of this study. Some key findings from this test segment were as follows:

- Reportedly, the test segment experienced heavy water currents as the water levels fluctuated during the flood event resulting in granular shoulder erosion, complete washout of a portion of the pavement, and erosion of the subbase layer beneath the pavement.
- Flowable cement grout was used to fill the voids formed beneath the pavement. The grout was very soft and did not set up even two days after placement. Longitudinal cracks were observed on a few panels where the subbase layer was eroded. Additional research is warranted in evaluating use of alternative materials of stabilizing grout for use below water.
- FWD tests at joints indicated an average LTE of about 93% to 95% at all testing times. Two of the test locations showed a reduction in LTE with time, from about 94% shortly after flooding to about 85% to 88% several months after flooding. These tests were located on panels underlain by cement grout. This test segment warrants performance monitoring over time to evaluate the effectiveness of the cement grout placement.
- FWD zero-load intercept values did not indicate any voids beneath the pavement. The $k_{FWD\text{-}static}$ values were on average about 15 to 20 kPa/mm (55 to 73 pci) and is rated as very poor, per AASHTO (1993).
- Average CBR of the grout layer increased from about 5.8 shortly after flooding to 10.4 after flooding. The CBR of the subgrade layer was about the same at both testing times

with an average of about 20 in the top 300 mm (1 ft) of subgrade.

- GPR scans detected dowel bars along the joint between the adjacent lanes. A potential void area was detected at about 0.3 to 0.6 m (1 to 2 ft) below the surface in one of the scans. The bottom of the grout layer was at about 250 to 300 mm (10 to 12 in.) below surface.

Bridge Abutments

- Erosion of bridge approach backfill materials was observed at the two bridge sites assessed in this study. These bridges consisted of timber back wall abutments. In one of the bridges, backfill on one of the approaches was completely washed out and was replaced prior to our testing. DCP-CBR profiles in the newly-placed backfill indicated poorly compacted layers of fill with depth (with CBR < 2) within about 0.6 m (2 ft) of the bridge, which is typically a result of thicker lifts placed during compaction.
- At the two bridge sites, approach backfill materials continued to erode over time resulting in voids beneath the surface gravel layer. At one of the bridge sites, DCP tests across the bridge approach (about 1 month after flood waters receded) indicated voids at depths of about 300 mm (11.8 in.) to 850 mm (33.5 in.) below the surface, which extended nearly down to a maximum depth of about 2 m (6.6 ft) below the surface.
- GPR scans detected areas of potential voids and backfill erosion beneath the gravel surface after about 8 months after flooding in spite of reconstruction.
- At one of the bridge sites, natural subgrade clay fill material was used to stabilize the bridge abutments and block erosion of the backfill materials through the abutment walls. This material can potentially be scoured away easily during a future flood event. Use of riprap material as scour protection for the abutment wall would be a better repair and mitigation alternative.

Post-Flood Geo-Infrastructure Assessment Techniques and Repair/Mitigation Solutions

A catalog of nine different field assessment techniques and twenty different potential repair/mitigation solutions are provided in this report. A flow chart relating the damages, assessment techniques, and potential repair/mitigation solutions is provided. These options are discussed for paved/unpaved roads, culverts, and bridge abutments, and are applicable for both primary and secondary roadways.

CHAPTER 1: INTRODUCTION

Problem Statement

The 2011 Missouri river flooding caused damage to levees, bridge abutments/foundations, paved and unpaved unpaved roadways, culverts, and embankment slopes along the Missouri river basin extending from Montana to Missouri. Several Iowa counties were affected by this flood event including Woodbury, Monona, Harrison, Pottawattamie, Mills, and Freemont. The total reported direct cost to repair flood damaged transportation infrastructure on primary and secondary roadways was about $63.5 million. The flooding resulted in closures on several interchanges along Interstate 29 and over 100 miles of secondary roads, causing severe inconvenience to residents and losses to local businesses (Iowa HSEMD 2011).

Flood-related damage has been more expensive than any other natural hazard related damages in the United States (Highfield and Brody 2013). Many studies documented the impacts of floods on transportation infrastructure (e.g., Copstead and Johansen 1998; Keller 2002; Doyle and Ketcheson 2007; Zhang et al. 2008; FHWA 2012). However, there has been limited documentation on the engineering characteristics and performance of flood-affected roadway infrastructure systems (e.g., Clark and Cosby 2007; Zhang et al. 2008; Stokoe et al. 2011; Ceylan et al. 2012). To the authors' knowledge, there have been no studies on flood-affected secondary roadway systems. Secondary roadways played a key role in Western Iowa during the flood event, serving as detour routes when primary highways were closed for repairs and as haul roads for construction traffic for repair work.

Post-flood assessment of the damage on secondary roadways by local and federal authorities was primarily based on visual observations. The visual assessment approach worked well where the damage was obvious (e.g., where segments of roadway were washed away), but was marginally effective in detecting subsurface damage (e.g., subsurface voids beneath roadways or around bridge abutments). In addition, repair measures mostly involved removing damaged structures and replacing them to achieve target pre-flood conditions. This remove and replace approach is driven by the policies of the funding sources (e.g., FHWA Emergency Relief Program and Federal Emergency Management Agency). Doyle and Ketcheson (2007) pointed out that on forest roads, many sites experienced recurring failures/damage after flooding because of the remove and replace approach that was followed for nearly 25 years.

Goals and Research Objectives

The main goals of this research project were to assist County and City Engineers by deploying and using advanced technologies to rapidly assess the damage to geo-infrastructure, and develop effective repair and mitigation strategies and solutions for use during future flood events in Iowa. There is a need for information on this topic. Recently, the Federal Highway Administration also initiated a European Collaboration project on this topic (FHWA 2012). Very limited studies have been documented on this topic (e.g., Zhang et al. 2008) and to the authors' knowledge, there are no documented studies to-date on post-flood assessment of secondary unpaved roadways.

The specific research objectives of this project were as follows:

- Conduct field reconnaissance to review geo-infrastructure damage and challenges in the flood affected Counties and prioritize areas for detailed in situ testing and evaluation.
- Conduct in situ testing and evaluation on paved and unpaved secondary roadways.
- Develop a final report with guidance for geo-infrastructure damage evaluation, repair, and mitigation strategies.

Research Approach

The ISU research team visited various sites in Pottawattamie and Fremont Counties in western Iowa to conduct field reconnaissance along with the respective County Engineers, to document the practices followed in repairing the flood damaged areas, and to select areas for testing. The selected counties were determined from conference calls and expressed interest from the project technical advisory committee. Aerial imagery of Pottawattamie and Fremont counties and Geographic Information System (GIS) based spatial data available from Pottawattamie County were used to assess the extent and duration of the flood. Testing was conducted on bridge abutment backfills that were affected by floods, flooded and non-flooded secondary roadways, and culverts. In situ testing was conducted shortly after the flood waters receded (in September and October 2011), and several months after flooding (in April, May, and June 2012) to evaluate recovery and performance. Road test segments were selected with an objective to monitor performance of the flooded versus non-flooded areas by evaluating their subsurface foundation layer characteristics over time. Note that there was no information available as baseline data to compare measurements in the flooded areas. Therefore, the research team relied on measurements obtained in non-flooded areas to compare with measurements in flooded areas.

In situ testing involved falling weight deflectometer (FWD), dynamic cone penetrometer (DCP), and ground penetrating radar (GPR) testing, and performing hand auger soil borings. In situ testing was conducted on about 24 km (18.6 miles) of roadway, where the test segments varied in length from about 150 m (500 ft) to 7.0 km (4.3 miles). The test segments varied by flood condition (fully or partially flooded), and type of surfacing (gravel, chip seal surface over stabilized or unstabilized gravel base, portland cement concrete (PCC), and hot mix asphalt (HMA)).

CHAPTER 2: BACKGROUND

This chapter presents background information on two important aspects of this research: (1) how the 2011 Missouri river flooding occurred and a timeline of significant events that occurred during the flooding event and (2) a summary of previous studies where assessment of post flooding road conditions was performed.

2011 Missouri River Flooding

The 2011 Missouri River flooding information presented in this section is based on reports and articles published by the US Army Corps of Engineers (USACE), Missouri River Flood Task Force (MRFTF), Missouri River Post Flood Water Management Technical Review Panel (composed of experts from US Department of Agriculture, National Oceanic and Atmospheric Administration, US Geological Society, and Colorado State University), Iowa Homeland Security and Emergency Management Division (HSEMD), and an article published by the Prairie Fire Newspaper, Lincoln, Nebraska. The information useful for this research project are presented herein from these sources. Additional information regarding the flood event can be obtained from Mestl (2011), Iowa HSEMD (2011), Grigg et al. (2011), Grode (2012), Latka (2012), McMahon and Farhat (2012), and USACE (2012a,b).

Description of the Missouri River Basin and Causes of 2011 Flooding

The Missouri river extends 2,619 miles from its source at Hell Roaring Creek in southwestern Montana and flows generally east and south to join the Mississippi River just upstream from St. Louis, Missouri. The Missouri river basin has a total drainage area of 529,350 square miles including about 9,700 square miles in Canada. Maps of the Missouri river basin and Missouri river watershed with USACE operated dam locations are shown in Figure 1 and Figure 2, respectively. According to USACE (2006), the basin includes all of the Nebraska; most of the Montana, Wyoming, North Dakota, and South Dakota; about half of Kansas and Missouri; and parts of Iowa, Colorado, and Minnesota.

The 2011 Missouri river flooding event was a result of the highest runoff on record since 1898 (Figure 3) in the basin, with about 61.0 million acre-feet (MAF) which was about 246% of the normal annual runoff and exceeded the previous record annual runoff of 49 MAF in 1997 (Grigg et al. 2011, USACE 2012b). This annual runoff volume equals to an average daily rate of 83,980 ft^3/s over a 12 month period. During March through July 2011, about 48.7 MAF runoff entered the Missouri river, exceeding the flood storage capacity of all the dams and reservoirs in the basin. Due to the excess runoff, all major dams in the basin released record amounts of water, which led to flooding in numerous towns and cities along the Missouri river from Montana to Missouri. The National Oceanic and Atmospheric Administration (NOAA) reported that the direct costs to repair the flood damage occurred in Montana, North Dakota, South Dakota, Iowa, Nebraska, and Missouri was about $623.5 million (NOAA 2011).

Figure 1. Missouri river basin map with USACE operated dam locations (USACE 2012a)

Figure 2. Missouri river main stem system watershed with Civil Works boundary and USACE operated dam locations (McMahon and Farhat 2012)

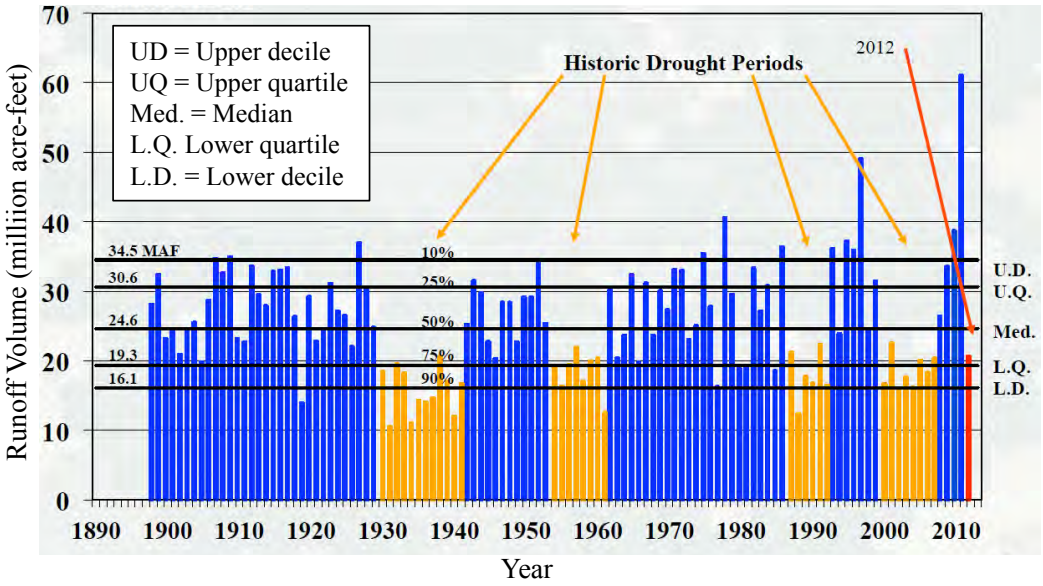

Figure 3. Missouri river basin annual runoff upstream of Sioux City, Iowa from 1898 to 2012 (Grode 2012)

The record runoff was triggered by a combination of three factors as illustrated in Figure 4 (USACE 2012b): (a) melting of above normal heavy plains snowpack from March and April 2011, (b) melting of above normal Rocky Mountain snowpack from May to July 2011, and (c) heavy rainfall in the upper Missouri river basin from March to October 2011. Compounding the problem was colder than normal temperatures which retained most of the snowpack in the upper river basin on the ground longer into the spring, setting the stage for a record runoff.

NASA's Aqua Satellite imagery from June 29, 2010 and June 30, 2011 (during flooding) are shown for comparison in Figure 5, which illustrates the width of the river during the flooding event. NASA's Landsat 5 image of Interstate 29 at the Iowa/Nebraska border during flooding is shown in Figure 6.

Figure 4. Main components of runoff (Latka 2012)

(a)

(b)

Figure 5. Moderate resolution imaging spectroradiometer (MODIS) images from NASA's Aqua satellite captured on (a) June 29, 2010, and (b) June 30, 2011 during flooding (Images Courtesy of MODIS Rapid Response Team, NASA's Goddard Space Flight Center, Greenbelt, Maryland)

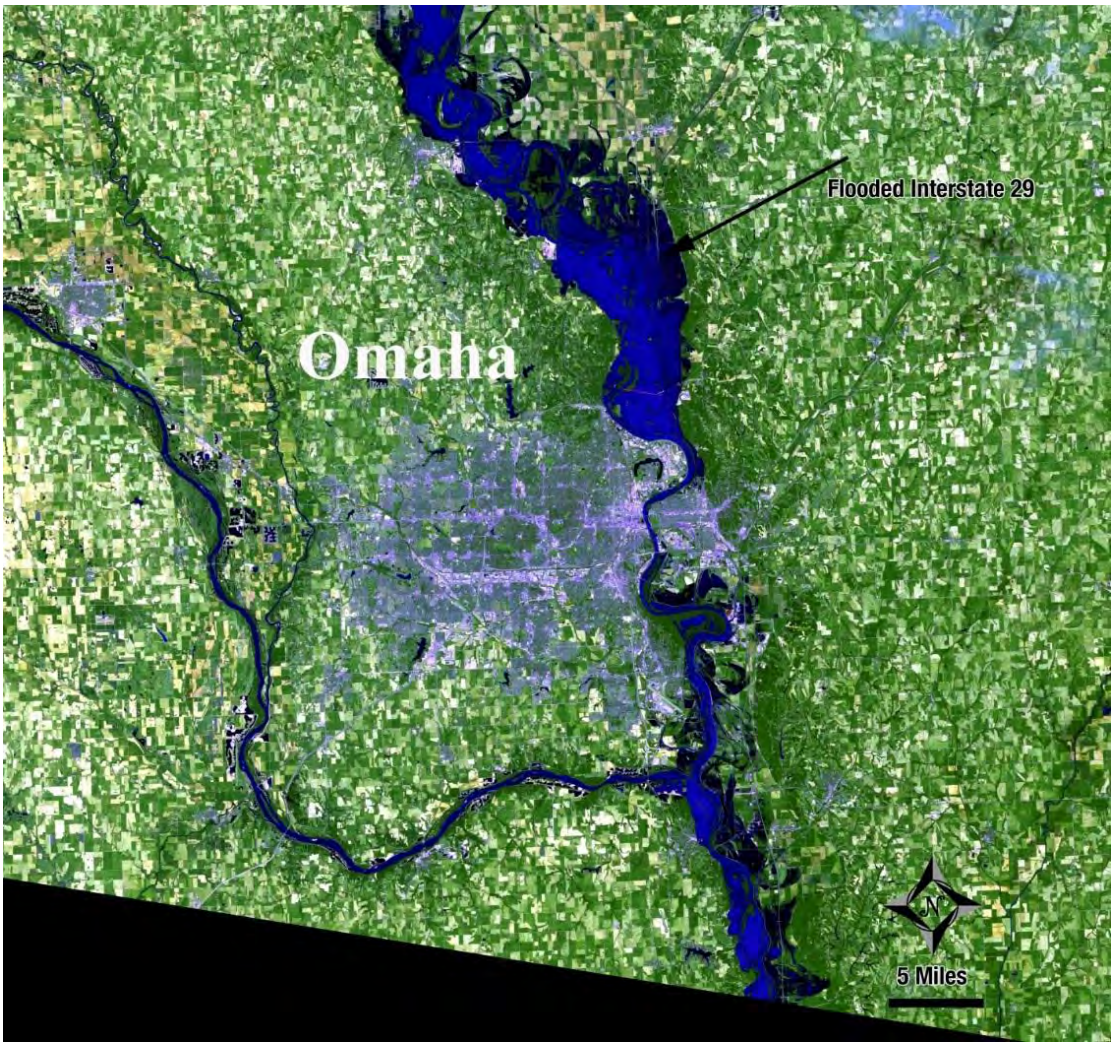

Figure 6. Landsat 5 image showing Missouri river flooding on Interstate 29 at Iowa/Nebraska border on July 6, 2011 (Images Courtesy of NASA's Goddard Space Flight Center, Greenbelt, Maryland)

Significant Events During and After Flooding

The chronology of significant events that occurred during the 2011 Missouri River flooding and after the flood waters receded is summarized in Table 1. The information in Table 1 is obtained from Iowa HSEMD (2011), Iowa DOT's Statewide Emergency Operations, newspaper articles (Kelleher and Bohan 2011, Mastre and Smollen 2011), and the ISU research team observations.

Selected aerial pictures obtained during the flooding event are shown in Figure 8 to Figure 13. A timeline of the daily average runoff released from Gavin's point dam located near the Nebraska-South Dakota border between May 27 and November 15, 2011, and significant events occurred during the period on Iowa DOT highway system is provided in Figure 14 and Figure 15.

Table 1. Chronology of significant events in Western Iowa during and after the 2011 Missouri River flooding

Date	Event
05/01/2011	Outflow at Gavin's Point dam reaches 45,000 ft^3/s.
05/20/2011	Outflow at Gavin's Point dam increased to 57,500 ft^3/s.
05/25/2011	Gov. Branstad directs the execution of the Iowa Emergency Response plan.
05/26/2011	Gavin's point dam releasing 62,000 ft^3/s – about twice the normal flow rate down to the Missouri river for that time of the year.
05/30/2011	Gavin's point dam releasing over 70,000 ft^3/s – exceeds all-time record flow
05/31/2011	USACE announces peak flow of 150,000 ft^3/s by mid-June
06/02/2011	Gov. Branstad issues State of Disaster Emergency Proclamation for Fremont, Harrison, Mills, Monona, Pottawattamie, and Woodbury Counties.
06/03/2011	Iowa Concern Hotline opens for calls. I-29 Hamilton Blvd exit (Exit 149) closed (Figure 8).
06/04/2011	Federal levee 575 near the City of Hamburg in Fremont County suffers partial collapse. USACE initiated an emergency contract to raise the levee immediately surrounding the town to protect it from an estimated 10 ft of flood water.
06/05/2011	Gavin's Point dam releasing 100,000 ft^3/s. Federal levee 575 suffered a second partial collapse.
06/07/2011	Federal levee 575 suffered a third partial collapse.
06/09/2011	I-29 closed in Council Bluffs area.
06/10/2011	Gavin's Point dam releasing 140,000 ft^3/s. I-680 closed in Council Bluffs area. Iowa HSEMD activates the SEOC to coordinate Federal, State, private sector, and volunteer agencies efforts in the affected areas. Iowa HSEMD launches Flood Watch Flickr page.
06/11/2011	IA-2 lane closure.
06/12/2011	I-29/I-680 north interchange closed. IA 175 shoulder protection project started. WinnaVegas Casino and Resort in Sloan, Iowa closes.
06/13/2011	Total breach at Federal levee 575 with about 300 feet gap (Figure 11).
06/14/2011	Gavin's point dam releasing 150,000 ft^3/s (Figure 9).
06/15/2011	I-29 and IA-333 closed in Hamburg between mileposts 1 and 10.
06/18/2011	IA-2 closed west of I-29.
06/21/2011	TrapBag mititgation on I-29 near Blencoe, IA between mileposts 107 and 109.
06/22/2011	USACE announces peak flow of 160,000 ft^3/s through August. Mills County declared a mandatory evacuation of all residents between Interstate 29 and the Missouri river.
06/23/2011	Fremont County orders evacuation of 661 residents.

Date	Event
06/24/2011	Gavin's point dam releasing 160,000 ft^3/s. Additional mandatory evacuation ordered for parts of Mills County.
06/25/2011	Levee breach north of Council Bluffs flooded an area of Harrison County.
06/27/2011	IA-175 Decatur bridge closed. Pres. Obama authorizes Presidential disaster Declaration for Public Assistance for six Iowa Counties (Fremont, Harrison, Mills, Monona, Pottawattamie, and Woodbury) affected by Missouri river flooding.
06/30/2011	Fremont County coordinator reports a 200 foot long breach in the levee north of Percival, Iowa, which lead to mandatory evacuation for the town of Percival. Iowa DOT reports that Interstate 29 is closed from the Bartlett, Iowa interchange (Exit 24) south to the I-29/US135 interchange in Missouri. I-29/I-680 north interchange mitigation project started.
07/01/2011	Pottawattamie County advised Iowa HSEMD the coalition for several drainage districts blew a hole in the privately owned Van Dam levee located about 10 river miles south of the reactor. The levee destruction was done to alleviate flooding in the bend of the river which was creating a water pool opposite to the reactor. TrapBag installation on US30 west of Missouri River valley. IA-175 Decatur bridge embankment mitigation project started.
07/08/2011	US Department of Agriculture declares an Agricultural Disaster Declaration for Fremont, Harrison, Mills, Monona, Pottawattamie, and Woodbury Counties, along with contiguous counties of Cass, Cherokee, Crawford, Ida, Montgomery, Page, Plymouth, and Shelby.
07/11/2011	USACE announces flow to be reduced to 150,000 ft^3/s by August 1st.
07/13/2011	I-29 mitigation project using 12" ACC overlay near milepost 103.5. SBA Disaster Assistance in the form of Economic Injury Disaster Loans (EIDL's) for small non-farm business, small agriculture cooperatives and private nonprofit businesses is available.
07/18/2011	State Individual Assistance Program activated.
07/22/2011	Levee breach reported in Harrison County on the north side of Soldier River between Mondamin and Little Sioux
07/29/2011	USACE announces plan to step-down to 90,000 ft^3/s by August 27th.
08/03/2011	Flow from Gavin's Point dam reduced to 150,000 ft^3/s.
08/04/2011	Federal Individual Assistance for Iowa denied.
08/08/2011	Mandatory evacuation order for the City of Hamburg lifted and changed to a voluntary order
08/12/2011	Gov. Branstad requests extended timeframe to appear FEMA denial due to unusual and ongoing nature of the flooding.
08/16/2011	Waters begin to recede on highways, exposing extensive debris and damage.

Date	Event
08/22/2011	FEMA amends Public Assistance Disaster Declaration activating Permanent Work categories of the Public Assistance Program for counties affected by Missouri River Flood. About 30 feet section of a non-Federal levee along St. Mary's Drainage District breached in Mills County.
08/24/2011	SBA assistance is available for Private Non-Profit organizations that provide essential government services.
08/26/2011	Iowa State University researchers submit a research proposal to Iowa Highway Research Board to assist in evaluation of damage on secondary roads in the flood affected counties.
09/01/2011	Flow from Gavin's Point dam reduced to 90,000 ft^3/s. I-29/Hamilton Blvd exit (Exit 149) re-opens. FEMA approves Gov. Branstad's request to extension to appeal the denial of Federal Individual Assistance.
09/19/2011	Iowa State University researchers submit a revised proposal to Iowa Highway Research Board to assist in evaluation of damage on secondary roads in the flood affected counties.
09/21/2011	Iowa State University researcher's visit Pottawattamie County for field reconnaissance of the flood affected secondary roads and conduct in situ testing.
09/23/2011	I-29 in Council Bluffs area (between mileposts 55 and 71) re-opens. Letting for I-680 reconstruction.
10/03/2011	Flow from Gavin's Point dam reduced to 40,000 ft^3/s.
10/05/2011	Letting for IA-175 Decatur bridge project.
10/08/2011	I-29 near Hamburg between mileposts 0 and 32 re-opens.
10/18/2011	Iowa receives Presidential Disaster Declaration for Federal Individual Assistance in Harrison, Fremont, Mills, Monona, and Pottawattamie Counties. Woodbury County not included in the declaration due to insufficient relevant damages. State Individual Assistance Program suspended. Following Federal Individual Assistance declaration, SBA assistance available for private homeowners in covered counties.
10/25/2011	Iowa State University researcher's visit Pottawattamie County to conduct follow-up in situ testing as flood waters receded.
10/26/2011	Iowa State University researcher's visit Fremont County for field reconnaissance of the flood affected secondary roads and conduct in situ testing. Pottawattamie County Disaster Recovery Center (DRC) opens.
10/27/2011	Fremont County DRC opens.
10/28/2011	Monona County DRC opens.

Date	Event
11/01/2011	Crisis counseling request sent to FEMA.
11/02/2011	I-680 re-opening ceremony.
11/03/2011	I-680 between mileposts 1 and 3 in Council Bluffs area re-opens. IA-175 Decatur bridge re-opens.
11/10/2011	Monona County DRC closes
11/11/2011	IA-333 near Hamburg re-opens.
11/17/2011	Fremont County DRC closes.
11/30/2011	Case Management request sent to FEMA.
12/8/2011	Pottawattamie County DRC closes.
04/04/2012	Iowa State University researchers visit Fremont and Pottawattamie Counties for performance monitoring testing on secondary roads affected during flooding.
05/29/2012	Iowa State University researchers visit Pottawattamie County for performance monitoring testing on secondary roads affected during flooding.
06/19/2012	Iowa State University researchers visit Fremont County for performance monitoring testing on secondary roads affected during flooding.

Figure 7. Aerial photo taken over Sioux City, Iowa on June 1, 2011 (Image Courtesy of Tim Hynds, AP Photos/Sioux City Journal)

Figure 8. Aerial photo of the Hamilton Blvd exit of I-29 (Exit 149) on June 3, 2011 (Image Courtesy of Mercy Aircare, Sioux City, Iowa)

Figure 9. Gavin's Point dam releases 150,000 ft^3/s of runoff volume on June 14, 2011 (Image Courtesy of Jay Woods, USACE)

Figure 10. Aerial photo of the flooding on I-29 between Council Bluffs and Hamburg, Iowa on June 16, 2011 (Image Courtesy of Rodney White, The Register)

Figure 11. Aerial photo of the full breach at Federal levee 575 near Hamburg, Iowa, on June 14, 2011 (Image Courtesy of USACEhttp://www.flickr.com/photos/usacehq/5837117182/in/photostream/**)**

Figure 12. Aerial photo of the flooding near the Fort Calhoun nuclear power plant near Blair, Nebraska on June 17, 2011 (Image Courtesy of Omaha Public Power District)

Figure 13. Aerial photo of the overtopping of Federal levee 550 near Highway 136 in Atchison County, Missouri, on June 19, 2011 (Image Courtesy of USACE http://www.flickr.com/photos/usacehq/5849817627/in/photostream/)

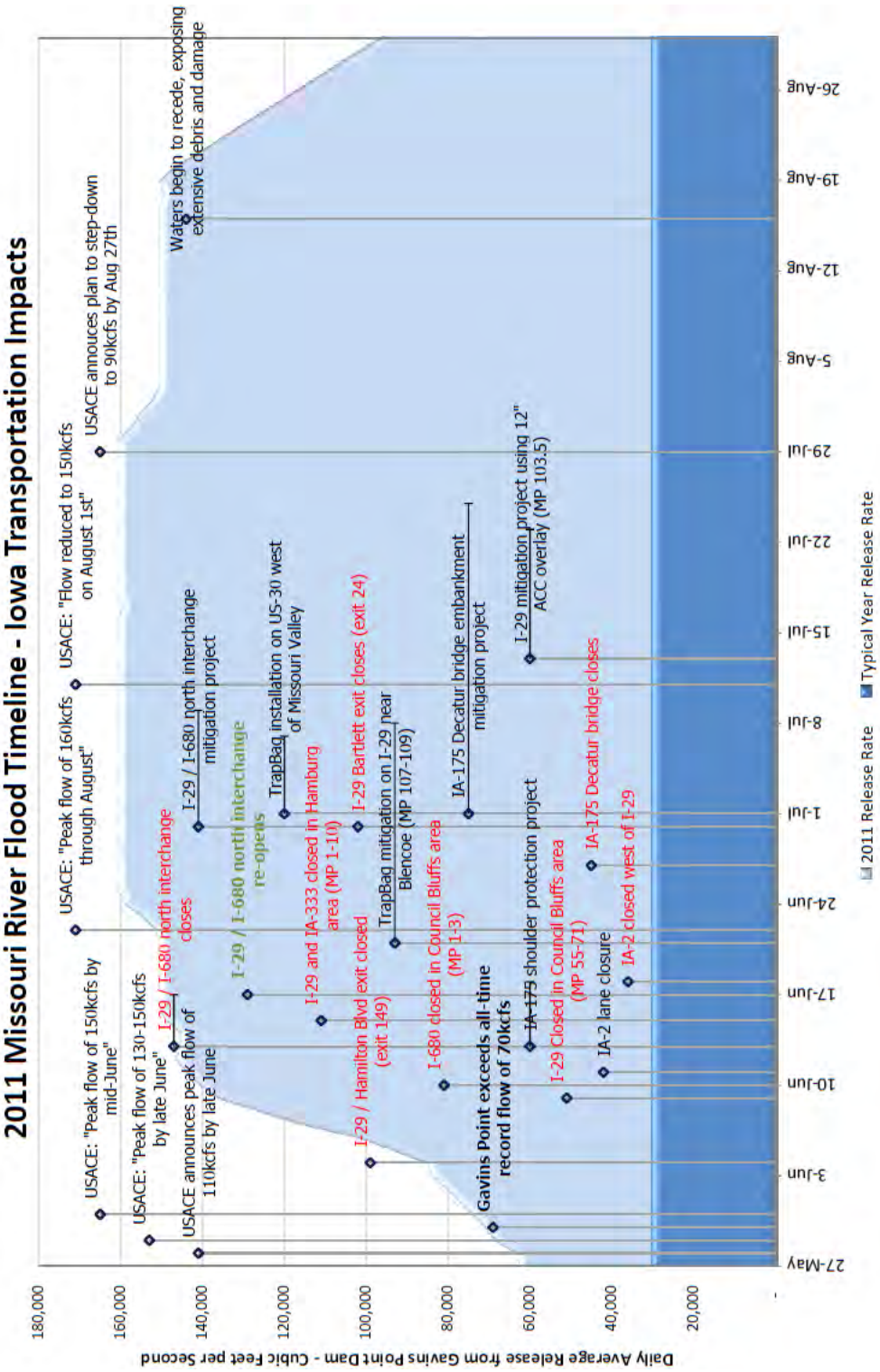

Figure 14. Timeline of daily average release of runoff from Gavins Point dam and significant events related to Iowa Transportation occurred during between 05/27/11 and 08/29/11 (Image Courtesy of Bonnie Castillo, Disaster Operations Manager, Iowa DOT State Emergency Operations)

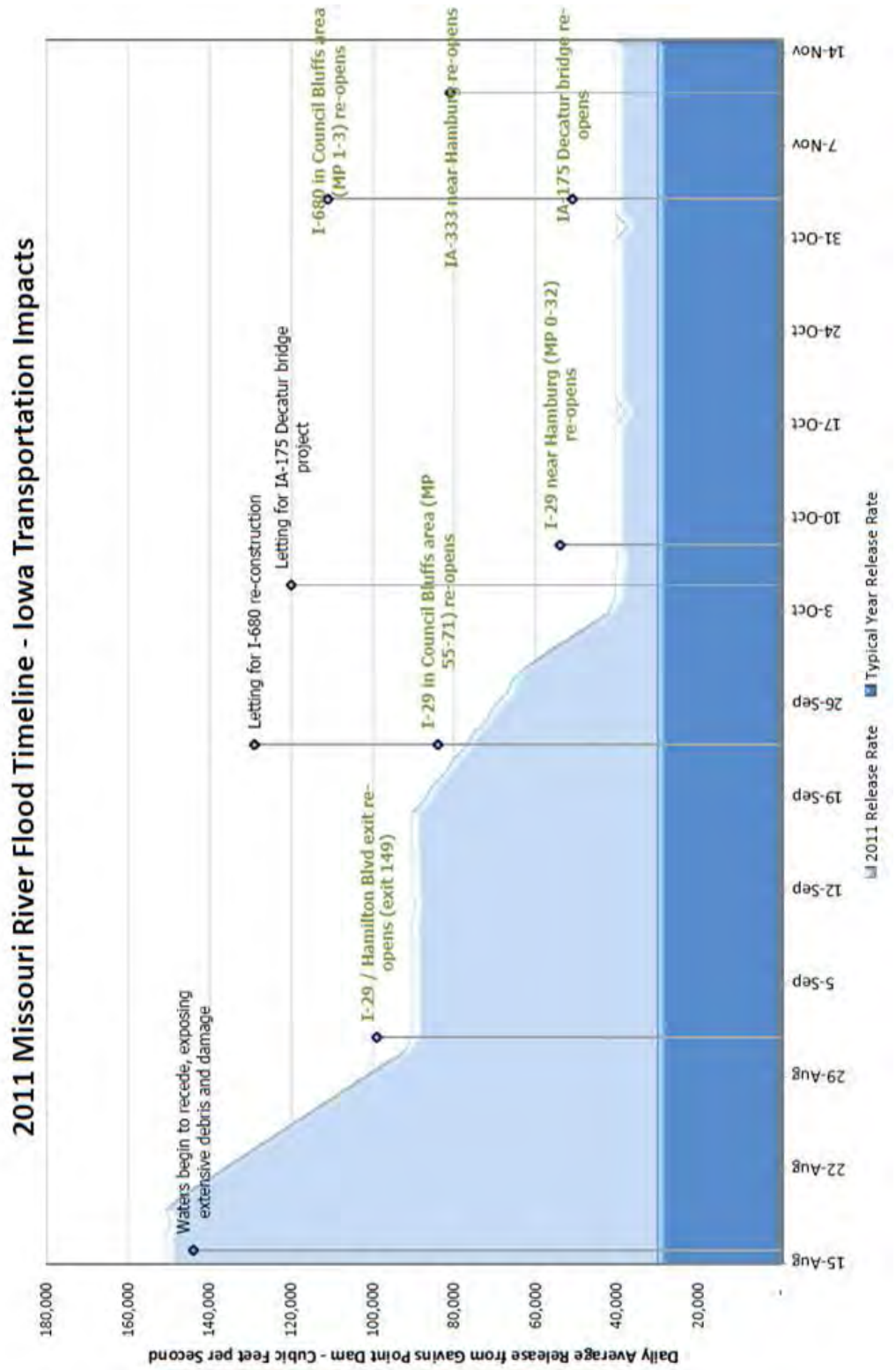

Figure 15. Timeline of daily average release of runoff from Gavins Point dam and significant events related to Iowa Transportation occurred during between 08/29/11 and 11/15/11 (Image Courtesy of Bonnie Castillo, Disaster Operations Manager, Iowa DOT State Emergency Operations)

Previous Studies on Assessment of Flood Damaged Roadway

An extensive literature search was conducted as part of this project to find previous studies that reported post-flood evaluation of roadways. Limited studies were found and are summarized below. Zhang et al. (2008) was the only comprehensive published study that was found, which evaluated PCC, HMA, and composite pavement structures after Hurricane Katrina using FWD testing on primary roadways. To the author's knowledge, no studies were documented to-date evaluating unpaved roadways after flooding.

Pavement Structures Damage after Hurricane Katrina Flooding, New Orleans, Louisiana (2005)

Zhang et al. (2008) reported in situ FWD test results on approximately 383 km (238 miles) of urban highways that were both inside and outside the area that was flooded during the 2005 Hurricane Katrina in New Orleans, Louisiana. The FWD data were imported in to a geographical information system (GIS) and plotted against a United States Geological Survey (USGS), FEMA, and NOAA geo-referenced soil and flood maps. The geo-referenced maps were used to compare FWD results in flooded versus non-flooded areas, short versus long flood durations, shallow versus deep flooding, and thin versus thick pavements. Limited pre- and post-flooding comparison data on HMA pavements indicated that the average structural number (SN) was about 5.1 before flooding but reduced to 4.2 after flooding, which is attributed to a reduction in the average subgrade modulus from 44 MPa to 33 MPa due to the effects of saturation. Results also indicated that HMA pavements in lower elevations were affected more by flooding than the ones at higher elevations. HMA pavements were impacted more than PCC pavements, and no conclusions could be drawn on composite pavements. Thinner pavements were affected comparatively more than thicker pavements on city-parish roadways.

HMA Pavement on State Highway 24 in McClain County, Oklahoma (2007)

Clarke and Cosby (2007) reported FWD test results on State Highway 24 in McClain County, Oklahoma, surfaced with HMA pavement. The subgrade soils consisted of red platy to blocky shale material. Results showed an average FWD surface deflection of 25.1 μm and 22.1 μm in flooded and non-flooded areas, respectively, which were flooded for about 8 to 14 hours. The authors concluded those flood durations were not long enough to cause significant damage to subgrade.

Evaluating "Unseen" Pavement Damage by Flooding after Hurricane Sandy (2012) and Katrina (2005)

PRWEB (2012) reported that Infrasense, Inc. worked on evaluating pavement damage, particularly to detect subsurface voids caused due to flooding after Hurricane Sandy in North Eastern United States and Hurricane Katrina in Louisiana. To this report author's knowledge, no results and findings of those studies were published at the time of this report.

Investigation of Galveston Airport Pavements after Hurricane Ike, Galveston, Texas (2008)

Stokoe et al. (2011) reported surface deflections under rolling dynamic deflectometer (RDD) results on Galveston airport pavements about 3 months after flooding due to Hurricane Ike in Galveston, Texas. Comparison of post-flooding results to pre-flooding results were not possible for this project as records of most of the pre-flooding results were lost during the hurricane. Based on small deflections observed in sections constructed several years before flooding, the authors concluded that water inundation into the pavement system during flooding had little effect on the performance of the airport runway pavements.

Iowa DOT Primary Roads Evaluation after 2011 Missouri River Flooding (2011)

Ceylan (2012) reported FWD and GPR tests conducted by the Iowa DOT on primary roadways (i.e., interstate and state highways) in western Iowa after the 2011 Missouri river flooding. FWD test results showed comparatively higher deflections in lanes where water had encroached up to the shoulders. FWD zero load intercept values detected voids beneath the pavement at few locations. GPR detected areas of voids beneath the pavement due to erosion of subdrain structures.

CHAPTER 3: LOW VOLUME ROAD FOUNDATION LAYER DESIGN INPUTS

AASHTO (1993) provides design guidance with typical foundation layer input values for design of low volume flexible, rigid, and aggregate-surfaced (gravel) roads. A summary of that information is provided herein, which is later used in this report to assess the condition of the roadway foundation layers after flooding.

The performance of gravel or surfaced roadways is directly dependent upon the stiffness of the underlying subgrade. Step-by-step design procedures based on the subgrade resilient modulus (M_r) or effective modulus of subgrade reaction (k) values are provided in the AASHTO (1993) design guide. In cases where this information is not available, the following suggestions are made in the design guide:

- Estimate the season lengths based on the six different climatic regions of the US (Figure 16) and the environmental characteristics associated with each using Table 2. Note that the state of Iowa falls under climate region III.
- Select typical seasonal subgrade M_r values shown in Table 3 with reference to the relative quality of the material.

A catalog with typical values for flexible, rigid, and gravel road design are provided in the AASHTO (1993) design guide. The design catalog for flexible pavements includes typical structural number (SN) values as a function of different subgrade soil quality, US climatic region, traffic levels, and reliability in design. Similarly, for rigid pavements the catalog includes typical pavement layer thickness values with and without granular subbase. The subgrade relative quality was differentiated by the k value for rigid pavement design as follows:

- k > 149 kPa/mm (550 pci) – Very Good
- k = 108 to 149 kPa/mm (400 to 550 pci) – Good
- k = 68 to 95 kPa/mm (250 to 350 pci) – Fair
- k = 41 to 68 kPa/mm (150 to 250 pci) – Poor
- k < 41 kP/mm (<150 pci) – Very Poor

For gravel roads, typical gravel layer thicknesses are provided as summarized in Table 4. It must be noted that these typical values were developed assuming an effective aggregate base material modulus of 207 MPa (30,000 psi). For roads that have poor to very poor subgrade soils and experience medium to high traffic levels, AASHTO (1993) recommends “higher type pavement design,” although it is not defined what that should be in the guide. Alternatives to improve upon poor to very poor subgrade conditions are presented in the last chapter of this report.

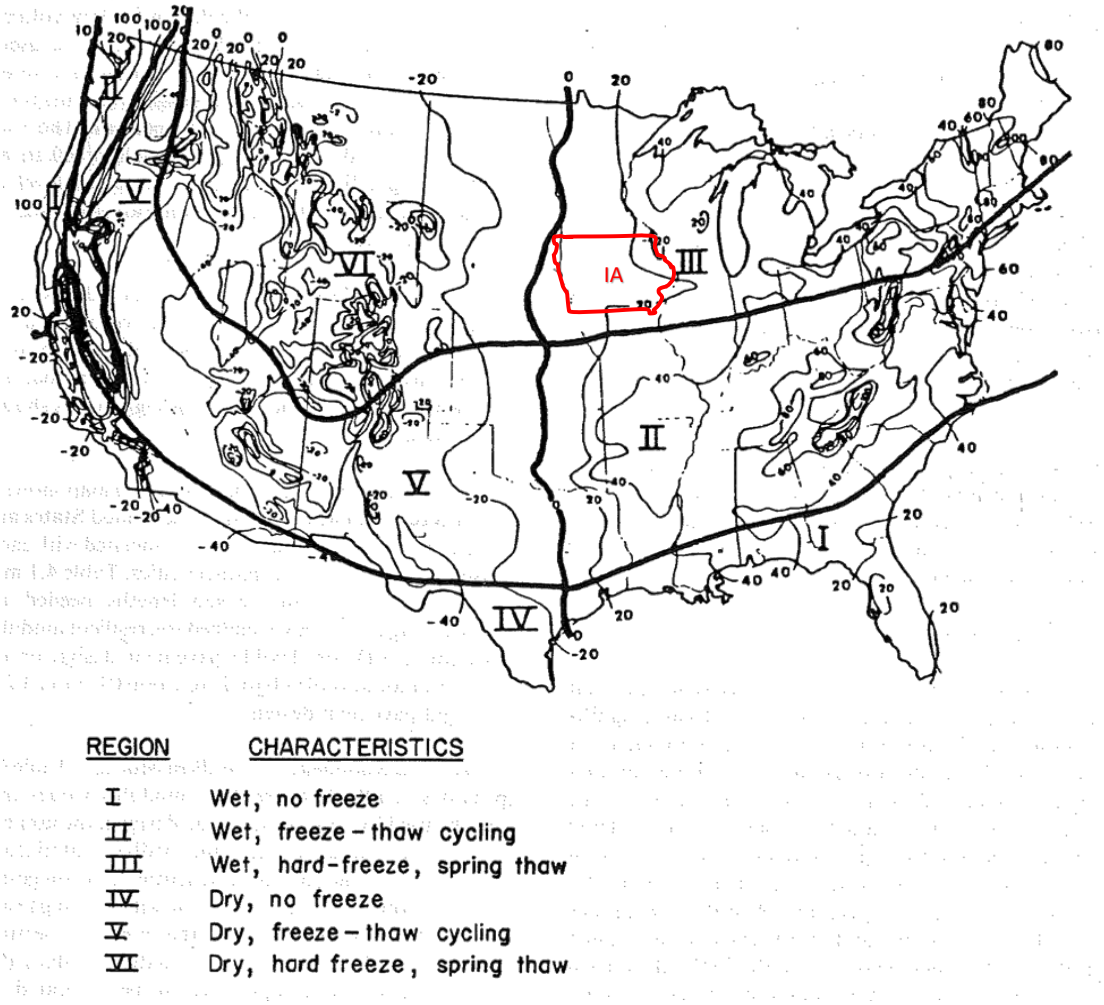

Figure 16. Six climatic regions in the United States (AASHTO 1993)

Table 2. Seasonal lengths for different climatic regions (AASHTO 1993)

U.S. Climatic Region	Season Length (months)			
	Winter (Frozen)	Spring-Thaw (Saturated)	Spring/Fall (Wet)	Summer (Dry)
I	0.0	0.0	7.5	4.5
II	1.0	0.5	7.0	3.5
III	2.5	1.5	4.0	4.0
IV	0.0	0.0	4.0	8.0
V	1.0	0.5	3.0	7.5
VI	3.0	1.5	3.0	4.5

Note: Highlighted shows climatic zone for the state of Iowa.

Table 3. Suggested seasonal subgrade soil resilient moduli as a function of the relative quality of the material (AASHTO 1993)

Relative quality of subgrade soil	Subgrade Resilient Modulus (MPa) for different Seasons			
	Winter (Frozen)	Spring-Thaw (Saturated)	Spring/Fall (Wet)	Summer (Dry)
Very Good	138	17	55	138
Good	138	14	41	69
Fair	138	14	31	45
Poor	138	10	23	34
Very Poor	138	10	17	28

Table 4. Recommended gravel layer thickness (in mm) for different climatic regions, relative qualities of roadbed soil, and three levels of traffic (AASHTO 1993)

Relative quality of subgrade soil	Traffic Level*	Recommended minimum gravel base thickness in mm for each US Climatic Region					
		I	II	III	IV	V	VI
Very Good	High	203	254	381	178	229	381
	Medium	152	203	279	127	178	279
	Low	102	102	152	102	102	152
Good	High	279	305	432	254	279	432
	Medium	203	229	305	178	229	305
	Low	102	127	178	102	127	178
Fair	High	330	356	432	305	330	432
	Medium	279	279	305	254	254	305
	Low	152	152	178	127	127	178
Poor	High	**	**	**	**	**	**
	Medium	**	**	**	381	381	**
	Low	229	254	229	203	203	229
Very Poor	High	**	**	**	**	**	**
	Medium	**	**	**	**	**	**
	Low	279	279	254	203	203	229

*High – 60,000 to 100,000; Medium – 30,000 to 60,000; Low – 10,000 to 30,000 18-kip ESAL applications.
**Higher type pavement design recommended.
Note: Highlighted shows climatic zone for the state of Iowa.

Measuring *k* values requires plate load testing, which is time-consuming and expensive. AASHTO (1993) suggests an empirical equation (Eq. 1) to estimate *k* values based on M_r and M_r can be estimated using empirical relationship with CBR (Eq. 2).

$$k\ (pci) = \frac{M_r(psi)}{19.4} \quad (1)$$

$$M_r\ (\text{psi}) = 1941.49(CBR^{0.684}) \quad (2)$$

Using these relationships, the seasonal soil modulus values are converted to subgrade CBR values as a function of the relative quality of the material as summarized in Table 5.

Table 5. Seasonal subgrade CBR values as a function of the relative quality of the material

Relative quality of subgrade soil	Subgrade CBR (%) for different Seasons			
	Winter (Frozen)	Spring-Thaw (Saturated)	Spring/Fall (Wet)	Summer (Dry)
Very Good	30	1.4	7.9	30
Good	30	1.0	5.2	11
Fair	30	1.0	3.4	5.8
Poor	30	0.7	2.2	3.9
Very Poor	30	0.7	1.4	2.9

CHAPTER 4: TESTING METHODS AND STATISTICAL DATA ANALYSIS

This chapter describes the laboratory and field testing methods used in this project and the statistical analysis methods followed. For tests where an American Standard for Testing and Materials (ASTM) standard was followed, the standard is simply referenced. Any deviations from the ASTM standard procedures are briefly described. For test methods where no ASTM standard is available or not followed, appropriate references are cited or the test procedure followed is briefly described.

In Situ Testing

Dynamic Cone Penetrometer

Dynamic cone penetrometer (DCP) tests (Figure 17) were performed in accordance with ASTM D6951-03 *"Standard Test Method for Use of the Dynamic Cone Penetrometer in Shallow Pavement Applications."* The tests involved dropping a 8 kg (17.6 lb) hammer from a height of 574 mm (22.6 in.) and measuring the resulting penetration depth. California bearing ratio (CBR) values were determined using either Eq. 3 or 4, as appropriate, where the penetration index (PI) is in units of mm/blow.

$$CBR\ (\%) = \frac{292}{PI^{1.12}} \text{ for all soils with CBR} > 10 \quad (3)$$

$$CBR\ (\%) = \frac{1}{(0.017019 \times PI)^2} \text{ when CBR} < 10 \text{ on CL soils} \quad (4)$$

Figure 17. Dynamic cone penetrometer (DCP)

On gravel road test segments, the tests were conducted directly on the surface. On PCC and HMA pavement test segments, tests were conducted by drilling a 25 mm diameter hole through the pavement using a hammer drill.

The DCP-CBR values are presented in this report as CBR with depth profiles and weighted average CBR for a given layer (gravel base or subgrade). The weighted average value was calculated using Eq. 5, where CBR_i = CBR of the i^{th} layer and H_i = is the thickness of the i^{th} layer. The thickness of the gravel layer was determined based on the DCP profile and the for the subgrade, the weighted average of the top 300 mm of the subgrade was reported, as illustrated in Figure 18.

$$CBR\ (\%) = \frac{(CBR_i \times H_i)+(CBR_{i+1} \times H_{i+1})+\cdots(CBR_n \times H_n)}{\sum H_n} \quad (5)$$

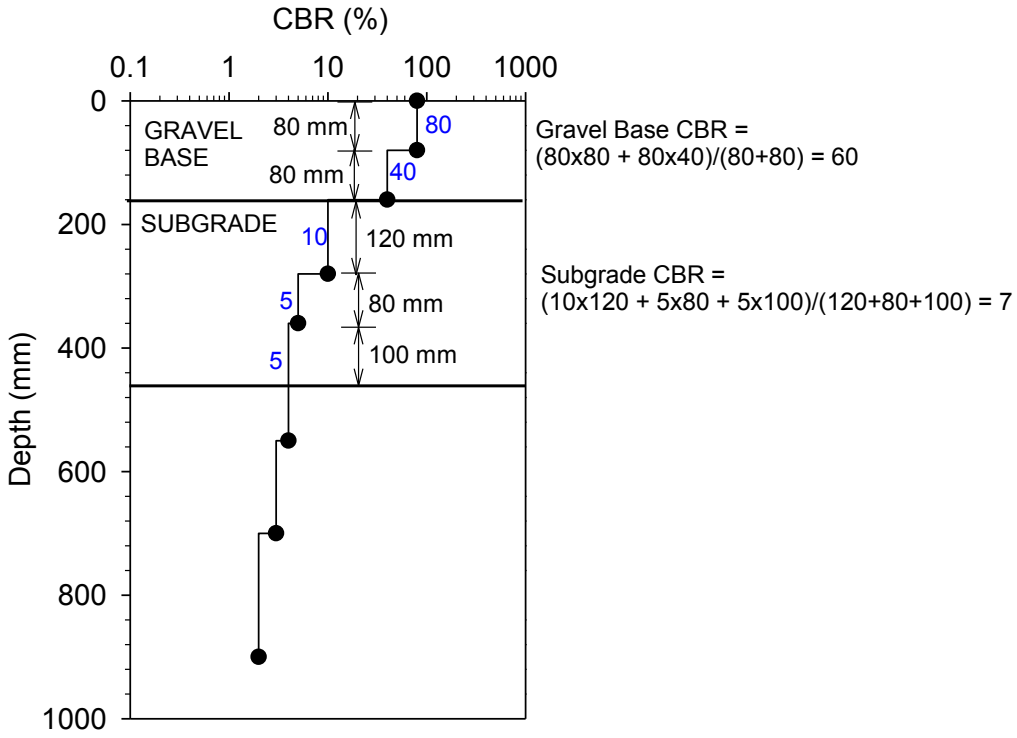

Figure 18. Ilustration of weighted average CBR calculation

Falling Weight Deflectometer

Falling weight deflectometer (FWD) tests were conducted using a Kuab FWD setup with a 300 mm (11.81 in.) diameter loading plate by applying one seating drop and four loading drops (Figure 2). The applied loads varied from about 5,000 to 15,000 lb in the four loading drops. The actual applied forces were recorded using a load cell, and deflections were recorded using seismometers mounted on the device, per ASTM D4694-09 *"Standard Test Method for Deflections with a Falling-Weight-Type Impulse Load Device."* The FWD plate and deflection

sensor setup, and a typical deflection basin is shown in Figure 20. To compare deflection values from different test locations at the same applied contact stress, the values at each test location were normalized to a 40 kN (9,000 lb) applied force.

On gravel roads, chipseal surface roads, and HMA pavements, surface modulus values were determined using Eq. 6 and the subgrade modulus values were determined using Eq. 7 (AASHTO 1993):

$$E_{FWD} = \frac{(1-\upsilon^2)\sigma_0 a}{D_0} f \quad (6)$$

$$E_{SG} = \mathrm{C}\left(\frac{(1-\upsilon^2)\sigma_0 a^2}{r\, D_{0(\mathrm{r})}}\right) \quad (7)$$

where:
a = radius of the plate = 150 mm,
E_{FWD} = elastic modulus at the surface determined from FWD (MPa),
E_{SG} = modulus of subgrade (MPa),
D_0 = measured deflection under the plate (mm),
ν = Poisson's ratio (assumed as 0.4),
σ_0 = applied stress (MPa),
f = shape factor assumed as 2 because of uniform stress distribution — the loading plate used in the test is a segmented (four-part) plate and according to the manufacturer, the segmented plate results in a uniform stress distribution,
r = radial distance of the sensor away from the center of the loading plate,
$d_{0(r)}$ = measured deflection at the sensor located at distance r (mm), and
C = adjustment factor assumed as 0.33 (per AASHTO 1993)

According to AASHTO (1993), the modulus values estimated from FWD tests exceed the laboratory measured resilient modulus values by a factor of three or more. Therefore an adjustment factor $C \leq 0.33$ is recommended. AASHTO (1993) suggests that the $d_{o(r)}$ must be far enough away that it provides a good estimate of the subgrade modulus, independent of the effects of any layers above, but also close enough that it does not result in a too small value. A graphical solution is provided in AASHTO (1993) to estimate the minimum radial distance based on an assumed effective modulus of all layers above the subgrade and the d_0 value. Salt (1998) indicated that if E_{SG} values are plotted against radial distance r, in linear elastic materials such as sands and gravels, the modulus values decrease with increasing distance and then level off after a certain distance. The distance at which the modulus values level off can be used as r in Eq. 7. In some cases the modulus values decrease and then increase with distance. Such conditions represent either soils with moderate to high moduli with poor drainage at the top of the subgrade or soft soils with low moduli. In those cases the distance where the modulus is low can be used as r in Eq. 7. In this study, r = 914 mm (36 in.) and r = 304 mm (12 in.), were used to determine E_{SG} under HMA pavements and gravel roads, respectively (Figure 21).

Figure 19. KUAB falling weight deflectometer (FWD)

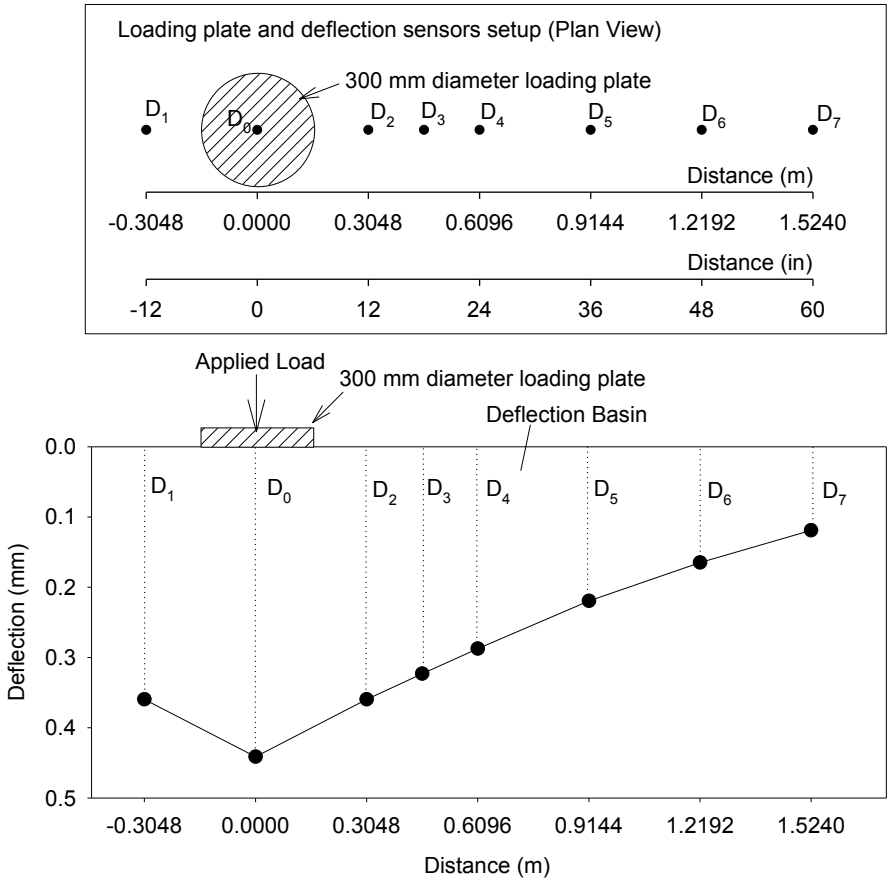

Figure 20. FWD plate and sensor setup (top), and typical deflection basin (bottom)

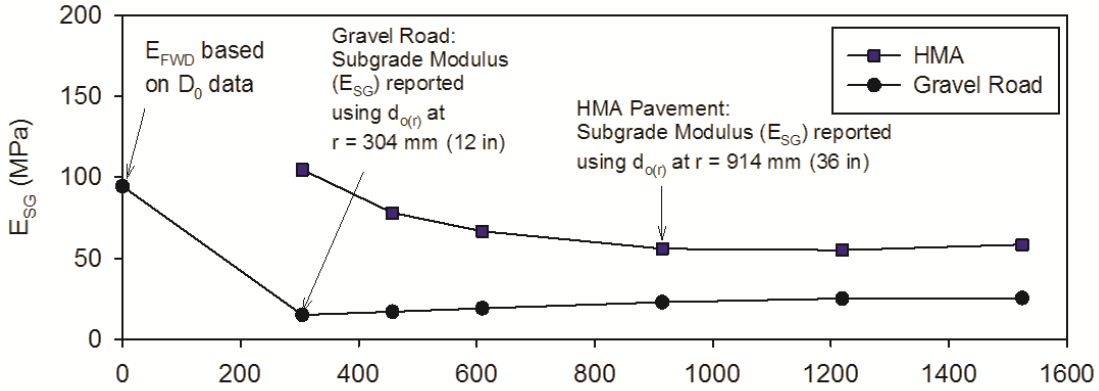

Figure 21. Interpretation of E_{SG} from FWD deflection basin results

FWD tests conducted on PCC pavements involved testing at the center of the slabs and at the joints. Tests at the joints were conducted to determine the joint load transfer efficiency (LTE) by obtaining deflections under the plate on the loaded slab (d_0) and deflections of the unloaded slab (d_1) using a sensor positioned about 0.3 m (12 in.) away from the center of the plate. The LTE was calculated using Eq. 8.

$$LTE\ (\%) = \frac{d_1}{d_0} \times 100 \tag{8}$$

If the entire applied load is transferred over to the adjacent slab, then the LTE would be 100%. If any loss of support exists under the slab, the LTE will be reduced.

FWD tests at the center for the slabs were conducted to determine the modulus of subgrade reaction values. The deflection basin data was used to back-calculate effective dynamic modulus of subgrade reaction ($k_{FWD\text{-}Dynamic}$) values using the Engineering and Research International (ERI) data analysis software. The ERI software uses deflections obtained from D_0, D_2, D_4, and D_5, and the AREA method as described in AASHTO (1993) to determine $k_{FWD\text{-}Dynamic}$. The AREA of each deflection basin is computed using Eq. 9:

$$AREA = 6 \times \left[1 + 2\left(\frac{D_2}{D_0}\right) + 2\left(\frac{D_2}{D_0}\right) + 2\left(\frac{D_4}{D_0}\right) + 2\left(\frac{D_5}{D_0}\right)\right] \tag{9}$$

where:
D_0 = measured deflection under the plate (mm),
D_2 = measured deflection at 304.8 mm (12 in.) away from the center of the plate,
D_4 = measured deflection at 609.6 mm (24 in.) away from the center of the plate, and
D_5 = measured deflection at 914.4 mm (36 in.) away from the center of the plate.

The dynamic $k_{FWD\text{-}Dynamic}$ is determined using Figure 22, using the calculated AREA, applied load (40 kN (9,000 lb)), and D_0 corresponding to the 40kN applied load. The $k_{FWD\text{-}Dynamic}$ value is then converted to effective static modulus of subgrade reaction ($k_{FWD\text{-}Static}$) using Eq. 10.

$$k_{FWD-Static} = \frac{k_{FWD-Dynamic}}{2} \quad (10)$$

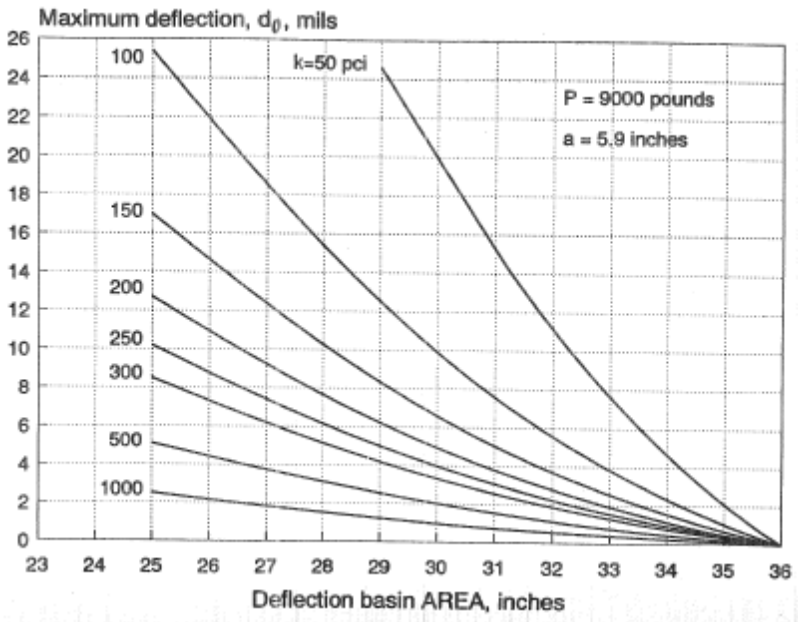

Figure 22. Determination of $k_{FWD\text{-}dynamic}$ using the AREA method (AASHTO 1993)

Voids underneath PCC pavements were predicted by plotting the applied load measurements on the x-axis and the corresponding deflection measurements on the y-axis, and plotting a best fit linear regression line as illustrated in Figure 23. AASHTO (1993) suggests I = 0.05 mm (2 mils) as a critical value for void detection. According to Quintus and Simpson (2002), if I ≤ -0.01 apr ≥ +0.01 mm, then the response would be considered elastic. If I > 0.01 then the response would be considered deflection hardening, and if I < -0.01 then the response would be considered deflection softening.

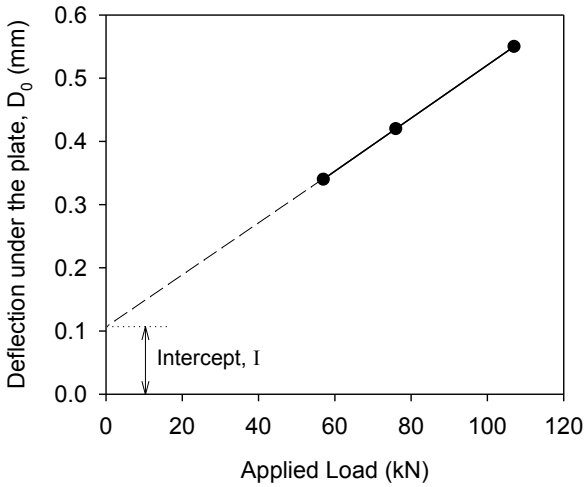

Figure 23. Void detection using load-deflection data from FWD test

Hand Auger Soil Sampling

Disturbed soil samples were obtained from various depths with a hand auger (Figure 24). The soil samples extracted from the bore holes were sealed and transported to lab for moisture content and classification testing.

Figure 24. Extracting soil samples using a hand auger equiped with a Dutch auger head

Ground Penetrating Radar

Ground penetrating radar (GPR) scanning was performed by Mr. David Eisenmann with Center for Non-Destructive Evaluation (CNDE) at Iowa State University, in accordance with ASTM D6432 *"Standard Guide for Using the Surface Ground Penetrating Radar Method for Subsurface Investigation."* The GSSI SIR-20 multi-channel data acquisition unit along with 200 MHz, 400 MHz, and 900 MHz antennas, was used in this study (Figure 25). The data was analyzed using GSSI's RADAN version 7.0.4.5 software with the manufacturer recommended filter settings for each antenna. In this report, GPR scanning results are presented using these analysis results and some of the key anomalies identified in the scans (D. Eisenmann, unpublished internal report, August 2012).

The GPR sends a pulse of energy into the ground and records the strength and time required for the return of any reflected signal. When a series of pulses are sent over a single area, then it is referred to as a scan. Signal reflections are produced when the energy pulse enters into materials with different electrical conductivities (i.e. dielectric permittivity), from the material it left. The strength or amplitude of the reflection is determined by the contrast in the dielectric constants of the two materials (Geophysical Survey Systems, Inc. 2009). For example, when a pulse moves from dry sand (with a dielectric constant of about 5) to wet sand (with a dielectric constant of about 30), it will produce a strong reflection. On the other hand, when a pulse moves from dry sand to limestone (with a dielectric constant of about 7) it will not produce a strong reflection.

While some of the transmitted energy is reflected back to the antenna, some energy keeps travelling through the material until it is dissipated (or attenuated) or until the control unit has

closed its time window. The rate of signal attenuation is dependent on the dielectric properties and conductivity of the materials. If the materials are highly conductive (e.g., wet clays), the signal is attenuated rapidly (Geophysical Survey Systems, Inc. 2009).

During GPR scans, the antenna receives the electrical pulse produced by the control unit, amplifies it, and transmits it into the ground at a particular frequency (Geophysical Survey Systems, Inc. 2009). The frequency of the antenna used is a major factor in the depth of penetration into the ground. The higher the frequency of the antenna, the shallower into the ground it will penetrate. Table 6 provides a summary of the appropriate depth ranges for difference frequency antennas. However, the maximum depth of penetration values will be lower when high conductivity materials are encountered (e.g., wet clays).

Figure 25. Ground penetrating radar scanning using GSSI SIR-20 data acquisition system

Table 6. Summary of depth ranges for different frequency GPR antenna's (Geophysical Survey Systems, Inc. 2009)

Depth Range (Approximate)	Primary Antenna Choice	Secondary Antenna Choice	Applications
0 to 0.5 m	1500 MHz	900 MHz	Structural concrete, roadways, bridge decks
0 to 1 m	900 MHz	400 MHz	Structural concrete, shallow soils, archeology
0 to 3 m	400 MHz	200 MHz	Shallow geology, utilities, underground storage tanks, archaeology
0 to 9 m	200 MHz	100 MHz	Geology, environmental, utilities, archaeology
0 to 30 m	100 MHz	Sub-Echo 40	Geologic profiling
> 30 m	80 to 16 MHz		Geologic profiling

Laser Scanning

A road breach was scanned using a Trimble CX 3D laser scanner (Figure 26). This scanning was performed to demonstrate a rapid survey method to do volumetric calculations in-situ. The scanner is built with WAVEPULSE^{TM} technology that offers efficient and highly accurate data capture over an approximate 80 m operating range. It provides clean and low noise data with 50,000 points per second data capture with a 360^{o} x 300^{o} field of view. The spatial data can be visualized in real time using a hand-held tablet. The data was post-processed and analyzed using Trimble RealWorks office software.

Figure 26. Trimble CX 3D laser scanner

Laboratory Testing

Soil Classification

Particle-size analysis tests were conducted on soil samples collected from field in accordance with ASTM D422-63 *"Standard test method for particle-size analysis of soils."* Atterberg limits tests (i.e., liquid limit—LL, plastic limit—PL, and plasticity index—PI) were performed in accordance with ASTM D4318-10 "*Standard test methods for liquid limit, plastic limit, and plasticity index of soils*" using the dry preparation method. Using the results from particle size analysis and Atterberg limits tests, the samples were classified using the unified soil classification system (USCS) in accordance with ASTM D2487-10 *"Standard practice for classification of soils for engineering purposes (Unified Soil Classification System)"* and American Association of State Highway and Transportation Officials (AASHTO) classification system in accordance with ASTM D3282-09 "*Standard practice for classification of soils and soil-aggregate mixtures for highway construction purposes."*

Moisture Content

Moisture content of samples obtained from hand augers was determined in general accordance with ASTM D4643 "*Standard Test Method for Determination of Water Moisture.*"

Statistical Data Analysis

To make statistically valid comparisons between flooded and non-flooded areas, it is important to obtain an adequate number of test measurements in each area. The minimum number of tests was determined using an approach described by Belle (2002) that is based on the coefficient of variation in the measurements and the percentage difference in the mean values in each area. The formulae to determine the minimum number of tests are:

$$n = \frac{16\,(CV \times 100)^2}{PD^2} \tag{11}$$

$$PD = \frac{\mu_0 - \mu_1}{\mu} \times 100 \tag{12}$$

$$\mu = \frac{\mu_0 + \mu_1}{2} \tag{13}$$

where, n = number of measurements required in each area; CV = coefficient of variation calculated as the ratio of standard deviation and mean; PD = percentage difference; μ_0 = mean values in non-flooded; and μ_1 = mean values in flooded areas. The number of measurements was adjusted in each test segment based on the observed CV and the percentage difference in the mean values observed during the first round of testing. Tests were repeated at the same locations during subsequent performance testing. It must be noted from Eq. (11) that as PD decreases, the number of test measurements increase. In one test segment, this resulted in a minimum number of tests > 300. Due to budget and time constraints, only a few tests (16 to 20) were conducted.

Student *t*-test analysis (Ott and Longnecker 2001) was conducted on the FWD test measurements to assess statistical significance in differences between the flooded and non-flooded areas. The t-values were determined using:

$$t = \frac{\mu_0 - \mu_1}{s_p\sqrt{\frac{1}{n_0} + \frac{1}{n_1}}} \tag{14}$$

$$s_p = \sqrt{\frac{(n_0 - 1)s_0^2 + (n_1 - 1)s_1^2}{n_0 + n_1 - 2}} \tag{15}$$

where, n0 and n1 = number of measurements obtained in non-flooded and flooded areas, respectively; sp = pooled standard deviation, and s0 and s1 = standard deviation of measurements obtained in non-flooded and flooded areas, respectively. The observed t-values were compared with the minimum t-value for a one-tailed test with degree of freedom (df) = n_0 + n_1 – 2, for 95% confidence level (i.e., $\alpha = 0.05$). If the observed t-values were greater than the minimum t-value, then it was concluded that there is sufficient evidence that the measurements in the flooded areas were different when compared to the measurements in the non-flooded areas.

DCP test results were used to compute the CBR values of the gravel and the underlying subgrade layers and were compared with FWD measurements (composite dynamic stiffness) obtained at the surface. Multivariate analysis was performed by incorporating CBR of the top 300 mm of the subgrade ($CBR_{Subgrade}$) and gravel (CBR_{Gravel}) layers into a multivariate linear regression model to predict E_{FWD}, as shown in Eq. 16:

$$E_{FWD} = b_0 + b_1 CBR_{Gravel} + b_2 CBR_{Subgrade} \quad (16)$$

where, b_0, b_1, and b_2 are regression coefficients. The statistical significance of each parameter was assessed using the p-value and t-value statistics (p-value < 0.05 and t-value > 2 are considered as statistically significant). The relative influence of subgrade and gravel layers on the surface FWD measurements were assessed using Eqs. 17 and 18:

$$Influence\ of\ Gravel\ (\%) = \frac{b_1}{b_1+b_2} \times 100 \quad (17)$$

$$Influence\ of\ Subgrade\ (\%) = \frac{b_2}{b_1+b_2} \times 100 \quad (18)$$

CHAPTER 5: EMERGENCY OPERATIONS AND REPAIR OF FLOOD-DAMAGED GEO-INFRASTRUCTURE

This chapter presents a summary of the emergency operations and repair measures taken by the Federal and State agencies in the State of Iowa, associated costs, and field damage evaluation procedures, based on the information provided by the Iowa DOT and a field reconnaissance survey conducted by the ISU research team along with Pottawattamie and Fremont County Engineers. Extensive damage occurred to levees with up to several hundred feet long breaches at seven locations along the Missouri river (see Table 1), during the flood event. Evaluation of levee damage is not part of this study, rather the focus is on roadway repair.

Reported Costs of Emergency Operations and Repair Measures

Emergency operations and repairs to damages on federal-aid routes, i.e., all primary roads and secondary roads classified as a major collector or above, have been sponsored by the Federal Highway Administration (FHWA) under the Emergency Relief (ER) program. Federal Emergency Management and Assistance (FEMA) Public Assistance (PA) program provided funding for all other routes that were not eligible for the FHWA ER program. The costs reported to conduct emergency operations and repairs to transportation infrastructure (including roads, bridges, culverts, etc.) on primary and secondary (County) roads in Iowa are summarized in Table 7. The total reported cost of flood damage to transportation infrastructure was about $63.5 million. A more detailed summary of the damages, emergency operations, and costs on different primary and secondary roads sites is provided in Appendix A. The damages occurred to geo-infrastructure and the associated repair measures taken by the State and County Engineers on primary and secondary roadways are discussed in the following sections of this report.

Table 7. Reported costs for emergency operations and repair under the FHWA ER and FEMA PA programs in Iowa

Highway System	FEMA PA Program	FHWA ER Program
Primary Roads	$149, 071	$50,708,535
Secondary Roads	$7,129,177	$5,480,670
TOTAL	**$7,278,248**	**$56,189,207**

Geo-Infrastructure Damages and Repair Measures

The Iowa DOT collected detailed damage inspection reports (DDIRs) from the DOT District Engineers and County Engineers, which described the damages and the associated costs of emergency operations and repair for the projects that were eligible under the FHWA ER program (i.e., on primary roadways and secondary roadways that are major collectors). This section presents a summary of damages, repair measures undertaken, and the associated costs reported in the DDIRs for primary and secondary roadways. Similar information was required by the FEMA PA program from the County Engineers on secondary low volume roadways. The information from the FEMA PA program was not available for our review at the time of this report.

A field reconnaissance survey of the flood affected areas was conducted by the ISU research team along with the Pottawattamie and Fremont County Engineers. The survey included documenting various damages to geo-infrastructure (i.e., paved and unpaved roadways, embankment slopes, bridges, abutments, approach embankments, ditches, culverts, etc.), and discussions with the County Engineers on the emergency measures taken to repair flood affected roadways and measures taken to evaluate damage. The information on the repair measures undertaken by the County Engineers is summarized in the following sections of this report. Cost information for those repair measures was not available.

Primary Roadways

Pictures showing the extent of damages on the primary roadways are provided in Figure 27. A summary of the various damages noted, the repair/emergency measures followed to fix the damages, and the reported costs on primary roadways are summarized in Table 8. The damages observed on primary roadway geo-infrastructure can be broadly categorized as follows:

A. Paved Roadways:
    1. Voids at shallow depths (< 150 mm (6 in)) due to erosion of underlying base material.
    2. Voids at deeper depths (> 150 mm (6 in)) due to erosion of subsurface material (some cases cracks/damage observed on pavements after spring/thaw about 6 to 8 months after flooding)
    3. Partial to complete erosion of PCC, HMA, composite pavements, and underlying base material
    4. Erosion of granular shoulders
B. Bridges:
    1. Erosion of bridge approach backfill material
    2. Erosion of embankment foreslopes
C. Culverts:
    1. Erosion of culvert backfill
    2. Separation of culverts
    3. Water outflow blockage

Repairs generally involved clearing damaged areas by removal of debris (deposited by the flood water, broken culverts, pavements, and pipes, etc.) and re-construction (replace with new material) to achieve pre-flood conditions. In some instances, flowable mortar grouting was used to fill voids beneath pavements and bridge approaches, and geosynthetics were used in bridge backfills and for drainage ditch levee foreslope erosion protection.

Field evaluation of damage was extensively based on visual survey of the locations, review of satellite imagery and Light Detection and Ranging (LiDAR) imagery by the DOT/County personnel. During the flood event, Iowa DOT and County officials used LiDAR data to evaluate which roadways and facilities were in potential danger of being flooded, which allowed for better utilization of resources and protection of infrastructure (Iowa HSEMD 2011). Iowa DOT conducted FWD and GPR testing on primary roadways after flooding, where accessible, to assess voids beneath pavements and compare conditions between flooded versus non-flooded areas.

Figure 27. Pictures taken near I-29 and I-680 intersection north of Council Bluffs on 9/21/2013

Table 8. Geo-infrastructure damages and associated repair measures followed on primary roadways

Description	Repair/emergency measures followed and reported costs
Debris, silt, and water scum deposited on pavements	• Cleaning and washing ($95 to $100 per station) • Removal of flood debris and landfill loads ($45 to $75 per ton) • Landfill loads ($60 per ton) • Removal of field fence ($3 per linear ft.) • Hazardous waste removal (lump sum prices variable) • Mobilization and traffic control
Damage to culverts (separated pipe joints, washed out culverts, eroded backfill)	• Storm sewer pipe removal (> 36 in. dia) ($15 per linear ft) • 48 in. concrete apron ($2,000 each) • 48 in. concrete culvert pipe ($200 per linear ft.) • Excavation for roadway culvert ($20 per cubic yd.) • Remove and re-install concrete pipe aprons ≤ 36 in. ($600 each) • Remove and re-install concrete pipe aprons >36 in. ($700 each) • Remove and re-install concrete pipe culvert ≤36 in. ($55 per linear ft.) • Remove and re-install concrete pipe culvert >36 in. ($105 per linear ft.) • Install 42 in. concrete pipe culvert ($400 per linear ft.) • Remove and replace concrete slope protection ($100 per sq. yd.) • Excavation of class 10 waste material ($20 per cubid yd.) • Remove and replace RF-19E subdrain outlets ($170 to $200 each)
Undermined bridge approaches, erosion of embankment foreslopes, and damaged bridge abutments	• Flowable mortar ($100 to 200 per cubic yd.) • Removal and replacement of bridge approach sections ($200 per sq. yd.) • Fixing eroded embankments ($15 to $20 per cubic yd.) • Culverts and ditch shaping near embankments ($15 per cu. yd.) • Slope reshaping ($20 per sq. yd.) • Cleaning subdrain outlets (lump sum prices variable) • Granular backfill ($11 to $20 per ton) • Class 10 excavation roadway and borrow ($10 per cubic yd.) • Class 13 excavation roadway and borrow ($20 per cubic yd.) • Class 23 excavation ($16 to $100 per cubic yd.) • Geosynthetic fabric ($3 to 5 per sq. yd.) • Class E revetment ($40 to $55 per ton) • Subdrain tile, 4 in. dia. ($12.50 per linear ft.) • Labor ($25 per hour) • Equipment mobilization and traffic control
Pavement undermining due to erosion of subbase, complete damage to PCC pavements, delaminated HMA overlays, and granular and HMA shoulder erosion	• Trap bag materials – emergency measure ($40 per linear ft.) • Rock to fill trap bags – emergency measure ($10 to $17 per ton) • Sand barrel arrays – emergency measure to prevent flooding ($2500 each) • Generators, sump pumps, detour signing, traffic control, labor, fuel, equipment for emergency measures • Trap bag removals ($3 per linear ft.) • Pavement markings ($32 per station) • Painted pavement marking ($6 per station) • Removable tape markings ($165 per station) • Painted symbols and legends ($80 per station) • Removal of pavement markings ($6 per station) • Temporary flood lighting luminaire ($5000 each) • Flowable mortar for undermined pavements ($110 to $200 per cu. yd.) • Full depth composite pavement patch ($100 per cu. Yd.) • Full depth PCC patch ($400 each) and subbase in each patch ($17 per sq. yd.) • Remove and replace HMA overlay ($15 per sq. yd)

	• Removal of pavement ($5 to $6 per sq. yd) • Removal of shoulder pavement ($6 per sq. yd) • Replace paved shoulder with 8 in. HMA ($36 to $40 per sq. yd.) • Double reinforced PCC patch ($286 per sq. yd) • 2 in. mill and overlay with HMA ($12 per sq. yd.) • 6 in. granular subbase ($6 per sq. yd.) • Replace granular shoulder ($16 to $34 per ton) • Full depth HMA patch ($75 to $150 per sq. yd.) • Remove and replace HMA pavement ($100 per sq. yd.) • Milled shoulder rumble strip, HMA with fog seal ($500 per sq. yd. or $12 per station) • Polymer geogrid for subgrade stabilization ($4 per sq. yd) • Special backfill ($34 per ton) • Excavation, class 10 waste ($15 per cu. yd.) • Cleaning subdrain outlets (lump sum prices variable) • Detour pavements ($59 per square yd.) • Reshaping ditches ($400 per station) • Pavement testing • Mobilization, traffic control, temporary traffic cushion
Erosion of drainage ditch levees (within DOT right-of-way)	• Excavation of class 10 roadway and borrow ($5 per cubic yd.) • Excavation of class 10 waste ($17 per cubic yd.) • Excavation of class 13 channel ($20 per cubic yd.) • Topsoil, furnish, and spread ($20 to $40 per cubic yd.) • Reshaping ditches ($210 to $370 per station) • Granular backfill ($25 per cubic yd.) • Aprons with 24 in. diameter ($500 each) • Aprons with 30 in. diameter ($1000 each) • 24 in. diameter culvert pipe ($40 per linear ft.) • 30 in. diameter culvert pipe ($80 per linear ft.) • Outlet control gates ($1000 to $3000 each) • Geosynthetic fabric ($5 to $20 per sq. yd.) • Class E revetment ($56 to $60 per ton) • Silt fence ($3 to $10 per linear ft.) • Floating silt curtain ($38 per linear ft.) • Mobilization and traffic control
Cracks on PCC pavements and subsidence during freeze thaw in 2012	• Full depth patching in isolated areas ($100 per sq. yd) • Mobilization and traffic control

Secondary Roadways

Prior to and after the field reconnaissance, the ISU research team conducted an extensive review of aerial imagery available from Google Earth. Aerial infrared imagery showing extent of floods in Woodbury to Fremont Counties in western Iowa are provided in Figure 28 to Figure 34. In addition, GIS maps showing the extent of flood waters were provided by the Pottawattamie County Engineer (see Figure 37 and Figure 38; see Appendix B for maps at different times). These maps were reportedly developed based on field water level measurements and observations multiple times during the flood event. The aerial imagery and the GIS maps from Pottawattamie County were used to find key test site locations, features along each test site (i.e., flooded area versus non-flooded area, pre-flood ponded areas), and the duration of flooding in each test site. GIS maps were not available in Fremont County, therefore, the exact duration of

flood event could not be determined. Fremont County maintained a FEMA site map, showing project locations that were funded under the FEMA PA program (Figure 39). The test sites in Fremont County were selected based on visits to various sites, type of damage observed, and site access. More detailed discussion on the test sections is provided in the next chapter of this report.

A summary of the various damages noted, the repair/emergency measures followed to fix the damages, and the reported costs are summarized in Table 9. Pictures showing the extent of damages on secondary roadways in Pottawattamie and Fremont Counties are provided in Figure 40 to Figure 54. The damages observed on secondary roadway geo-infrastructure can be broadly categorized as follows:

A. Paved Roadways:
    1. Voids at shallow depths (< 150 mm (6 in.)) due to erosion of underlying base material.
    2. Voids at deeper depths (> 150 mm (6 in.)) due to erosion of subsurface material.
    3. Partial to complete erosion of PCC and HMA pavements, and underlying base material.
    4. Erosion of granular shoulders.
B. Bridges:
    1. Erosion of bridge approach backfill material.
    2. Erosion of embankment foreslopes.
C. Culverts:
    1. Erosion of culvert backfill
    2. Separation of culverts
    3. Water outflow blockage
D. Unpaved Roadways:
    1. Erosion of gravel surface.
    2. Rutting under traffic loading (on gravel roads and other detoured roadways due to excessive loading, although not flooded).
    3. Full breach of roadway embankments.

Similar to repair on primary roadways, repairs on secondary roadways also generally involved clearing damaged areas by removal of debris and re-construction by replacing damaged areas with new material to achieve targeted pre-flood condition. In some instances, flowable mortar grouting was used to fill voids beneath pavements, and emulsified-oil (bitumen) stabilization was used to stabilize the gravel layer (for damage D2). Field evaluation of damage was primarily based on visual inspection. A push T-bar (see Figure 47) was used in some cases to detect weep holes under gravel roads during the visual inspection.

Of the areas that were surveyed during the field visits, two areas posed significant safety concerns to traffic due to damage that was not apparent at the surface (i.e., due to damage that occurred beneath the surface). One of those areas resulted in deep potholes on a gravel road due to eroded backfill around a culvert In Pottawattamie County (see Figure 46) and the other resulted in deep voids beneath roadway due to eroded backfill around a bridge abutment in Fremont County (see Figure 54). Such areas can go undetected with just visual surveys at the surface and pose a significant risk to traffic.

Table 9. Geo-infrastructure damages and associated repair measures followed on secondary roadways

Description	Repair measures followed
Debris, silt, and water scum deposited on roadways	• Cleaning and washing (on paved roadways) • Clearing and grading (on unpaved roadways) • Filling washed out areas, removing silt and debris, and providing temporary access roads for residents ($200,000 per mile) • Labor ($22 per hour + fringe) • Overtime labor ($32 per hour + fringe) • Equipment ($35 per hour) • Hazardous waste removal
Damage to Culverts (separated pipe joints, washed out culverts, eroded backfill)	• Removal and replacement of culverts • Replacement of backfill materials
Erosion of bridge abutment backfill	• Replaced backfill material • Other measures not reported
Damaged double seal coat (stripping)	• Replace with double seal coat ($4 per sq. yd.) [cost includes materials, labor, and equipment)
Gravel shoulder erosion	• Replace granular shoulders, type B ($10 per ton)
Destroyed PCC pavements, double seal coat pavements, and underlying foundation layers	• Construction of new pavements including surface and base course layers, labor, and equipment ($190,000 to $250,000 per mile)
Eroded gravel surfacing and undermining (with weep holes)	• Labor ($21 per hour + fringe) • Overtime labor ($32 per hour + fringe) • Equipment ($40 per hour) • Replace with new gravel surfacing (lumpsum values reported: approximately $11,300 per mile for clearing debris and installing gravel surfacing) • Areas with weep holes were excavated and replaced with new gravel.
Full breach of roadway embankment	• Reconstruction of the embankment with new fill (sand/silt deposited from flood waters were used in some locations to fill the breach)
Stripping of single chipseal coat over stabilized base	• No repair performed or reported at the time of this report.
Undermined and failed HMA pavement due to base layer erosion	• Replaced with 2½ to 3 in. of HMA ($120 per ton)
Undermined PCC pavement due to base layer erosion (about 200 ft of PCC washed away)	• Pumping flowable grout in undermined areas and replaced with new PCC pavement over a 200 ft length where the pavement was completely damaged ($43,000 lumpsum)
Damaged pavements (wheel track rutting and stress cracking) due to excessive construction traffic on detoured roads (non-flooded areas)	• Milling exising surface ($1.8 per sq. yd.) • 2 in. HMA overlay ($32 per ton) • Asphalt binder at 6% ($504 per ton) • 6 in. base stabilization wit • h seal coat ($140,000 per mile) • Labor ($24 per hour) • 6 in. base stabilization with seal coat ($140,000 per mile) • Equipment and mobilization

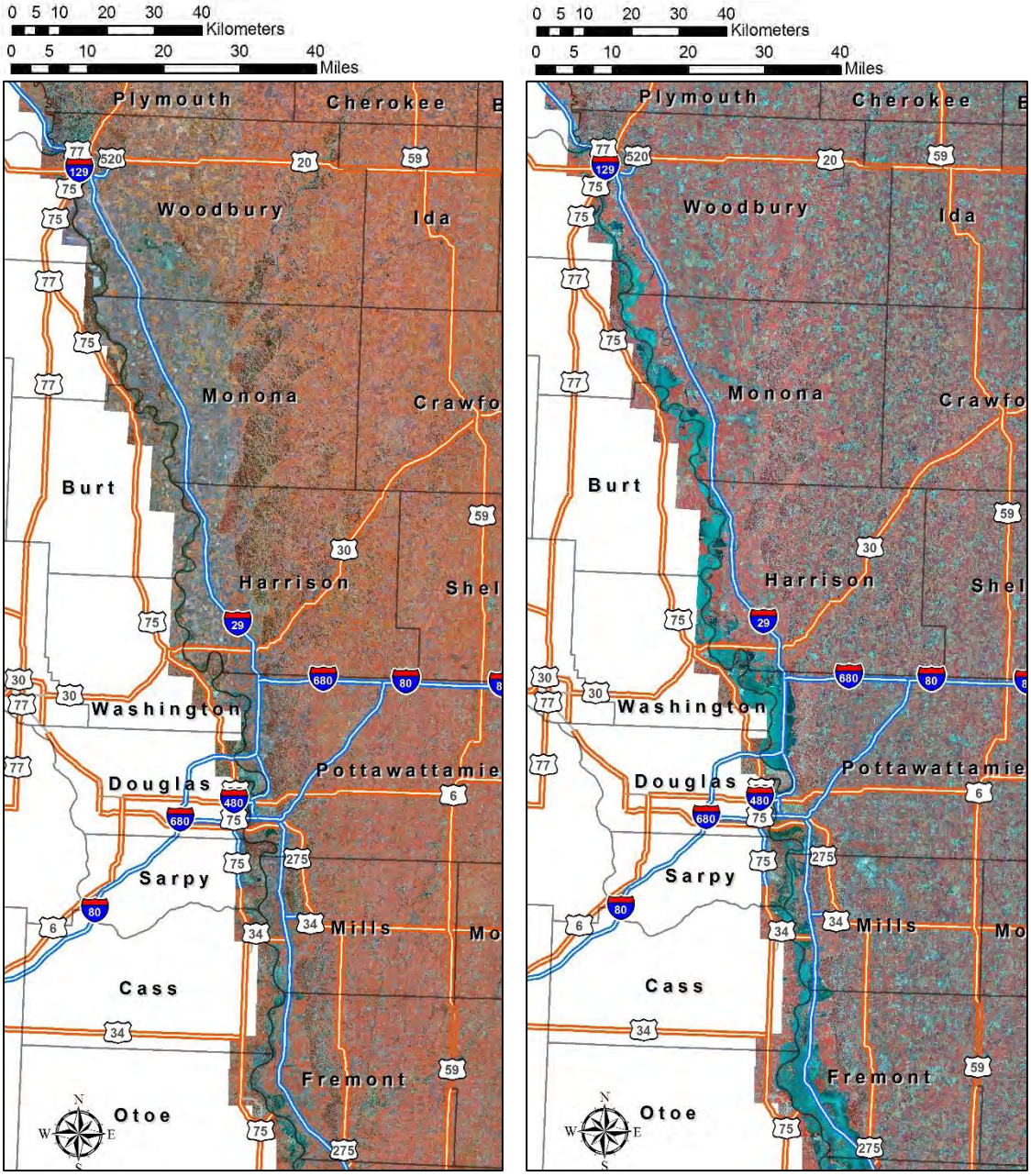

Figure 28. Aerial infrared imagery showing extent of Missouri River in Summer 2010 (left) and Summer 2011 (right) in western Iowa

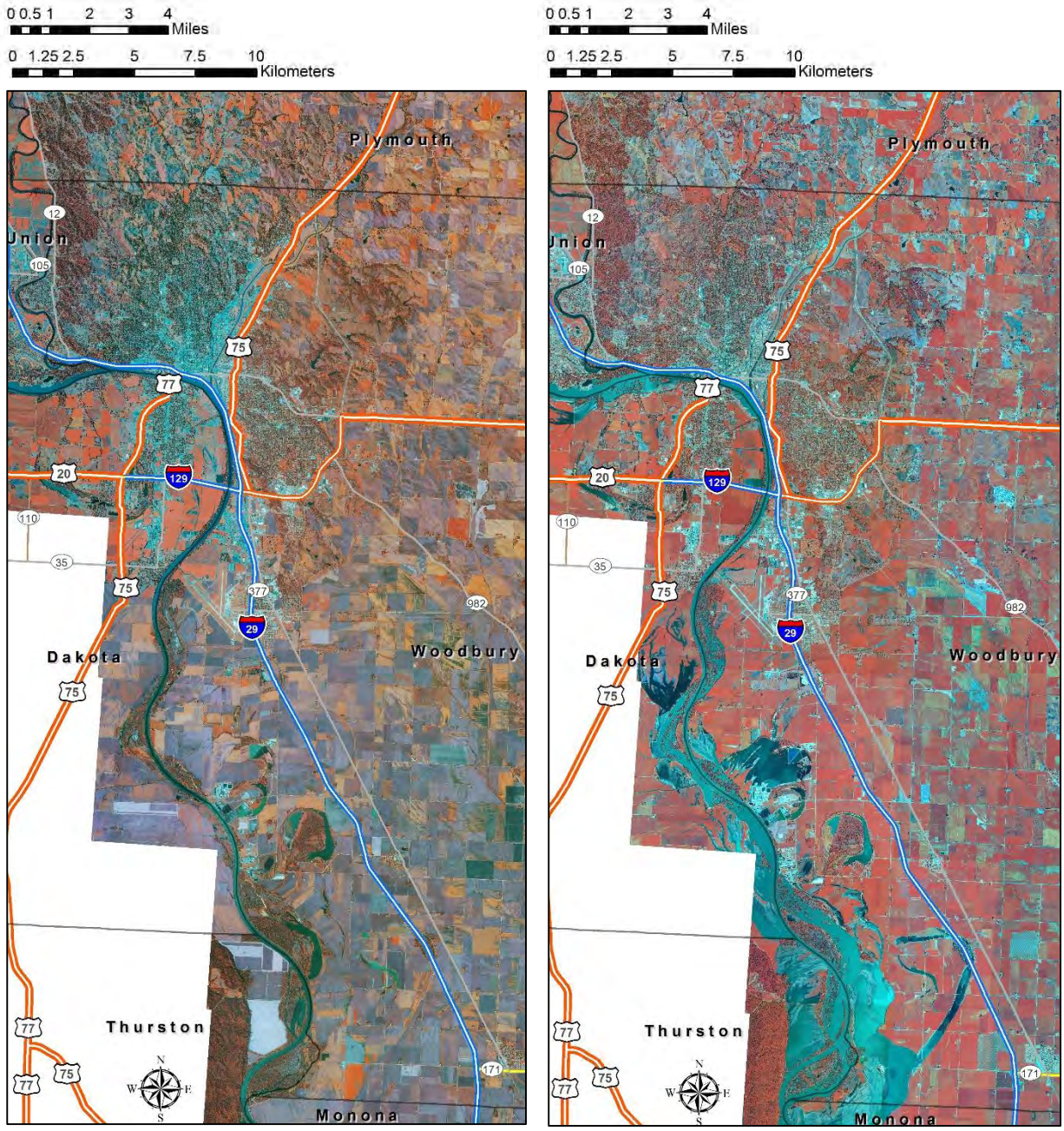

Figure 29. Aerial infrared imagery showing extent of Missouri River in Summer 2010 (left) and Summer 2011 (right) in Woodbury County

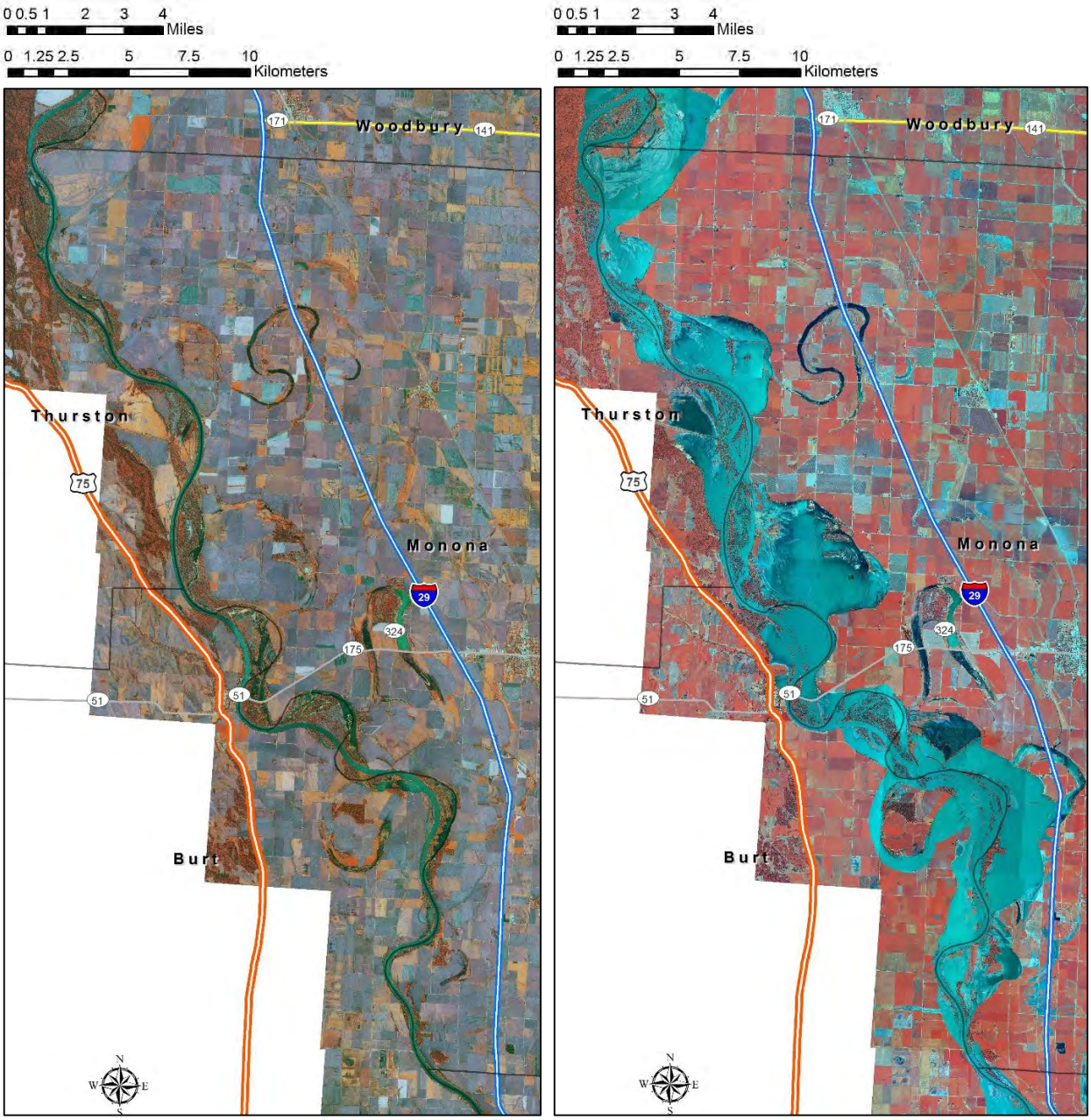

Figure 30. Aerial infrared imagery showing extent of Missouri River in Summer 2010 (left) and Summer 2011 (right) in Monona County

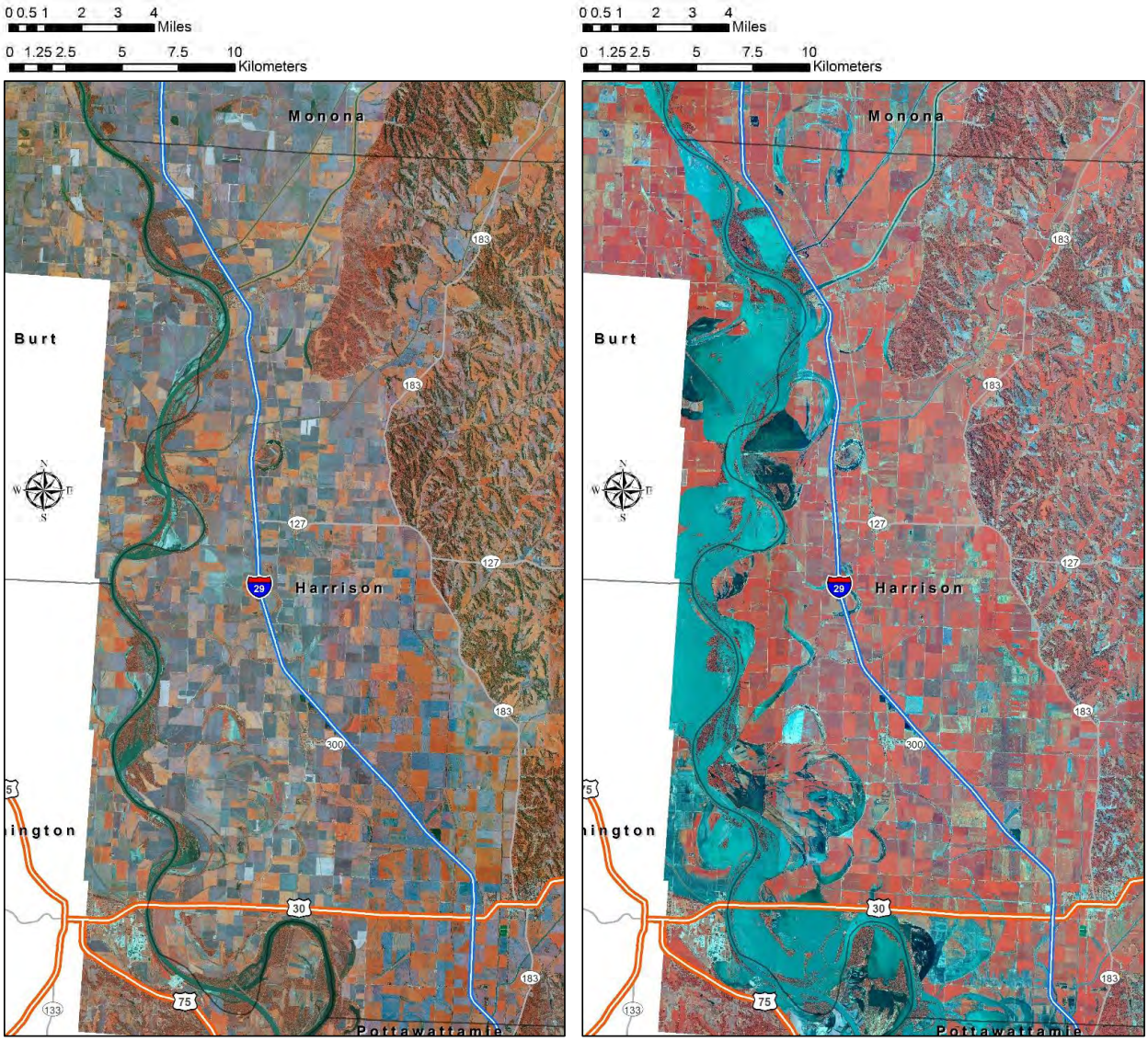

Figure 31. Aerial infrared imagery showing extent of Missouri River in Summer 2010 (left) and Summer 2011 (right) in Harrison County

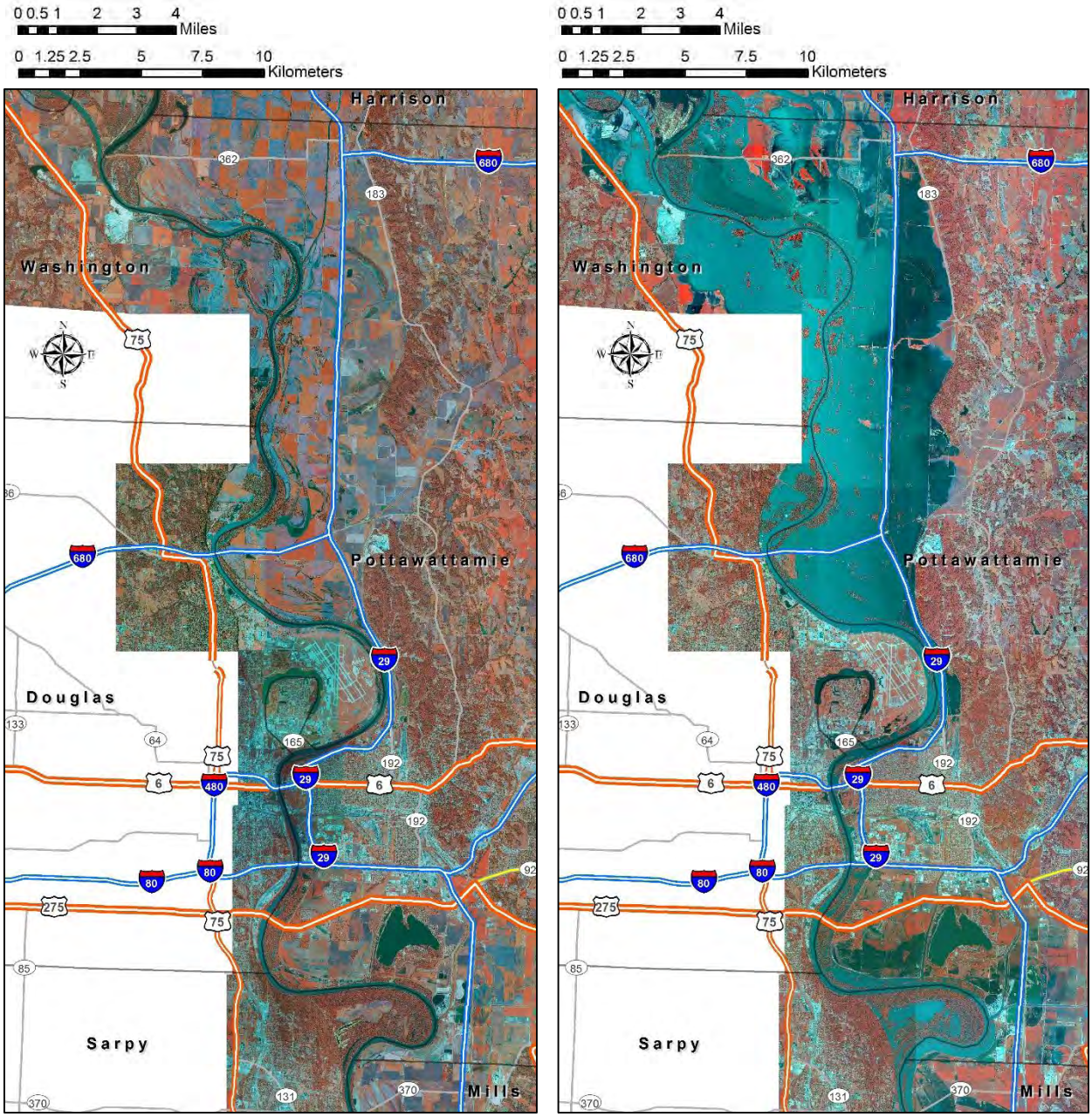

Figure 32. Aerial infrared imagery showing extent of Missouri River in Summer 2010 (left) and Summer 2011 (right) in Pottawattamie County

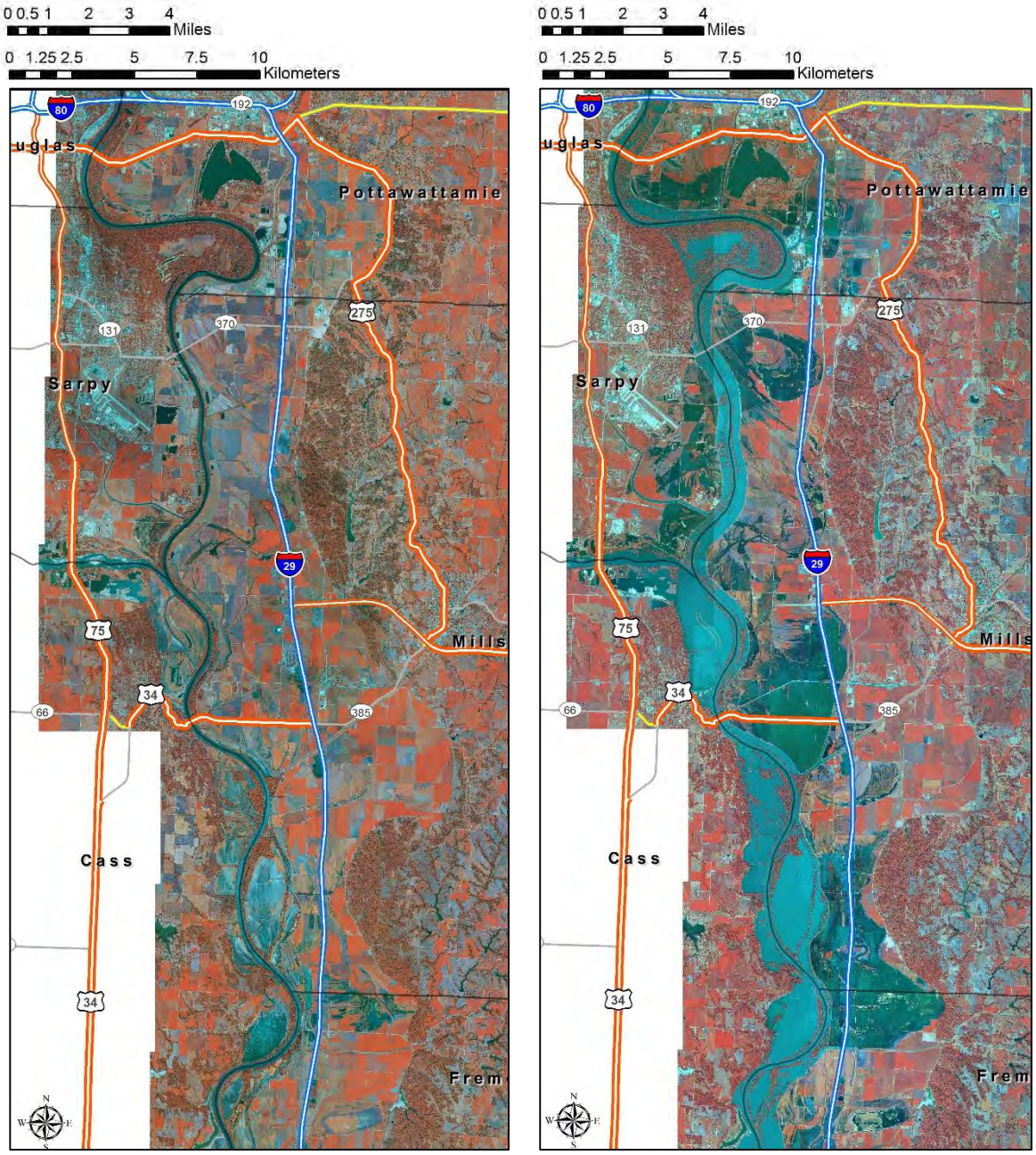

Figure 33. Aerial infrared imagery showing extent of Missouri River in Summer 2010 (left) and Summer 2011 (right) in Mills County

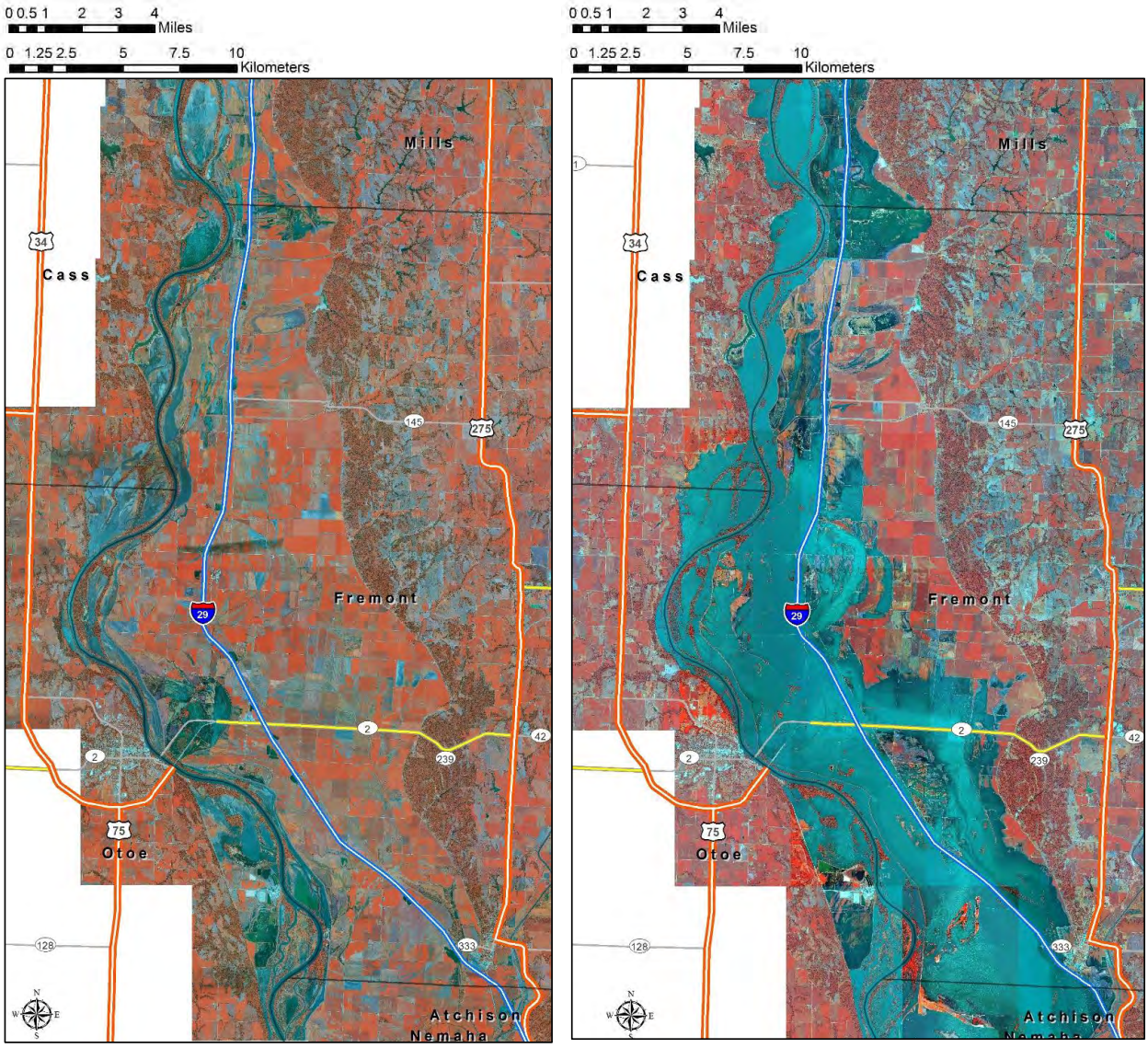

Figure 34. Aerial infrared imagery showing extent of Missouri River in Summer 2010 (left) and Summer 2011 (right) in Fremont County

Figure 35. Levee breach in north part of Fremont County (images updated on 6/9/10 and 8/11/11)

Figure 36. Levee breach in southern part of Fremont County (images updated on 6/9/10, 7/17/11, and 8/11/11)

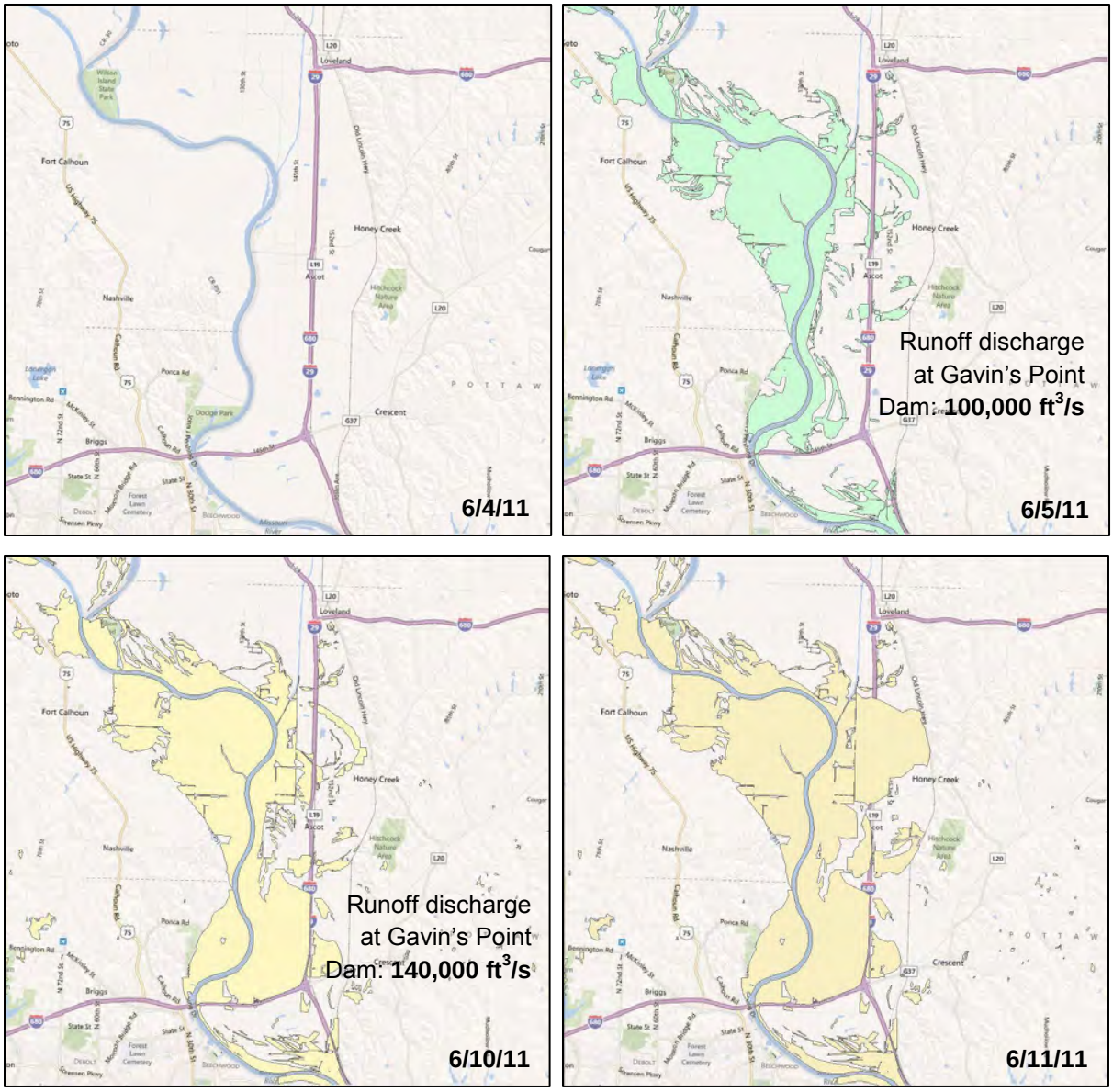

Figure 37. Flood water coverage maps north of Council Bluffs from 6/4/11 to 6/11/11 – Pottawattamie County

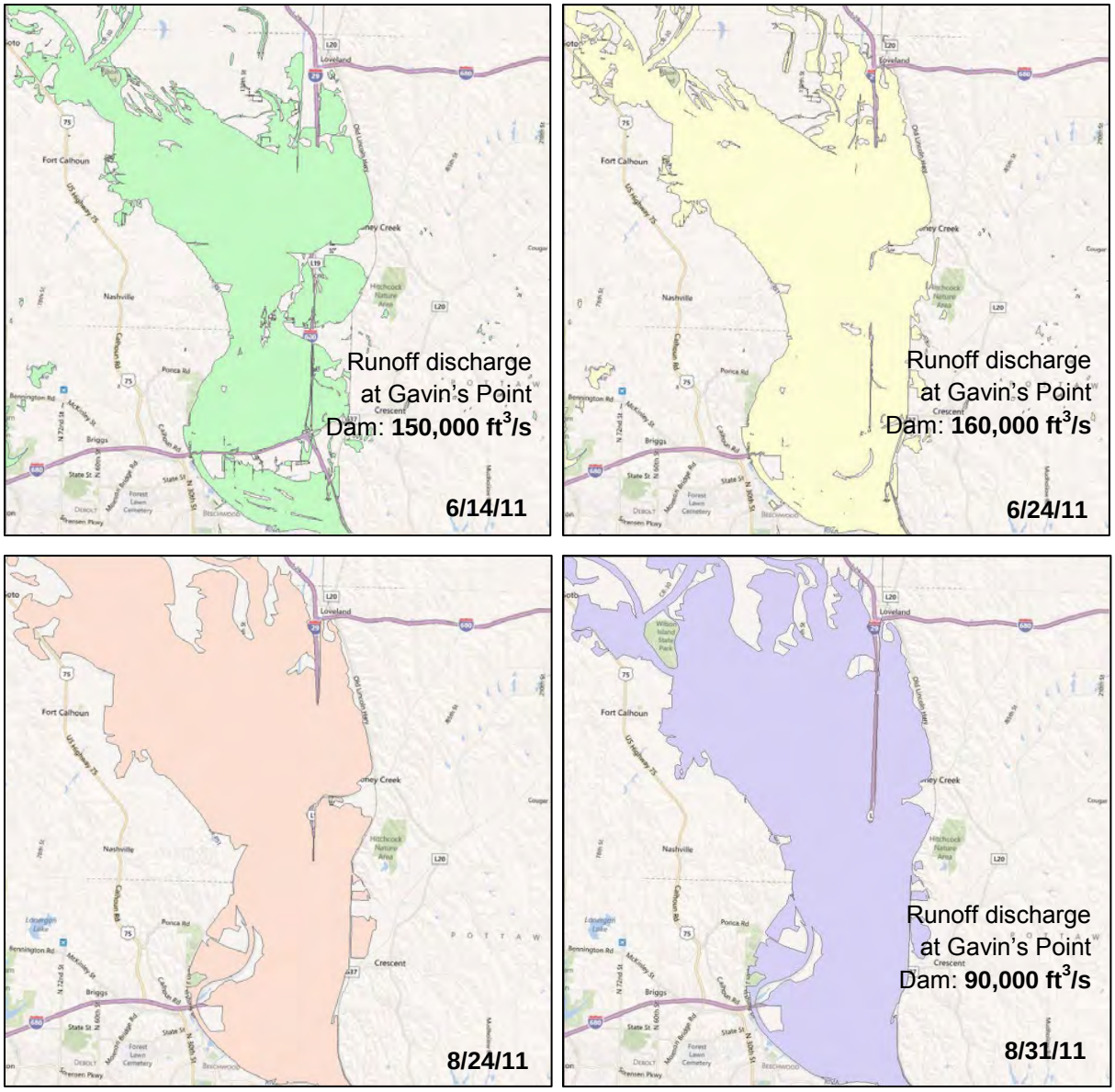

Figure 38. Flood water coverage maps north of Council Bluffs from 6/14/11 to 8/31/11 – Pottawattamie County

Figure 39. Fremont county map with flood affected areas showing sites funded by FEMA for damage repair

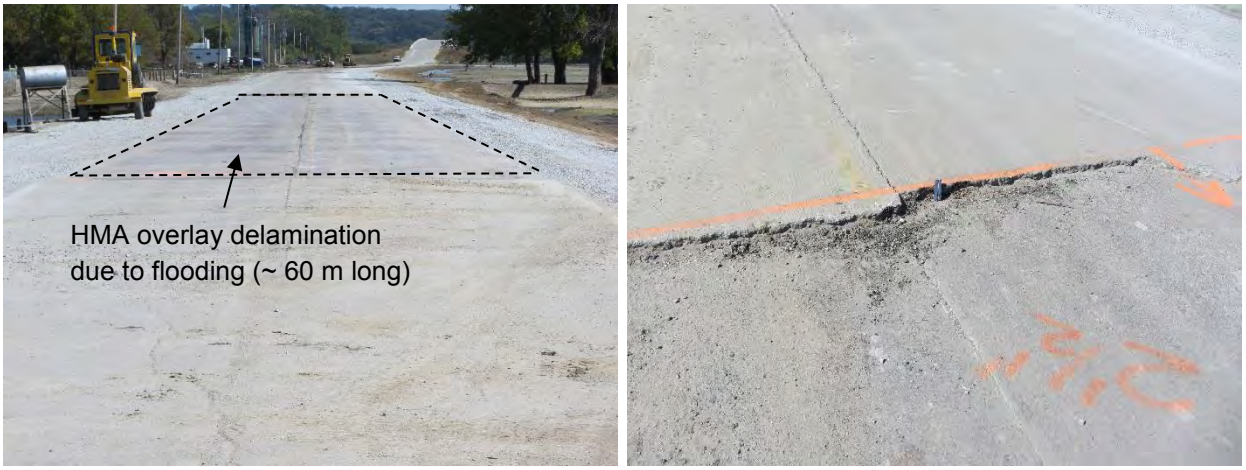

Figure 40. Delaminated HMA overlay over PCC pavement and eroded shoulders refilled with crushed limestone – Old Mormon Road (looking east), Pottawatamie County (Photos taken on 9/21/11)

Figure 41. Eroded shoulder next to PCC pavement being reconstructed on 9/21/11 – Old Mormon Road (looking west towards I-680 and I-29 intersection), Pottawatamie County (Photos taken on 9/21/11)

Figure 42. Water overtopping a thin chipseal coat surfaced road underlain by oil stabilized granular base on 9/21/11 showing delamination of chipseal and rolled asphalt at the surface – Desoto Avenue, Pottawattamie County (Photos taken on 9/21/11)

Figure 43. Clogged culvert inlets due to scouring and erosion of embankment material beneath chipseal coat surfaced road on 9/21/11 – Desoto Avenue, Pottawatamie County (Photos taken on 9/21/11)

Figure 44. Scouring and erosion of bridge backfill material around a timber abutment supporting a concrete bridge deck – Pottawatamie County (Photos taken on 9/21/11)

Figure 45. Full breach of about 150 m (500 ft) long unsurfaced access road – Pottawatamie County (Photo taken on 9/21/11)

Figure 46. Potholes (with about 0.5 m (1.5 ft) diameter) under gravel road due to erosion of backfill material around a culvert located beneath the road – Pottawatamie County (Photos taken on 9/21/11 and 9/23/11)

Figure 47. Weep holes detected under a gravel road – Meadowlark Loop Road, Pottawatamie County (Photos taken on 9/22/11)

Figure 48. Rutting along right wheel path on chipseal surfaced gravel road and erosion of granular shoulder during flooding – 220th Street, Fremont County (Photo taken 10/26/11)

Figure 49. Erosion of shoulder and roadbed on a chip seal surfaced gravel road – Fremont County (Photo taken on 10/26/11)

Figure 50. Delaminated or stripped chipseal surfacing – Fremont County (Photo taken on 10/26/11)

Figure 51. Full breach of a gravel road (about 100 m (330 ft) long) – Fremont County (Photo taken on 10/26/11)

Figure 52. Gravel road segments washed away during floods – Fremont County (Photo taken on 10/26/11)

Figure 53. Reconstruction of a gravel road washed away during floods and deposited with silt and sand– Fremont County (Photo taken on 10/26/11)

Figure 54. Erosion of backfill material around timber back wall supporting a timber bridge crossing a creek – Fremont County (Photos taken on 10/26/11)

CHAPTER 6: FIELD EVALUATION OF GEO-INFRASTRUCTURE ON SECONDARY ROADWAYS

The ISU research team visited various sites in Pottawattamie and Fremont Counties in Western Iowa to conduct in situ testing shortly after the flood waters receded (in September and October 2011), and several months after flooding (in April, May, and June 2012) to evaluate performance. Road test segments were selected with an objective to monitor performance of the flooded versus non-flooded areas by evaluating their subsurface foundation layer characteristics over time. Testing was conducted on about 24 km (18.6 miles) of roadway. In situ testing involved conducting FWD and DCP testing in all test segments, obtaining hand auger soil samples in selected areas, and conducting GPR scans in selected areas. The test segments varied in length from about 150 m (500 ft) to 7.0 km (4.3 miles), by flood condition (fully or partially flooded), and type of surfacing (gravel, chip seal surface over emulsified oil stabilized gravel base or untreated gravel base, PCC, and HMA).

In situ test results and field observations from each test segment (TS) are presented in this chapter. Based on the test results, the relative quality of the subgrade was evaluated using subgrade modulus (E_{SG}) values determined from FWD tests and DCP-CBR measurements (per AASHTO 1993), using the rating system described earlier in Table 3 (per AASHTO 1993). The seasonal variation in the subgrade modulus was considered in evaluating the relative quality rating. Based on temperature profile results obtained from a Iowa DOT monitoring station in Sioux City, Iowa (Appendix C), it was determined that September to November 2011 was fall (wet), December to March 2012 was winter (freeze) and spring (thaw), and April to August 2012 was summer (dry). Therefore, results obtained in September and October 2011 were compared with fall (wet) conditions ratings, and results obtained in April and June 2012 were compared with summery (dry) condition ratings.

Pottawattamie County

Field testing in Pottawattamie County was conducted on seven test segments: Old Mormon Road, 110th Street, Desoto Avenue West and East, 140th Street, 145th Street, and River Road North. These test segments varied in length from about 150 m (500 ft) to 6.05 km (3.75 miles), by flood condition (fully or partially flooded), and type of surfacing (gravel, chip seal coat over emulsified oil stabilized gravel base, PCC, and HMA). A summary of all test segments with tests conducted, field notes, and subgrade soil information (from Pottawattamie County USDA Soil Survey Report) is provided in Table 10. Locations of the test segments are shown in Figure 55.

FWD tests were conducted at 20 to 40 locations, while DCP testing was conducted at 1 to 2 selected test locations in each test segment. GPR scans were performed on a PCC roadway (TS2) where flowable concrete grout was used to fill voids beneath pavement, gravel road (TS3) where only a portion of the test segment was flooded, and chipseal coat surfaced emulsified stabilized base section (TS7) where portions of the chipseal was stripped off and weep holes were observed during flooding beneath the surface. Detailed results from each test segment along with aerial imagery showing the extent of flood water are presented in the following subsections of this report.

Table 10. Summary of field test segments — Pottawattamie County

TS	Date	In Situ Tests	Comments
TS1	Old Mormon Road — Hot Mix Asphalt [about 750 m from the west bridge joint]		
	9/21/2011	20 FWD tests 2 DCP tests	Segment was partially submerged for about two months during flooding. No structural failures were observed on the pavement. Shoulder was scoured at isolated locations. The natural subgrade soils consisted of silty alluvium material in the top 600 mm of the subgrade and are classified as A-4, A-6, and A-7 or CL, CL-ML, and CH soils. The saturated hydraulic conductivity of the material vary from about 1 to 9 μm/s.
	4/5/2012	20 FWD tests	
	6/19/2012	20 FWD tests 2 DCP tests	
TS2	Old Mormon Road — Concrete [about 160 m from the utility pole labeled BG-03 east of I-29/I-680 interchange]		
	9/21/2011	24 FWD tests 1 DCP test	Segment was completely submerged for about two months during flooding. The roadway base layer and gravel shoulder were eroded along the south side. Cement grout was pumped (on 9/20/11) into the base layer to fill voids under the pavement. Longitudinal cracking was observed on some concrete slabs with eroded base material. 12 FWD tests were taken at the center of slab and 12 FWD tests were taken at the joints to measure load transfer efficiency and detect voids. A portion of the test segment consisted of a newly replaced PCC pavement. The natural subgrade soils consisted of silty alluvium material in the top 600 mm of the subgrade and are classified as A-4 and A-6 or CL-ML and CL soils. The saturated hydraulic conductivity of the material is about 9 μm/s.
	4/5/2012	24 FWD tests	
	6/19/2012	24 FWD tests 1 DCP test 1 GPR scan	
TS3	110th St. — Gravel [about 590 m from the corner post south of a residential drive way nearest to Desoto Ave.]		
	9/22/2011	25 FWD tests 4 DCP tests 1 soil profile	Segment was partially submerged for about two months during flooding. Some gravel was washed away in the area that was under water and the County maintenance crew replaced it with about 50 mm (2 in) thick gravel layer shortly after the flood water receded (before 9/22/11). The natural subgrade soils consisted of silty alluvium material in the top 600 mm of the subgrade and are classified as A-4 and A-6 or CL-ML and CL soils. The saturated hydraulic conductivity of the material is about 9 μm/s.
	10/25/2011	25 FWD tests 2 DCP tests	
	4/5/2012	25 FWD tests 2 DCP tests	
	5/29/2012	25 FWD tests 4 DCP tests	
	6/19/2012	1 GPR scan	
TS4	Desoto Ave. and 140th St. — Emulsified oil stabilized base surfaced with chip seal coat [about 5215 m from the utility pole east of 110th St./Desoto Ave. intersection]		
	9/23/2011	40 FWD tests 4 DCP tests	Segment was partially submerged under water for about two months during flooding. Chipseal coat was delaminated at several locations that were submerged. The material was peeled and washed away or rolled-up on the roadway. Shoulder material was eroded at high water locations. Rutting and settlement was observed north of 140th St. and
	10/25/2011	40 FWD tests	
	4/5/2012	40 FWD tests	

	5/29/2012	40 FWD tests 4 DCP tests	Desoto Ave. intersection in the NB lane. The natural subgrade soils consisted of silty to clayey alluvium material in the top 600 mm of the subgrade and are classified as A-4, A-6, and A-7 or CL-ML, CL, and CH soils. The saturated hydraulic conductivity of the material vary from about 0.04 to 9 μm/s.
TS5	145th St. — Gravel [about 6050 m from the 90 degree curve north of 130th St. and I-680 overpass]		
	9/23/2011	29 FWD tests 2 DCP tests 1 Hand auger	Segment was fully submerged for about one to three months. Roadway was graded to remove silt and flood debris prior to 9/23/11. Road surface collapses were observed due to erosion of backfill material at Sta. 10+62 m. Weep holes were observed at the culvert inlets on 10/25/11. Laser scan performed on an access road connecting to 145th St. that was breached. The natural subgrade soils consisted of silty to clayey to sandy alluvium material in the top 600 mm of the subgrade and are classified as A-4, A-6, A-7, and A-2-4 or CL-ML, CL, CH, SM, and SP soils. The saturated hydraulic conductivity of the material vary from about 0.04 to 189 μm/s.
	10/25/2011	29 FWD tests 1 DCP test	
	4/5/2012	29 FWD tests 1 DCP test	
	5/29/2012	29 FWD tests 2 DCP tests 1 Laser scan	
TS6	River Road North — Gravel [about 5170 m from the utility pole east of 130th St/River Road N intersection]		
	9/23/2011	16 FWD tests 1 DCP tests	Segment was fully submerged for about one to three months. Rutting was occurring at isolated locations during 9/23/11 testing. Weep holes were observed at culvert inlets during 10/25/11 testing. The natural subgrade soils consisted of silty to clayey alluvium material in the top 600 mm of the subgrade and are classified as A-4, A-6, and A-7 or CL-ML, CL, and CH soils. The saturated hydraulic conductivity of the material vary from about 0.04 to 9 μm/s.
	10/25/2011	20 FWD tests	
	4/5/2012	20 FWD tests 1 DCP test	
	5/29/2012	20 FWD tests 1 DCP test	
TS7	Desoto Ave. (West) — Emulsified oil stabilized base surfaced with chip seal coat [about 1629 m from Desoto National Wildlife Refuge monument east to 110th St.]		
	10/25/2011 4/5/2012	22 FWD tests 22 FWD tests	Segment was fully submerged for about one to three months. Chip seal was washed away during floods at many isolated locations. GPR scans performed in areas with surface stripping, culverts, and weep holes. The natural subgrade soils consisted of silty to clayey to sandy alluvium material in the top 600 mm of the subgrade and are classified as A-4, A-6, A-7, and A-2-4 or CL-ML, CL, SM, and SP soils. The saturated hydraulic conductivity of the material vary from about 0.04 to 9 μm/s.
	5/29/2012	22 FWD tests	
	6/19/2012	3 GPR scans	

NOTE: The soil classification information and saturated hydraulic conductivity values are obtained from the Pottawattamie County Soil Survey Information (USDA 1985).

Figure 55. Locations of test sections – Pottawattamie County (Image updated on 6/28/2010)

TS1 – Old Mormon Bridge Road (HMA)

TS1 is a HMA pavement segment located on Old Mormon Bridge Road just west of the bridge over Pigeon Creek, north of Council Bluffs, Iowa. Testing was conducted over a length of about 750 m on the west bound lane. The segment consisted of about 360 mm (14 in.) thick HMA layer underlain by about 300 mm (12 in.) thick base and subgrade (note: depths determined from DCP test results at two locations along the test segment). The Pottawattamie County soil survey report indicates that the natural subgrade soils in this region consist of silty alluvium material in the top 600 mm of the subgrade and are classified as A-4, A-6, and A-7 or CL, CL-ML, and CH soils. According to the soil survey report, these soils exhibit moderately high drainability with saturated hydraulic conductivity varying from about 1 to 9 μm/s (0.3 to 2.6 ft/day).

During the 2011 flood event, the test segment was partially submerged for about two months (Figure 56). Reportedly, the flood waters receded in the area on 9/1/11. No structural failures

were observed on the pavement, but the granular shoulder was scoured at a few isolated locations. In situ testing was conducted on this test segment in flooded and non-flooded areas for comparison, about 20 days after the flood waters receded (9/21/11) and after about 6 and 9 months (on 4/5/12 and 6/19/12). FWD tests were conducted at 20 locations (8 in non-flooded area and 12 in flooded area) (Figure 57) and DCP tests were conducted at 2 locations (1 each in flooded and non-flooded areas).

E_{FWD} and E_{SG} results from three different testing times along the test segment are shown in Figure 58, identifying the flooded and non-flooded zones. The E_{SG} values were calculated based on deflections from the sensor located at 914 mm (36 in.) away from the center of the loading plate. DCP-CBR profiles at the two test locations from two different testing times are shown in Figure 59. Box plots of E_{SG} values comparing measurements in the flooded and non-flooded areas at different test times are shown in Figure 60. In the box plots, the box boundary closest to zero indicates the 25th percentile; solid line within the box indicate median, and box boundary farthest from zero indicates the 75th percentile. Error bars above and below box indicate the 90th and 10th percentiles. Points beyond the error bards indicate the 95th and 5th percentiles. Some key findings from this test segment are as follows:

- E_{FWD} and E_{SG} values were on average about 1.3 to 1.4 times higher in the non-flooded zone than in the flooded zone, at all times of testing. FWD results obtained about 6 months after flooding were on average higher in the non-flooded zone and the results obtained about 9 months after flooding were on average similar in both flooded and non-flooded zones, when compared to the results obtained shortly after flooding.
- When compared to the relative subgrade quality ratings per AASHTO (1993), results indicated that the subgrade in the flooded zone was mostly of "fair" to "good" quality, while the subgrade in the non-flooded zone was mostly of "good" to "very good" quality.
- The CBR of the base layer was about the same in both flooded and non-flooded zones (>50), but the CBR of subgrade (at depths below 650 mm) was on average about 10 times higher in the non-flooded zone than in the flooded zone (Figure 61). No significant difference was noted in the measurements obtained shortly after flooding and about 9 months after flooding.
- CBR values obtained shortly after flooding indicated that the subgrade in both the flooded and the non-flooded zones were of "very good" quality, per AASHTO (1993) relative quality ratings.
- No structural failures were observed on the pavement, despite some minor granular shoulder erosion in areas close to the high water line.

Figure 56. Aerial imagery showing pre-flood (left from 6/28/10) and during flood (right from 7/17/11) conditions on TS1 – Pottawattamie County

Figure 57. FWD testing on HMA pavement on TS1 (Photo taken on 9/21/11) – Pottawattamie County

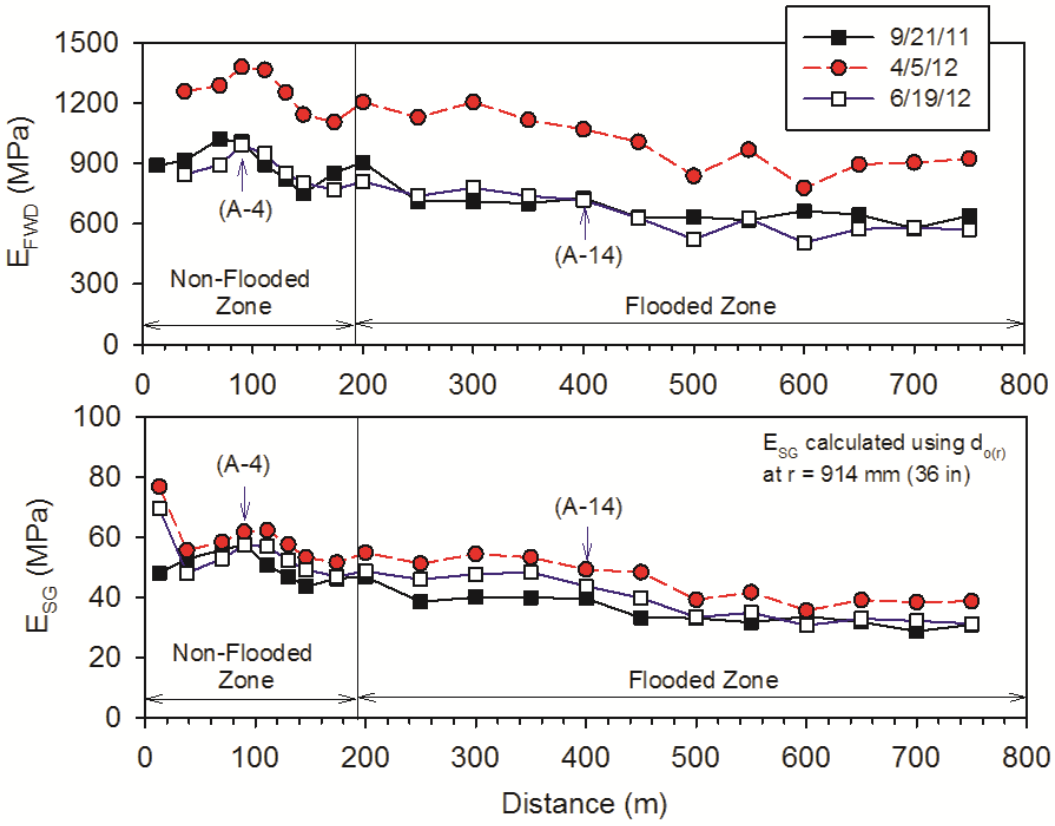

Figure 58. Surface modulus and subgrade E_{SG} at three different times after flooding on TS1 – Pottawattamie County

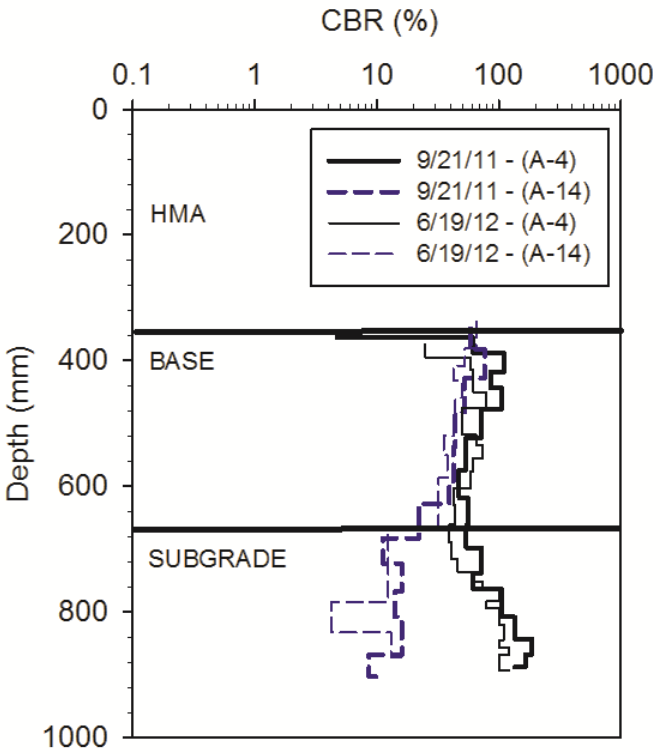

Figure 59. DCP-CBR profiles at two test locations at two different times after flooding on TS1 – Pottawattamie County

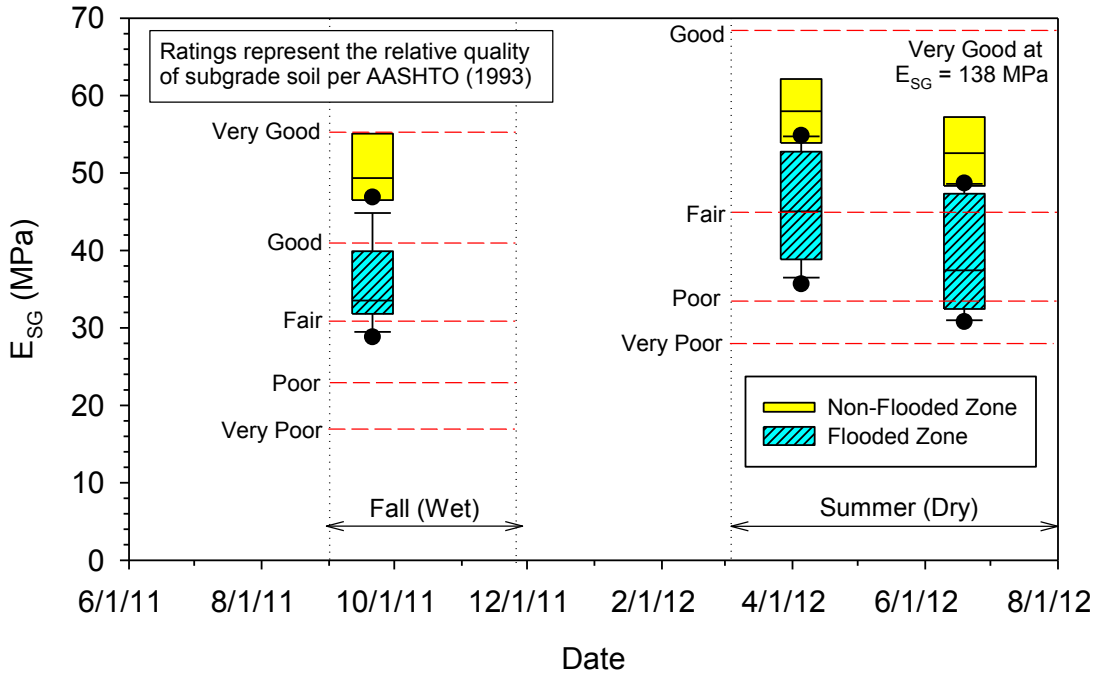

Figure 60. Box plots of subgrade modulus values in flooded and non-flooded zones in comparison with relative quality ratings on TS1 – Pottawattamie County

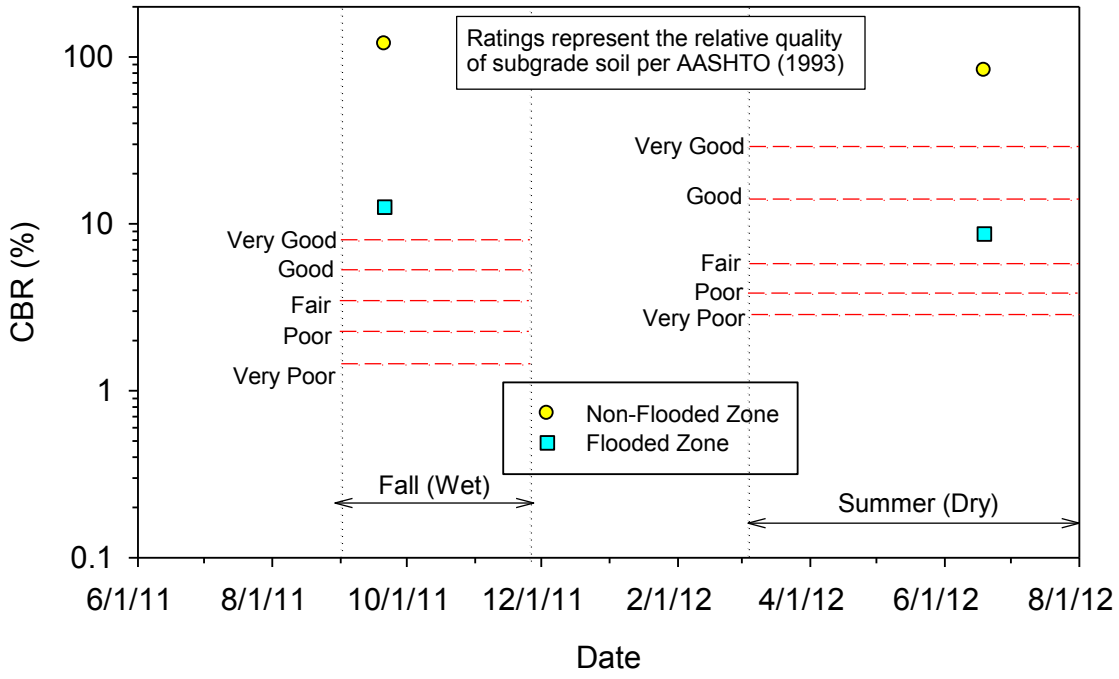

Figure 61. Comparison of subgrade CBR values in flooded and non-flooded zones with relative quality ratings on TS1 – Pottawattamie County

TS2 – Old Mormon Bridge Road (PCC)

TS2 is a PCC pavement segment located on Old Mormon Bridge Road just east of the I-29 and I-680 interchange, north of Council Bluffs, Iowa. Testing was conducted over a length of about 160 m on the east bound lane. The segment originally (before flooding) consisted of about 250 mm (9.8 in.) thick PCC layer underlain by about 150 mm (6 in.) thick subbase and natural subgrade. The Pottawattamie County soil survey report indicates that the natural subgrade soils in this region consist of silty alluvium material in the top 600 mm of the subgrade and are classified as A-4 and A-6 or CL and CL-ML soils. According to the soil survey report, these soils exhibit moderately high drainability with saturated hydraulic conductivity of about 9 μm/s (2.6 ft/day).

During the 2011 flood event, the test segment was fully submerged for about two months (Figure 62). Reportedly, the flood waters receded in the area on 9/1/11. The TS reportedly experienced heavy water currents as the water levels fluctuated during the flood event. The granular shoulders were completely eroded, a portion of the pavement was washed away, and subbase layer under the pavement was eroded in a portion of the TS (Figure 63). The section where the pavement was washed away was replaced with a new 230 mm (9 in.) thick PCC pavement placed directly over the subgrade. Flowable cement grout was used to fill the voids formed due to subbase layer erosion. Pictures taken two days after cement grout was placed are shown in Figure 63. The grout was very soft and did not setup even two days after placement. Field engineers indicated that there could have been water beneath pavement during grouting. Longitudinal cracks were observed on a few panels where the subbase layer was eroded (Figure 64).

In situ testing was conducted on this TS about 20 days after the flood waters receded (9/21/11) and after about 6 and 9 months (on 4/5/12 and 6/19/12). FWD tests were conducted at 24 locations and DCP test was conducted at 1 location. FWD tests were conducted at mid-panel and at joints, both on the old pavement (stabilized with cement grout) and the new pavement.

FWD test results from three different testing times along the TS are shown in Figure 65. DCP-CBR profiles at the two test locations from two different testing times are shown in Figure 66. Some key findings from these in situ testing are as follows:

- FWD tests at joints indicated an average LTE of about 93% to 95% at the three testing times. Two of the test locations showed a reduction in LTE with time, from about 94% shortly after flooding to about 85% to 88% several months after flooding. These tests were located on panels underlain by cement grout.
- FWD zero-load intercept values did not indicate any voids beneath the pavement. The $k_{FWD\text{-}static}$ values were on average about 15 to 20 kPa/mm, which is significantly lower than 41 kPa/mm (150 pci) and is rated as "very poor," per AASHTO (1993).
- Average CBR of the grout layer increased from about 5.8 to 10.4, from shortly after flooding to 9 months after flooding. The CBR of the subgrade layer was about the same at both testing times with an average of about 20 in the top 300 mm of subgrade, which can be rated as "good" to "very good" quality, per AASHTO (1993).

GPR scanning was conducted on 6/19/12 to detect any potential voids beneath the pavement. Scanning was originally planned on both east and west bound lanes in multiple scanning lines longitudinally along the pavement, with multiple frequency antennas (200 MHz, 400 MHz, 900 MHz, and 1500 MHz). However, due to traffic control restrictions, GPR scans were performed using only the 400 MHz antenna (Figure 67) along the south side, middle, and north sides of the east bound lane. Scanning was performed between the 38 m and 68 m station of the TS, as noted on Figure 65. GPR scan results longitudinally along the north side, middle, and south side of the pavement are shown in Figure 68, Figure 69, and Figure 70, respectively. Some key features observed in the GPR scans are as follows:

- Scanning along the north side detected joint dowel bars within the first 5 m (16 ft) and from the last 12 m (40 ft) of the scanned zone (Figure 68).
- A potential void area (with changing conductivity) was detected at about 0.3 to 0.6 m below surface in the middle of the scanned zone, along the south side scan (Figure 70).
- Bottom of the grout layer appears to be at about 250 to 300 mm below surface (Figure 70).

Figure 62. Aerial imagery showing pre-flood (top from 6/28/10) and during flood (bottom from 7/17/11) conditions on TS2 – Pottawattamie County

Figure 63. Eroded base material and voids under PCC pavement filled with cement grout – TS2 [Note: Cement grout was placed two days prior to taking these photos] (Photos taken on 9/21/11) – Pottawattamie County

Figure 64. Longitudinal cracks on PCC pavement with undermined base material on TS2 (Photo taken on 9/21/11) – Pottawattamie County

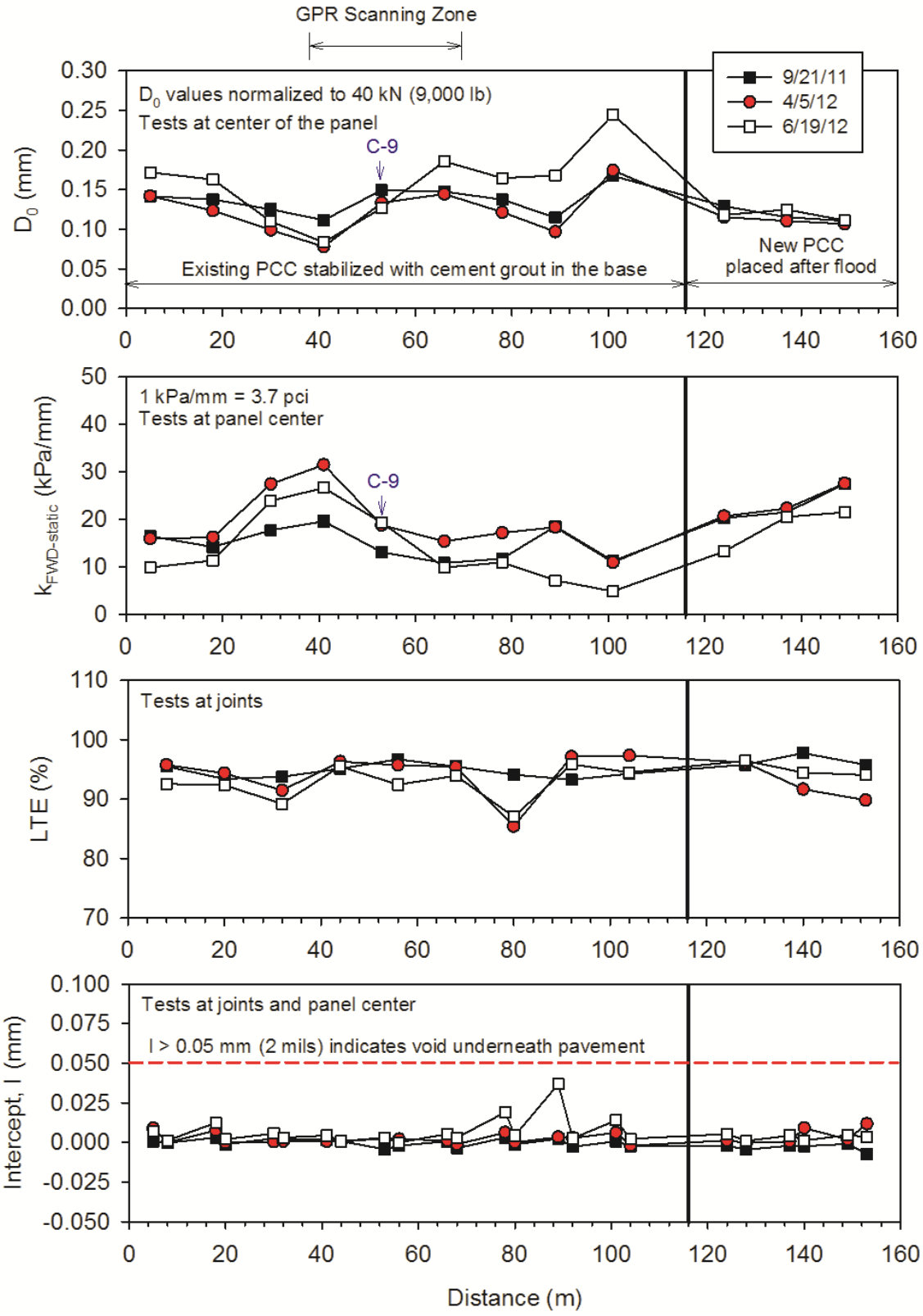

Figure 65. FWD results from three different testing times after flooding on TS2 – Pottawattamie County

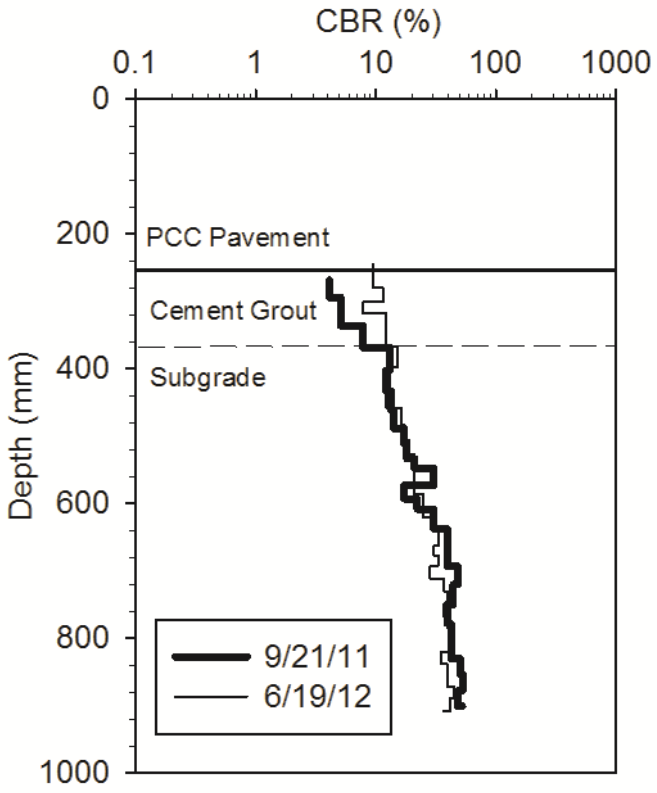

Figure 66. DCP-CBR profiles at one test locations at two different times after flooding on TS2 – Pottawattamie County

Figure 67. GPR scanning setup with 400 MHz antenna along the south side of the east bound lane on TS2 – Pottawattamie County

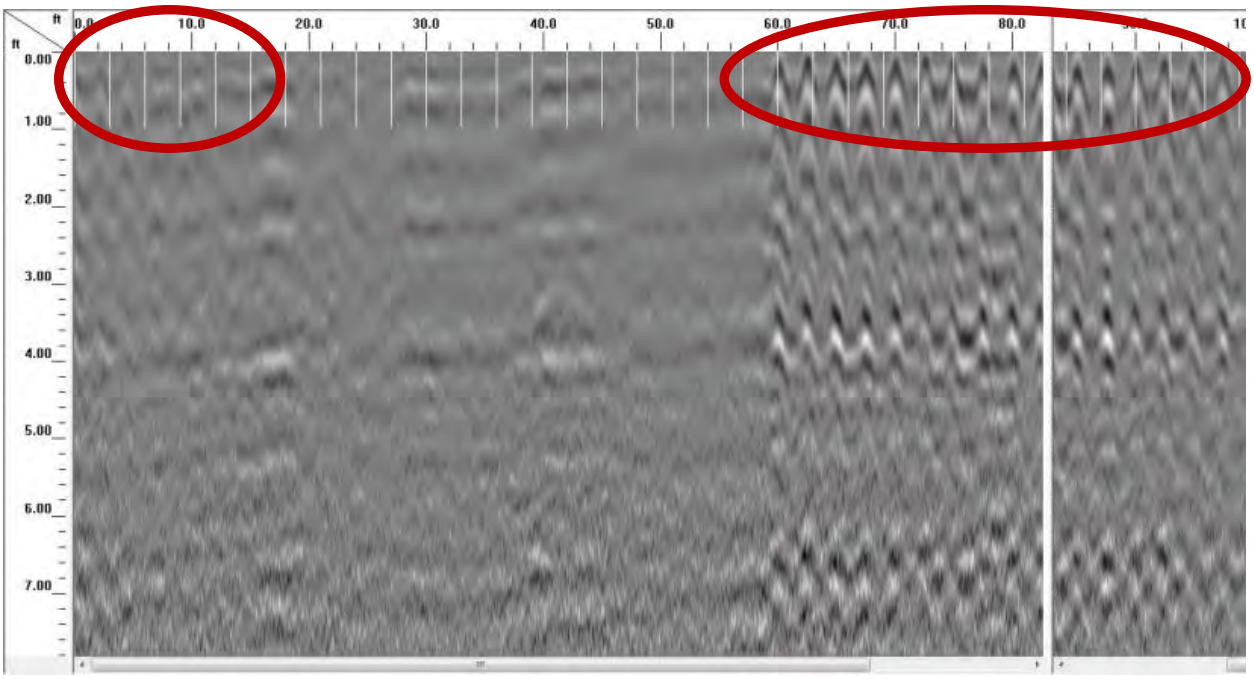

Figure 68. GPR scan using 400 MHz antenna along the north side of the east bound lane on TS2 (note 0 ft on the figure represents the 38 m station and the 100 ft on the figure represents the 68 m station of the TS) – areas circled in red denote rebars in pavement – Pottawattamie County

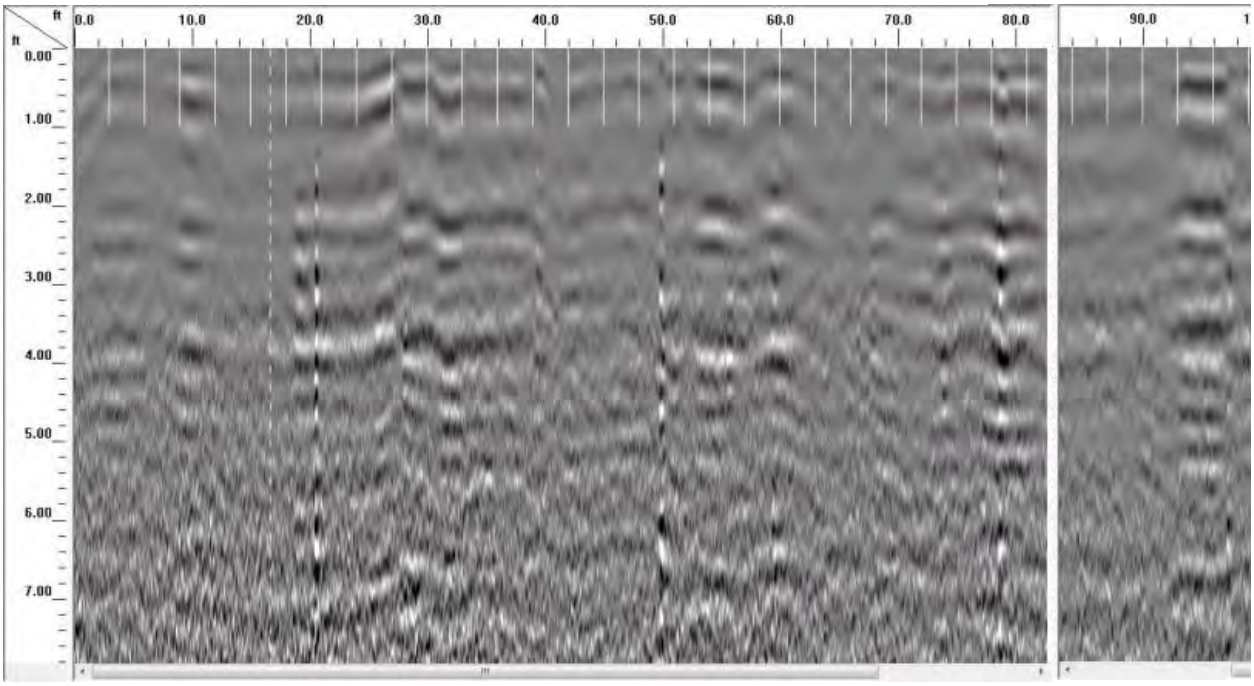

Figure 69. GPR scan using 400 MHz antenna along the middle of the east bound lane on TS2 (note 0 ft on the figure represents the 38 m station and the 100 ft on the figure represents the 68 m station of the TS) – Pottawattamie County

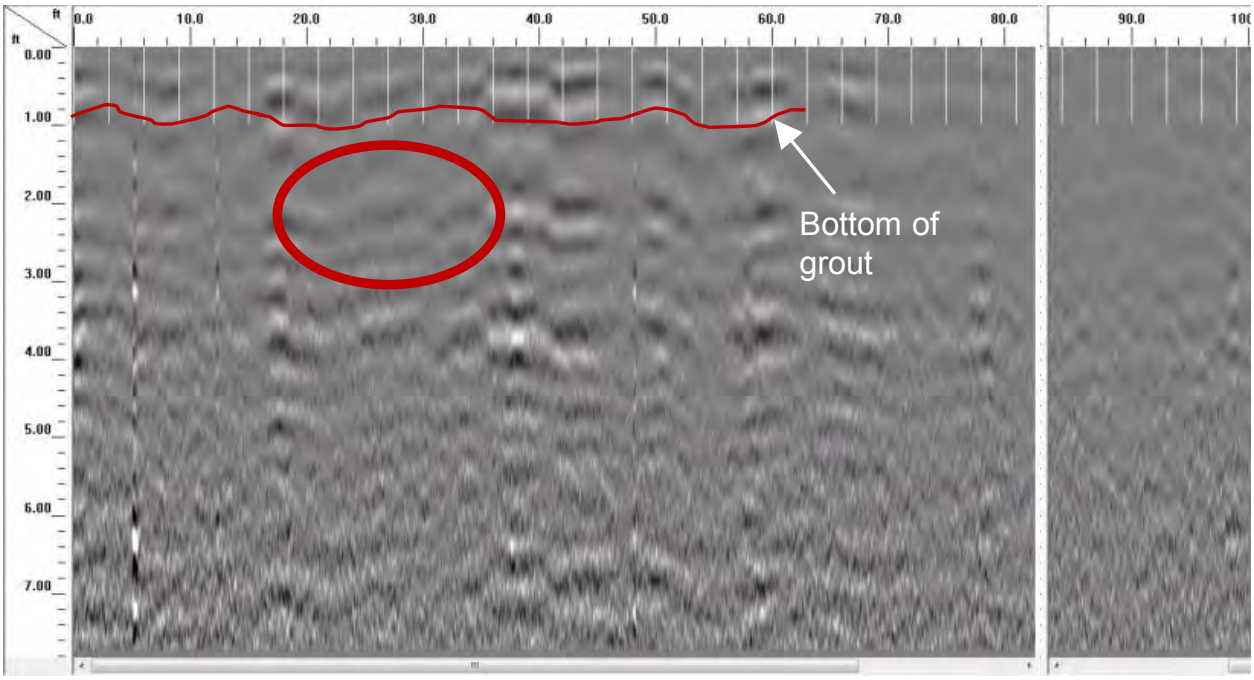

Figure 70. GPR scan using 400 MHz antenna along the south side of the east bound lane on TS2 (note 0 ft on the figure represents the 38 m station and the 100 ft on the figure represents the 68 m station of the TS) – area circled in red denote a potential void zone beneath pavement – Pottawattamie County

TS3 – 110th Street (Gravel)

TS3 is a gravel road segment located on 110th Street just north of Desoto Avenue, north of Council Bluffs, Iowa. Testing was conducted over a length of about 590 m along the middle of the lane. The segment consisted of 130 mm to 150 mm thick gravel layer underlain by natural subgrade (note: depths determined from DCP tests). The Pottawattamie County soil survey report indicates that the natural subgrade soils in this region consist of silty alluvium material in the top 600 mm of the subgrade and are classified as A-4 and A-6 or CL-ML and CL soils. According to the soil survey report, these soils exhibit moderately high drainability with saturated hydraulic conductivity varying from about 1 to 9 μm/s (0.3 to 2.6 ft/day).

During the 2011 flood event, the TS was partially submerged for about two months (Figure 65). Reportedly, the flood waters receded in the area on 9/1/11. During the flood event, some of the surface gravel was washed away in a portion of the TS. The washed out portion was located at a lower elevation where a small drainage culvert was present. County personnel replaced the eroded surface with some new gravel (Figure 65). Photos taken during field visits are shown in Figure 72 and Figure 73.

In situ testing was conducted on this TS in flooded and non-flooded areas for comparison, about 21 days after the flood waters receded (9/22/11), 54 days after flood waters receded (10/25/11), and after about 6 and 8 months (on 4/5/12 and 5/29/12). FWD tests were conducted at 25

locations (9 in non-flooded area and 16 in flooded area) and DCP tests were conducted at 4 locations (2 each in flooded and non-flooded areas). GPR scans were performed on 6/19/12.

Hand auger boring to a depth of about 1.5 m below surface was performed on 9/22/11 at a location near the culvert to obtain soil samples for moisture content and determine the depth of water table. Results from this testing are shown in Figure 74. E_{FWD} and E_{SG} results from four different testing times along the TS are shown in Figure 75, identifying the flooded and non-flooded zones. Review of aerial images indicated pre-flood ponding in areas close to the culvert and those zones are also identified Figure 75. E_{SG} values were calculated based on deflections from the sensor located at 300 mm (12 in.) away from the center of the loading plate. DCP-CBR profiles at the four test locations from different testing times are shown in Figure 76. Box plots of E_{SG} values comparing measurements in the flooded and non-flooded areas at different test times are shown in Figure 77. Some key findings from these in situ testing are as follows:

- Ground water level was located at about 1.27 m below surface under the roadway, while the water level in the ditches was about 0.15 m below the gravel surface during 9/22/11 testing (about 21 days after flooding). Moisture contents varied from about 18 to 22% above the water table. During field visit on 10/25/11, some subsurface weep holes were observed around the culvert (Figure 73), indicating erosion of material around the culvert.
- On average, E_{FWD} and E_{SG} values at 21 days after flooding were on average about 1.6 to 1.8 times higher in the non-flooded zone than in the flooded zone. The difference between the average values in the two zones decreased with time and the E_{SG} values obtained after about 54 days were not significantly different.
- The E_{SG} values in the whole TS were low and the quality is rated as “very poor,” per AASHTO (1993). Lowest values were located in zones where pre-flood ponding was evident.
- The CBR of the surface gravel layer was higher in the non-flooded zone compared to the flooded zone, by nearly 10 times at 21 days after flooding. Similar to FWD results, the difference between the flooded and non-flooded zone gravel layer CBR values decreased with time and were about the same at 8 months after flooding.
- The CBR of the gravel layer increased with time at all test locations. For example at G-14 (weakest location), average CBR of the gravel was about 5, 20, 40, and 80 testing at 21 days, 54 days, 6 months, and 8 months after flooding.
- The subgrade CBR values (averaged over the top 300 mm) in the flooded zone increased (from 1.7 to 6.4 and 4.0 to 8.5 at the two locations) from 21 to 54 days after flooding. At 21 days after flooding, subgrade CBR values in the non-flooded zone were higher (4.5 and 8.2) than the values in flooded zone (1.7 and 4.0), but they were about the same (10 to 12) at 8 months after flooding.
- The DCP and FWD test results on this test segment illustrate that both subgrade and the surface gravel layers gained strength with time, likely because of subgrade material drying over time.

Figure 71. Aerial imagery showing pre-flood (left from 6/28/10) and during flood (right from 7/17/11) conditions on TS3 – Pottawattamie County

Figure 72. New gravel placed at the middle of the segment following flooding on TS3 (Photo taken on 9/21/2011) – Pottawattamie County

Figure 73. Weep holes near culvert on TS3 (Photo taken on 10/25/2011) – Pottawattamie County

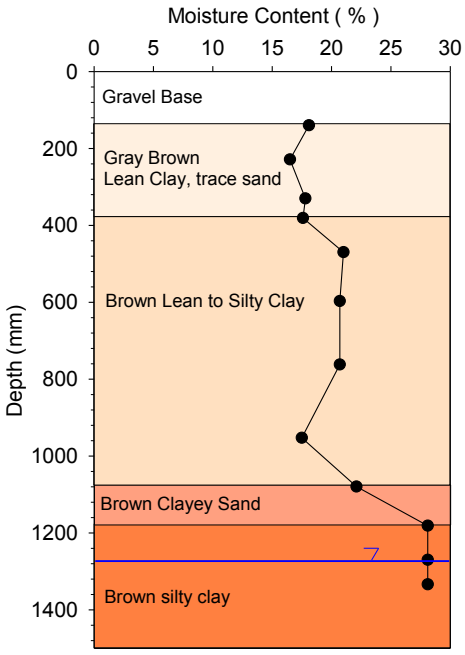

Figure 74. Soil moisture content profile with depth to water table at G-14 on 9/22/11 – Pottawattamie County

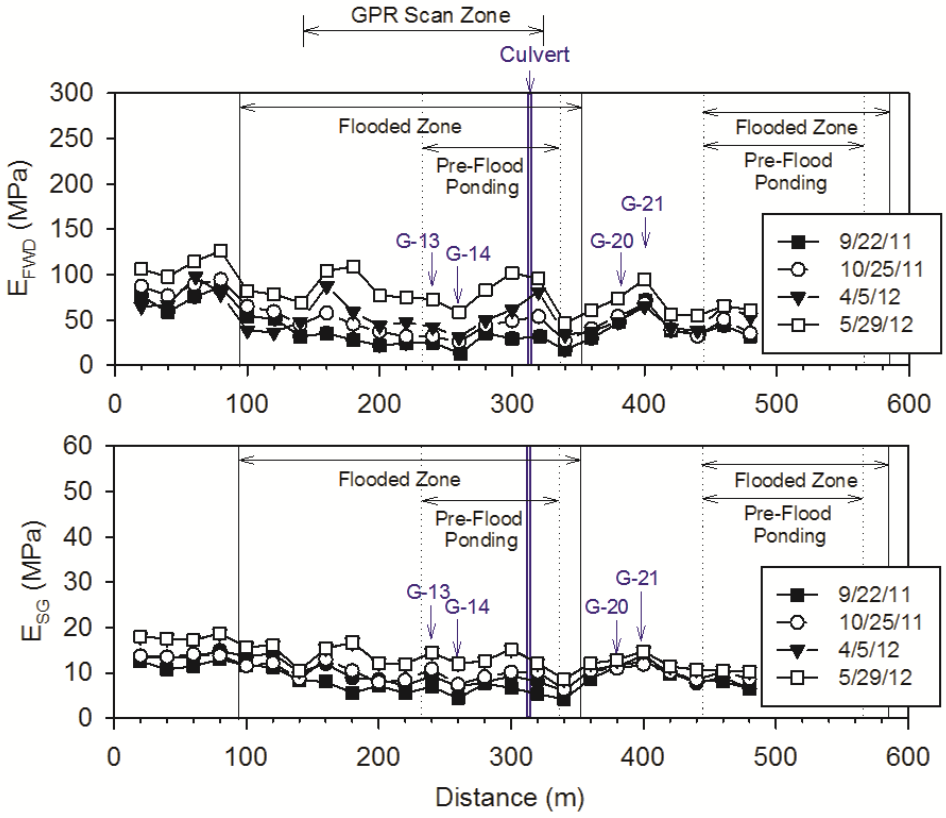

Figure 75. Surface FWD modulus and subgrade modulus at four different times after flooding on TS3 – Pottawattamie County

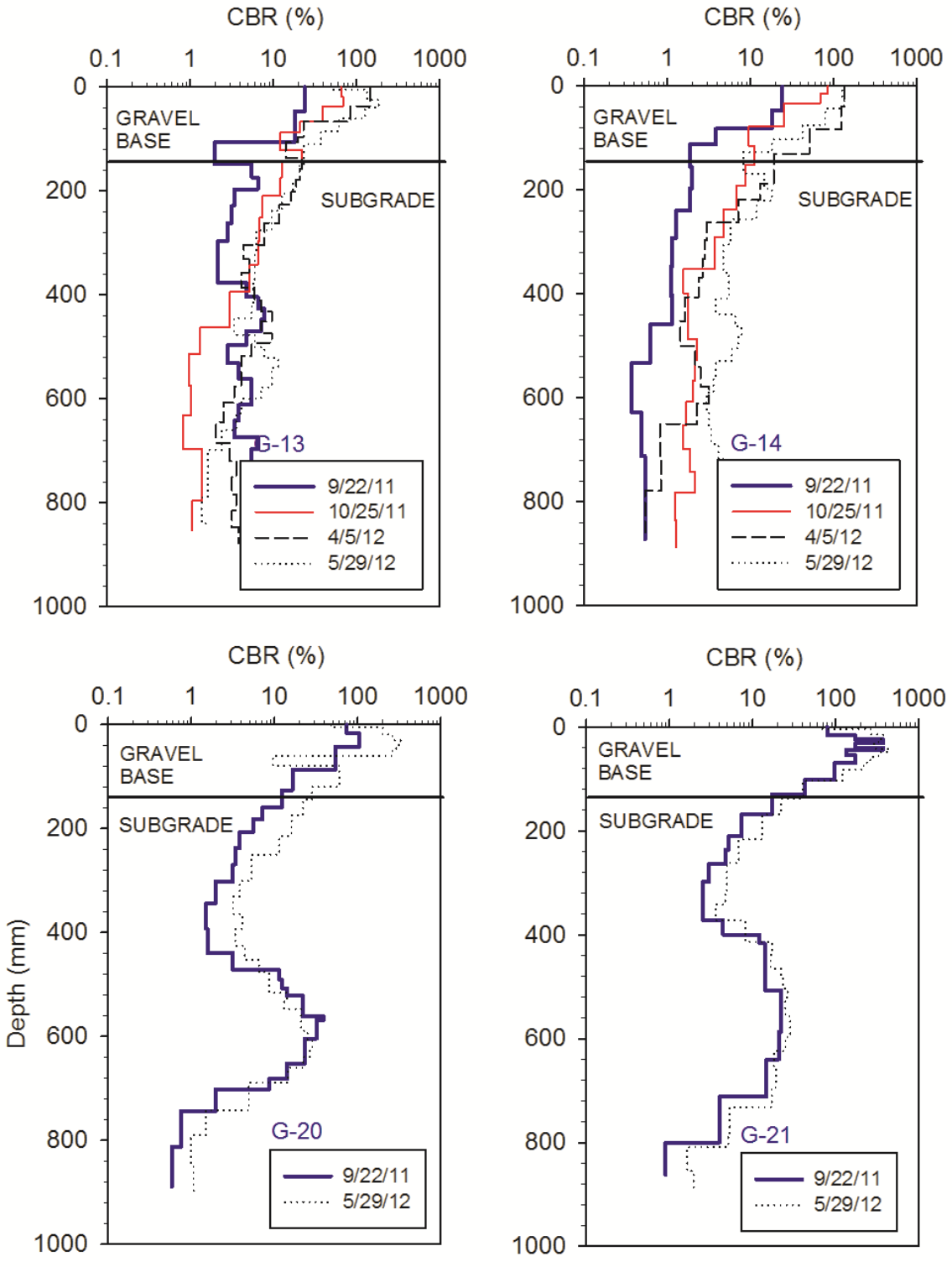

Figure 76. DCP-CBR profiles at four test locations from four different testing times on TS3 – Pottawattamie County

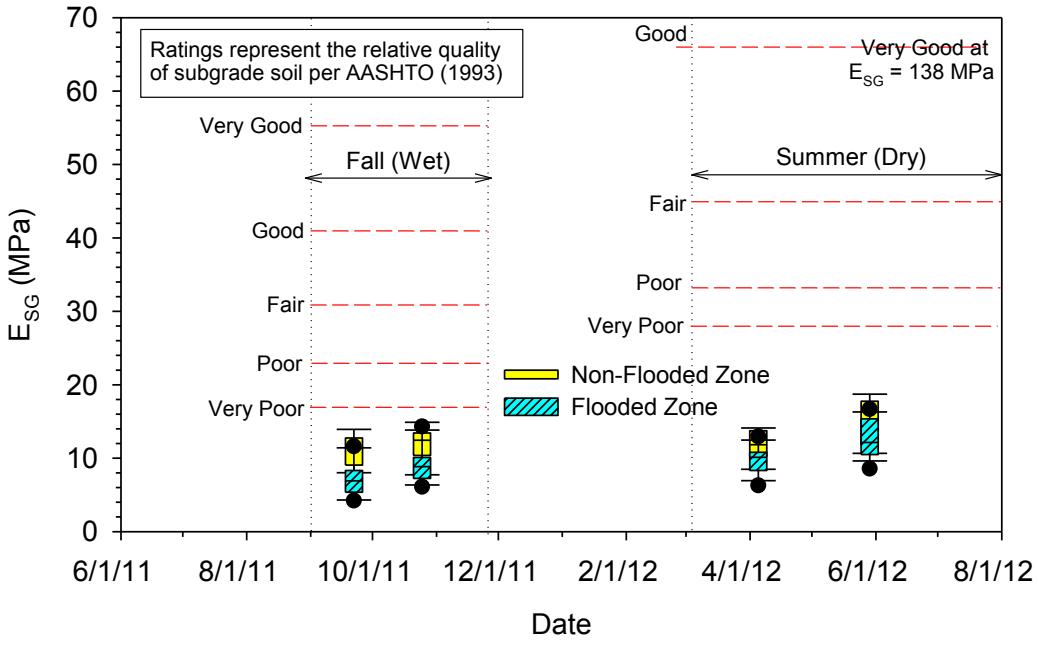

Figure 77. Box plots of subgrade modulus values in flooded and non-flooded zones in comparison with relative quality ratings on TS3 – Pottawattamie County

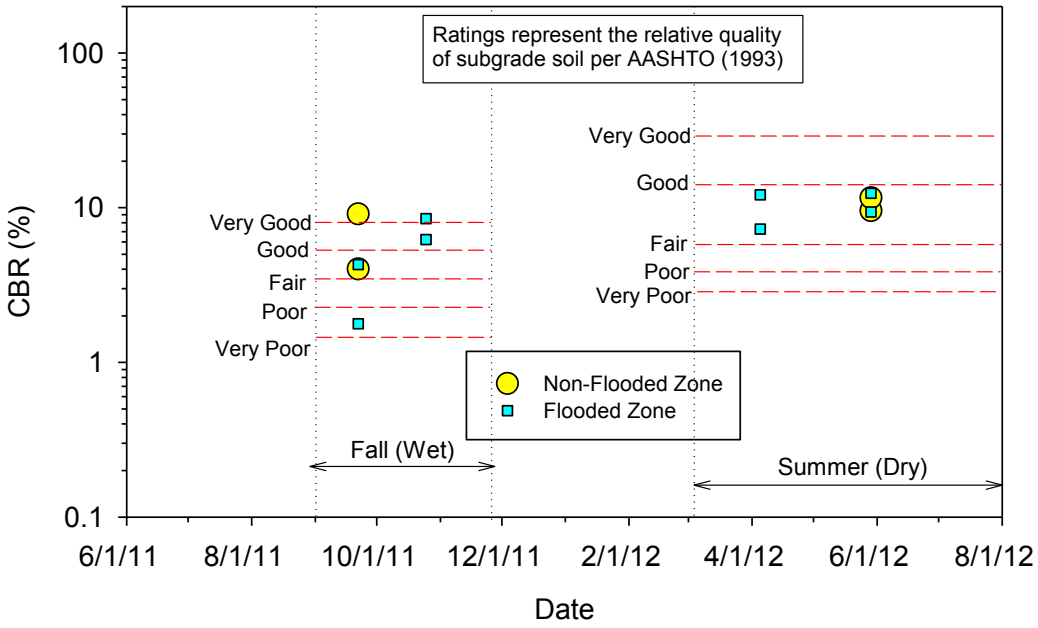

Figure 78. Comparison of subgrade CBR values in flooded and non-flooded zones with relative quality ratings on TS3 – Pottawattamie County

GPR scans were performed using 200 and 400 MHz antennas on 6/19/12 along the roadway between 140 m and 320 m stations, as noted on Figure 75. The scanning was conducted to: (a) identify culverts or any other features beneath the surface (e.g., weep holes), (b) determine

thickness of the gravel layer, and (c) determine the depth to water table. GPR scan results longitudinally along the roadway are shown in Figure 79 and Figure 80. Some key features observed in the GPR scans are as follows:

- Changes in gravel layer thickness along the roadway were identified in both 200 MHz and 400 MHz antenna scans (Figure 68). Note that the depths on the vertical scale were not calibrated with the actual depth measurements and they must be considered approximate. However, if calibrated (i.e., if verified with a known feature at known depth in situ), gravel layer thickness can be obtained accurately.
- Culvert location was identified in the scans as shown in Figure 80.
- No weep holes were noted in the scans. Although they were visible near the culvert during 10/25/11 field visit, they were not seen at the time of scanning on 6/19/12.
- Although water was present in the ditches near the culvert at the time of scanning, it was not identified in the GPR scans (note that the water table depth under the roadway was much deeper than the depth of water seen in ditches during 9/22/11 field testing as discussed earlier).

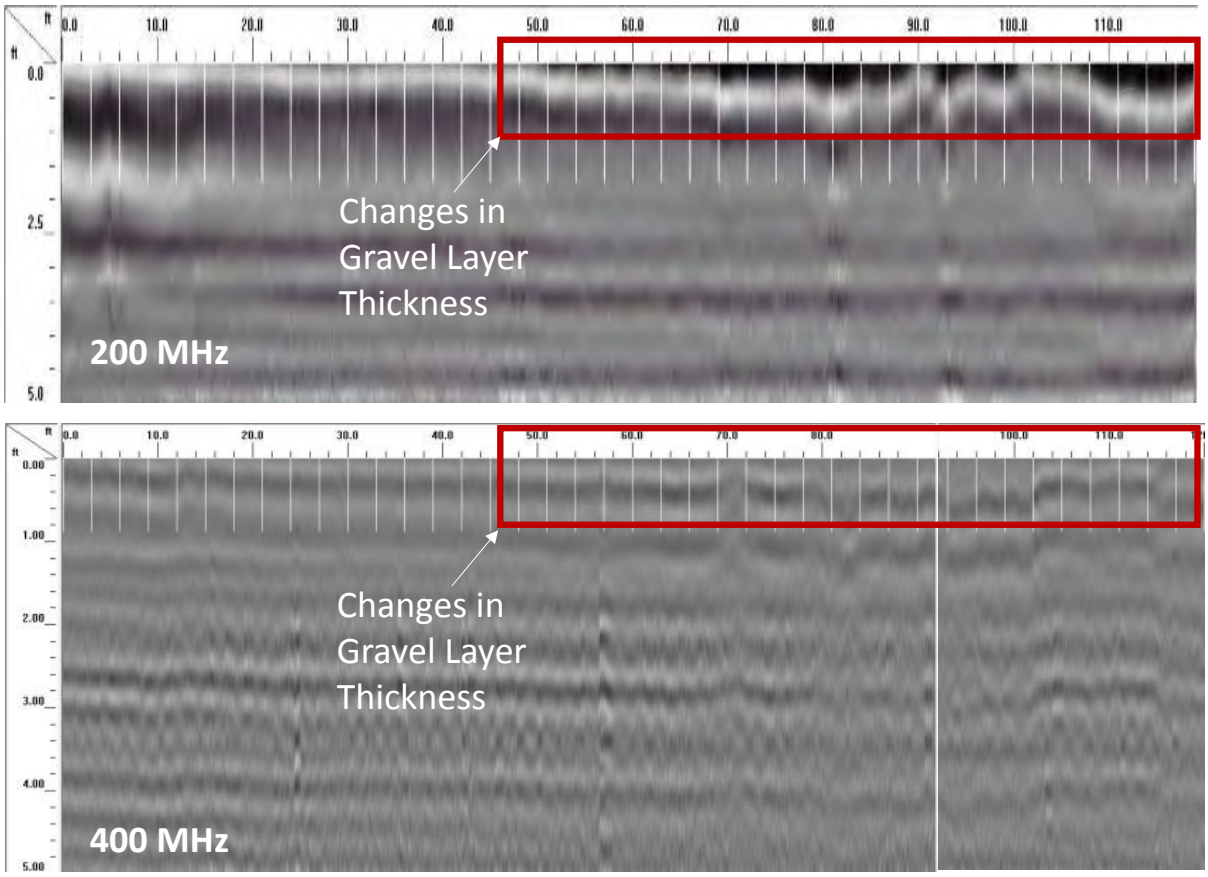

Figure 79. GPR scans using 200 and 400 MHz antennas on TS3 (note 0 ft on the figure represents the 130 m station of the TS) – Pottawattamie County

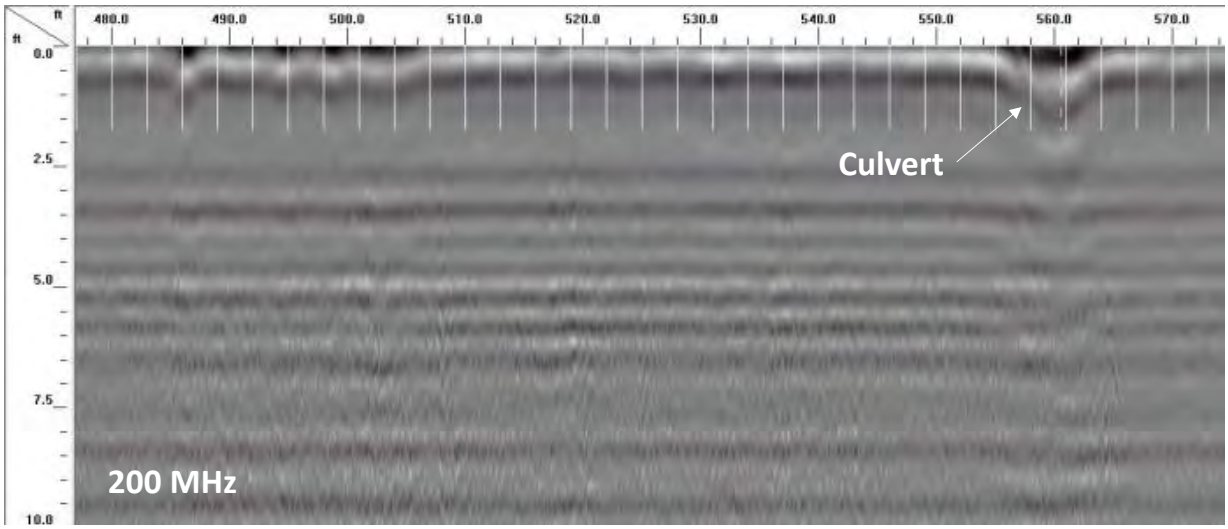

Figure 80. GPR scan using 200 MHz antenna on TS3 (note that 560 ft on the figure represents the 310 m station (at culvert) of the TS) – Pottawattamie County

TS4 – Desoto Avenue East (Emulsified Oil-Stabilized Base)

TS4 is a chipseal surfaced roadway over emulsified oil-stabilized base located on Desoto Avenue, north of Council Bluffs, Iowa. Testing was conducted over a length of about 5,215 m along the east bound lane. The segment consisted of thin chipseal at the surface over about 200 mm thick emulsified oil-stabilized base underlain by natural subgrade (depths determined based on DCP tests). The Pottawattamie County soil survey report indicates that the natural subgrade soils in this region consist of silty to clayey alluvium material in the top 600 mm of the subgrade and are classified as A-4, A-6, and A-7 or CL-ML, CL, and CH soils. The saturated hydraulic conductivity of the material vary from about 0.04 to 9 μm/s (0.01 to 2.6 ft/day).

During the 2011 flood event, portions of the TS was submerged under water, portions of the TS had water encroached up to the shoulders but did not overtop the road, and portions of the TS did not experience flooding (Figure 81). The flood event existed for nearly two months in this TS. Reportedly, the flood waters receded in the area on 9/1/11. During the flood event, chipseal coat was stripped off (delaminated) at a few locations and granular shoulder material was eroded at isolated locations. A culvert along the roadway was clogged due to scouring and erosion of embankment materials beneath the surface (Figure 44). Rutting under wheel paths was observed north of 140th St. and Desoto Avenue intersection (near the end of the test segment) (Figure 82).

In situ testing was conducted on this TS in flooded and non-flooded areas for comparison, about 22 days after the flood waters receded (9/23/11), 55 days after flood waters receded (10/25/11), and after about 6 and 8 months (on 4/5/12 and 5/29/12). FWD tests were conducted at 40 locations (8 in the flooded areas, 15 in the encroached areas, and 17 in the non-flooded areas) and DCP tests were conducted at 4 locations (1 in the flooded area, 2 in the encroached areas, and 1 in the non-flooded areas). GPR scans were performed on 6/19/12.

E_{FWD} and E_{SG} results from four different testing times along the TS are shown in Figure 83, identifying the flooded and non-flooded zones. Review of aerial images indicated encroached water areas and pre-flood ponding in lower elevation areas, and those zones are also identified Figure 83. E_{SG} values were calculated based on deflections from the sensor located at 300 mm (12 in.) away from the center of the loading plate. DCP-CBR profiles at the four test locations from different testing times are shown in Figure 84. Box plots of E_{SG} values comparing measurements in the flooded and non-flooded areas (encroached areas are not included) at different test times are shown in Figure 77. Some key findings from these in situ testing are as follows:

- On average, E_{FWD} and E_{SG} values were on average about 1.3 to 1.6 times higher in the non-flooded zone (including data from the encroached zone) than in the flooded zone, at all times of testing. FWD results in the encroached areas were on average similar to the results in areas where there was no encroachment.
- The E_{SG} values in the flooded zone are rated as "very poor" to "poor," and the values in the non-flooded zone are rated as "very poor" to "fair," per AASHTO (1993).
- The CBR of the stabilized gravel layer was about the same in flooded and non-flooded zones (>50), but the CBR of the subgrade layer (in the top 300 mm) was not. At 22 days after flooding, the subgrade CBR was about 3.7 in the flooded zone, 7.7 in the encroached zone, and about 14 in the non-flooded zone. This trend remained the same but the values decreased slightly during testing at 8 months after flooding (see Figure 86).
- The DCP and FWD test results on this TS illustrate that flooded areas were comparatively softer than the non-flooded areas and remained the same even at 8 months after flooding.

Figure 81. Aerial imagery showing pre-flood (left from 6/28/10) and during flood (right from 7/17/11) conditions on TS4 – Pottawattamie County

Figure 82. Rutting observed near the east end of the test segment (near test location D-38) (photo taken on 9/23/11) on TS4 – Pottawattamie County

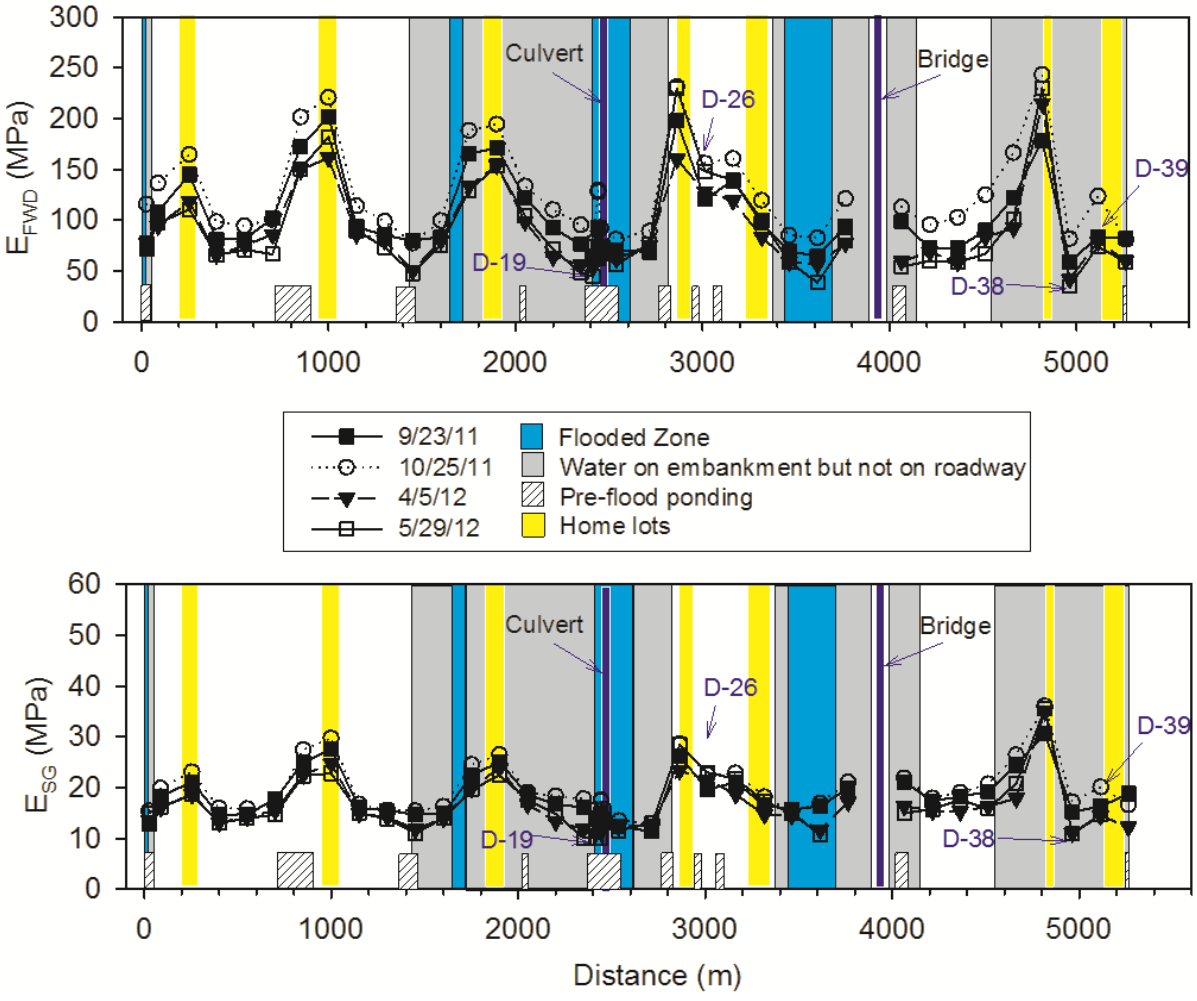

Figure 83. Surface FWD modulus and subgrade modulus at four different times after flooding on TS4 (highlighted in color are drainage, flooding, and home lot features observed from aerial maps) – Pottawattamie County

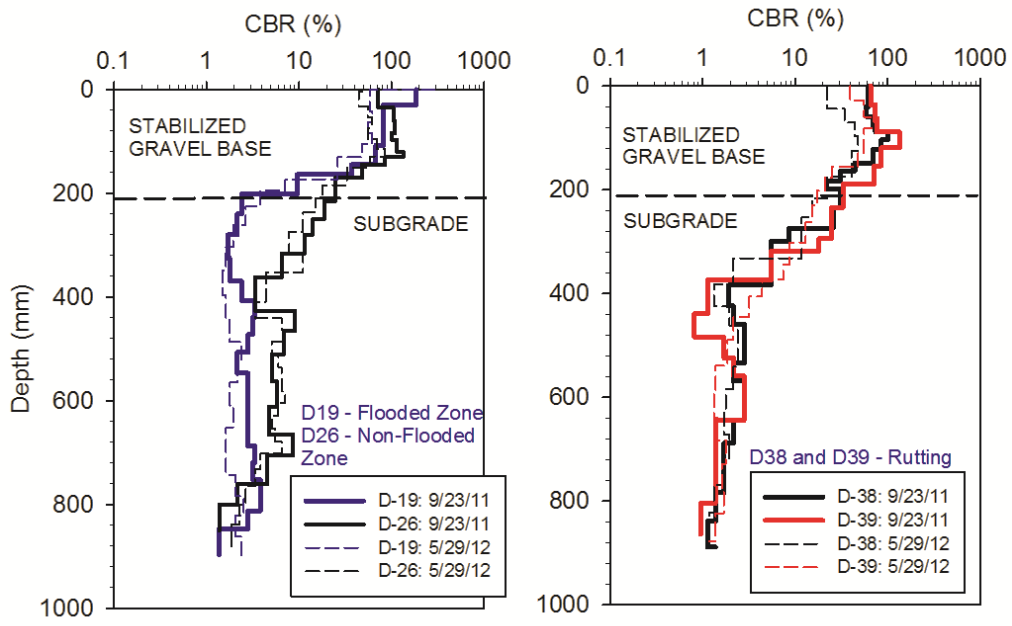

Figure 84. DCP-CBR profiles at four test locations from two different testing times on TS4 – Pottawattamie County

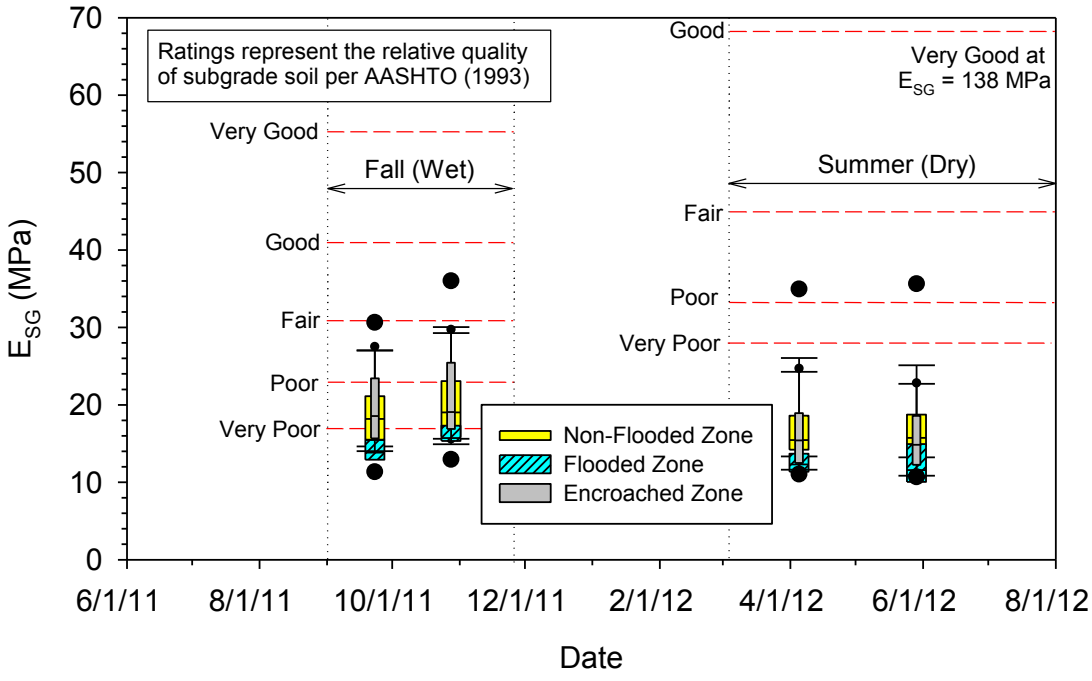

Figure 85. Box plots of subgrade modulus values in flooded and non-flooded zones in comparison with relative quality ratings on TS4 – Pottawattamie County

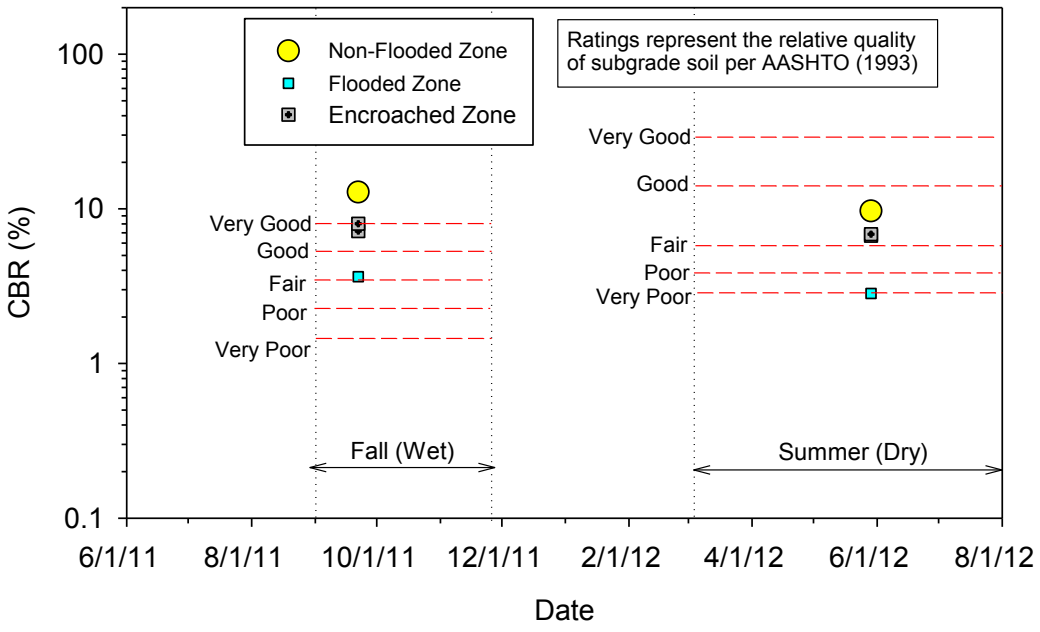

Figure 86. Comparison of subgrade CBR values in flooded and non-flooded zones with relative quality ratings on TS4 – Pottawattamie County

TS5 – 145th Street (Gravel)

TS5 is a gravel road segment located on 145th Street, north of Council Bluffs, Iowa. Testing was conducted over a length of about 6050 m along the middle of the lane. The segment consisted of 130 mm to 140 mm thick gravel layer underlain by natural subgrade (note: depths determined from DCP tests). The Pottawattamie County soil survey report indicates that the natural subgrade soils in this region consist of silty to clayey to sandy alluvium material in the top 600 mm of the subgrade and are classified as A-4, A-6, A-7, and A-2-4 or CL-ML, CL, CH, SM, and SP soils. According to the soil survey report, the CL-ML, CL, and CH soils exhibit low to moderate drainability with saturated hydraulic conductivity varying from about 0.04 to 9 μm/s (0.3 to 2.6 ft/day) and the SM and SP soils exhibit high drainability with saturated hydraulic conductivity of about 189 μm/s (54 ft/day).

During the 2011 flood event, the TS was fully submerged for about one to three months (Figure 87, Figure 88). Reportedly, the flood waters receded in the area on 9/1/11. Roadway damages noted on this TS include eroded gravel surface layer, eroded culvert backfill materials, and weep holes beneath the surface (Figure 90 to Figure 89).

Erosion of culvert backfill materials resulted in formation of about 0.5 m diameter pothole on the middle of roadway and was observed during the field reconnaissance on 9/21/11 (see Figure 89). At that time, the flood water level was close to the road surface. There was about 0.2 m deep void beneath the surface gravel layer. A small water vortex was observed as shown in Figure 46 indicating a culvert at this location. On 9/23/11, two additional pot holes were formed in that same location, shortly after a utility truck passed the area. These pot holes were undetected until they were formed and posed a significant safety concern to traffic. After the flood waters

receded, it was found that there is a 1.2 m diameter concrete culvert and several weep holes around the culvert at this location (Figure 91). Field observations on 4/5/12 indicated that the backfill material placed around the culvert was very loose Figure 92).

In situ testing was conducted on this TS about 23 days after the flood waters receded (9/23/11), 54 days after flood waters receded (10/25/11), and after about 6 and 8 months (on 4/5/12 and 5/29/12). FWD tests were conducted at 29 locations and DCP tests were conducted at 2 locations. Hand auger boring to a depth of about 0.72 m below surface was performed on 9/23/11 at a location near the culvert to obtain soil samples for moisture content and determine the depth of water table (note: flood water was close to the road surface at that time).

E_{FWD} and E_{SG} results from four different testing times along the TS are shown in Figure 93. E_{SG} values were calculated based on deflections from the sensor located at 300 mm (12 in.) away from the center of the loading plate. DCP-CBR profiles at the two test locations from different testing times are shown in Figure 94. Soil moisture profile and water table depth from hand auger boring are also shown in Figure 94. Box plots of E_{SG} values at different test times are shown in Figure 95. Some key findings from these in situ testing are as follows:

- Ground water level was located at about 0.58 m below surface under the roadway, while the water level in the ditches was close to the gravel surface during 9/23/11 testing (about 21 days after flooding). Moisture contents varied from about 12 to 18% above the water table and the material consisted of clayey to fine sand material.
- On average, the E_{SG} values in the whole TS were low and the quality is rated as "very poor" to "poor," per AASHTO (1993). The E_{SG} values improved slightly over time (on average from about 17 to 23 MPa), likely because of subgrade material drying.
- Although limited, DCP-CBR results were in contrast with the E_{SG} values. Subgrade CBR values at two locations were > 10 on 9/23/11, which is rated as "very good," per AASHTO (1993). Results increased over time to about 30 on 5/29/12 (Figure 96).

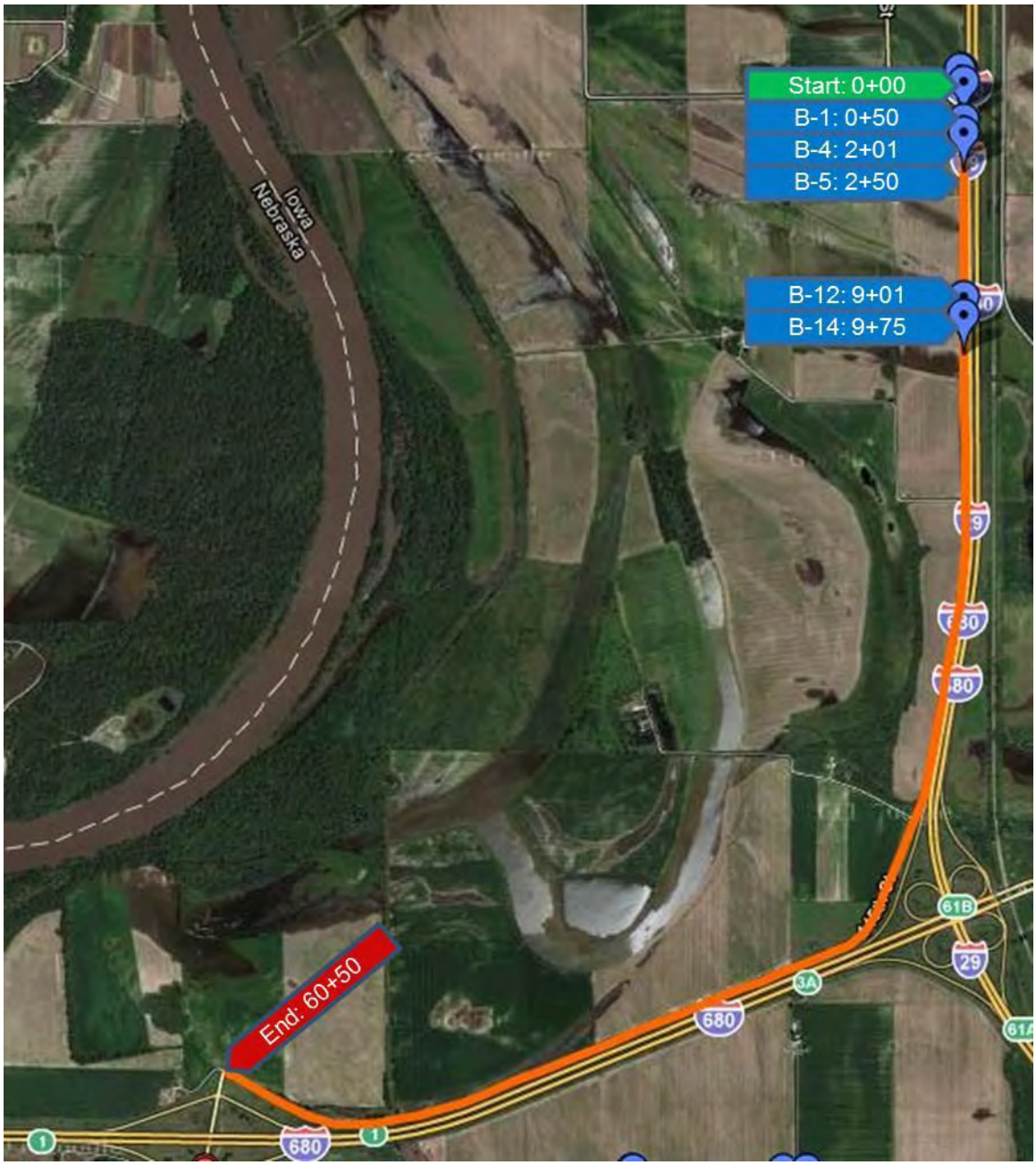

Figure 87. Aerial imagery showing pre-flood (from 6/28/10) conditions and test locations on TS5 – Pottawattamie County

Figure 88. Aerial imagery showing during flood (from 7/17/11) conditions and test locations on TS5 – Pottawattamie County

Figure 89. Potholes (with about 0.5 m (1.5 ft) diameter) under gravel road due to erosion of backfill material around a culvert located beneath the road TS 5 (Photos taken on 9/21/11 and 9/23/11) – Pottawatamie County

Figure 90. FWD testing on TS5 with floodwater up to the edge of the road (Photo taken 9/23/11) – Pottawattamie County

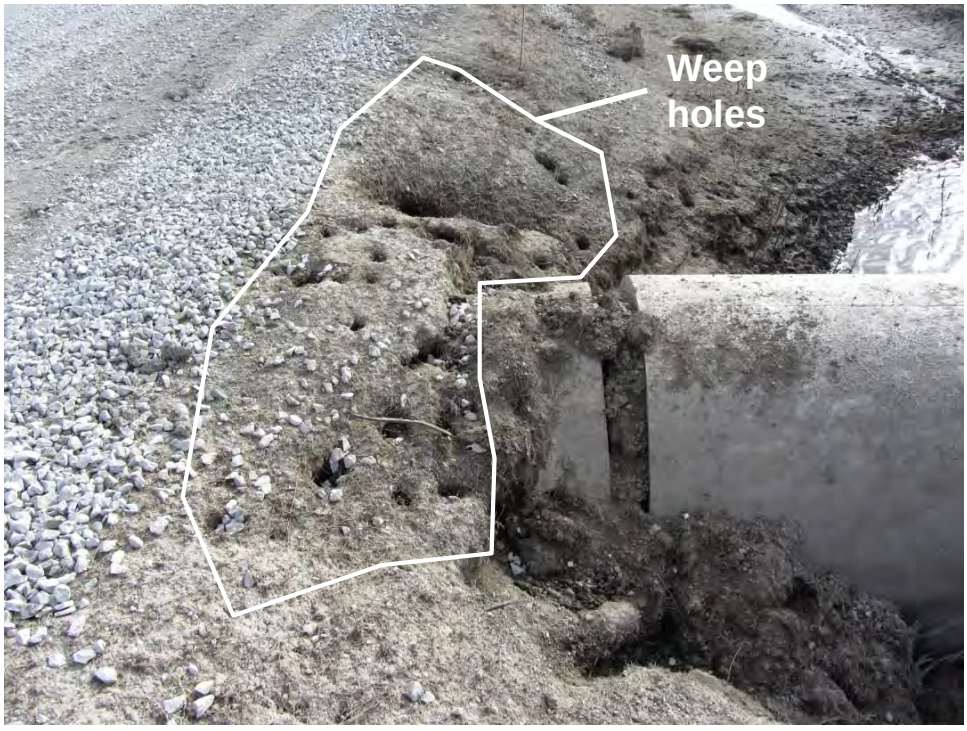

Figure 91. Weep holes (20+) around the culvert observed after flood waters receded on TS5 (Photo taken on 10/25/11) – Pottawattamie County

Figure 92. Loose backfill material around culvert replaced after flood waters receded on TS5 (Photo taken on 4/5/12) – Pottawattamie County

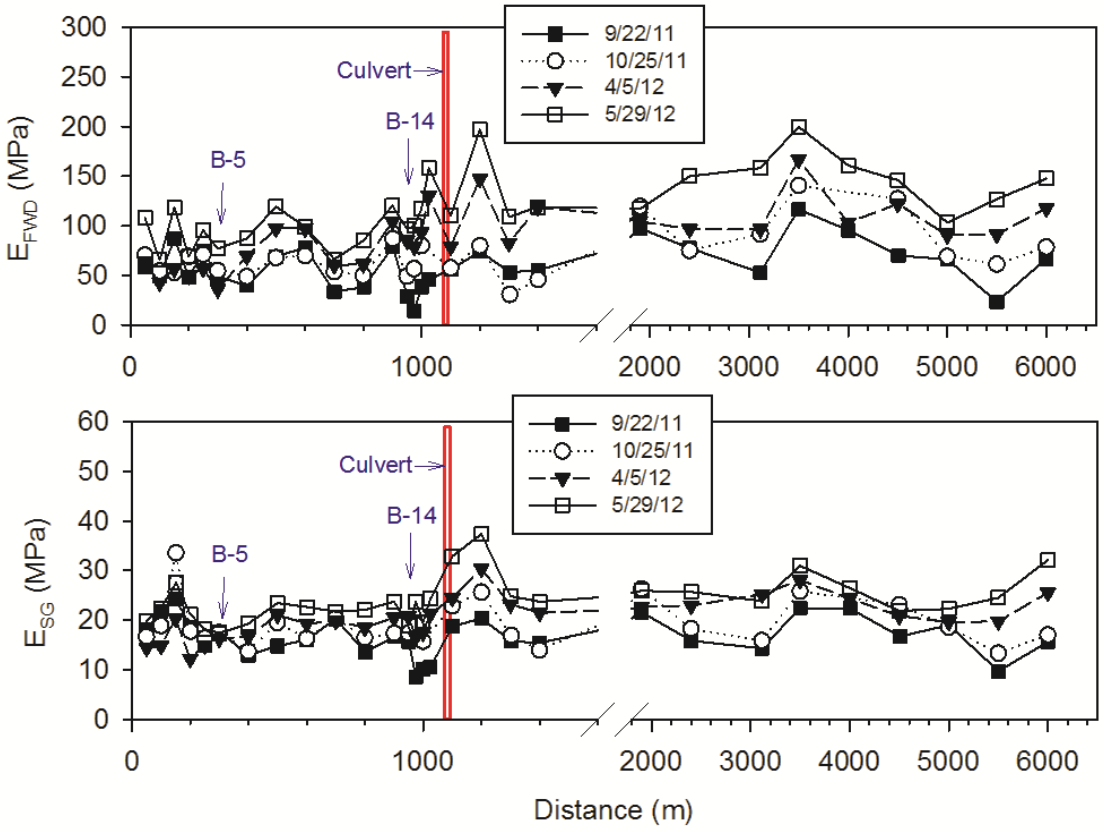

Figure 93. Surface FWD modulus and subgrade modulus at four different times after flooding on TS5 – Pottawattamie County

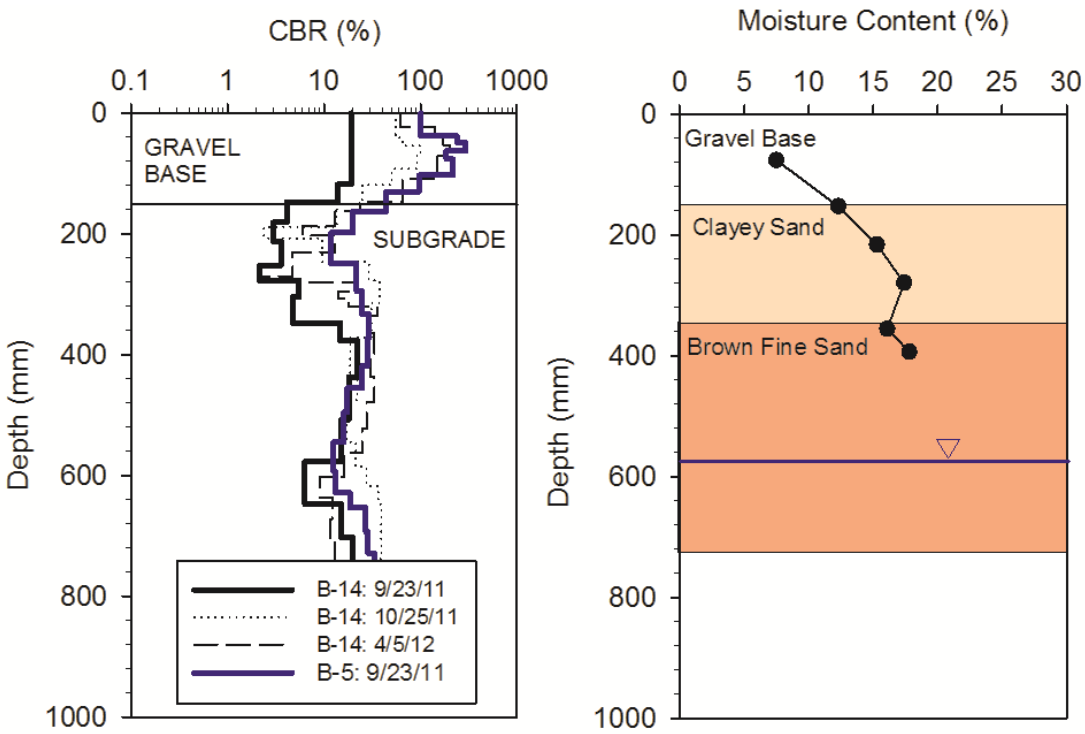

Figure 94. DCP-CBR profiles from three different testing times and soil moisture content profile at B14 from 9/23/11 on TS5 – Pottawattamie County

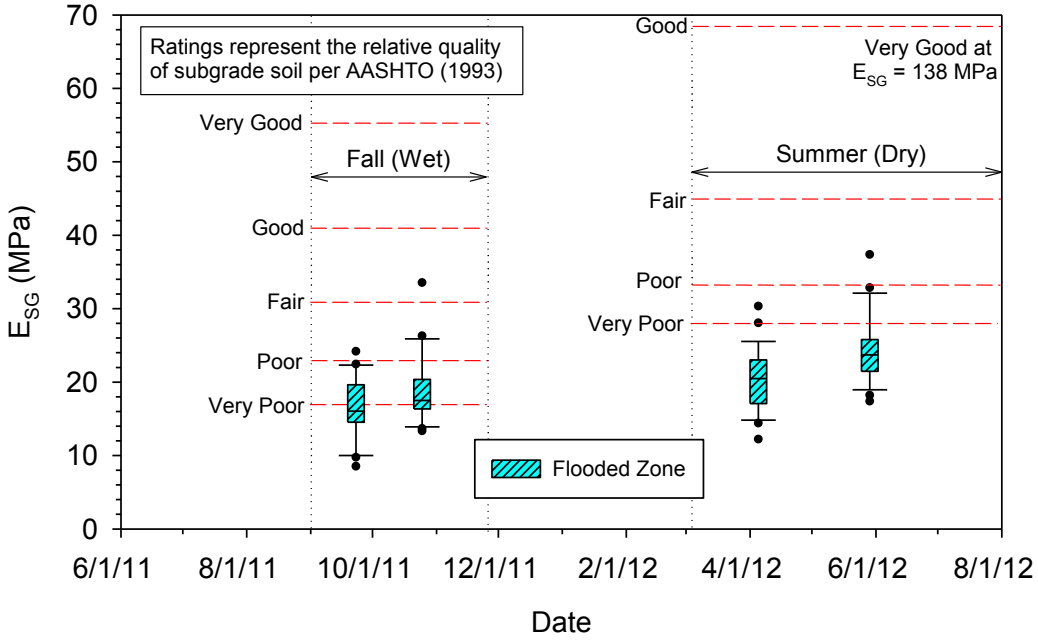

Figure 95. Box plots of subgrade modulus values in comparison with relative quality ratings on TS5 – Pottawattamie County

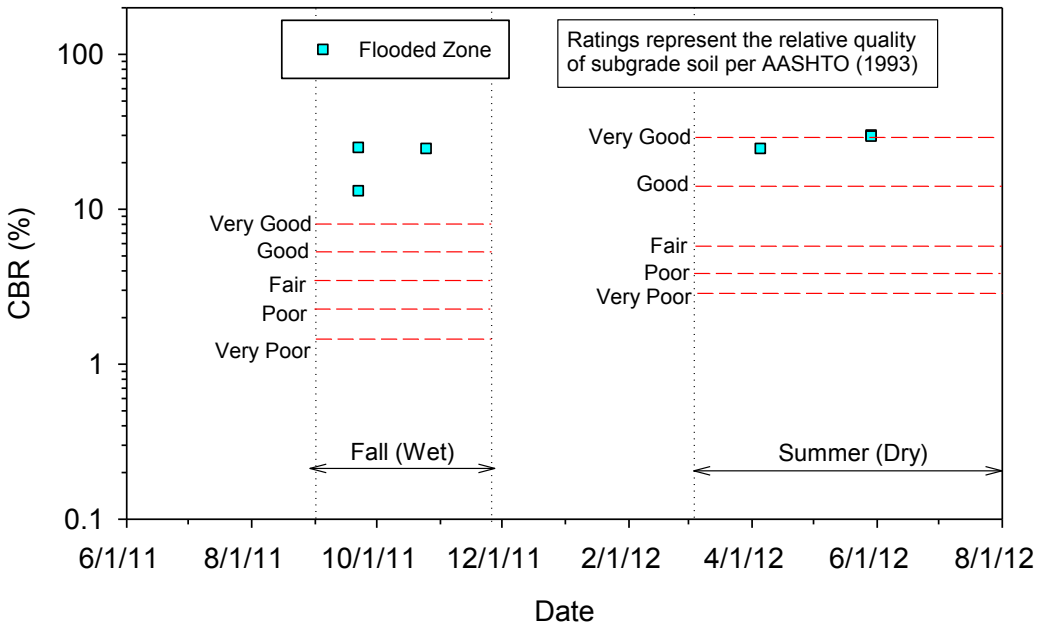

Figure 96. Subgrade CBR values at different testing times with relative quality ratings on TS5 – Pottawattamie County

TS5 – Laser Scanning of a Breach next to 145th Street

3D laser scanning was performed at a breach site located next to 145th Street on TS5 to demonstrate rapid and accurate volumetric calculations. Aerial imagery of the breach site is shown in Figure 97. Photos taken during laser scanning are shown in Figure 98. Results obtained from the laser scanning showing point clouds, contour maps, and colored mesh surfaces are shown in Figure 99 to Figure 106. Rendering of volume calculations are shown in Figure 107.

Figure 97. Aerial imagery of the breach site located next to TS5 145th St. (Google image from 3/7/12) – Pottawattamie County

Figure 98. 3D laser scan setup at the levee breach site on TS5 145th St. – Pottawattamie County

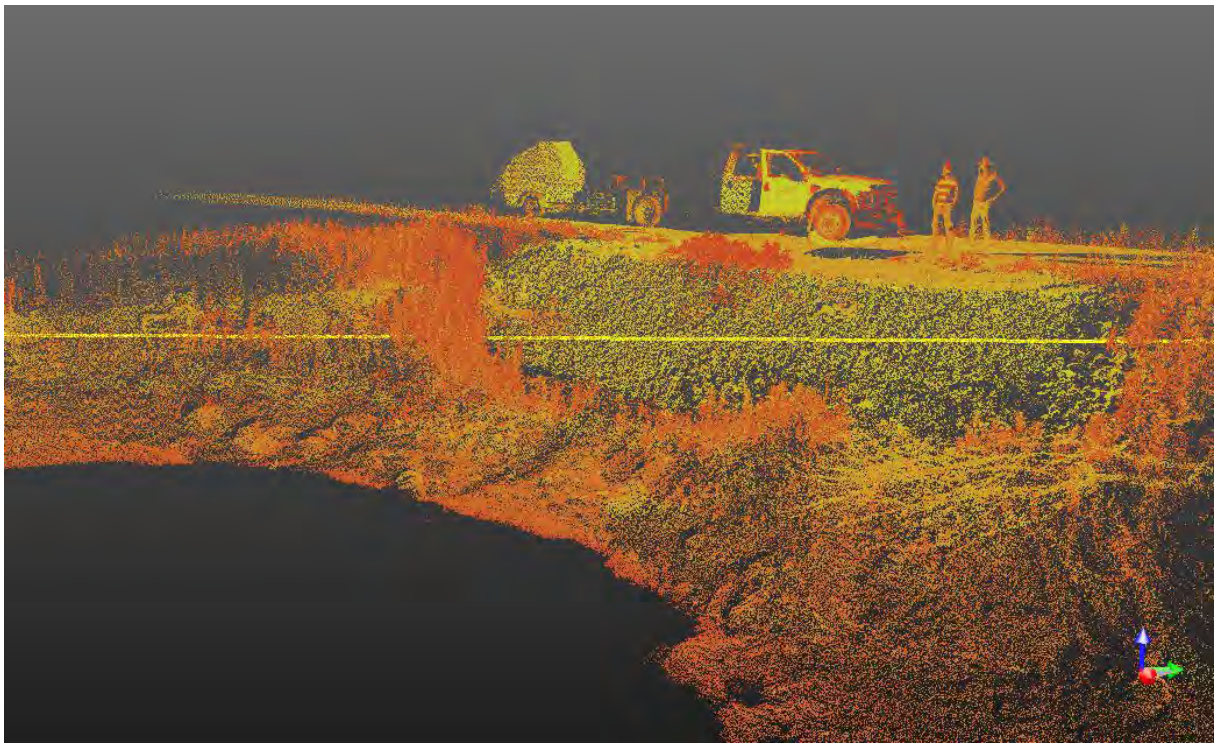

Figure 99. Raw point cloud data showing intensity contrast – TS5 Pottawattamie County

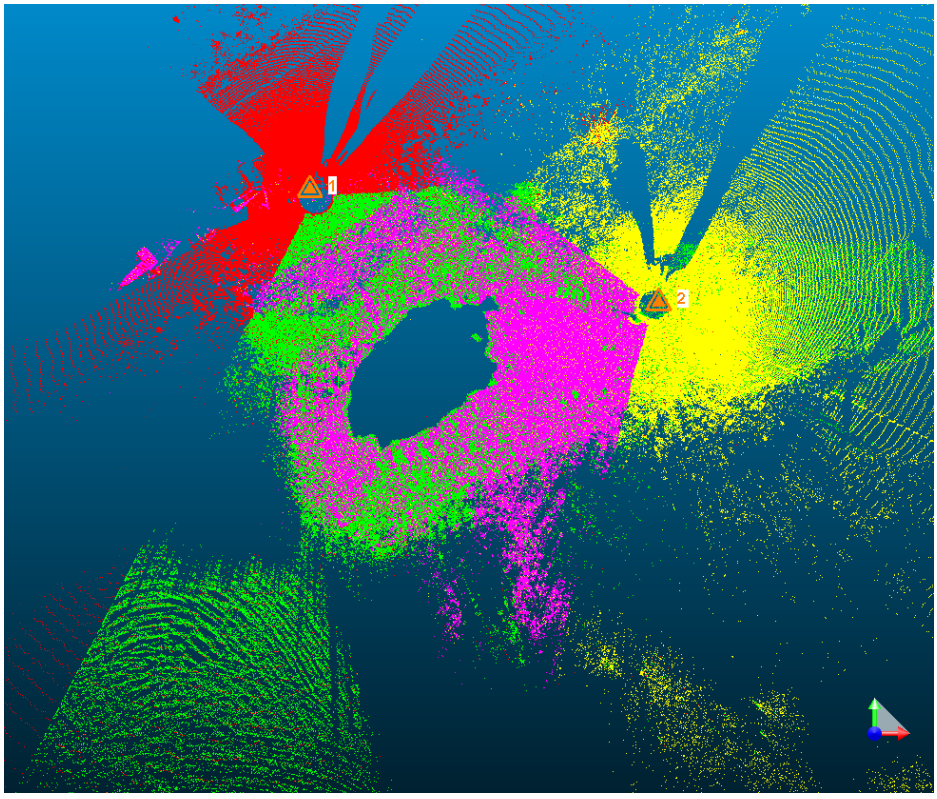

Figure 100. Overhead view of scanned point cloud – TS5 Pottawattamie County

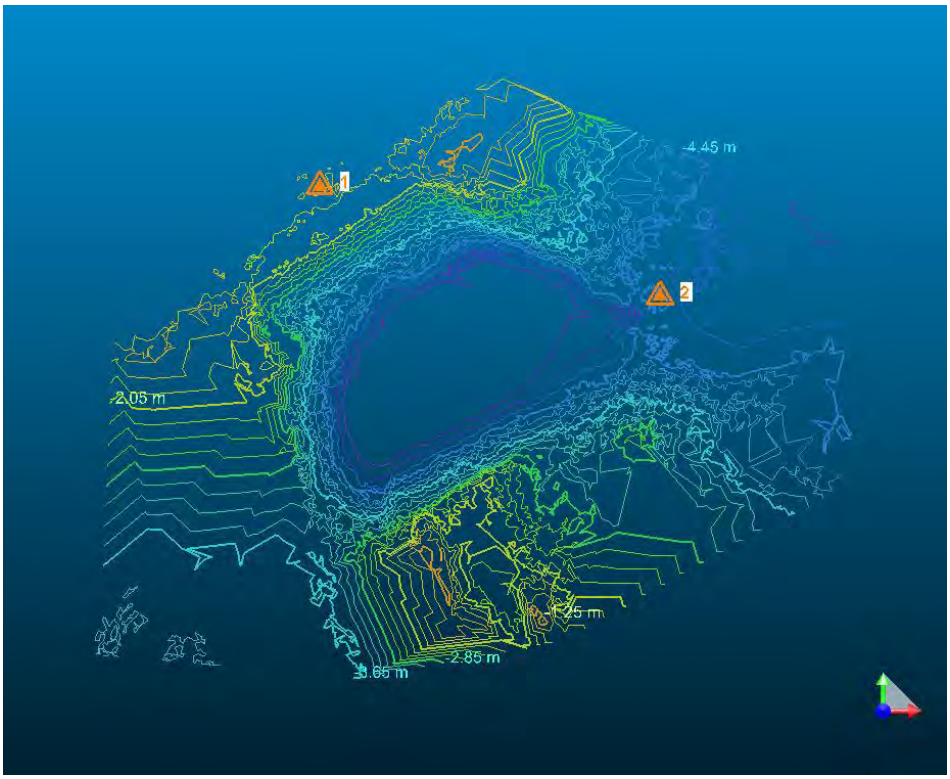

Figure 101. Contour map of site used for volumetric calculations – TS5 Pottawattamie County

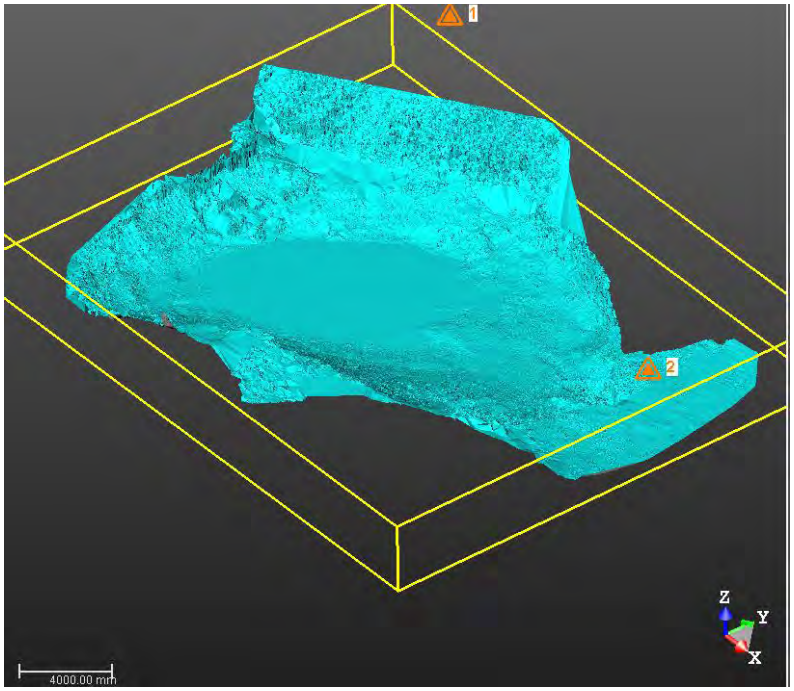

Figure 102. Meshed surface used for volumetric calculations – TS5 Pottawattamie County

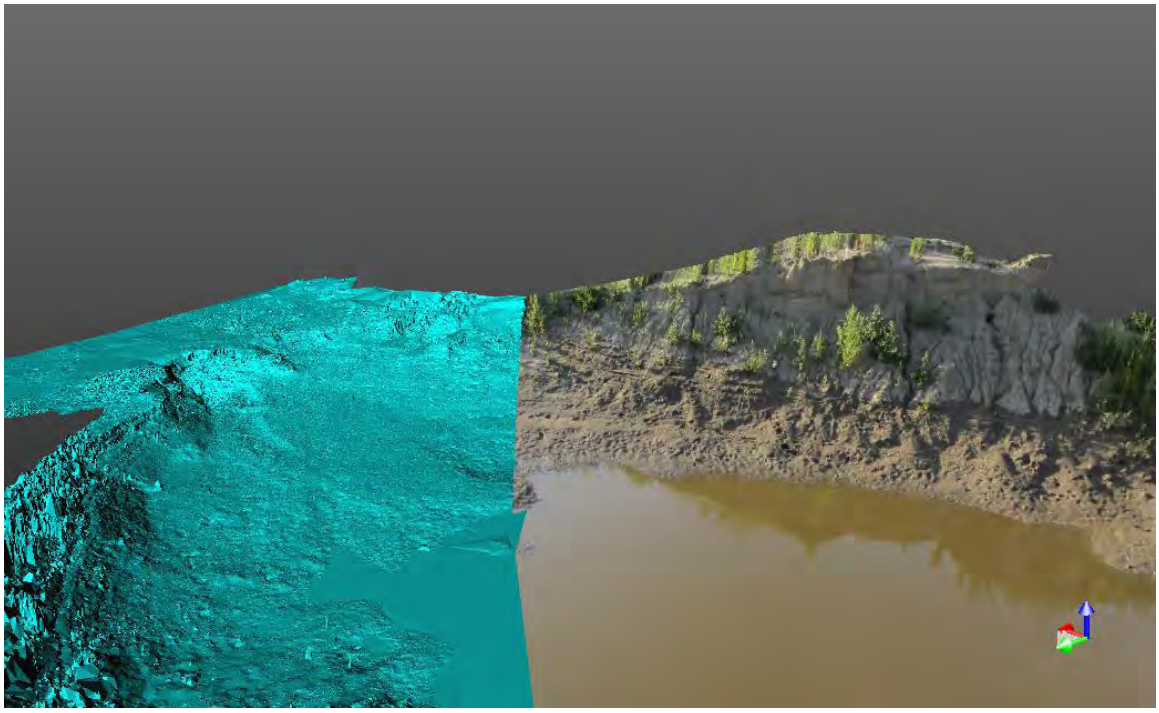

Figure 103. Meshed surface with photo overlay to show colored mesh surface – TS5 Pottawattamie County

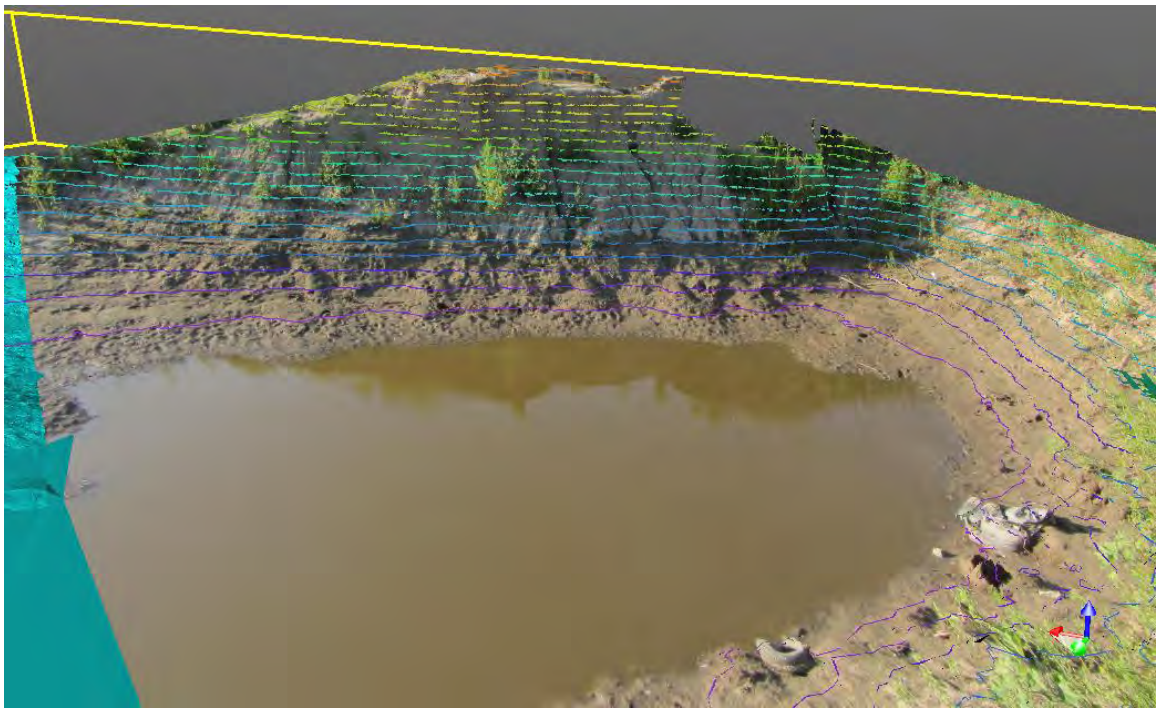

Figure 104. Colored mesh surface with 0.6 m (2 ft) contour lines – TS5 Pottawattamie County

Figure 105. Colored point cloud data – TS5 Pottawattamie County

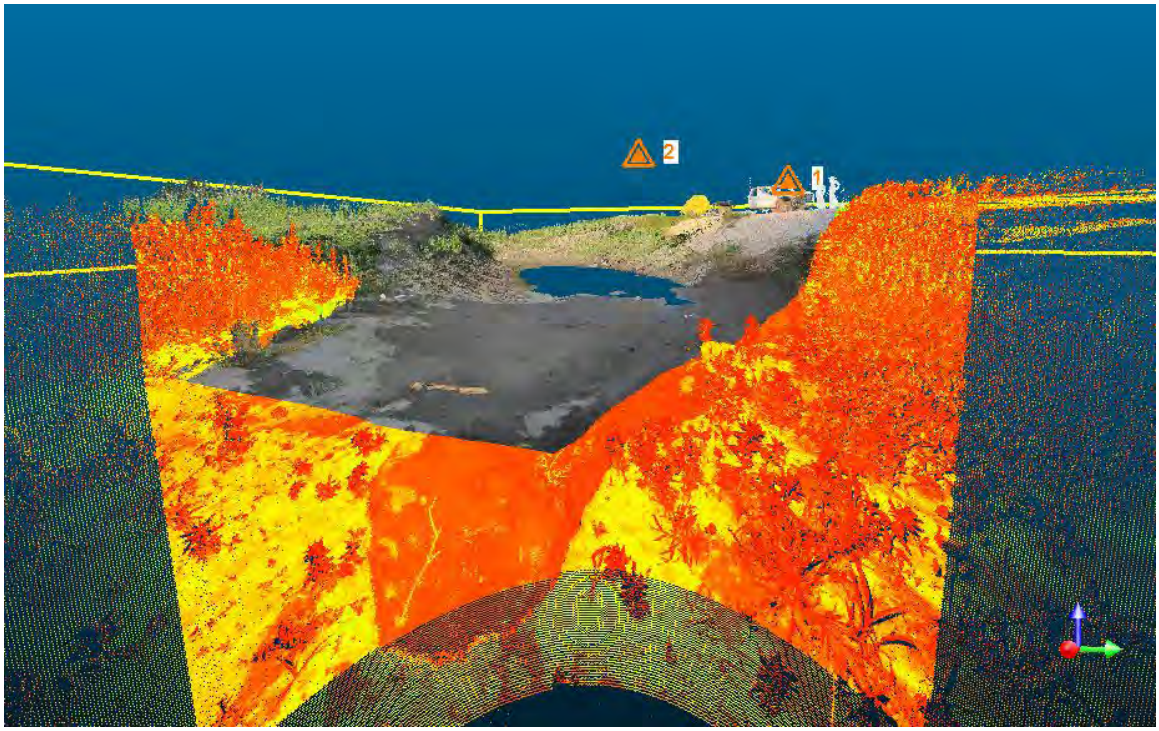

Figure 106. Merged point cloud with colored surface from photo – TS5 Pottawattamie County

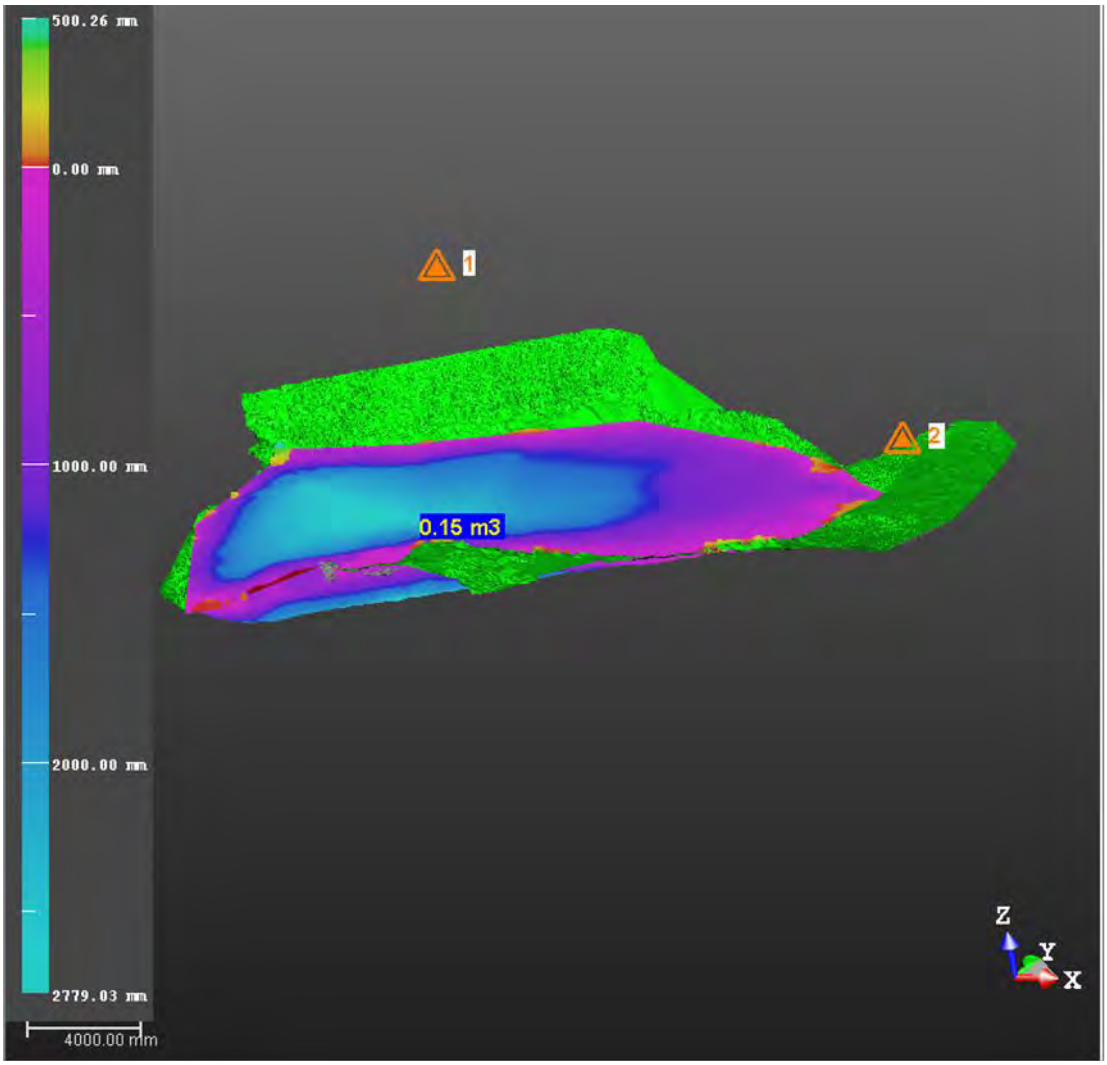

Figure 107. Rendering of volume calculations – TS5 Pottawattamie County

TS6 – River Road North (Gravel)

TS6 is a gravel road segment located River Road North, north of Council Bluffs, Iowa. Testing was conducted over a length of about 5170 m along the middle of the lane. The segment consisted of about 160 mm thick gravel layer underlain by natural subgrade (note: depth determined from DCP tests). The Pottawattamie County soil survey report indicates that the natural subgrade soils in this region consist of silty to clayey alluvium material in the top 600 mm of the subgrade and are classified as A-4, A-6, and A-7, or CL-ML, CL, and CH soils. According to the soil survey report, these soils exhibit low to moderate drainability with saturated hydraulic conductivity varying from about 0.04 to 9 μm/s (0.3 to 2.6 ft/day).

During the 2011 flood event, the TS was fully submerged for about one to three months (Figure 108and Figure 109). Reportedly, the flood waters receded in the area on 9/1/11. Roadway damages noted on this TS include eroded gravel surface layer, washed out culverts, and weep holes beneath the surface. Eroded gravel surface layers and washed out culverts were replaced at

the time of our first testing (Figure 113). Some pictures taken during testing are shown in Figure 110 to Figure 113.

In situ testing was conducted on this TS about 23 days after the flood waters receded (9/23/11), 54 days after flood waters receded (10/25/11), and after about 6 and 8 months (on 4/5/12 and 5/29/12). FWD tests were conducted at 16 to 20 locations and DCP tests were conducted at 1 location.

E_{FWD} and E_{SG} results from four different testing times along the TS are shown in Figure 114. E_{SG} values were calculated based on deflections from the sensor located at 300 mm (12 in.) away from the center of the loading plate. DCP-CBR profiles at the two test locations from different testing times are shown in Figure 115. Box plots of E_{SG} values at different test times are shown in Figure 116. Some key findings from these in situ testing are as follows:

- The E_{SG} values in the whole TS were low and the quality is rated as "very poor," per AASHTO (1993). The E_{SG} values improved slightly over time (on average from about 11 to 19 MPa), likely because of subgrade material drying.
- The FWD test results showed soft conditions ($E_{SG} \leq 10$ MPa) in areas close to culverts, where the gravel was washed away and new gravel was placed, at all times of testing.
- DCP-CBR results also indicated "very poor" subgrade conditions (with CBR < 2 within the top 200 mm of subgrade) at 23 days after flooding, at a test location that showed the lowest E_{SG} value (9 MPa). The test area was located near a culvert, where gravel was washed away and new gravel was placed. The subgrade CBR values improved to "fair" to "good" conditions (with CBR = 6.0 and 8.8) at 6 and 8 months after testing (Figure 117).
- CBR of the gravel layer was about 3.0 on 9/23/11, but improved to > 60 on 4/5/12. This improvement is likely due to densification under traffic loads.

Figure 108. Aerial imagery showing pre-flood (from 6/28/10) conditions and test locations on TS6 – Pottawattamie County

Figure 109. Aerial imagery showing during flood (from 7/17/11) conditions and test locations on TS6 – Pottawattamie County

Figure 110. FWD plate depression and rutting under truck wheels near culvert (Picture taken on 9/23/2011) – Pottawattamie County

Figure 111. Newly placed gravel showing rutting near culvert (Picture taken on 9/23/2011) – Pottawattamie County

Figure 112. Replacement gravel cover over culvert (Picture taken on 9/23/2011) – Pottawattamie County

Figure 113. Location of newly placed gravel on TS6 over a metal pipe culvert (Picture taken on 9/23/11) – Pottawattamie County

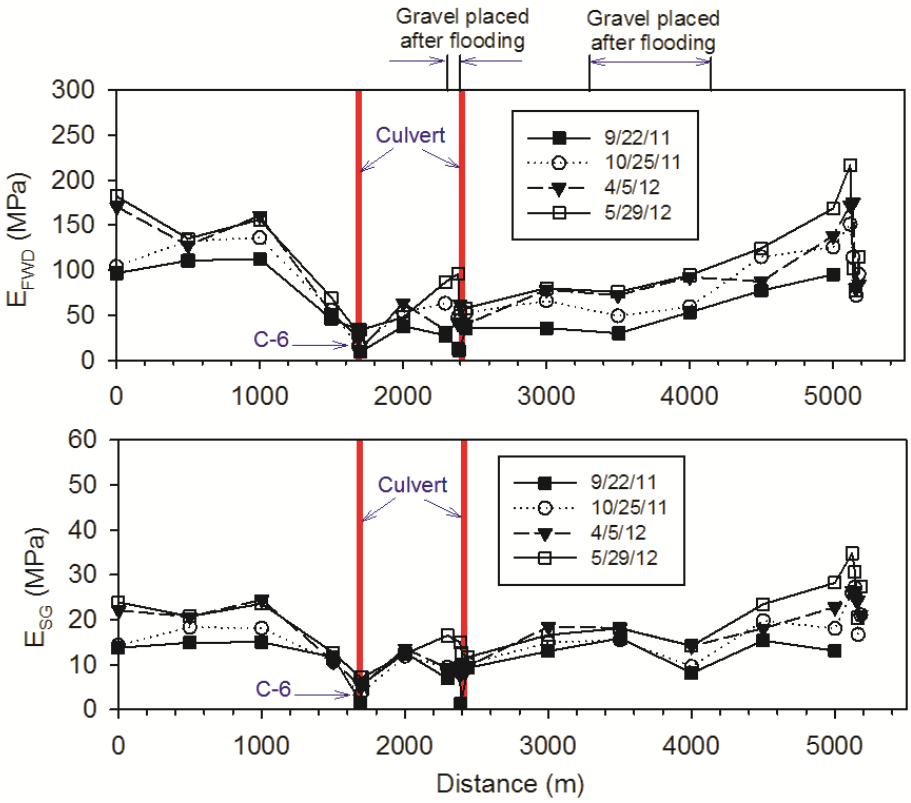

Figure 114. Surface FWD modulus and subgrade modulus at four different times after flooding on TS6 – Pottawattamie County

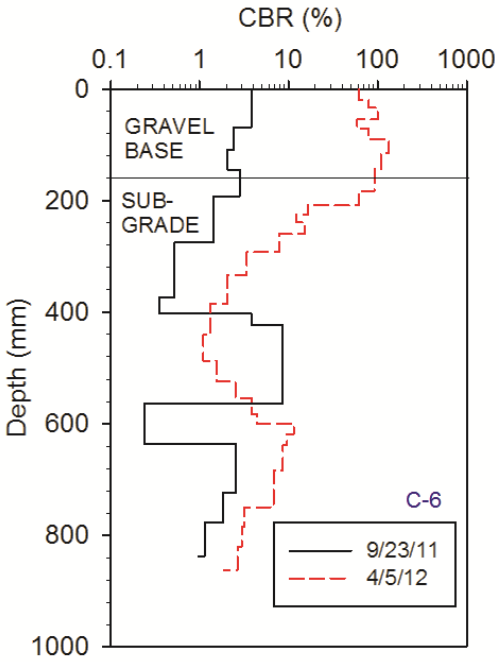

Figure 115. DCP-CBR profiles from two different testing times at C-6 test location on TS6 – Pottawattamie County

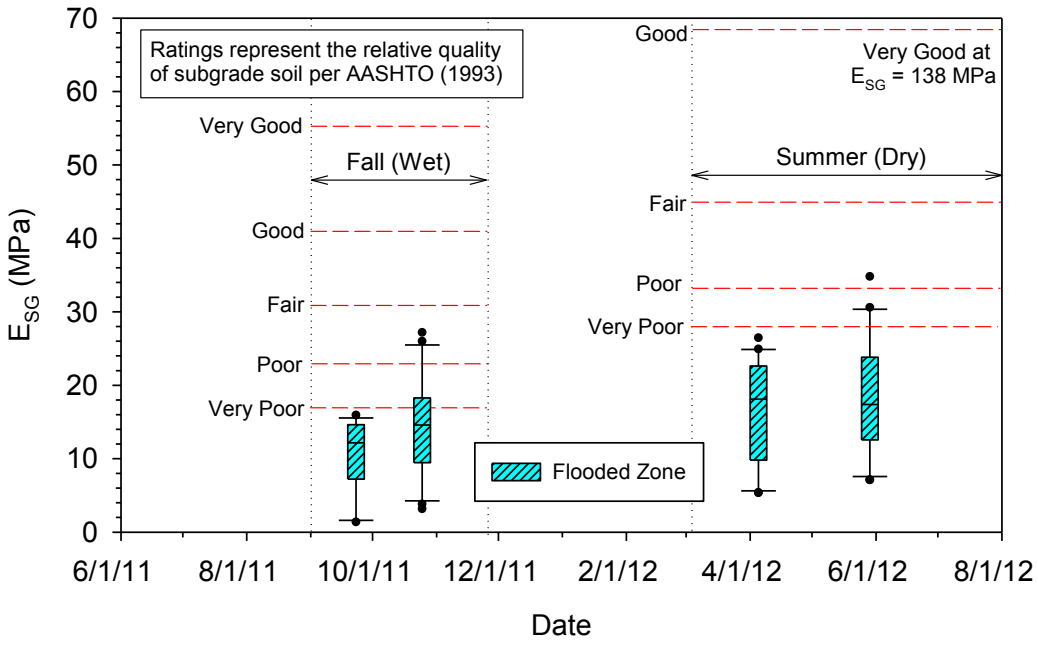

Figure 116. Box plots of subgrade modulus values in comparison with relative quality ratings on TS6 – Pottawattamie County

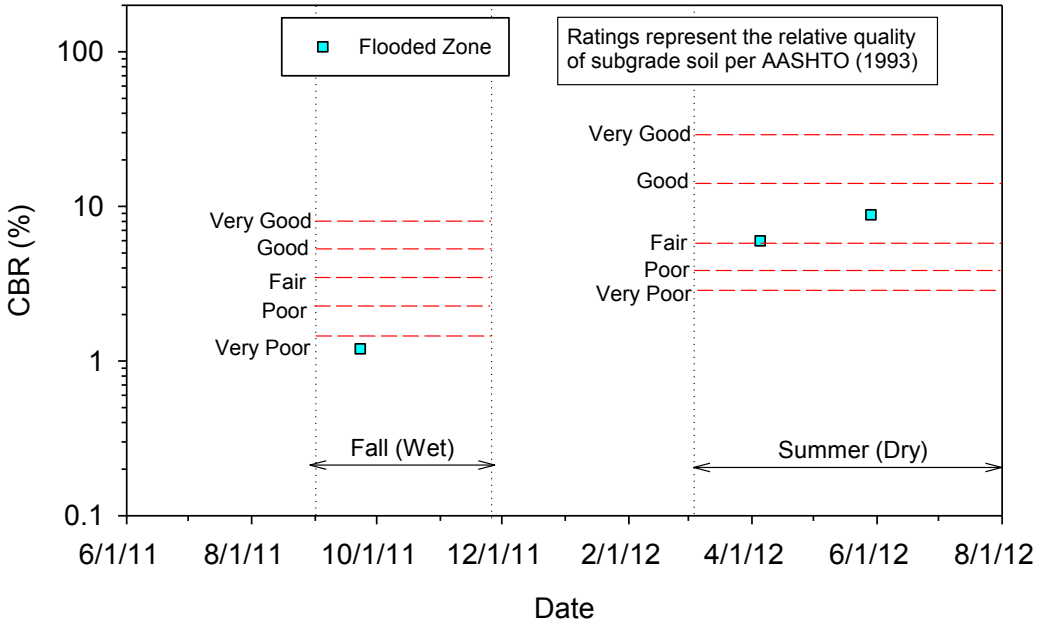

Figure 117. Subgrade CBR values at different testing times with relative quality ratings on TS6 – Pottawattamie County

TS7 – Desoto Avenue West (Oil Stabilized Base)

TS7 is a chipseal surfaced roadway over emulsified oil-stabilized base located on Desoto Avenue, north of Council Bluffs, Iowa. This TS is located west of TS4 (Desoto Avenue East) and TS3 (110th Street). Testing was conducted over a length of about 1629 m along the east bound lane. Similar to TS4, the segment consisted of thin chipseal at the surface over about 200 mm thick emulsified oil-stabilized base underlain by natural subgrade. The Pottawattamie County soil survey report indicates that the natural subgrade soils in this region consist of silty to clayey alluvium material in the top 600 mm of the subgrade and are classified as A-4, A-6, and A-7 or CL-ML, CL, and CH soils. The saturated hydraulic conductivity of the material vary from about 0.04 to 9 μm/s (0.01 to 2.6 ft/day).

During the 2011 flood event, this TS was fully submerged under water for nearly one to three months (Figure 118 and Figure 119). The flood waters receded in a portion of this TS on 9/1/11, but in some areas flood waters overtopped the roadway till 9/31/11. During the flood event, chipseal coat was stripped off (delaminated) at a few locations and granular shoulder material was eroded at isolated locations (shown as road scour in Figure 119). Weep holes were observed around culverts along the TS. Photos taken during field testing are shown in Figure 120 and Figure 122.

In situ testing was conducted on this TS about a month after flood waters receded on 10/25/11, and after about 6 and 8 months (on 4/5/12 and 5/29/12). FWD tests were conducted at22 locations. In addition, GPR scans were performed on 6/19/12.

E_{FWD} and E_{SG} results from three different testing times along the TS are shown in Figure 123. Review of aerial images indicated pre-flood ponding in lower elevation areas, and those zones are also identified Figure 123. E_{SG} values were calculated based on deflections from the sensor located at 300 mm (12 in.) away from the center of the loading plate. Box plots of E_{SG} values with measurements at different test times are shown in Figure 124. Some key findings from these in situ testing are as follows:

- The E_{SG} values in the whole TS were low and the quality is rated as "very poor" to "poor," per AASHTO (1993). The E_{SG} values did not change over time (varied on average from 16 to 17 MPa).
- With the exception of granular shoulder loss at a few locations, which was replaced shortly after the flood event, no significant distresses or damages were noted on this roadway. Some weep holes were observed around culvert locations and were also found in GPR scans as discussed below.

Figure 118. Aerial imagery before flooding (from 6/28/10) and during flooding (from 7/17/11) on TS7 – Pottawattamie County

Figure 119. Aerial imagery before flooding (from 6/28/10) and during flooding (from 7/17/11) showing road scour and culvert locations on TS7 – Pottawattamie County

Figure 120. Water overtopping Desoto Avenue on 9/21/11 and delamination of chipseal coat at the surface (Pictures taken on 9/21/11) – Pottawattamie County

Figure 121. Delaminated surface chipseal on Desoto Avenue due to flood waters overtopping the roadway (Pictures taken on 10/25/11) – Pottawattamie County

Figure 122. Weep holes around culvert inlets on TS7 (Picture taken on 10/25/11) – Pottawattamie County

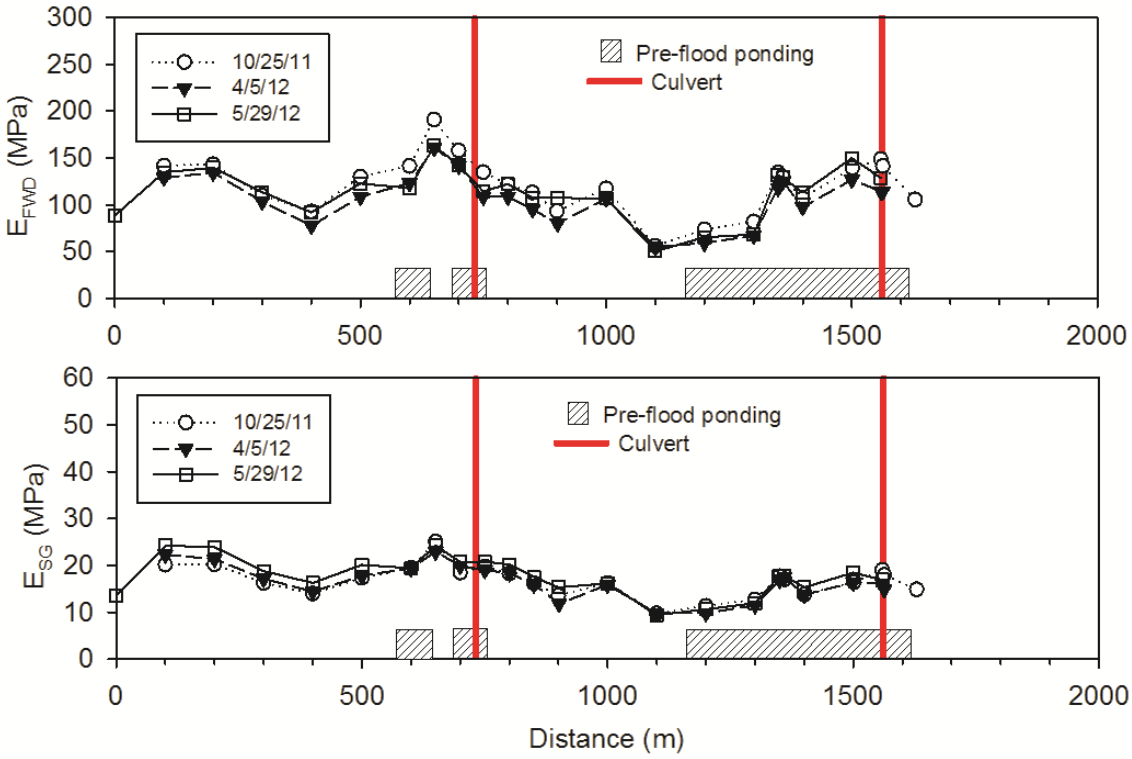

Figure 123. Surface FWD modulus and subgrade modulus at three different times after flooding on TS7 (entire TS was flooded and pre-flood ponding zones identified from aerial maps) – Pottawattamie County

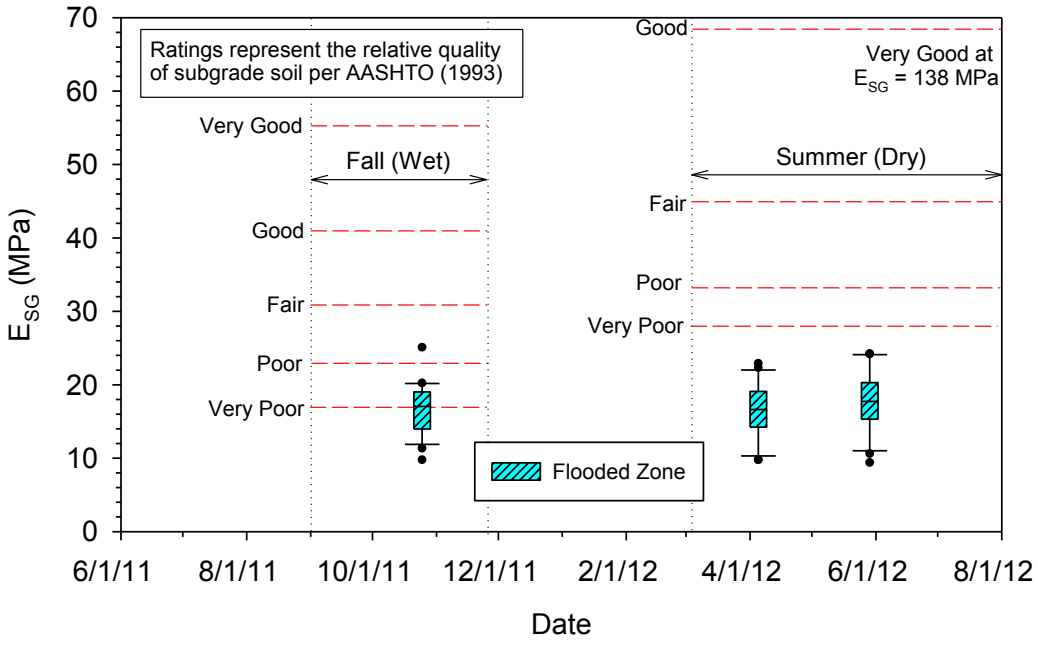

Figure 124. Box plots of subgrade modulus values in comparison with relative quality ratings on TS7 – Pottawattamie County

GPR scans were performed using 400 and 900 MHz antennas on 6/19/12 along the roadway between 720 m and 750 m stations, and 1550 m and 1580 m. The scanning was conducted to: (a) identify culverts or any other features beneath the surface (e.g., weep holes), and (b) delamination at the interface of chipseal and the stabilized gravel surface. GPR scan results longitudinally along the roadway are shown in Figure 125 to Figure 126. Some key features observed in the GPR scans are as follows:

- Culvert location was not clearly identified in the scans shown in Figure 125.
- Weep holes were noted at several locations in the scans as shown in Figure 126 and Figure 127.

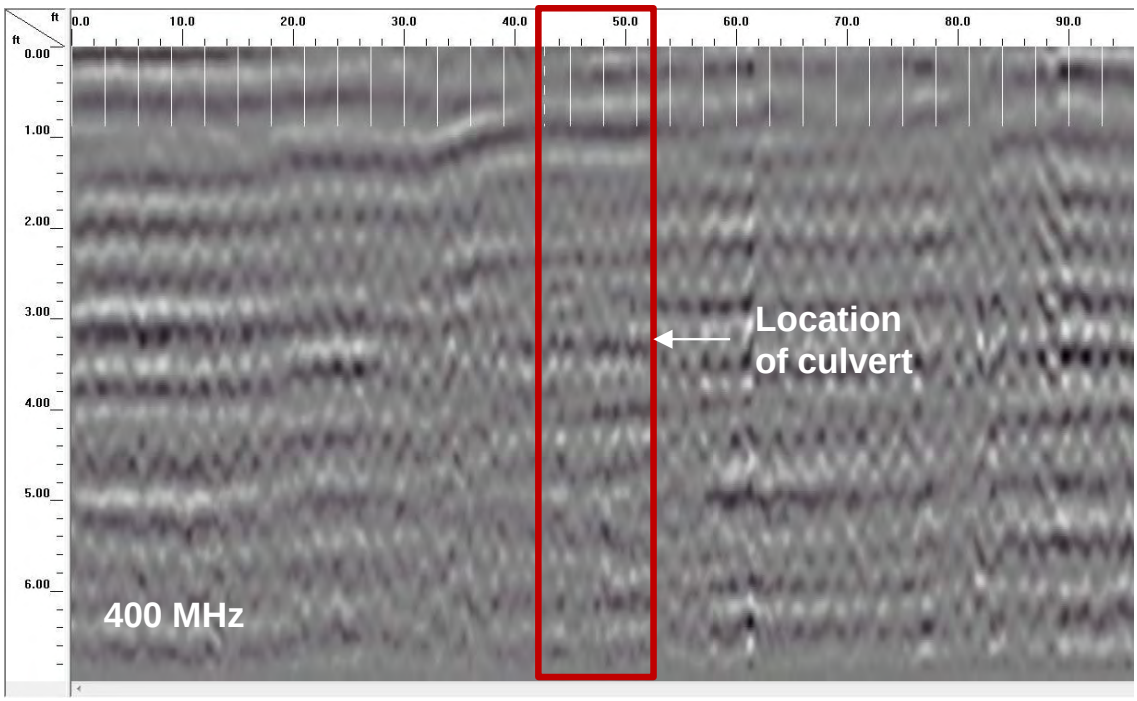

Figure 125. GPR scan using 400 MHz antennas on TS7 showing location of culvert (at station 724 m) – Pottawattamie County

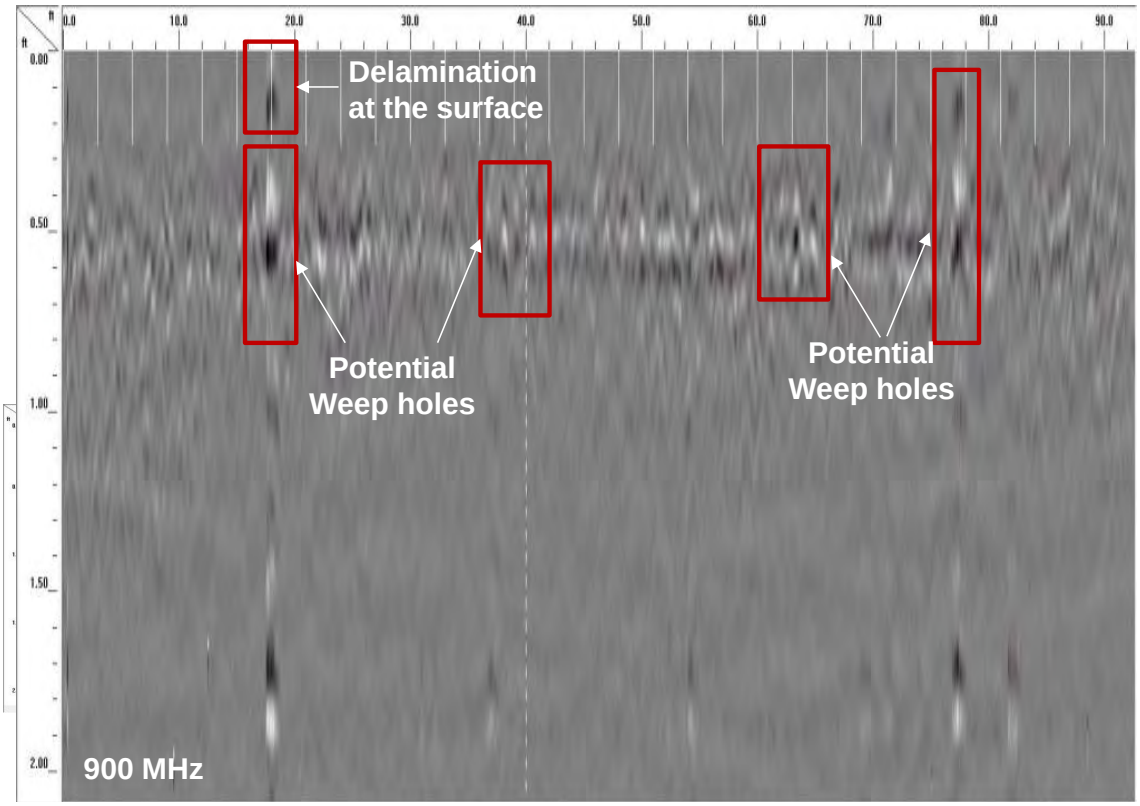

Figure 126. GPR scan using 900 MHz antenna on TS7 showing potential weep holes in the subgrade (between 720 m and 750 m stations on east bound lane) – Pottawattamie County

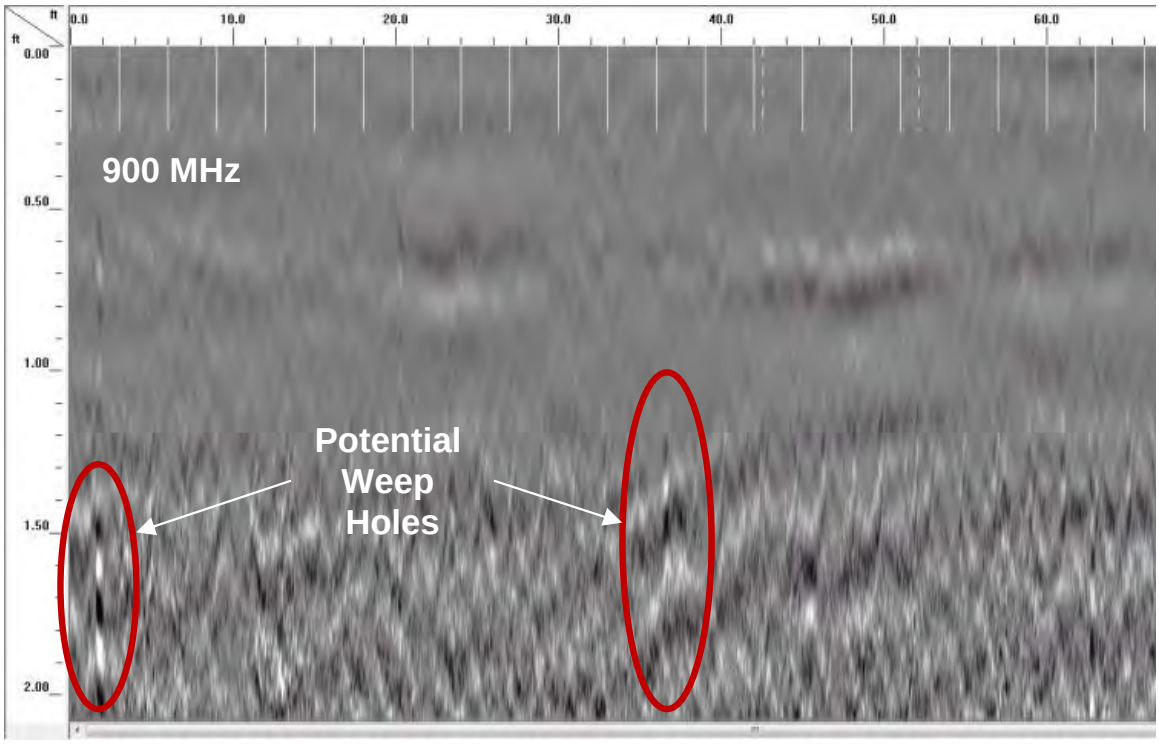

Figure 127. GPR scan using 900 MHz antenna on TS7 showing potential weep holes in the subgrade (between 1550 m and 1580 m stations on east bound lane) – Pottawattamie County

Fremont County

Field testing in Fremont County was conducted on four test segments: 260th Street, 285th Street, 185th Avenue, and 220th Street. These test segments varied in length from about 355m (500 ft) to 6.67 km (4.1 miles), by flood condition (fully or partially flooded), and type of surfacing (gravel and chip seal coat). A summary of all test segments with tests conducted, field notes, and subgrade soil information (from Fremont County USDA Soil Survey Report) is provided in Table 11. Locations of the test segments are shown in Figure 128.

FWD tests were conducted at 16 to 47 locations, while DCP testing was conducted at 2 to 6 selected test locations in each TS. GPR scans were performed two test segments (TS1 and TS2) where bridge backfill material was eroded away during flooding. Detailed results from each TS along with aerial imagery showing the extent of flood water are presented in the following subsections of this report.

Table 11. Fremont County - Summary of field testing

TS	Date	In Situ Tests	Comments
TS1	260th Street — Gravel (FEMA Site # 7) [355 m from 100 ft. west of the second bridge west of Bluff Rd. heading east toward Bluff Rd.		
	10/26/2011	35 FWD tests 4 DCP tests	Segment was partially submerged. Water covered approximately 125 m of the roadway segment. All tests performed on east bound lane in the right wheel path. Bridge backfill material was eroded at one of the bridge abutments. GPR scanned along bridge approaches to detect voids. The natural subgrade soils consisted of alluvium to clayey alluvium material in the top 600 mm of the subgrade and are classified as A-4 and A-7 or CL and CH soils. The saturated hydraulic conductivity of the material vary from about 0.04 to 9 μm/s.
	4/4/2012	34 FWD tests 3 DCP tests	
	6/19/2012	34 FWD tests 2 DCP tests 1GPR test	
TS2	285th Street — Gravel (FEMA Site # 37) [2100 m from the utility pole labeled "1" near the telephone tower west of Bluff Rd. heading east toward Bluff Rd.]		
	10/26/2011	35 FWD tests 5 DCP test	Segment was partially submerged. Water covered approximately 1050 m of the roadway segment. A scour hole was visible on the west side of the bridge approach. FWD and DCP tests weer conducted near bridge approaches to detect voids. GPR scanned along bridge approaches to detect voids. The natural subgrade soils consisted of alluvium to silty alluvium material in the top 600 mm of the subgrade and are classified as A-4 and A-7 or CL soils. The saturated hydraulic conductivity of the material vary from about 6.4 to 9 μm/s.
	4/4/2012	35 FWD tests 2 DCP tests	
	6/19/2012	35 FWD tests 2 DCP tests 1 GPR test	
TS3	185th Avenue — Gravel (FEMA Sites # 18 and 19) [6678 m from the survey marker at the s-curve south of the 225th St. to 200th St.]		
	10/27/2011	47 FWD tests 6 DCP tests 1 hand auger boring	Segment was mostly submerged. Approximately 450 m segment of gravel was washed away. Some sand deposits were observed (< 50 m). Rutting was observed at several locations along the segment. Gravel depth was generally about 140 mm, but varied from about 65 to 100 mm in a few locations. The natural subgrade soils consisted of silty to clayey to sandy alluvium material in the top 600 mm of the subgrade and are classified as A-2-4, A-4, A-6, and A-7 or SM, CL, ad CH soils. The saturated hydraulic conductivity of the material vary from about 0.04 to 190 μm/s.
	4/4/2012	47 FWD tests 2 DCP tests	
	5/30/2012	47 FWD tests 6 DCP tests	
TS4	220th Street — Chip seal [1200 m from the utility pole located on the south side of roadway, east of the railroad tracks, and near the elevated railroad control building heading east]		
	10/28/2011	16 FWD tests 2 DCP tests	Segment was partially submerged. Approximately 180 m of road segment showed severe rutting and alligator cracking distresses. About 2 m long segment experienced surface stripping. Locations with severe stripping have been patched. Water covered approximately 500 m of the roadway segment. The natural subgrade soils consisted of alluvium to silty alluvium material in the top 600 mm of the subgrade and are classified as A-4 and A-7 or CL soils. The saturated hydraulic conductivity of the material vary from about 6.4 to 9 μm/s.
	4/4/2012	16 FWD tests 2 DCP tests	
	5/30/2012	16 FWD tests 2 DCP tests	

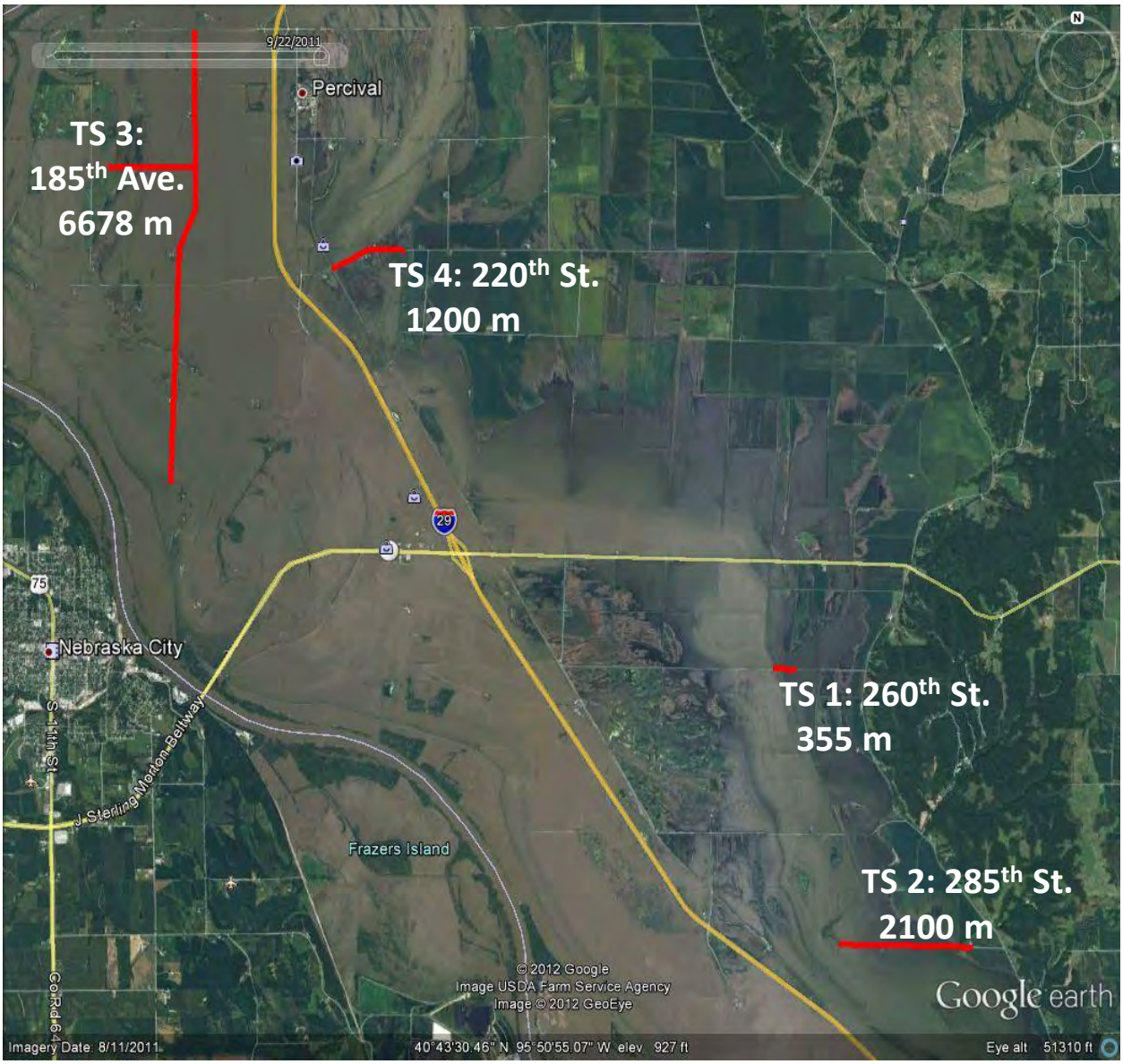

Figure 128. Location of all test segments – Fremont County (Image updated on 8/11/2011)

TS 1 – 260th Street (Gravel)

TS1 is a gravel road segment located on 260th Street, between I-29 and Bluff Road, north of Hamburg, Iowa. Testing was conducted over a length of about 355 m along the middle of the lane, on the gravel roadway and on the bridge approach backfill materials. The bridge structure consisted of a timber bridge and timber back wall abutments. Backfill materials used in the abutment were natural subgrade fill materials surfaced with gravel. The segment consisted of about 120 to 150 mm thick gravel layer underlain by subgrade (note: depths determined from DCP tests). The Fremont County soil survey report indicates that the natural subgrade soils in this region consist of alluvium to clayey alluvium material in the top 600 mm of the subgrade and are classified as A-4 and A-6 or CL and CH soils. According to the soil survey report, these soils exhibit moderately high drainability with saturated hydraulic conductivity varying from about 0.04 to 9 μm/s (0.01 to 2.6 ft/day).

During the 2011 flood event, the TS was partially submerged for about two to three months (Figure 129). Reportedly, the flood waters receded in the area during mid-September 2011. During the flood event, backfill material behind the east bridge approach was eroded away and new fill was placed prior to testing (Figure 130). The bridge crosses a drainage ditch. The drainage ditch embankment slopes (close to the bridge abutments) were scoured during the flood event (see pictures from 10/25/11 in Figure 131 to Figure 133). Field observations during 4/4/12 indicated continued erosion of backfill materials abutment, and scoured embankments (Figure 134). The scoured embankment slopes and bridge abutments were repaired by 6/19/12 using on-site clay fill material (Figure 135).

In situ testing was conducted on this TS in flooded and non-flooded areas for comparison, about 1 month after the flood waters receded (10/25/11), and after about 5 and 8 months (on 4/4/12 and 6/19/12). FWD tests were conducted at 34 to 35 locations (11 in non-flooded area and 6 in flooded area, and 18 on bridge approaches) and DCP tests were conducted at 4 locations (2 on bridge approaches, and 1 each in flooded and non-flooded areas). DCP tests on bridge approach was conducted to evaluate the compaction state of the newly placed backfill material. GPR scans were performed on 6/19/12 to detect potential voids/weep holes in the bridge abutment backfill material.

E_{FWD} and E_{SG} results from three different testing times along the TS are shown in Figure 136 and Figure 137, respectively, identifying the flooded/non-flooded areas and the bridge. E_{SG} values were calculated based on deflections from the sensor located at 300 mm (12 in.) away from the center of the loading plate. DCP-CBR profiles at the four test locations from different testing times are shown in Figure 138. Box plots of E_{SG} values comparing measurements in the flooded and non-flooded areas at different test times are shown in Figure 139. Some key findings from these in situ testing and observations are as follows:

- On average, E_{FWD} values were about 1.7 to 3.4 times higher in the non-flooded area than in the flooded area, at all times of testing. Similarly, E_{SG} values were about 1.3 to 1.5 times higher in the non-flooded area than in the flooded area. The values, however, have increased over time. On average, the E_{FWD} values increased from about 86 to 125 MPa in

the non-flooded area, and from about 33 to 75 MPa in the flooded area, from 1 month after flooding to 8 months after flooding.

- The E_{SG} values in the whole TS were low and the quality is rated as "very poor" to "poor," per AASHTO (1993). Lowest values were located in the middle of the flooded zone.
- DCP-CBR profiles (see PT13 on 10/26/11 in Figure 138) indicated that the approach backfill material close to the bridge approach (about 0.6 m away from the abutment) consisted of poorly compacted layers of fill with depth (with CBR < 2) , which is typically a result of thicker lifts placed during compaction.
- The CBR of the surface gravel layer was higher in the non-flooded zone compared to the flooded zone, by nearly 10 times at about one month after flooding. The CBR of the gravel layer increased in the flooded zone from about 7 to 25, from one month after flooding to 8 months after flooding.
- The subgrade CBR values (averaged over the top 300 mm) in the non-flooded zone was about 4 times higher than in the flooded zone. The subgrade CBR increased in the flooded zone from about 9 to 20, from one month after flooding to 8 months after flooding.
- The DCP and FWD test results on this TS illustrate that both subgrade and the surface gravel layers gained strength with time, likely because of subgrade material drying over time.
- Field observations indicated that clay fill material was used to stabilize the bridge abutments and block erosion of the backfill materials through the abutment walls. However, this material can be scoured away easily during a future flood event. Use of rip rap material as scour protection for the abutment wall would be a better repair and mitigation alternative.

GPR scans were performed using a 200 MHz antennas on 6/19/12 along the east and west approaches at 0.6 m to 2.4 m away from the north and south edges of the bridge. The scanning was conducted to identify potential voids/erosion beneath the surface in the backfill material, which can potentially cause gradual or sudden subsidence of the backfill material. GPR scan results are shown in Figure 141 and Figure 142. Some key features observed in the GPR scans are as follows:

- Backfill material layers sloped towards the bridge abutment are detected in the scans. This sloping is more apparent in scans closer to the edges (within 1m of the edge) than in scans that are close to the center.
- Areas with potential voids/backfill erosion are detected at about 0.76 m to 2.4 m beneath the surface.

Figure 129. Aerial imagery before flooding on left (from 10/28/10) and during flooding on right (from 8/11/11) on TS1 – Fremont County

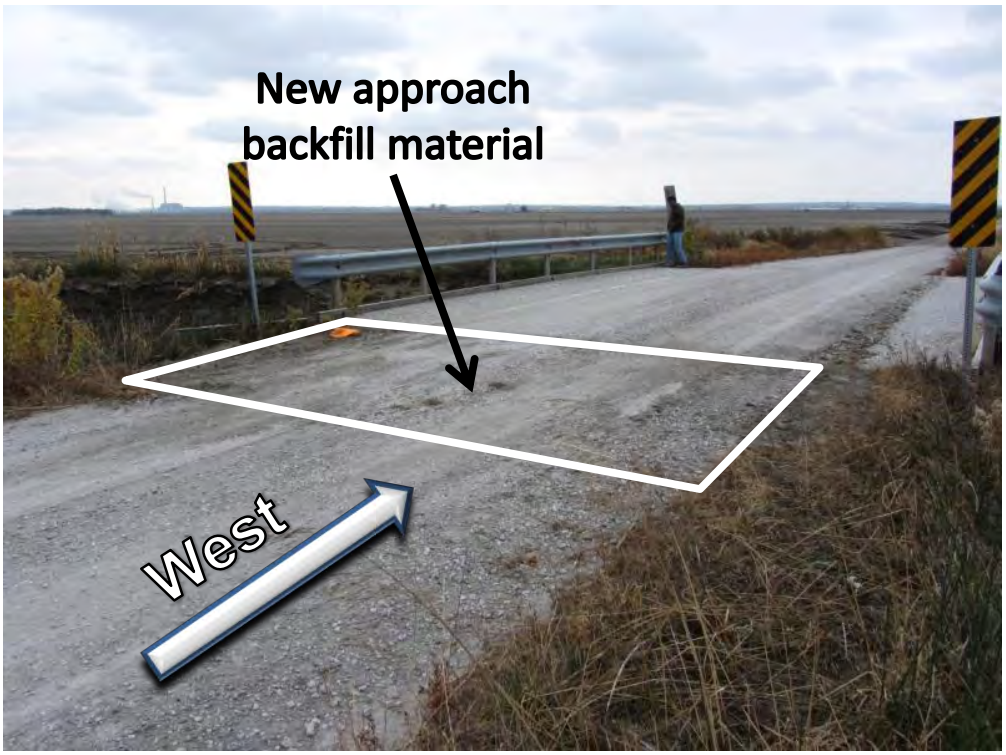

Figure 130. New bridge approach backfill material placed along the east approach on TS1 (Picture taken on 10/26/11) – Fremont County

Figure 131. ***Erosion of embankment material along the west bank on TS1*** **(Picture taken on 10/26/11) – Fremont County**

Figure 132. Erosion of embankment material along the west bank near abutment wing walls on TS1 (Picture taken on 10/26/11) – Fremont County

Figure 133. Erosion of backfill material behind the wing wall on TS1 (Picture taken on 10/26/11) – Fremont County

Figure 134. Bridge conditions on TS1 on 4/4/12 – Fremont County

Figure 135. Bridge conditions on TS1 on 6/9/12 – Fremont County

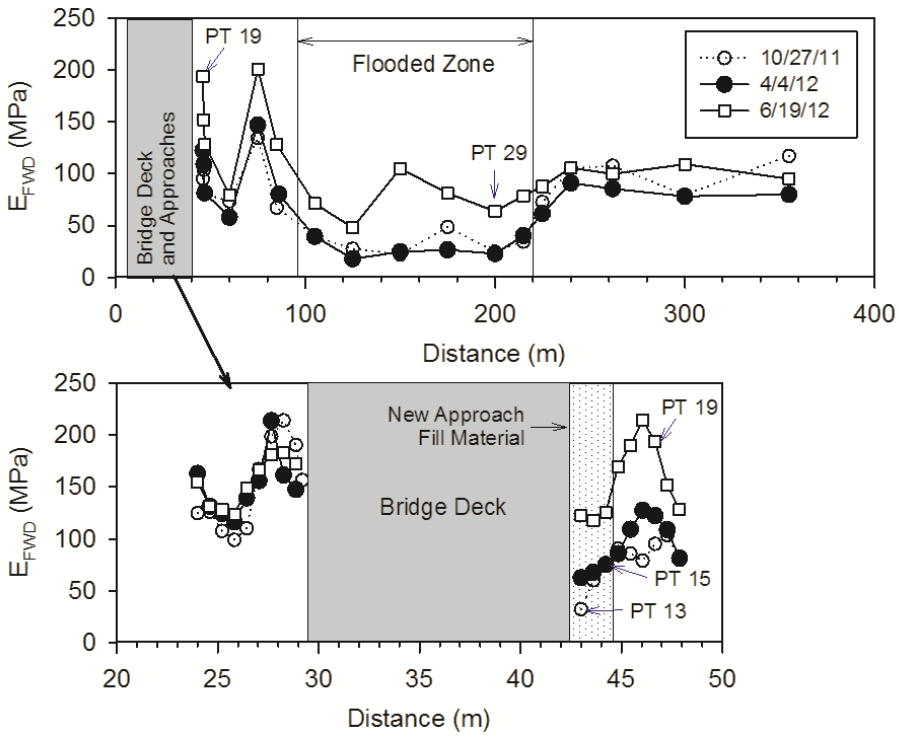

Figure 136. Surface FWD modulus at three different times after flooding on TS1 – Fremont County

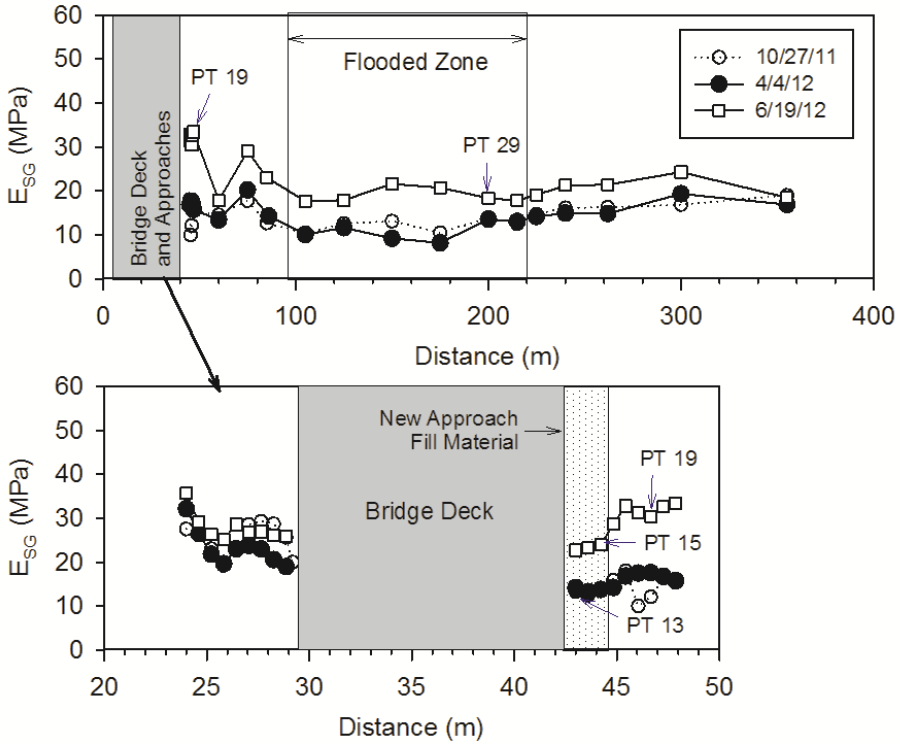

Figure 137. Subgrade modulus measurements at three different times after flooding on TS1 – Fremont County

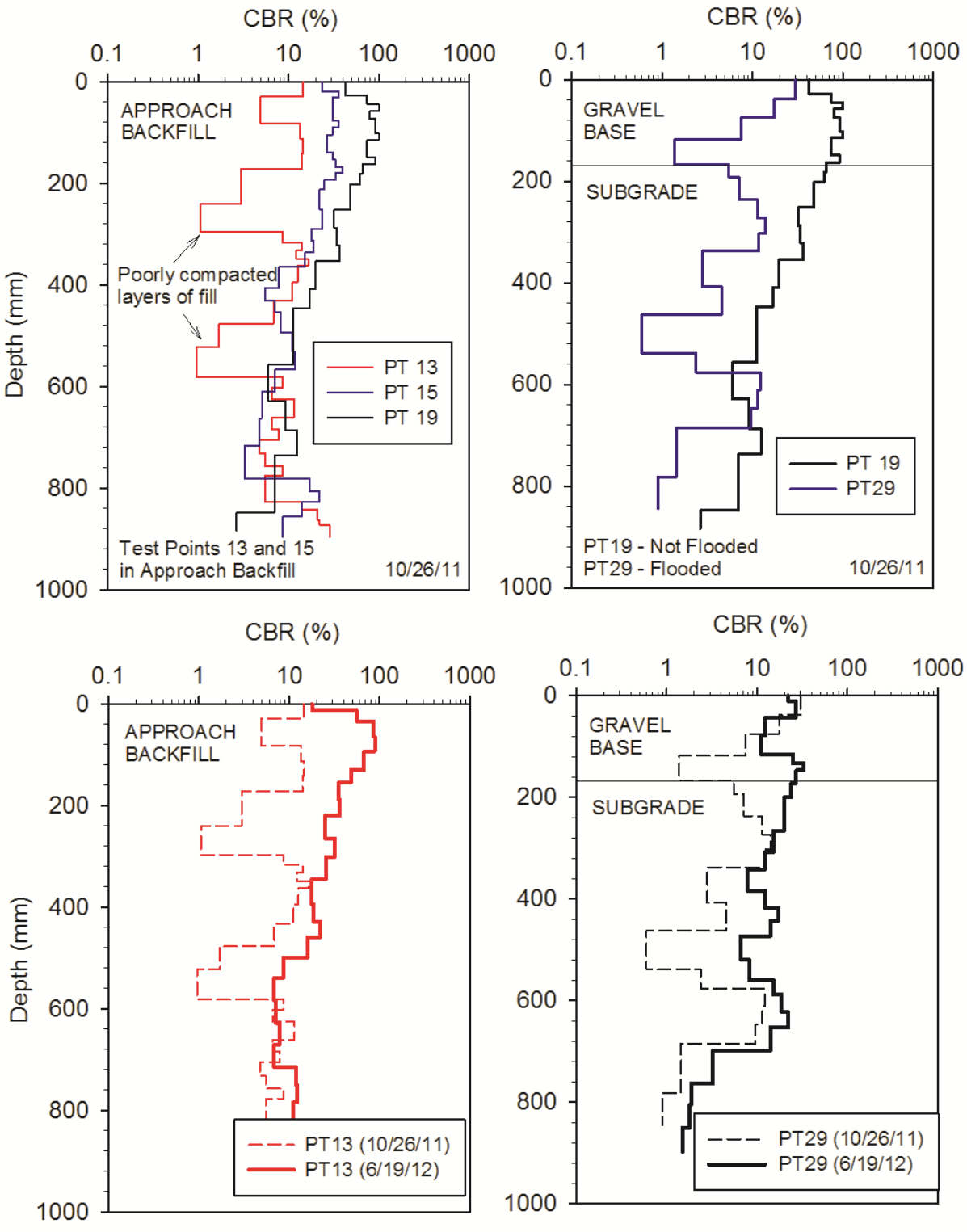

Figure 138. DCP-CBR profiles from two different testing times at five test locations on TS1 – Fremont County

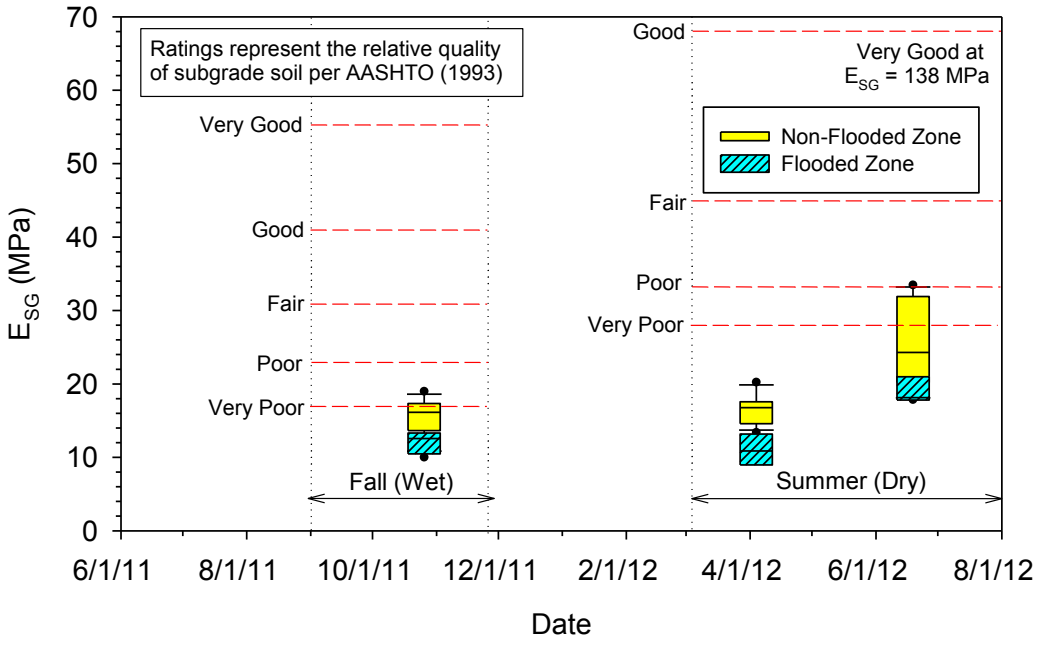

Figure 139. Box plots of subgrade modulus values in flooded and non-flooded zones in comparison with relative quality ratings on TS1 – Fremont County

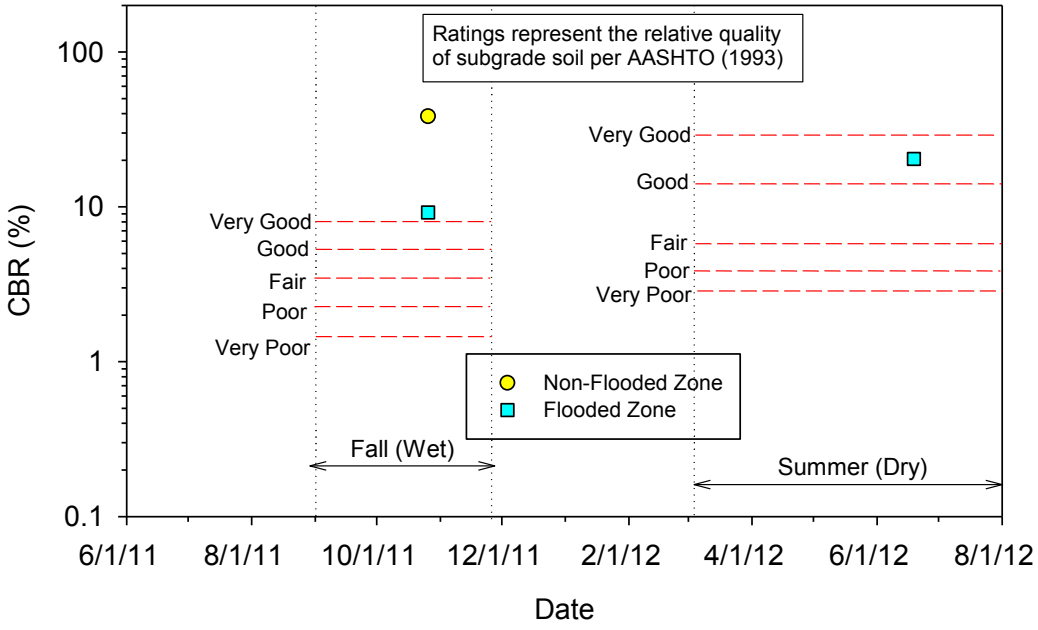

Figure 140. Comparison of subgrade CBR values in flooded and non-flooded zones with relative quality ratings on TS1 – Fremont County

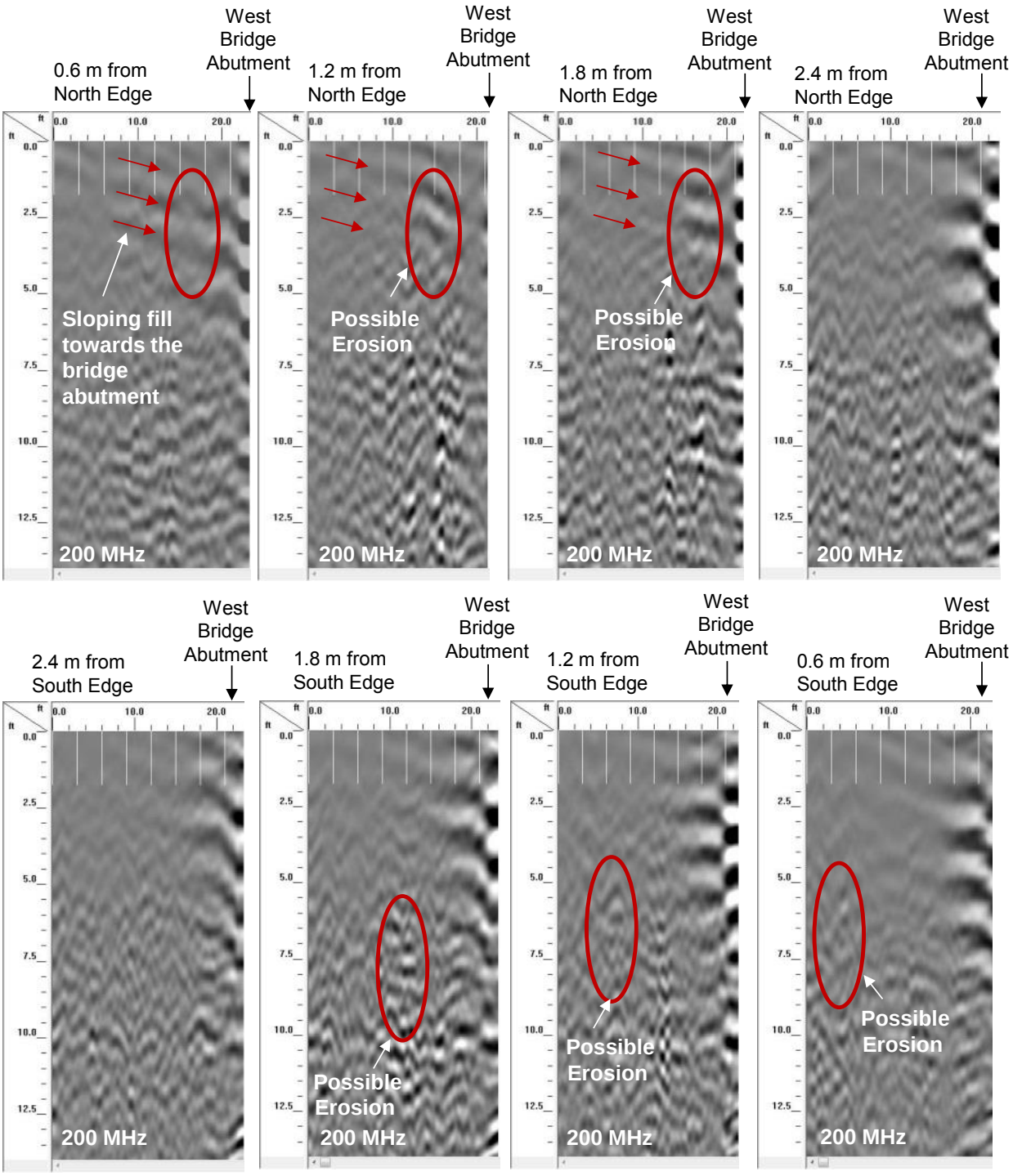

Figure 141. GPR scans using 200 MHz antenna on TS1 longitudinally along the west bridge approach backfill at 0.6 to 2.4 m away from the north and south edges of the bridge (note: 0 ft mark on the horizontal scale represents about 6.7 m (22 ft) away from the west abutment) – Fremont County

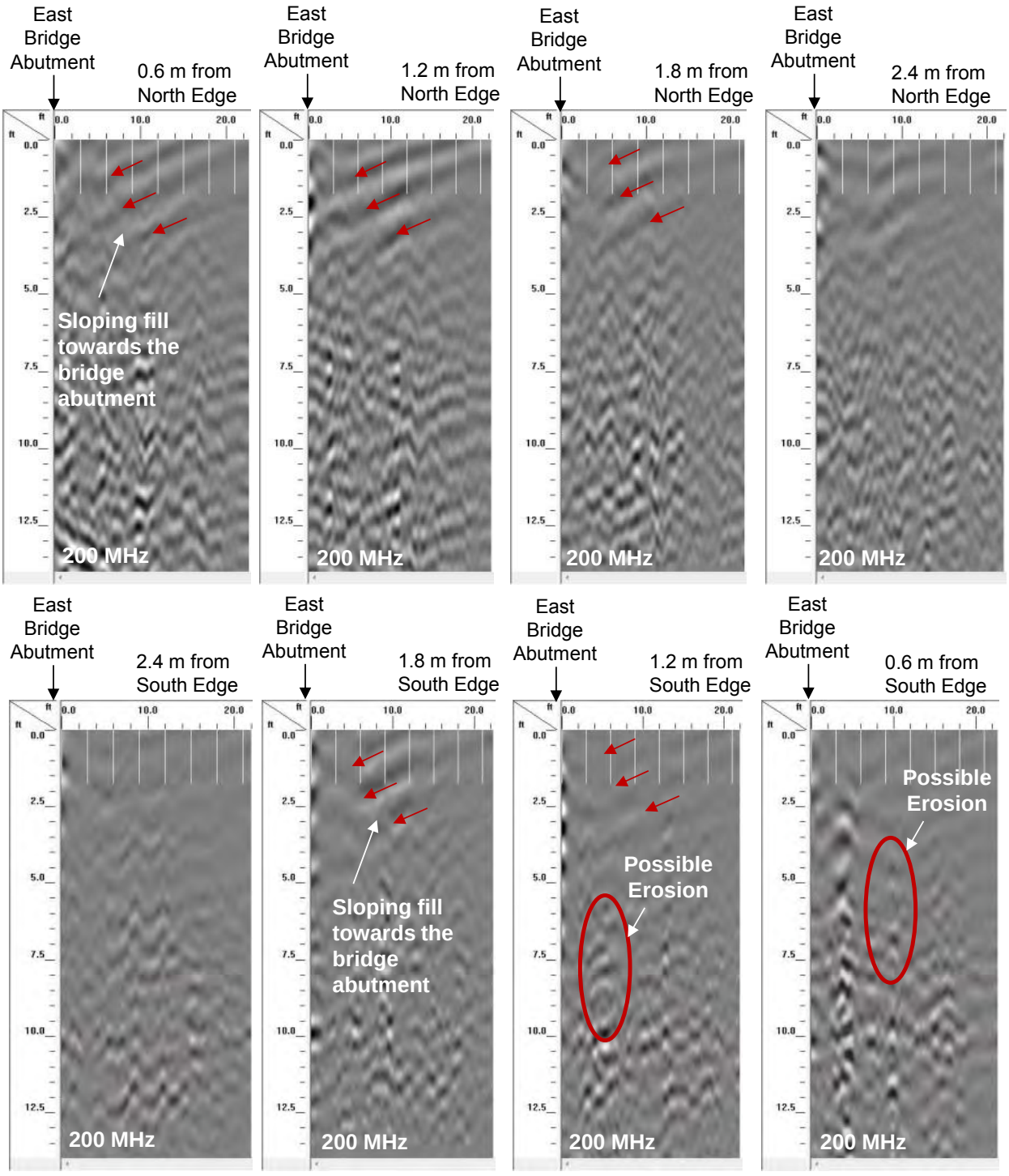

Figure 142. GPR scans using 200 MHz antenna on TS1 longitudinally along the east bridge approach backfill at 0.6 m to 2.4 m away from the north and south edges of the bridge (note: 0 ft mark on the horizontal scale represents about 6.7 m (22 ft) away from the west abutment – Fremont County

TS 2 – 285th Street (Gravel)

TS2 is a gravel road segment located on 285th Street (south of TS1) between I-29 and Bluff Road, north of Hamburg, Iowa. Testing was conducted over a length of about 2100 m along the middle of the lane, on the gravel roadway and on the bridge approach backfill materials. The bridge structure consisted of a timber bridge and timber back wall abutments. Backfill materials used in the abutment were natural subgrade fill materials surfaced with gravel. The segment consisted of about 120 to 150 mm thick gravel layer underlain by subgrade (note: depths determined from DCP tests). The Fremont County soil survey report indicates that the natural subgrade soils in this region consist of alluvium to silty alluvium material in the top 600 mm of the subgrade and are classified as A-4 and A-6 or CL soils. According to the soil survey report, these soils exhibit moderately high drainability with saturated hydraulic conductivity varying from about 6.4 to 9 μm/s (1.8 to 2.6 ft/day).

During the 2011 flood event, the TS was partially submerged for about two to three months (Figure 143). Reportedly, the flood waters receded in the area during mid-September 2011. During the flood event, backfill material behind the west bridge approach was eroded away forming voids beneath the surface gravel layer. Pictures taken on 10/26/11 are show in Figure 144 to Figure 146. Field observations on 4/4/12 indicated that the eroded backfill material on the west abutment was repaired, but some surface subsidence was observed, and new voids were observed on the east abutment (Figure 147).

In situ testing was conducted on this TS in flooded and non-flooded areas for comparison, about 1 month after the flood waters receded (10/26/11), and after about 5 and 8 months (on 4/4/12 and 6/19/12). FWD tests were conducted at 35 locations (14 in non-flooded area and 16 in flooded area, and 5 on bridge approaches) and DCP tests were conducted at 5 locations on the bridge approach to evaluate depth to void beneath the surface and at 1 location in the flooded area. GPR scans were performed on 6/19/12 to detect potential voids/weep holes in the bridge abutment backfill material.

E_{FWD} and E_{SG} results from three different testing times along the TS are shown in Figure 148 and Figure 149, respectively, identifying the flooded/non-flooded areas and the bridge. E_{SG} values were calculated based on deflections from the sensor located at 300 mm (12 in.) away from the center of the loading plate. Void profile perpendicular to the bridge in the bridge approach backfill is shown in Figure 150. DCP-CBR profiles at the middle of the roadway in the bridge approach and in the flooded area are shown in Figure 151. Box plots of E_{SG} values comparing measurements in the flooded and non-flooded areas at different test times are shown in Figure 152. Some key findings from these in situ testing and field observations are as follows:

- On average, E_{FWD} and ESG values were about the same in the flooded and non-flooded areas (ratio of non-flooded to flooded area values were about were about 0.8 to 1.1). The values, however, have increased over time. On average, the E_{FWD} values increased from about 79 to 112 MPa in the non-flooded area, and from about 80 to 105 MPa in the flooded area, from 1 month after flooding to 8 months after flooding.
- The E_{SG} values in the whole TS were low and the quality is rated as “very poor” to

"poor," per AASHTO (1993). Lowest values were located in the flooded zone (close to D-27 as noted on Figure 148 and Figure 149) that is located at a lower elevation (i.e., area that experienced deep waters above the roadway).
- DCP tests indicated void at depths of about 300 to 850 mm below surface (Figure 150).

GPR scans were performed using a 200 MHz antennas on 6/19/12 along the west approach at 1.2 m to 3.0 m away from the north and south edges of the bridge. The scanning was conducted to identify potential voids/erosion beneath the surface in the backfill material, which can potentially cause gradual or sudden subsidence of the backfill material. GPR scan results are shown in Figure 153. Some key features observed in the GPR scans are as follows:

- Similar to observations on TS1, backfill material layers sloping towards the bridge can be seen in the scans, within about 8 m of the bridge abutment.
- Areas with potential voids/backfill erosion are detected at about 1 m to 1.5 m beneath the surface.

Figure 143. Aerial imagery before flooding on left (from 10/28/10) and during flooding on right (from 8/11/11) on TS2 – Fremont County

Figure 144. Gravel surface on TS2 at the time of testing (Picture taken on 10/26/11)

Figure 145. Bridge approach on TS2 (Picture taken 10/26/11)

Figure 146. Void behind the west abutment wall due to erosion of backfill material at TS2 bridge (Pictures taken on 10/26/11) – Fremont County

Figure 147. West and east abutments on TS2 bridge (Pictures taken on 4/4/11) – Fremont County

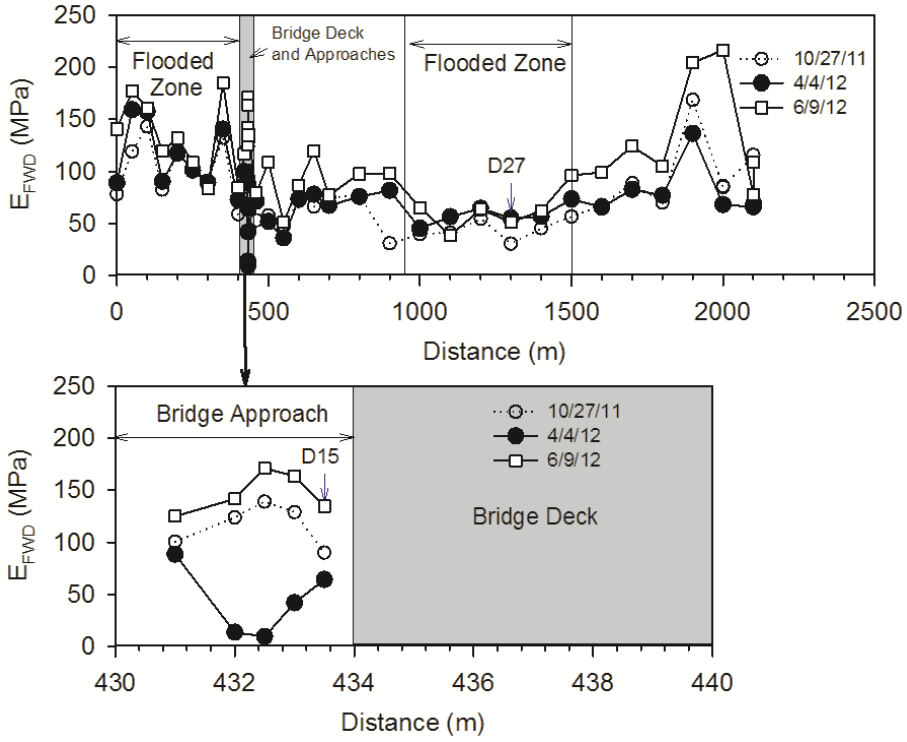

Figure 148. Surface FWD modulus at three different times after flooding on TS2 – Fremont County

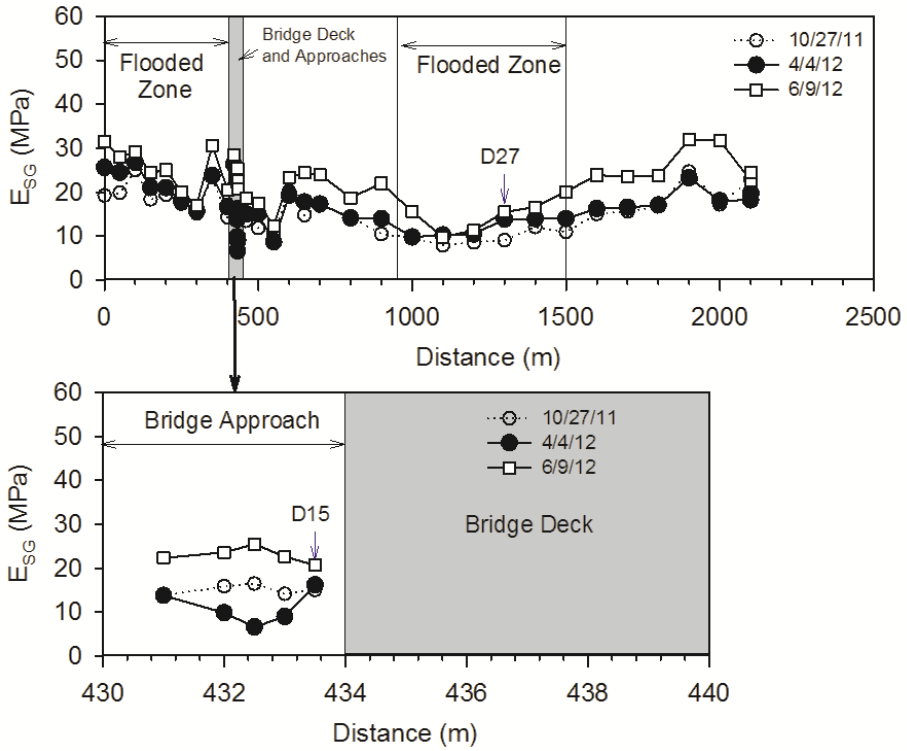

Figure 149. Subgrade modulus measurements at three different times after flooding on TS2 – Fremont County

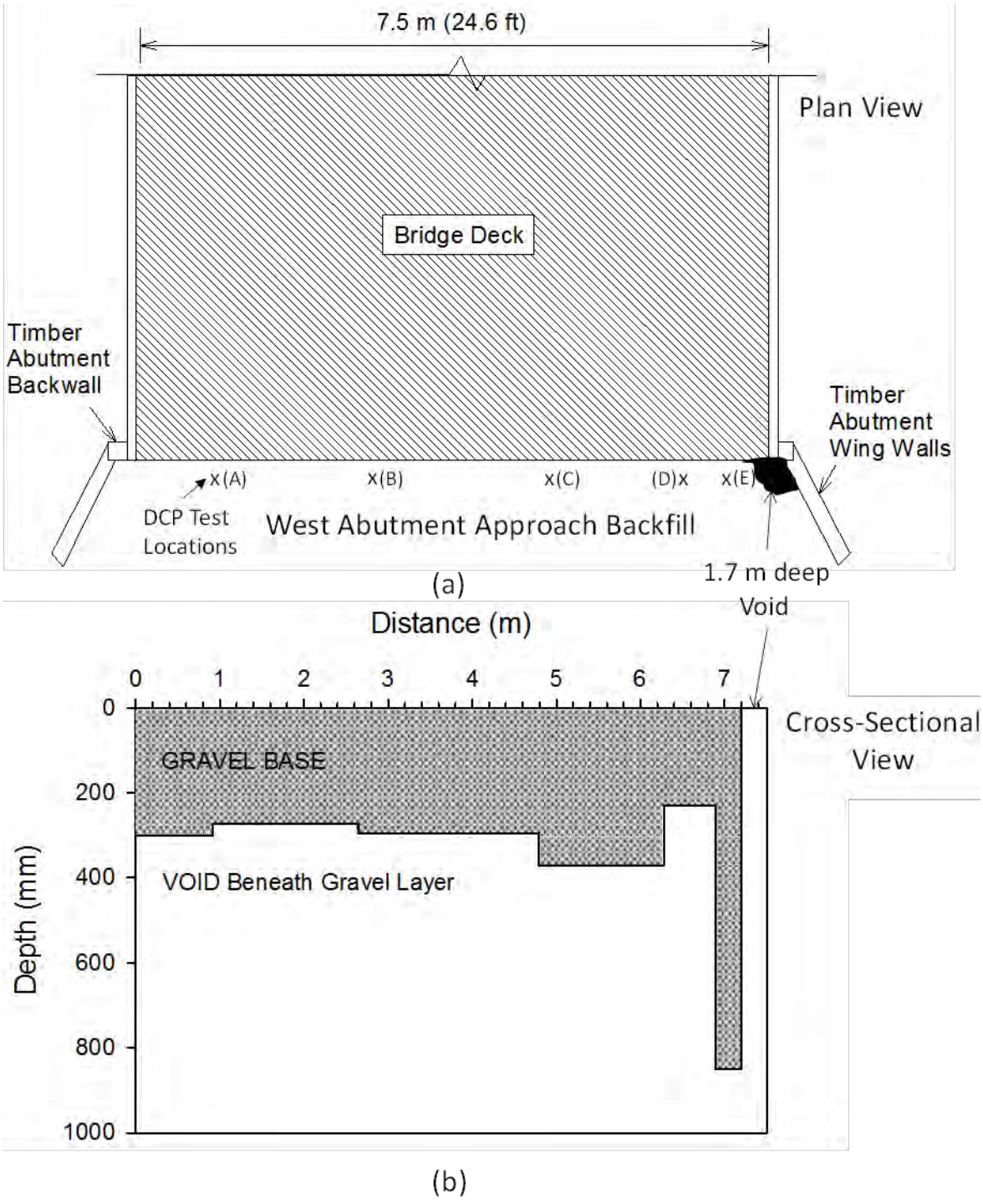

Figure 150. TS2 bridge approach: (a) Bridge deck plan view showing DCP test locations on the approach backfill, and (b) cross-sectional view showing thickness of gravel base and void beneath the gravel layer across the bridge (tests conducted on 10/25/11) – Fremont County

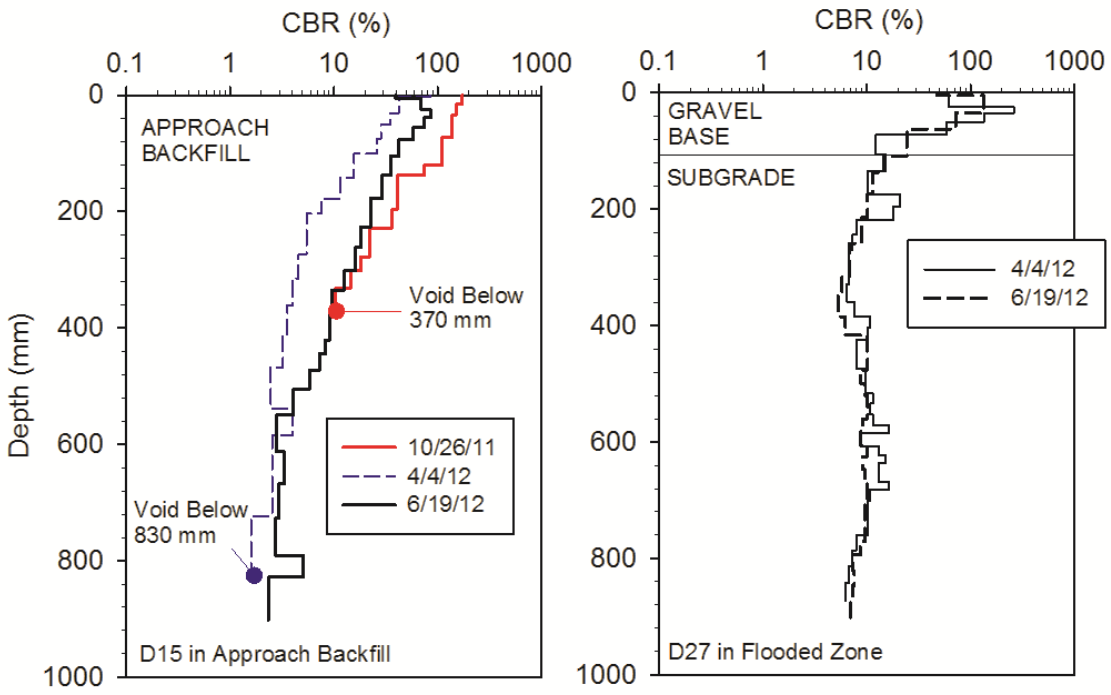

Figure 151. DCP-CBR profiles from three different testing times on TS2 – Fremont County

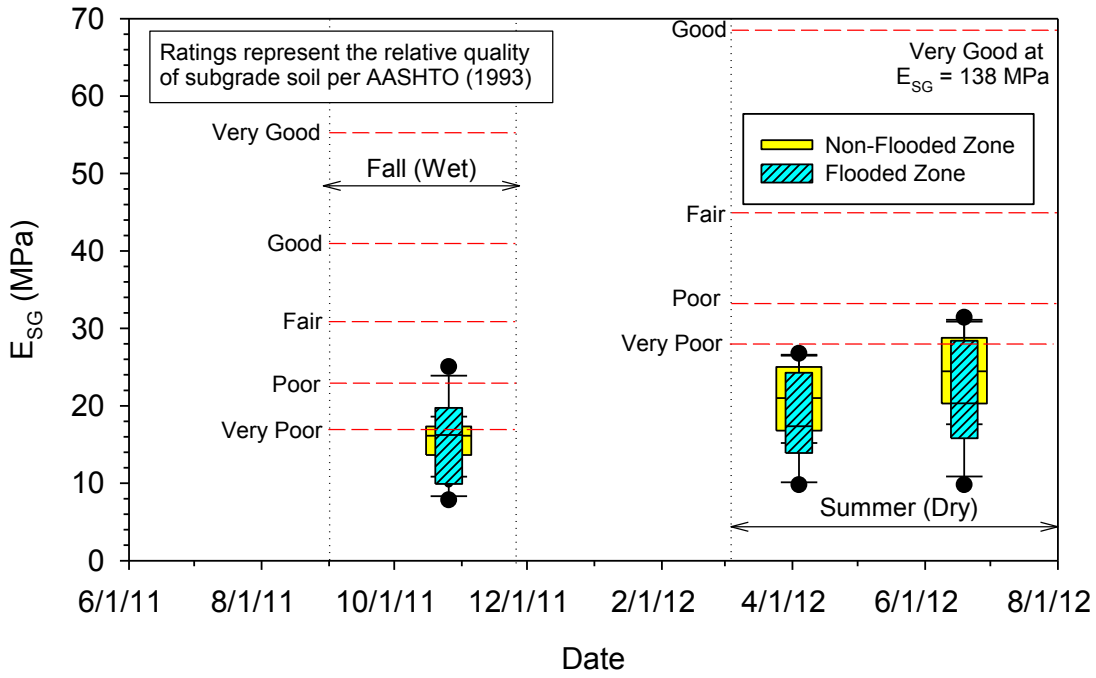

Figure 152. Box plots of subgrade modulus values in flooded and non-flooded zones in comparison with relative quality ratings on TS2 – Fremont County

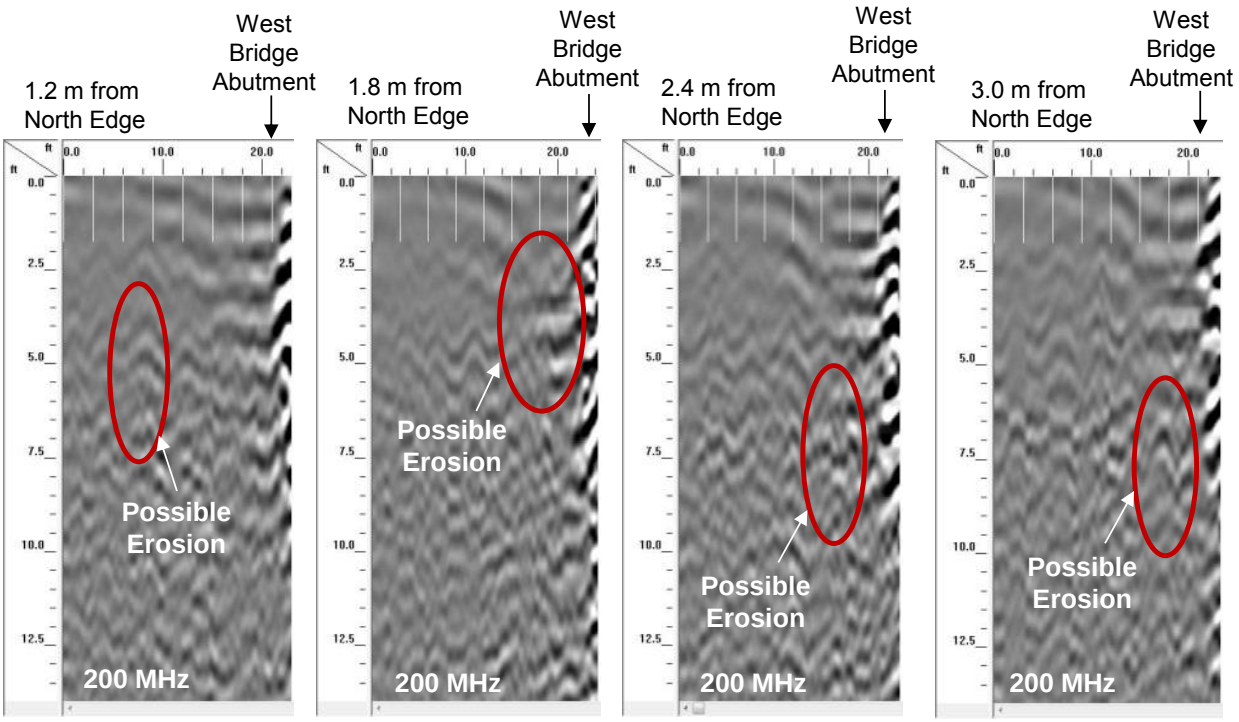

Figure 153. GPR scans using 200 MHz antenna on TS2 longitudinally along the west bridge approach backfill at 1.2 to 3.0 m away from the north edge of the bridge (note: 0 ft mark on the horizontal scale represents about 6.7 m (22 ft) away from the west abutment) – Fremont County

TS 3 – 185th Avenue (Gravel)

TS3 is a gravel road segment located on 185th Avenue located between I-29 and Iowa-Nebraska border in Fremont County. Testing was conducted over a length of about 6678 m along the middle of the lane. The segment generally consisted of about 140 mm thick gravel layer underlain by natural subgrade (note: depths determined from DCP tests), but it was about 65 to 100 mm in a few locations along the test segment. The Fremont County soil survey report indicates that the natural subgrade soils in this region consist of silty to clayey to sandy alluvium material in the top 600 mm of the subgrade and are classified as A-2-4, A-4, A-6, and A-7 or SM, CL, ad CH soils. The saturated hydraulic conductivity of the material vary from about 0.04 to 190 μm/s (0.01 to 54 ft/day).

During the 2011 flood event, the test segment was fully submerged for about one to three months (Figure 154). Reportedly, the flood waters receded in the area during mid-September. Roadway damages noted on this test segment include eroded gravel surface layer, sand/silt deposits on the road, rutting under wheel loads at isolated locations (Figure 155, Figure 156).

In situ testing was conducted on this test segment about 1 month after the flood waters receded (10/27/11), and after about 5 and 7 months (on 4/4/12 and 5/30/12). FWD tests were conducted at 47 locations and DCP tests were conducted at 6 locations.

E_{FWD} and E_{SG} results from four different testing times along the test segment are shown in Figure 157. E_{SG} values were calculated based on deflections from the sensor located at 300 mm (12 in.) away from the center of the loading plate. DCP-CBR profiles at the two test locations from different testing times are shown in Figure 158. Box plots of E_{SG} values at different test times are shown in Figure 159. Subgrade CBR values (averaged in the top 300 mm of subgrade) at two different test times are shown in Figure 160. Some key findings from these in situ testing are as follows:

- Most of the E_{SG} values in the whole TS were low and the quality is rated as "very poor" to "poor," per AASHTO (1993). A few test locations are rated between "poor" to "fair." The E_{SG} values improved slightly over time (on average from about 14 to 17 MPa)
- Subgrade CBR values (in the top 300 mm of subgrade) indicated mixed results with quality varying from "poor" to "very good." Some locations with low CBR values in the subgrade showed improvement over time (e.g., at PT2 from about 5.2 to 17), while some locations did not (e.g., at PT25 which remained at about 1.8).
- Significant rutting (about 125 mm) was observed under wheel paths near PT25 (near Sta. 3000), where the subgrade CBR was about 1.9. Rutting was also observed at PT 35 (near Sta. 4700), where subgrade CBR (averaged in the top 300 mm) was higher than at PT 25 (7.9). Examining the full CBR profile indicated that CBR in the subgrade ranged from about 0.3 to 2.0 below about 420 mm.

Figure 154. Aerial imagery before flooding on left (from 10/28/10) and during flooding on right (from 8/11/11) on TS3 – Fremont County

Figure 155. Newly placed gravel near a culvert at about 4700 m station on TS2 (Picture taken 10/27/11)

Figure 156. Rutting observed near 3000 m station on TS2 (Picture taken 4/4/12)

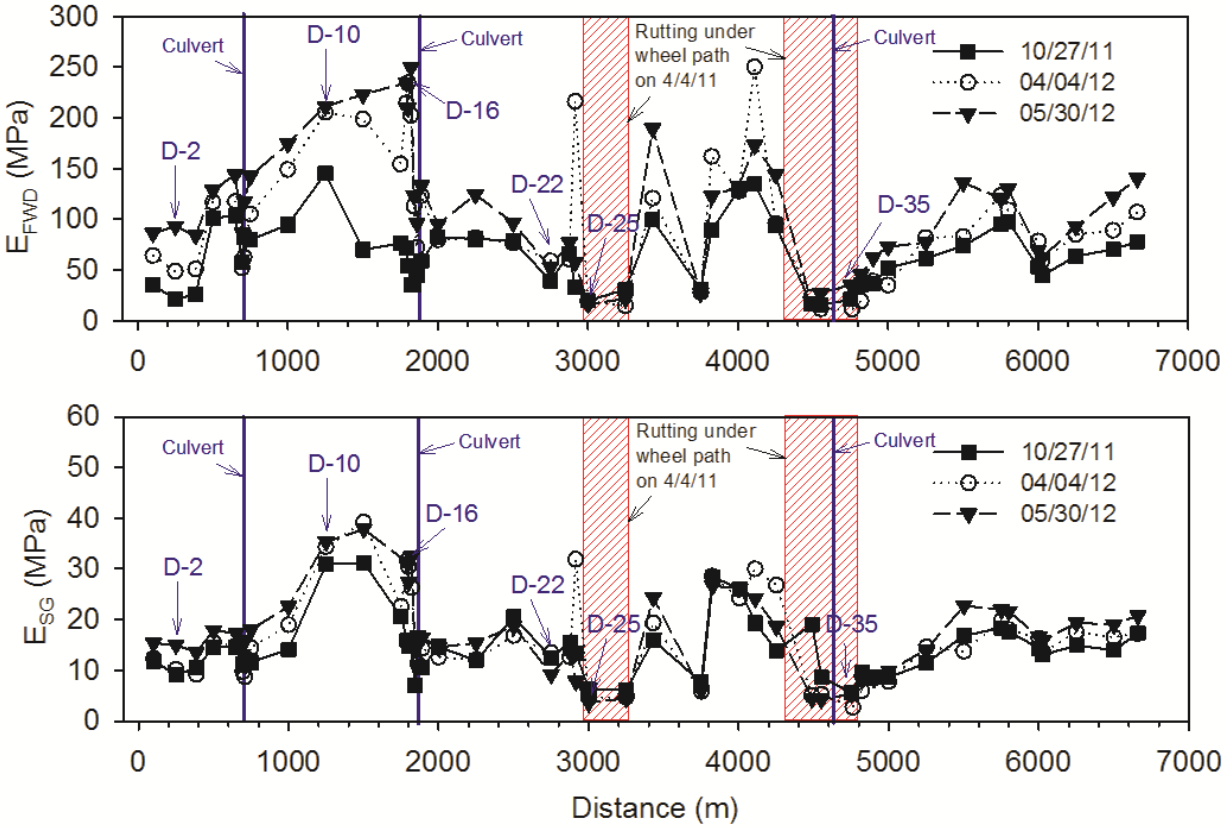

Figure 157. Surface FWD modulus (top) and subgrade modulus (bottom) at three different times after flooding on TS3 – Fremont County

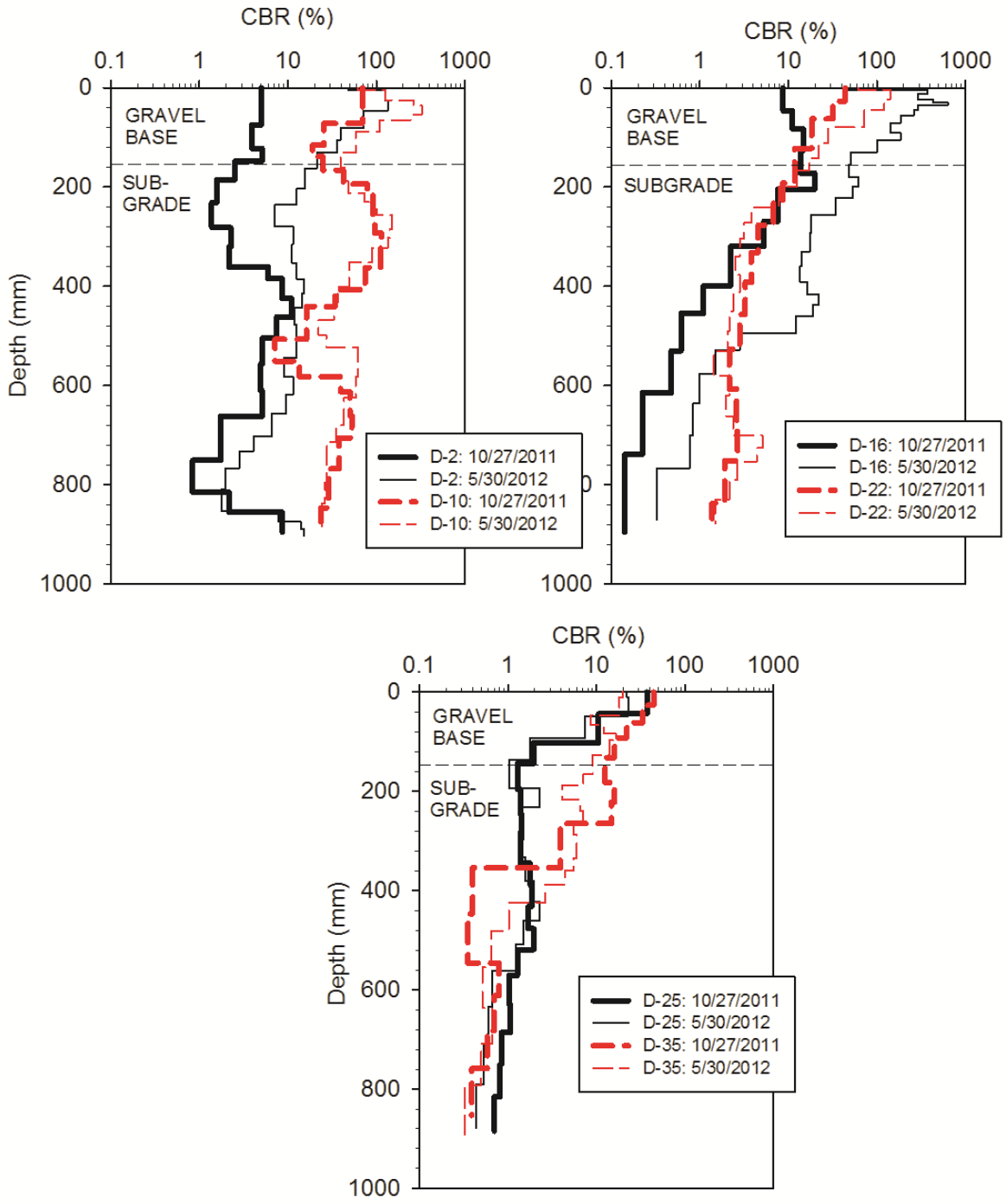

Figure 158. DCP-CBR profiles at three different times after flooding at six test locations on TS3 – Fremont County

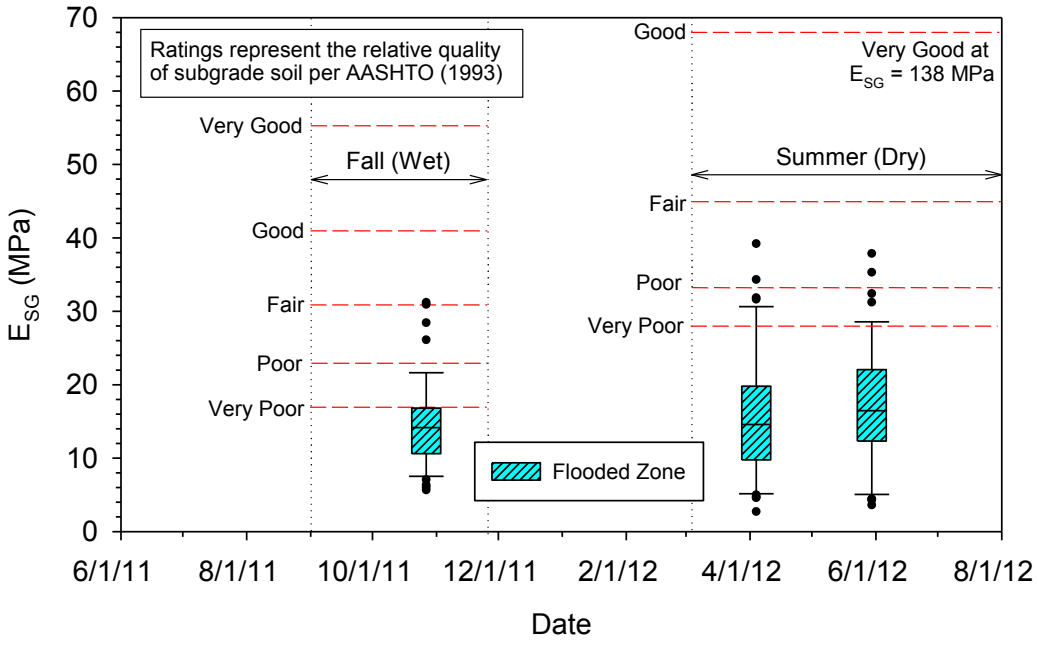

Figure 159. Box plots of subgrade modulus values in comparison with relative quality ratings on TS3 – Fremont County

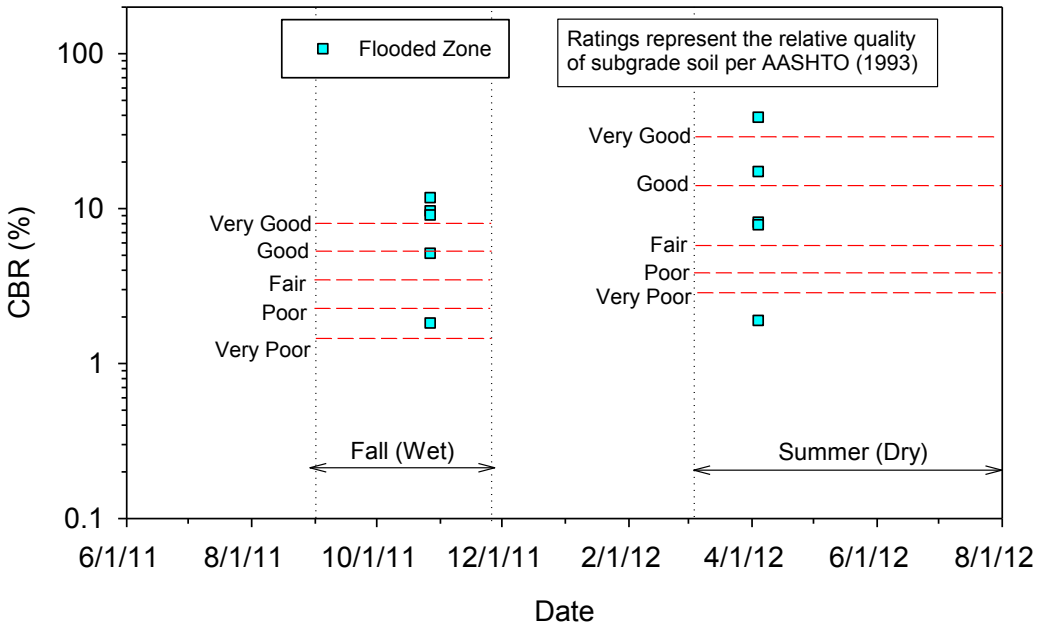

Figure 160. Comparison of subgrade CBR values with relative quality ratings on TS3 – Fremont County

TS 4 – 220th Street (Chipseal Surfacing over Gravel)

TS4 is a gravel road segment surfaced with chipseal coat located on 220th Street, starting from just east of the railroad intersection (east of 195th Avenue intersection), south of Percival, iowa. Testing was conducted over a length of about 1200 m along the east bound lane. The Fremont County soil survey report indicates that the natural subgrade soils in this region consist of silty alluvium in the top 600 mm of the subgrade and are classified as A-4 and A-7 or CL soils. According to the soil survey report, these soils exhibit moderately high drainability with saturated hydraulic conductivity of about 6.4 to 9 μm/s (1.8 to 2.6 ft/day).

During the 2011 flood event, the test segment was partially submerged for about two to three months Figure 161). Reportedly, the flood waters receded in the area during mid-September 2011. Roadway damages noted on this test segment include rutting under wheel paths and cracks on the chipseal surfacing, eroded chipseal and gravel over culvert location (patched prior to testing), and eroded granular shoulders. Pictures from this test segment are shown in Figure 162 and Figure 163.

In situ testing was conducted on this test segment in flooded and non-flooded areas for comparison, about 1 month after the flood waters receded (10/28/11), and after about 5 and 7 months (on 4/4/12 and 5/30/12). FWD tests were conducted at 16 locations (7 in non-flooded area and 9 in flooded area) and DCP tests were conducted at 2 locations (1 each in flooded and non-flooded areas).

E_{FWD} and E_{SG} results from three different testing times along the test segment are shown in Figure 164, identifying the flooded/non-flooded areas and the bridge. E_{SG} values were calculated based on deflections from the sensor located at 300 mm (12 in.) away from the center of the loading plate. DCP-CBR profiles at the four test locations from different testing times are shown in Figure 165. Box plots of E_{SG} values comparing measurements in the flooded and non-flooded areas at different test times are shown in Figure 166. Some key findings from these in situ testing and observations are as follows:

- On average, E_{FWD} values were about 1.3 to 1.7 times higher in the non-flooded area than in the flooded area, at all times of testing. Similarly, E_{SG} values were about 1.3 times higher in the non-flooded area than in the flooded area. The E_{FWD} values, however, have decreased over time. On average, the E_{FWD} values decreased from about 71 to 46 MPa in the non-flooded area, and from about 42 to 36 MPa in the flooded area, from about 1 month after flooding to about 7 months after flooding. The E_{SG} values did not vary much over time (varied from 15 to 13 MPa in non-flooded area and 11 to 10 MPa in flooded area).
- The E_{SG} values in the whole TS were low and the quality is rated as “very poor,” per AASHTO (1993). Lowest values were located in the middle of the flooded zone.

Figure 161. Aerial imagery before flooding on left (from 10/28/10) and during flooding on right (from 8/11/11) on TS4 – Fremont County

Figure 162. Rutting observed on the surface and washed out shoulders during flooding on TS4 – Fremont County (Picture taken 10/28/11)

Figure 163. Surface patch repair over a culvert on TS4 – Fremont County (Picture taken 10/28/11)

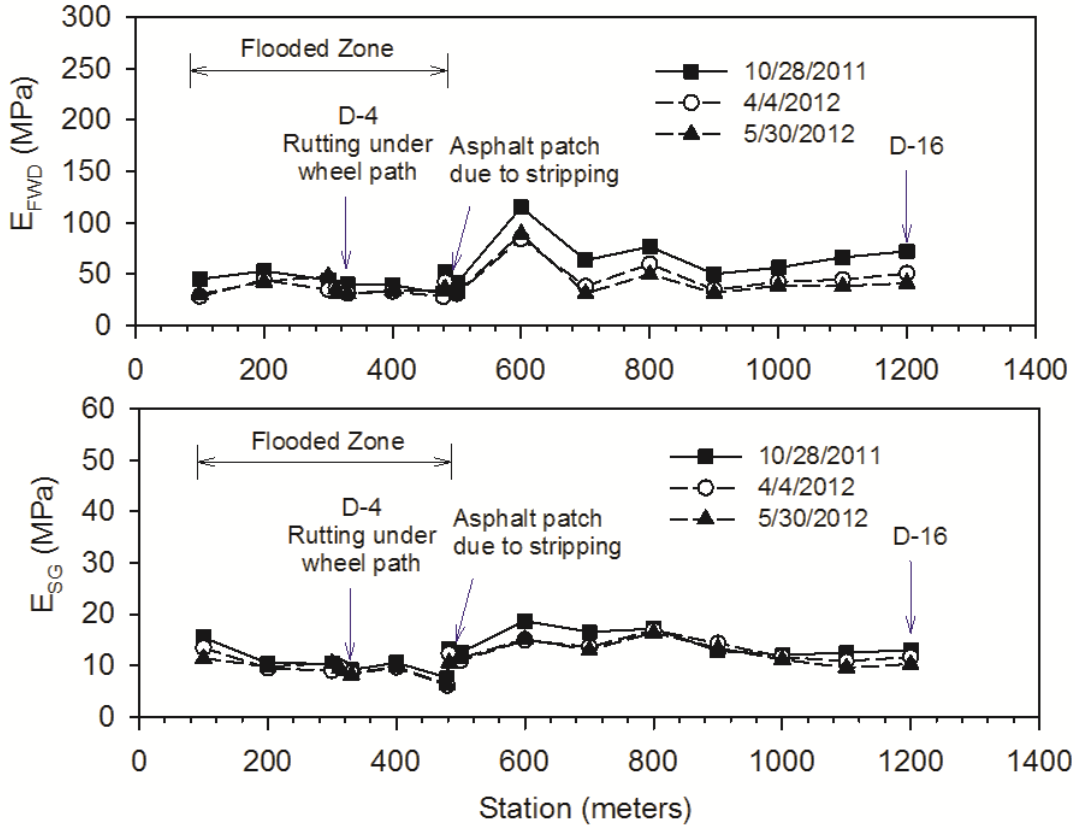

Figure 164. Surface FWD modulus (top) and subgrade modulus (bottom) at three different times after flooding on TS4 – Fremont County

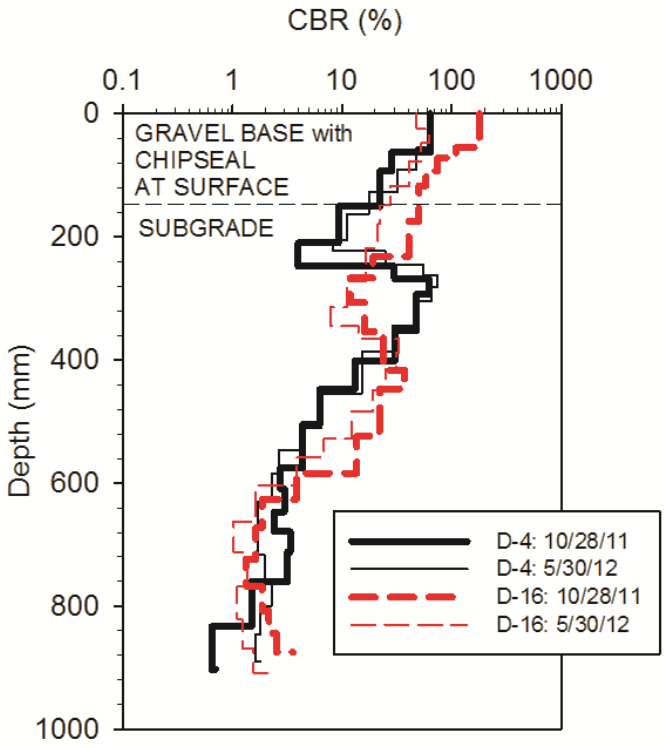

Figure 165. DCP-CBR profiles at two test locations from two different testing times on TS4 – Fremont County

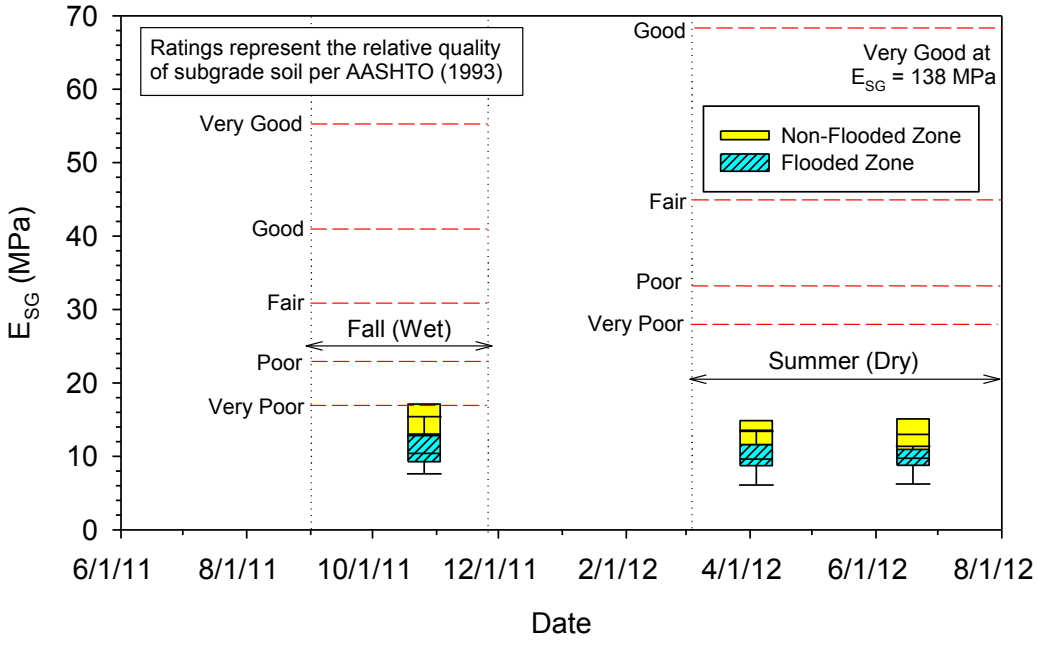

Figure 166. Box plots of subgrade modulus values in flooded and non-flooded zones in comparison with relative quality ratings on TS4 – Fremont County

Statistical Analysis

Comparison between Flooded and Non-Flooded Areas

Box plots of E_{FWD} and E_{SG} measurements obtained from each test segment in Pottawattamie and Fremont Counties, comparing results from flooded and non-flooded zones obtained shortly after flooding (about 1 month or less) and about 7 to 8 months after flooding, are shown in Figure 167 and Figure 168, respectively. Statistical t-test analysis was conducted on these results to compare differences between the flooded and non-flooded zones, and determine if the results are statistically different from each other. The selected criteria for identifying the statistical significance included: p-value < 0.05 and t-value > 2. Results of statistical t-tests are provided in Table 12 and Table 13 for Pottawattamie and Fremont County test segments, respectively.

The comparisons presented in Figure 167 and Figure 168 and the statistical t-test results indicate that out of the 6 test segments (where non-flooded and flooded zones sections were present within a test segment), 5 test segments had statistically significant difference between flooded and non-flooded zones. On average, the E_{FWD} and E_{SG} values in non-flooded zones were about 1.3 to 3.6 times greater than the values in non-flooded zones, in the test segments where the difference was statistically significant. Results obtained about 7 to 8 months after flooding were statistically significant in only 3 out the 6 test segments. This indicates that in those test segments, the foundation layers in the flooded zone gained strength over time, likely as drainage occurred and the degree of saturation in the subgrade layers decreased.

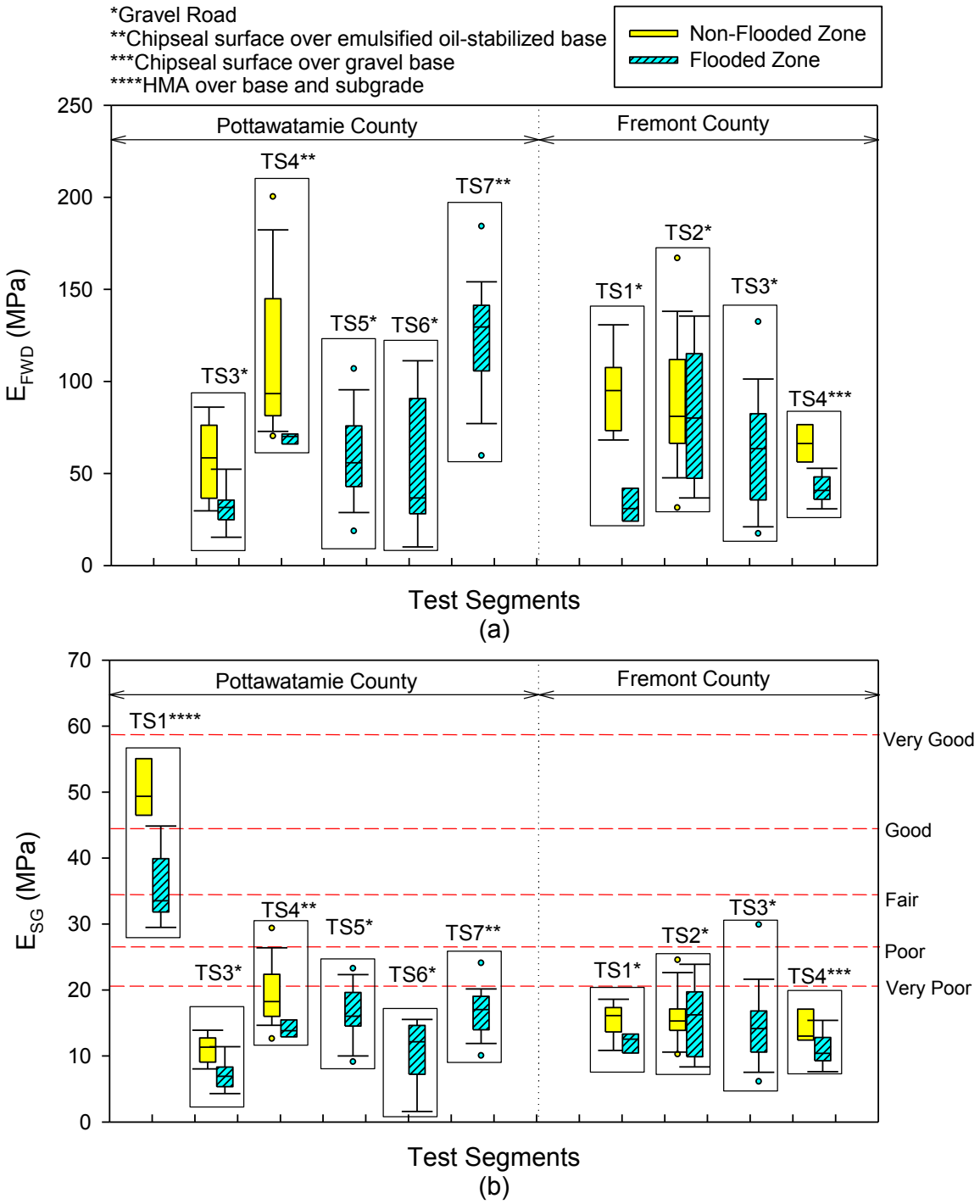

Figure 167. Box plots of (a) E_{FWD} and (b) E_{SG} obtained shortly after flooding (about 20 to 30 days) from all test segments in flooded and non-flooded zones

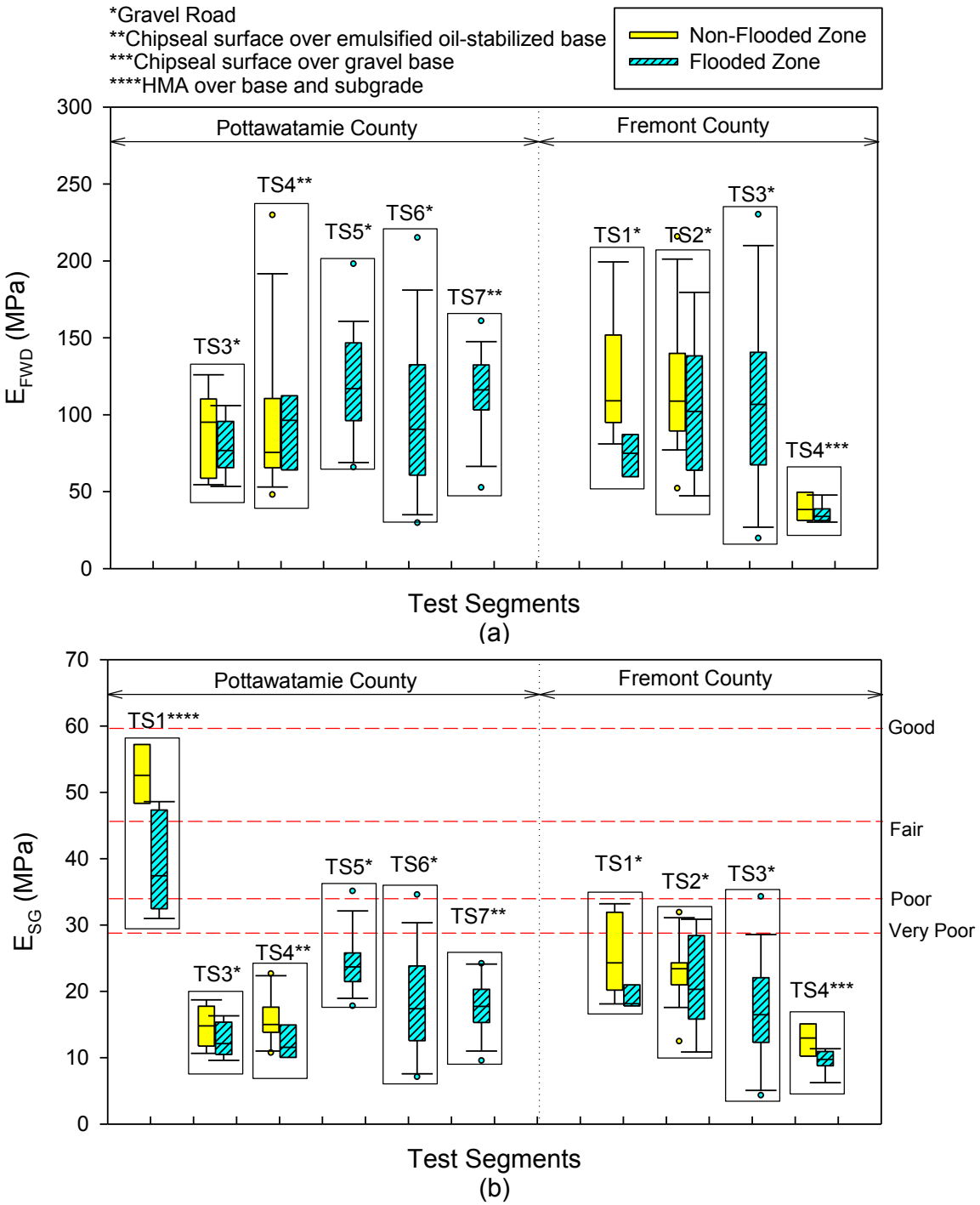

Figure 168. Box plots of (a) E_{FWD} and (b) E_{SG} obtained about 7 to 8 months after flooding from all test segments in flooded and non-flooded zones

Table 12. Summary of statistical t-test results comparing flooded and non-flooded areas on each test segment – Pottawatamie County

TS	Parameter	Duration after flooding	Mean Values		Ratio of Mean	Diff. in Mean	t-Ratio	Prob > t	Statistically significant difference*
			Non-Flooded Zone	Flooded Zone					
1	E_{FWD} (MPa) on HMA	20 days	894	681	1.3	213	-5.327	< 0.0001	Yes
		6 months	1256	1003	1.3	253	-4.475	0.0004	Yes
		8 months	871	650	1.3	222	-5.270	< 0.0001	Yes
	E_{SG} (MPa)	20 days	50	36	1.4	14	-6.335	< 0.0001	Yes
		6 months	60	45	1.3	15	-4.118	0.0010	Yes
		8 months	54	39	1.4	15	-4.503	0.0004	Yes
3	E_{FWD} (MPa) on Gravel	21 days	58	32	1.8	26	-3.448	0.0055	Yes
		54 days	65	44	1.5	21	-2.435	0.0340	Yes
		6 months	60	52	1.2	8	-1.150	0.2665	No
		8 months	87	79	1.1	9	-0.861	0.4053	No
	E_{SG} (MPa)	21 days	11	7	1.6	4	-4.376	0.0003	Yes
		54 days	12	9	1.3	3	-2.895	0.0095	Yes
		6 months	12	10	1.2	2	-2.749	0.0143	Yes
		8 months	15	13	1.2	2	-1.513	0.1524	No
4	E_{FWD} (MPa) on stabilized gravel base	22 days	110	71	1.5	39	-4.481	<0.0001	Yes
		55 days	132	99	1.3	33	-2.764	0.0101	Yes
		6 months	94	68	1.4	26	-2.894	0.0066	Yes
		8 months	95	59	1.6	36	-3.421	0.0017	Yes
	E_{SG} (MPa)	22 days	19	14	1.4	5	-5.080	<0.0001	Yes
		55 days	21	16	1.3	4	-4.141	0.0002	Yes
		6 months	17	13	1.3	4	-4.024	0.0003	Yes
		8 months	17	13	1.3	4	-2.879	0.0091	Yes

*between non-flooded zone and flooded zone

Table 13. Summary of statistical t-test results comparing flooded and non-flooded areas on each test segment – Fremont County

TS	Parameter	Duration after flooding	Mean Values		Ratio of Mean	Diff. in Mean	t-Ratio	Prob > t	Statistically significant difference*
			Non-Flooded Zone	Flooded Zone					
1	E_{FWD} (MPa) on Gravel	1 months	86	33	2.6	53	7.350	< 0.0001	Yes
		5 months	98	29	3.4	69	7.982	< 0.0001	Yes
		8 months	125	75	1.7	51	3.469	0.0035	Yes
	E_{SG} (MPa)	1 months	15	12	1.3	3	3.529	0.0028	Yes
		5 months	16	11	1.5	5	5.166	0.0005	Yes
		8 months	26	19	1.4	7	3.762	0.0018	Yes
2	E_{FWD} (MPa) on Gravel	1 months	79	80	1.0	-1	0.081	0.9351	No
		5 months	73	92	0.8	-18	1.355	0.1870	No
		7 months	112	105	1.1	7	0.434	0.6681	No
	E_{SG} (MPa)	1 months	15	16	0.9	-1	0.188	0.8532	No
		5 months	21	18	1.2	3	1.707	0.1001	No
		7 months	25	21	1.2	4	1.410	0.1702	No
4	E_{FWD} (MPa) on Gravel	1 months	71	42	1.7	29	3.509	0.0095	Yes
		5 months	50	34	1.5	16	2.417	0.0459	Yes
		7 months	46	36	1.3	10	1.248	0.253	No
	E_{SG} (MPa)	1 months	15	11	1.4	4	2.895	0.0133	Yes
		5 months	13	10	1.3	3	3.227	0.0066	Yes
		7 months	13	10	1.3	3	2.748	0.0210	Yes

*between non-flooded zone and flooded zone

Correlations between DCP-CBR and FWD Measurements

Correlation analysis was performed between DCP-CBR measurements (of subgrade and gravel layers) and E_{FWD} measurements obtained from this study and the results are presented in Figure 169 and Figure 170. The motivation for this analysis was to assess the relative influence of surface gravel and underlying subgrade layers as they relate to FWD measurements. FWD tests provide a composite layer response to loading and have a measurement influence depth of up to 0.67 m (see White et al. 2013a).

The correlations between CBR of subgrade and FWD measurements yielded power relationships with higher R^2 values (0.63) than the correlation between CBR of gravel and E_{FWD} ($R^2 = 0.49$). Correlation between E_{FWD} and E_{SG} yielded a linear relationship with $R^2 = 0.81$. The standard error of the predictions are also shown in Figure 169.

The relative statistical significance of the subgrade and gravel layer CBR measurements on E_{FWD} was assessed using multivariate analysis results shown in Figure 169. The p-value and t-value statistics indicated that both CBR of subgrade and gravel layers are statistically significant. Using Eqs. 17 and 18, the subgrade layer has about 86% of influence on the surface layer FWD measurements while the gravel layer has about 14% influence. This finding has practical importance because it indicates that the response to dynamic traffic loading at the surface will be more dependent on the relatively soft subgrade layer. In cases where subgrade layer is "soft"

(CBR < 2 from this study) stabilization or treatment (e.g., chemical stabilization or placing geosynthetics) may be necessary to improve performance and reduce maintenance issues.

Using the multivariate regression relationship, a chart was developed to predict E_{FWD} from CBR of subgrade and gravel layer values, as shown in Figure 171. The chart shows the subgrade quality ratings per AASHTO (1993) and the in situ test measurements obtained from this study. Results from 7 out of the 44 test locations were outside of the predicted zone, due to uncertainity in the prediction. The curves presented in the charts are based CBR of subgrade = 1.2 to 93, CBR of gravel = 2.8 to 307, FWD modulus = 9 to 211 MPa (1,305 to 30,600 psi), and gravel layer thickness = 90 to 200 mm (3.5 to 7.9 in.). Figure 171 also includes light weight deflectomter modulus (E_{LWD}) on y-axis based on E_{FWD} versus E_{LWD} correlations presented in White et al. (2013a) from tests conducted on 150 mm (6 in.) thick gravel roads.

Typical CBR values for subgrade and gravel layers in wet condition (during spring-thaw), which were originally constructed using different stabilization techniques (from White et al. 2013b) are overlaid on this chart in Figure 172. Also included in Figure 172 is rut depth scale on x-asis based on relationships between CBR of subgrade (untreated) and rut depth under a 80 kN (18 kips) axle load for 100 loading cycles on a 152 mm (6 in.) thick gravel layer (untreated), as presented in White et al. (2007).

The chart presented in Figure 172 are developed to help determine target values in the field. A few example scenarios on how the chart can be used to determine target values is provided below:

Scenario 1: Assume that a gravel road is to be designed for an allowable rut depth of 50 mm. Based on the chart, a minimum CBR of subgrade = 6 and CBR of gravel = 6 are needed, as measured using a DCP test. As an alternate, LWD (using 300 mm diameter plate Zorn LWD) or FWD (using a 300 mm diameter plate Kuab FWD) tests can be conducted and the respective target values corresponding to CBR of subgrade and gravel = 6 are 48 MPa (6,960 psi) and 27 MPa (3,915 psi), respectively. If these values cannot be achieved, alternative treatments to subgrade (e.g., geosynthetics, chemical stabilization, mechanical stabilization) can be used. Note that the geosynthetic treatment zone highlighted on Figure 172 does not correspond to the rut depth measurements, as the CBR to rut depth relationship from White et al. (2007) was for mateirals without any geosynthetic. Use of geosynthetics can help reduce rutting under traffic loading.

Scenario 2: Assume that a new subgrade layer with a target design CBR = 10 in wet conditions, is required. Based on the chart, stabilization technologies to achieve a minimum CBR = 10 in the subgrade is with 20% fly ash stabilization, mechanical stabilization, or cement stabilization of subgrade. FWD and LWD target values can also be determined for the different stabilization technologies.

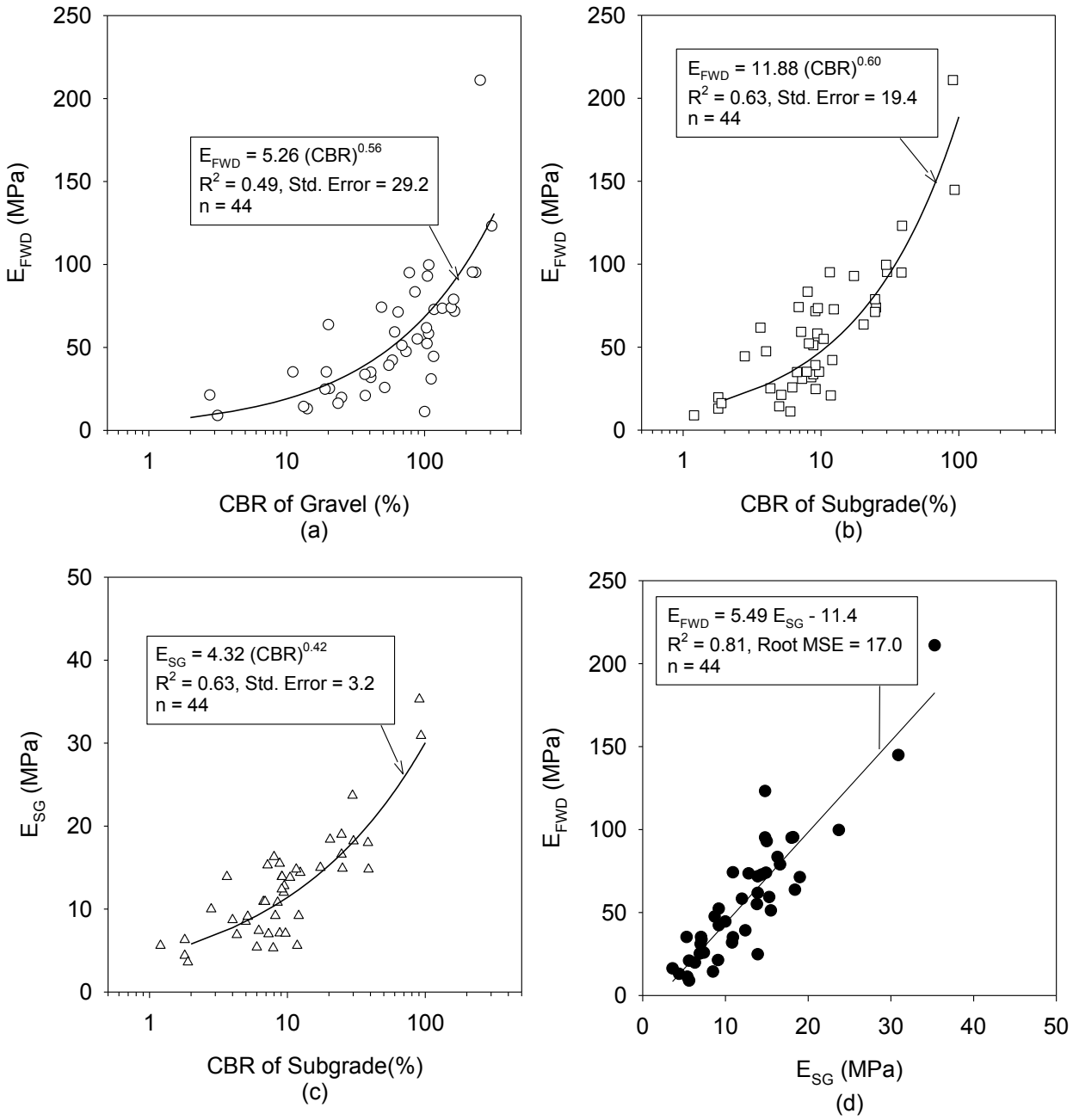

Figure 169. Regression analysis between: (a) CBR of Gravel and E_{FWD}, (b) CBR of subgrade and E_{FWD}, (c) CBR of subgrade and E_{SG}, and (d) E_{SG} and E_{FWD}

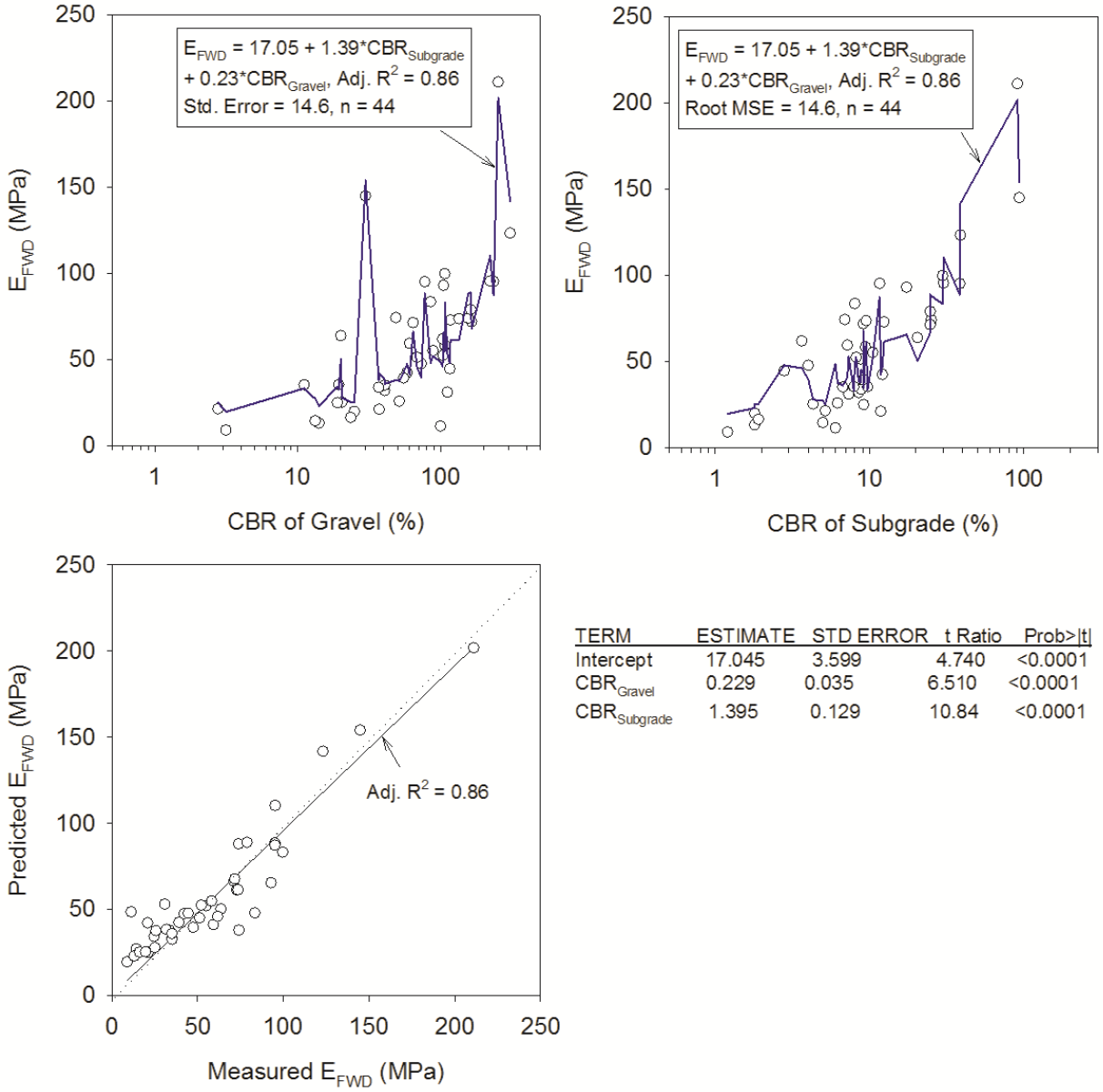

TERM	ESTIMATE	STD ERROR	t Ratio	Prob>|t|
Intercept	17.045	3.599	4.740	<0.0001
CBR_{Gravel}	0.229	0.035	6.510	<0.0001
$CBR_{Subgrade}$	1.395	0.129	10.84	<0.0001

Figure 170. Results of multivariate regression analysis to predict E_{FWD} from CBR of gravel and CBR of subgrade

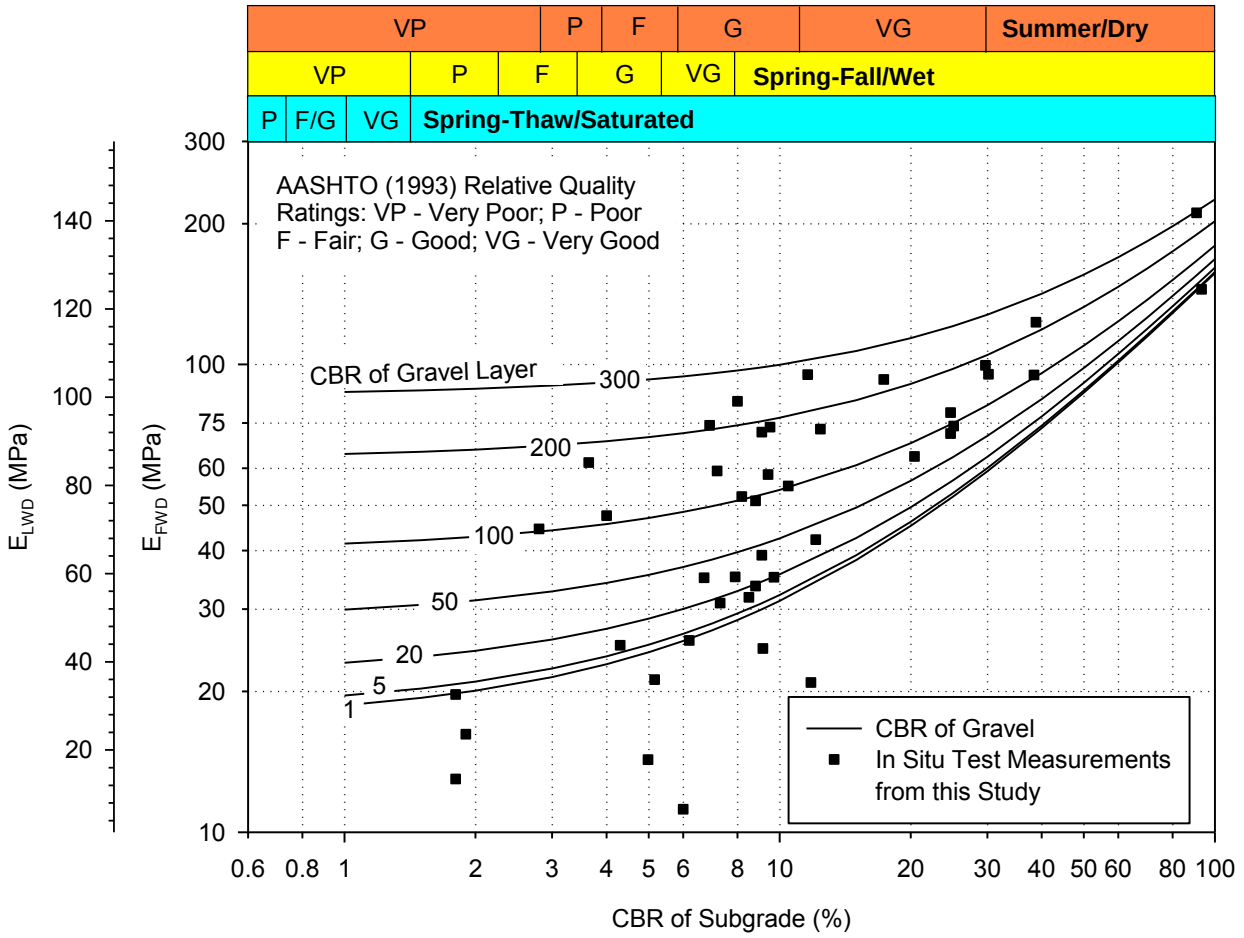

Figure 171. Chart to estimate FWD or LWD surface modulus from CBR of subgrade and gravel layers overlaid with in situ test measurements and AASHTO (1993) subgrade relative quality ratings

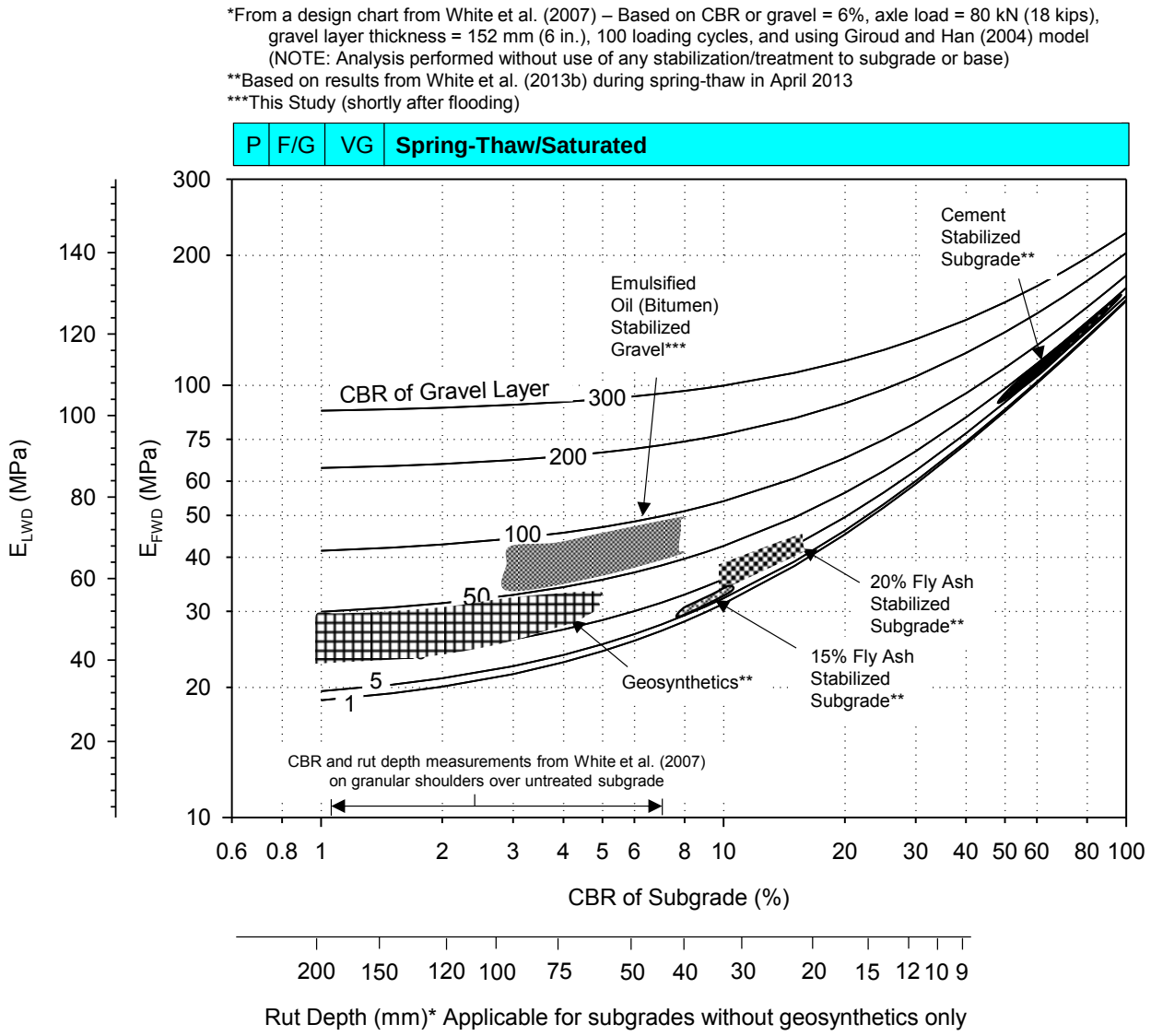

Figure 172. Chart showing relationship between CBR, rut depth, and FWD and LWD modulus, and typical range of CBR values observed after spring-thaw in Iowa (White et al. 2013b) for different stabilization methods

CHAPTER 7: KEY FINDINGS FROM FIELD TESTING AND OBSERVATIONS

Summary of Flood Damages to Secondary Roadways and Repair Measures

Based on field reconnaissance of the flood-damaged areas by the research team, review of the damage inspection reports submitted to the Iowa DOT, and interviews with county engineers, the damages observed on secondary roadway geo-infrastructure can be broadly categorized as follows:

A. Paved Roadways:
    1. Voids at shallow depths (< 150 mm (6 in.)) due to erosion of underlying base material
    2. Voids at deeper depths (> 150 mm (6 in.)) due to erosion of subsurface material
    3. Partial to complete erosion of PCC and HMA pavements and underlying base material
    4. Erosion of granular shoulders
B. Bridges:
    1. Erosion of bridge approach backfill material
    2. Erosion of embankment foreslopes
C. Culverts:
    1. Erosion of culvert backfill
    2. Separation of culverts
    3. Water outflow blockage
D. Unpaved Roadways:
    1. Erosion of gravel surface.
    2. Rutting under traffic loading (on gravel roads and other detoured roadways due to excessive loading, although not flooded)
    3. Full breach of roadway embankments

Repairs on secondary roadways generally involved clearing damaged areas by removal of debris and re-construction by replacing damaged areas with new material to achieve targeted pre-flood condition. In some instances, flowable mortar grouting was used to fill voids beneath pavements, and emulsified-oil (bitumen) stabilization was used to stabilize the gravel layer (for damage D2). The total reported cost of flood damage to transportation infrastructure on secondary roadways in western Iowa was about $12.6 million.

Field evaluation of damage by the county engineers and Federal Emergency Management Agency (FEMA) personnel was based primarily on visual inspection. A push T-bar was used in some cases to detect weep holes under gravel roads during the visual inspection. The visual assessment approach worked well where the damage was obvious, i.e., where segments of roadway were washed away, but was not effective in detecting subsurface damage that was not immediately visible at the surface (due to erosion of subsurface materials). The research team found two areas that posed significant safety concerns to traffic due to subsurface damage that was not apparent at the surface. One of those areas resulted in deep potholes on a gravel road due to eroded backfill around a culvert and the other resulted in deep voids beneath the roadway due

to eroded backfill around a bridge abutment. Use of in situ DCP tests and GPR scanning was effective in identifying these areas and are discussed below.

In Situ Test Results and Statistical Analysis

The research team visited selected sites in Pottawattamie and Fremont Counties in western Iowa to conduct in situ testing shortly after the flood waters receded (in September and October 2011) and 7 to 8 months after flooding (in April, May, and June 2012) to evaluate performance. Road test segments were selected with an objective to monitor performance of the flooded versus non-flooded areas over time.

In situ testing involved conducting FWD, DCP, and GPR testing and performing hand auger soil borings. Testing was conducted on about 30 km (18.6 miles) of roadway, where the test segments varied in length from about 150 m (500 ft) to 7.0 km (4.3 miles). The test segments varied by flood condition (fully or partially flooded) and type of surfacing (gravel, chip seal surface over stabilized or unstabilized gravel base, PCC, and HMA). Key findings from in situ testing and observations on test segments with gravel roads (treated and untreated) with and without chipseal surfacing, HMA pavement, PCC pavement, and bridge abutments are as follows.

Gravel Roads and Culvert Crossings

- Comparison of in situ FWD test measurements obtained in flooded and non-flooded areas shortly after flooding revealed statistically significant differences in five out of the six test segments. All test segments showed recovery over time. Testing conducted several months after flooding revealed that in three test segments, the differences between flooded and non-flooded areas became statistically insignificant, while in three other test segments the differences remained statistically significant. This finding emphasizes the need for in situ testing to characterize the often complex field conditions that result from flooding.
- Statistical analysis between CBR of subgrade and gravel layers and FWD modulus indicated that the subgrade layer had about 86% of influence on the FWD measurements while the gravel layer had about 14% influence. This finding has practical importance because it indicates that the response to dynamic traffic loading at the surface will be more dependent on the quality of the subgrade layer.
- Using the multiple regression relationship, a simple chart was developed to predict FWD and LWD modulus values from CBR of subgrade and gravel layers. This chart can be helpful in determining target values of LWD or FWD modulus, if CBR values are known, or vice-versa.
- Weep holes were observed at several culvert locations directly beneath the gravel layer, indicating erosion of backfill material around the culvert. Most of the weep holes were not noticeable until the flood waters receded. On one test segment, erosion of culvert backfill materials resulted in formation of about 0.5 m (1.5 ft) diameter potholes on the middle of roadway. These potholes were undetected until they were formed and posed a significant safety concern to traffic.
- Significant rutting (up to 125 mm (4.9 in.) deep) was observed under wheel paths at

several locations along a test segment (TS3) in Fremont County. DCP tests in some of those areas showed layers with CBR < 2 in the subgrade, which likely contributed to the rutting.
- GPR scanning using 200 and 400 MHz antennas identified changes in gravel layer thicknesses, culvert locations, and weep holes.

HMA Pavement

Only one pavement segment with 360 mm (14 in.) thick HMA underlain by 300 mm (12 in.) thick base and natural subgrade was tested as part of this study. Some key findings from this test segment were as follows:

- No structural failures were observed on the pavement. However, granular shoulder erosion was evident in areas close to the high water line.
- E_{FWD} and E_{SG} values were on average about 1.3 to 1.4 times higher in the non-flooded zone than in the flooded zone at all times of testing. FWD results obtained about 6 months after flooding were on average higher in the non-flooded zone and the results obtained about 9 months after flooding were on average similar in both flooded and non-flooded zones when compared to the results obtained shortly after flooding.
- The CBR of the base layer was about the same in both flooded and non-flooded zones (> 50), but the CBR of subgrade was on average about 10 times higher in the non-flooded zone than in the flooded zone. No significant difference was noted in the measurements obtained shortly after flooding and about 9 months after flooding.

PCC Pavement

Only one pavement segment with about 250 mm (9.8 in.) thick PCC, which was originally (before flooding) underlain by 150 mm (6 in.) thick subbase and natural subgrade, was tested as part of this study. Some key findings from this test segment were as follows:

- Reportedly, the test segment experienced heavy water currents as the water levels fluctuated during the flood event resulting in granular shoulder erosion, complete washout of a portion of the pavement, and erosion of the subbase layer beneath the pavement.
- Flowable cement grout was used to fill the voids formed beneath the pavement. The grout was very soft and did not set up even two days after placement. Longitudinal cracks were observed on a few panels where the subbase layer was eroded. Additional research is warranted in evaluating use of alternative materials of stabilizing grout for use below water.
- FWD tests at joints indicated an average LTE of about 93% to 95% at all testing times. Two of the test locations showed a reduction in LTE with time, from about 94% shortly after flooding to about 85% to 88% several months after flooding. These tests were located on panels underlain by cement grout. This test segment warrants performance monitoring over time to evaluate the effectiveness of the cement grout placement.
- FWD zero-load intercept values did not indicate any voids beneath the pavement. The $k_{FWD\text{-}static}$ values were on average about 15 to 20 kPa/mm (55 to 73 pci) and is rated as

very poor, per AASHTO (1993).

- Average CBR of the grout layer increased from about 5.8 shortly after flooding to 10.4 after flooding. The CBR of the subgrade layer was about the same at both testing times with an average of about 20 in the top 300 mm (1 ft) of subgrade.
- GPR scans detected dowel bars along the joint between the adjacent lanes. A potential void area was detected at about 0.3 to 0.6 m (1 to 2 ft) below the surface in one of the scans. The bottom of the grout layer was at about 250 to 300 mm (10 to 12 in.) below surface.

Bridge Abutments

- Erosion of bridge approach backfill materials was observed at the two bridge sites assessed in this study. These bridges consisted of timber back wall abutments. In one of the bridges, backfill on one of the approaches was completely washed out and was replaced prior to our testing. DCP-CBR profiles in the newly-placed backfill indicated poorly compacted layers of fill with depth (with CBR < 2) within about 0.6 m (2 ft) of the bridge, which is typically a result of thicker lifts placed during compaction.
- At the two bridge sites, approach backfill materials continued to erode over time resulting in voids beneath the surface gravel layer. At one of the bridge sites, DCP tests across the bridge approach (about 1 month after flood waters receded) indicated voids at depths of about 300 mm (11.8 in.) to 850 mm (33.5 in.) below the surface, which extended nearly down to a maximum depth of about 2 m (6.6 ft) below the surface.
- GPR scans detected areas of potential voids and backfill erosion beneath the gravel surface after about 8 months after flooding in spite of reconstruction.
- At one of the bridge sites, natural subgrade clay fill material was used to stabilize the bridge abutments and block erosion of the backfill materials through the abutment walls. This material can potentially be scoured away easily during a future flood event. Use of riprap material as scour protection for the abutment wall would be a better repair and mitigation alternative.

CHAPTER 8: GUIDANCE FOR GEO-INFRASTRUCTURE DAMAGE ASSESSMENT AND SELECTION OF REPAIR AND MITIGATION SOLUTIONS

This chapter presents a catalog of options for flood damage assessment, and potential repair and mitigation solutions. A flow chart relating the damages, assessment techniques, and potential repair/mitigation solutions is provided. These options are discussed for paved/unpaved roads, culverts, and bridge abutments, and are applicable for both primary and secondary roadways.

The list below shows the various flood damage assessment techniques and a brief description of each of these technologies is provided in Appendix D:

- Aerial and LiDAR imagery review
- Visual inspection
- Dynamic plate load tests (i.e., FWD, LWD, or Clegg Hammer)
- Penetration tests (Push T-bar or DCP tests)
- Roller-integrated compaction monitoring
- Ground penetrating radar (GPR)
- Surface Laser scanning
- Underwater sonar scanning
- Pipe Crawler for Culvert pipe inspection

The list below shows the various potential repair and mitigation solutions, and a brief description of these solutions is provided in Appendix D:

A. Bio-Stabilization
B. Bulk-Infill (Cement) Grouting
C. Chemical Grouting
D. Chemical Stabilization of Subgrade/Base
E. Combined Soil Stabilization with Vertical Columns
F. Electro-Osmosis
G. Excavation and Replacement
H. Excavation and Replacement (using non-erodible fill)
I. Fiber Reinforcement of Subgrade/Base
J. Geosynthetic Reinforced Soil for Approach Backfill
K. Geosynthetics for Reinforcement/Separation/ Drainage
L. Geocell Confinement of Granular Materials
M. High Energy Impact Roller Compaction
N. Injected Light Weight Foam Fill
O. Mechanical Stabilization (Blending)
P. On-Site Recycling of Pavement Materials
Q. Partial Encapsulation
R. Rapid Impact Compaction
S. Sheet Pile Abutments
T. Rip-Rap for Erosion Protection

The list of technologies have been developed based on author's experience, field observations, ad literature review. It must be noted that a few of these technologies (i.e., A, B, C, E, F, N, and Q) warrant additional research with field trials to evaluate their effectiveness. Table 14 summarizes the assessment techniques and repair/mitigation solutions related to various damages observed in this study.

Table 14. Summary of potential flood damage evaluation techniques and repair/mitigation solutions

Damage Description	Assessment Techniques	Repair/Mitigation* Solutions
Paved Roadways		
1. Isolated voids at shallow depths (< 0.5 ft)	Visual inspection, GPR, FWD, DCP	B, N
2. Isolated voids at deeper depths (> 0.5 ft)	GPR, DCP[3]	B, C, N
3. Partial to complete erosion of pavement and base	Visual inspection, Aerial survey, LiDAR	A, D*, F[1], G, I, K, L*, M[2], O, P, Q*, R[2]
4. Erosion of granular shoulders	Visual inspection, aerial survey, laser scan	A, D*, G, I, K, L*
Bridge Abutments		
1. Erosion of approach backfill	Visual inspection, GPR, DCP, laser scan	B, C, G[4], H*[4], J*, S[5], T
2. Embankment fore slope erosion	Visual inspection, laser scan	E*, H, T[6]
Culverts		
1. Erosion of culvert backfill	Visual inspection, GPR, DCP	B, G[4], H*[4], T*[6]
2. Culvert separation	Visual inspection, GPR	
3. Water outflow blockage	Visual inspection, pipe crawler, under water sonar	Clear debris, T*[6]
Unpaved Roadways		
1. Erosion of gravel surface	Visual inspection, laser scan, GPR	A, D*, G, I, K, L*
2. Rutting under traffic loading	Visual inspection, FWD[7], DCP[7]	A, D*, G, I, K, L*, M[8]
3. Full breach of roadway embankments	Visual inspection, aerial survey, laser scan, LiDAR	D[9], E, H*, G, K[9]

*Potential mitigation solution
[1]For dewatering in silts/clays only
[2]For rubbilizing concrete (only if voids are small enough for the equipment to safely drive over the concrete)
[3]At locations selected based on GPR scans for verification
[4]Control lift thickness as appropriate to compaction equipment
[5]On low-volume bridges
[6]Place rip-rap over geosynthetic placed over natural material
[7]Determine FWD modulus or CBR of subgrade to select appropriate treatment/stabilization option
[8]May not be a viable option if the subgrade layer is wet/saturated
[9]To serve as a construction working platform

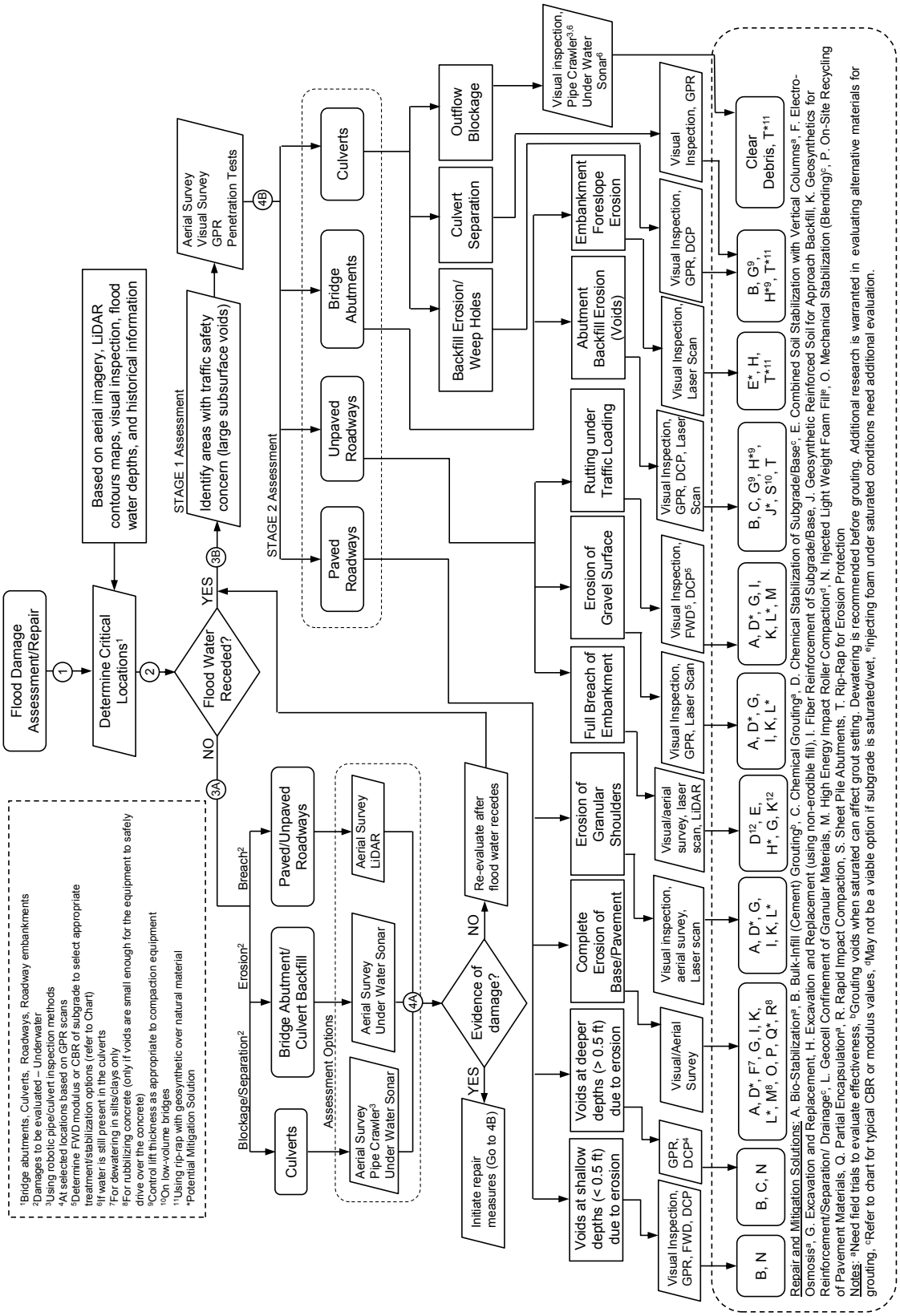

Figure 173. Flow chart to select assessment techniques and repair/mitigation solutions

REFERENCES

AASHTO. (1993). *AASHTO guide for design of pavement structures,* Published by the American Association of State Highway and Transportation Officials (AASHTO), Washington, D.C.

Adams, M.T., Collin, J.G. (1997). "Large Model Spread Footing Load Tests on Geosynthetic Reinforced Soil Foundations." *J. of Geotechnical and Geoenvironmental Engineering,* 123(1), 66-72.

Adams, M.T., Nicks, J.E., Stabile, T., Wu, J.T.H., Schlatter, W., and Hartmann, J. (2011a). *Geosynthetic Reinforced Soil Integrated Bridge System—Synthesis Report*. Report No. FHWA-HRT-11-027, Federal Highway Administration, McLean, VA.

Adams, M., Nicks, J., Stabile, T., Wu, J., Schlatter, W., and Hartmann, J. (2011b). *Geosynthetic Reinforced Soil Integrated Bridge System—Interim Implementation Guide.* Report No. FHWA-HRT-11-026, Federal Highway Administration, McLean, VA.

Austroads (1998). *Guide to Stabilisation in Roadworks*. National Association of Australian State Road Authorities, Australia.

Belle, G. V (2002). *Statistical rules of thumb,* Wiley Series in Probability and Statistics, John Wiley & Sons, Inc., New York.

Berg, R. R., Christopher, B. R., and Perkins. S. (2000). "Geosynthetic reinforcement of aggregate base/subbase courses of pavement structures – GMA White Paper II." Prepared for AASHTO Committee 4E by the Geosynthetic Materials Association, Roseville, MN, June 2000.

Bolander, P. (1999). "Laboratory testing of nontraditional additives for stabilization of roads and trail surfaces." *Transportation Research Record,* 1652, 24–31.

Bouazza, A., and Avalle, D. L. (2006). "Effectiveness of rolling dynamic compaction on an old waste tip." *ISSMGE 5th Intl. Congress on Environmental Geotechnics*, 26-30 June, Cardiff, Wales, United Kingdom.

Briaud, J.L., James, R.W., and Hoffman, S.B. (1997). *NCHRP synthesis 234: settlement of Bridge Approaches (the bump at the end of the bridge)*, Transportation Research Board, National Research Council, Washington, D.C. 71 pp.

Bushman, W. H., T. E. Freeman, and E. J. Hoppe. (2004). *Stabilization techniques for unpaved roads*. Charlottesville, VA: Virginia Transportation Research Council, Virginia Department of Transportation.

Carle, R. J., and Whitaker, S. S. (1989). "Sheet piling bridge abutments." *Realizing DFI's Potential, a Parallel to Baltimore's Renaissance*, 14th Annual Members Conference, Baltimore, Maryland.

Ceylan, H. (2012). "Condition assessment of Iowa's transportation infrastructure system after 2011 Missouri River flooding." Presented at 2012 ASCE Geotechnical Conference, Ames, Iowa.

Christopher, B. R., C. Schwartz, and R. Boudreau. (2005). *Geotechnical Aspects of Pavements*. FHWA-NHI-05-037, U.S. Department of Transportation, Federal Highway Administration, Washington DC.

Chu, T. Y., D. T. Davidson, W. L. Geocker, and C. Moh. (1955). "Soil stabilization with lime-fly ash mixtures: Studies with silty and clayey soils." Highway Research Board, 108, 102–112.

Clarke, C. R., and Cosby, S. (2007). "Flood effect evaluation on SH24 – North of Washington, Oklahoma in McClain County," Presented at a meeting held by the USGS Oklahoma Water Science Center, National Weather Center, Norman, Oklahoma. <http://ok.water.usgs.gov/projects/hurricane/Pdf%20Files/12_Clark_ODOT_FloodStudy.pdf> (accessed May 5, 2013).

Clegg, B., and Berrangé, A. R. (1971). "The development and testing of an impact roller," *Trans. S. Afr. Instn. Civ. Engs.* Vol. 13, No. 3, pp. 65-73.

Collings, D., R. Lindsay, and R. Shunmugam. (2004). "LTPP exercise on foamed bitumen treated base-evaluation of almost 10 years of heavy trafficking on MR 504 in Kwazulu-Natal." *Proceedings of the 8th Conference on Asphalt Pavements for South Africa*, Sun City, South Africa.

Cook, D. (2002). "Tree sap helps hold roadside shoulder together." *Road Management,* 72(5), 30–31.

Doyle, J., and Ketcheson, G. (2007). "Lessons learned from management response to flood damaged roads in the western Washington cascades." *Proc. Advancing the Fundamental Sciences: Proceedings of the Forest Service National Earth Sciences Conference*, M. Furniss, C. Clifton, and K. Ronnenberg, eds., PNW-GTR-689, U.S. Department of Agriculture, Forest Service, Pacific Northwest Research Station, Portland, Oregon.

Evans, R., White, D. J., Kaliber, W. (2012). *Modified sheet pile abutments for low-volume road bridges*. IHRB Project TR-568, Center for Earthworks Engineering Research and Bridge Engineering Center, Iowa State University, Ames, Iowa.

Fang, H. Y. (1990). *Foundation engineering handbook.* 2nd Ed. New York, NY: VanNostrans Reinhold.

FHWA. (2012). "European Collaboration – Flooded Pavement Assessment." Federal Highway Administration (FHWA) Research and Technology, United States Department of Transportation, Washington, D.C. <http://www.fhwa.dot.gov/research/partnership/eu-collaboration/flooded.cfm> (accessed August 5, 2013).

Giroud, J. P., and J. Han. (2004). "Design method for geogrid-reinforced unpaved roads. I. Development of design method." *Journal of Geotechnical and Geoenvironmental Engineering,* 130(8), 775–786.

Gopalakrishnan, K., Ceylan, H., and Kim, S. (2010). *Biofuel Co-Product uses for pavement geo-materials stabilization*. IHRB Project TR-582, Iowa State University, Ames, Iowa.

Grigg, N., McCarthy, C., Lawrence, B., and Ockerman, D. (2011). *Review of the Regulation of the Missouri River Mainstem Reservoir System During the Flood of 2011,* Missouri River Independent Review Panel, Missouri River Flood Task Force < http://www.nwd-mr.usace.army.mil/rcc/MRFTF/docs/MRIndependentReviewPanel.pdf> (accessed March 5, 2013).

Grode, K. (2012). "Missouri River Mainstem System 2012-2013 Draft Annual Operating Plan," US Army Corps of Engineers, Presented at the Missouri River Association of States and Tribes (MoRAST) Meeting, Bismarck, ND, September. <http://mo-rast.org/wp-content/uploads/2012/09/Grode_MoRAST_Sept20-2012_DraftAOP.pdf> (accessed March 5, 2013).

Highfield, W.E., and Brody, S.D. (2013). "Evaluating the effectiveness of local mitigation activities in reducing flood losses." *Nat. Haz. Rev*., in press.

Hopkins, T. C., T. L. Beckham, and D. Q. Hunsucker. (1995). *Modification of Highway Soil Subgrades.* Final Report KTC 94-11, Kentucky Transportation Center, University of Kentucky, Lexington, KY.

Huang, C. C., and Tatsuoka, F. (1990). "Bearing capacity of reinforced horizontal sandy ground." *Geotextiles and Geomembranes,* Vol. 9, 51-82.

Iowa DOT (2013). Flood Safety – Iowa Department of Transportation, Ames, Iowa. <http://www.iowadot.gov/floods/> (accessed August 5, 2013).

Iowa HSEMD (2011). *Missouri River Flood Coordination Task Force Report,* Prepared by the Missouri River Flood Coordination Task Force and Reviewed by the Task Force Chairman, Brigaidier General J. Derek Hill, Iowa Homeland Security and Emergency Management Division (HSEMD).

Kelleher, J. B, and Bohan, P. (2011). "Missouri River levee near Hamburg, Iowa fails," Reuters online edition, June 13. <http://www.reuters.com/article/2011/06/13/us-flooding-plains-idUSTRE75A1OX20110613 > (accessed March 5, 2013).

Kendall, M., B. Baker, P. Evans, and J. Ramanujan. (2001). "Foamed bitumen stabilization- The Queensland experience." *20th Australian Road Research Board (ARRB) Conference,* 1–32.

Keller, G.R. (2002). "Rural roads vulnerability reduction assessment, mitigation measures, and training." *Nat. Haz. Rev*., 3(4), 139-147.

Kettle, R. J., and E. Y. McCabe. (1985). "Mechanical stabilization for the control of frost heave." *Canadian Journal of Civil Engineering*, Vol. 12, 899–905.

Latka, D. (2012). "Missouri River Mainstem Reservoir System – Lessons Learned from 2011 Flood of Record and the Path Forward," US Army Corps of Engineers, Presented at the Missouri River Natural Resources Committee (MRNRC) Meeting, Jefferson City, Missouri, March. <http://www.mrnrc2012.com/LatkaMRNRCMarch2012.pdf> (accessed March 5, 2013).

Mastre, B., and Smollen, G. (2011). "Explosives used to breach levee, investigation underway." Online article by Wowt.com, July 1. <http://www.wowt.com/home/headlines/Explosives_Used_to_Breach_Levee_Investigation_Underway_124871614.html > (accessed March 5, 2013).

McMahon, J. R., and Farhat, J. (2012). *Technical Analysis of Missouri River Mainstem Flood Control Storage,* U.S. Army Corps of Engineers, Northwestern Division, Missouri River Basin Water Management Division, Omaha, Nebraska.< http://www.nwd-mr.usace.army.mil/rcc/reports/pdfs/PressKit.pdf > (accessed March 5, 2013).

Mestl, G. (2011). "The Missouri River Flood of 2011: New Report Examines Causes." *Prairie Fire,* September, Lincoln, NE < http://prairiefirenewspaper.com/2011/09/the-missouri-river-flood-of-2011-new-report-examines-causes> (accessed March 5, 2013).

Milligan, G. W. E., and Love, J. P. (1984). "Model testing of geogrids under an aggregate layer in soft ground." *Proc., Symp. on Polymer Grid Reinforcement in Civ. Engrg.,* ICI, London, England.

Muthen, K. M. (1998). *Foamed asphalt-mix design procedure*. Report CR-98/077. Pretoria, South Africa: SABITA Ltd. and CSIR Transportek.

NOAA. (2011). *United States Flood Loss Report – Water Year 2011*. National Weather Service, National Oceanic and Atmospheric Administration, US Dept. of Commerce, Silver Spring, Maryland. <http://www.nws.noaa.gov/hic/summaries/WY2011.pdf> (accessed August 5, 2013).

Ott, R.L., and Longnecker, M. (2001). *An introduction to statistical methods and data analysis,* 5th Ed., Published by Duxbury, Thomson Learning Academic Resource Center, Pacific Grove, California.

Portland Cement Association (1995). *Soil-Cement Construction Handbook*, Portland Cement Association (PCA), Skokie, Illinois.

Powell, W., Keller, G.R., and Brunette, B. (1999). "Application for geosynthetics on forest service low-volume roads." *Transportation Research Record,* 1652, 113–120.

Rollings, M. P., and R. S. Rollings. (1996). *Geotechnical Materials in Construction.* McGraw-Hill, New York, NY.

Salt, G. (1998). *Pavement deflection measurement and interpretation for the design of rehabilitation treatments*. Transit New Zealand Report No. 117, Tonkin and Taylor International Ltd.

Stokoe II, K.H., Lee, J.-S, Nam, B.-H, Cox, B.R., Oshinski, E. (2011). "Investigations of Galveston airport pavements after hurricane Ike in 2008 and liquefaction sites in residential areas after the New Zealand earthquake in 2010." *Geotechnical Engineering for Disaster Mitigation and Rehabilitation and Highway Engineering 2011*, S.P.R. Wardani, J. Chu, S.C. Robert Lo, S. Iai, K.K. Phoon, eds., World Scientific Publishing Co. Pte. Ltd., Singapore.

Terrel, R. L., J. A. Epps, E. J. Barenberg, J. K. Mitchell, amd M. R. Thompson. (1979). *Soil Stabilization in Pavement Structures—A User's Manual—Vol. 2: Mixture Design Considerations*, FHWA-IP-80-2, Federal Highway Administration, Washington, D.C.

USACE. (2006). *Missouri River Mainstem Reservoir System Master Water Control Manual*, Reservoir Control Center, U.S. Army Corps of Engineers, Northwestern Division – Missouri River Basin, Omaha, Nebraska, March. <http://www.nwd-mr.usace.army.mil/rcc/reports/mmanual/MasterManual.pdf > (accessed March 5, 2013).

USACE. (2012a). *Missouri River Mainstem Reservoir System – Post 2011 Flood Event Analysis of Missouri River Mainstem Flood Control Storage,* U.S. Army Corps of Engineers, Northwestern Division, Missouri River Basin Water Management Division, Omaha, Nebraska, April. < http://www.nwd-mr.usace.army.mil/rcc/reports/pdfs/Post2011FloodEventAnalysisofMainstemFloodControlStorage.pdf> (accessed March 5, 2013).

USACE. (2012b). *Missouri River Mainstem Reservoir System – Summary of Actual 2011 Regulation,* U.S. Army Corps of Engineers, Northwestern Division, Missouri River Basin Water Management Division, Omaha, Nebraska, July. < http://www.nwd-mr.usace.army.mil/rcc/reports/pdfs/rcc2011summary.pdf > (accessed March 5, 2013).

Vennapusa, P., and White, D.J. (2009). "Comparison of Light Weight Deflectometer Measurements for Pavement Foundation Materials." *Geotechnical Testing Journal*, Vol. 32, No. 3, pp. 239–251.

Vennapusa, P., White, D. J., and Klaiber, F. W. (2012). *Geosynthetic reinforced soil for low-volume bridge abutments*. IHRB Project TR-621 Final Report, Center for Earthworks Engineering Research, Iowa State University, Ames, Iowa.

White, D.J, Becker, P., Vennapusa, P., Dunn, M., White, C. (2013a). "Assessing soil stiffness of stabilized pavement foundations." *Transp. Res. Rec.: J. Transp. Res. Board*, 2335, 99-109.

White, D. J., Harrington. D., and Thomas, Z. (2005). *Fly Ash Soil Stabilization for Non-Uniform Subgrade Soils, Volume I: Engineering Properties and Construction Guidelines*. IHRB Project TR-461; FHWA Project 4. Iowa State University, Ames, Iowa, April 2005.

White, D. J., Mekkawy, M., Jahren, C., Smith, D., and Suleiman, M. (2007). *Effective Shoulder Design and Maintenance*, IHRB Project TR-531, Iowa State University, Ames, Iowa.

White, D. J., Vennapusa, P., and Becker, P. (2013b). *Boone County Expo Test Sections – Phase I*, Final Report, Center for Earthworks Engineering Research, Iowa State University, Ames, Iowa (in preparation).

White, D. J., Vennapusa, P., and Gieselman, H. (2011). "Field Assessment and Specification Review for Roller-Integrated Compaction Monitoring Technologies." Special Issue: Advances in Instrumentation and Monitoring in Geotechnical Engineering, *Advances in Civil* Engineering Journal, Hindawi Publishing Corporation, Vol. 2011, Article ID 783836.

Wu, J.T., Lee, K., Helwany, S., Ketchart, K. (2006). *Design and construction guidelines for geosynthetic-reinforced soil bridge abutments with a flexible facing*, NCHRP Report 556, Transportation Research board, Washington, D.C.

Zhang, Z., Wu, Z., Martinez, M., and Gaspard, K. (2008). "Pavement structures damage caused by hurricane Katrina flooding." *J. Geotech. Geoenviron. Eng.,* 134(5), 633-643.

Yu, T. (2012). "A new NDT Tool for Pavement Evaluation: Step-Frequency GPR," *Presented at the 2012 TTCC-National Concrete Consortium Meeting – Fall 2012,* Seattle, Washington. <http://www.cptechcenter.org/t2/SP2012_Presentations_Reports/08%20YU-NDT%20presentation.pdf>, Date Accessed August 11, 2013.

APPENDIX A: SUMMARY OF DAMAGES, EMERGENCY OPERATIONS, AND DAMAGE COSTS REPORTED BY THE IOWA DOT

Table A1. Summary of damages, emergency operations, and damage costs on primary roads in Iowa (information obtained from Bonie Castillo, Iowa DOT)

County	Location	Brief Description of Damage and Emergency Operations	Emergency Costs	Permanent Costs
Monona	I-29N and I-29S between MP 105 and 110	Trap bags placed on the outside shoulder and inside median to prevent flood waters from encroaching on pavement. Pumps used to de-water	$977,694	—
	I-29 between MP 107 and 110	Debris removal, damaged field fence, dead and fallen trees, destroyed vegetation, dead living snow fence, silt in culverts, emergency work done to keep I-29 open, construction of temporary bridge approaches at the SB Cleghorn bridge, trap bags over the Cleghorn bridge, placing temporary crash cushions at the end of the trap bags, utilizing incident response as part of the traffic control	$388,591	$418,000
	I-29 between MP 107.9 and 109.5	Traps bags placed at two locations on I-29 at risk to overtopping, trap bags removed & pre-flood traffic control restored after flood water receded using a detour of NB I-29, detour signing installed and removed, revision to include clearing and grubbing project	$130,250	$68,373
	IA175 between MP 0.0 to 0.1	Protection to avoid erosion and damage to east berm of the bridge connecting Nebraska and Iowa	$2,009,640	—
	IA175 between MP 0.0 to 0.7	Scour hole repair, protecting berm with revetment, repairing slide on south side of IA175, placing and removing sand bags, clearing dead trees, replacing damaged field fence, seeding and fertilizing, debris removal, patching damaged PCC, and replacing guard rail	$5,011,166	$587,170
	IA175E at MP 0.0	Detour implemented due to rising water flood waters at the Decatur bridge. Erosion of abutment fill under bridge approach	$152,440	$21,596
Woodbury	I-29 between MP146 north to the South Dakota border	Clearing and grubbing dead and downed trees, debris removal, reestablishing vegetation, replacing damaged fence, and repairing damage storm sewer	—	$304,900
	I-29 Exit 147A	Building levee to keep flood waters from encroaching on I29SB exit ramp, signing, and temporary detours	$5,333	—

	I-29 near Hamilton Blvd MP 148 to 149	Construction of temporary ramp built due to flooding on Hamilton Blvd.	$45,396	—
Woodbury	I-29S at MP149 and the Hamilton Blvd. exit.	Flooding on Hamilton Blvd, water pumps used to lower water table and maintain NB exit	$17,359	—
	I-29 between MP 149 and 149.1	Undermining and sloughing of material through a storm sewer pipe under the highway causing I29SB paved shoulder collapse, voids discovered under SB lanes filled with flowable mortar, sorm sewer pipe under highway partially crushed, double reinforced path installed to maintain traffic	$100,596	$78,001
	IA12 near MP 3.7	Temporary detour and traffic control, plugged storm sewer, pumping water to maintain traffic on the interchange ramps and loop	$6,683	—
Fremont	I-29 from MP 0 to 1.8	Damaged guardrail, undermined bridge approach slabs, dead tree hazard, eroded fore slopes and ditches, destroyed right of way vegetation, plugged culverts, and possible pipe separation	$101,102	$291,850
Multiple Counties	I-29 from MP 0 to 71.6.	Long-term saturation of underground electrical wiring and one damaged luminary	—	$222,295
Fremont	I-29N MP 1.4	Damage to district levees within the right of way	—	$53,440
	I-29N near MP 1.4	Revetment repairs	$432,534	—
	I-29N between MP 0.8 and 3.2	Undermining of the bridge approaches at MP 1.5, construction of cross overs, replacement of bridge approaches	$1,009,882	—
	I-29S from MP 1.8 to 10.1	Damage to shoulder and ramps, eroded ditches and fore slopes, damage to right of way fence, destroyed vegetation, and damaged signs and pavement markings	$335,586	$878,060
	I-29S from MP 10.1 to 15.5	Damage to shoulder and ramp, pipe separations, crushed and missing subdrain outlets, buried pipe outlets, eroded fore slopes and ditches, flood debris in ditches, and damaged right of way fence and vegetation	$93,600	$872,140
	I-29S near MP 10.2	Damage to a roadside weather station power and control box, and damage to surface sensor cable near IA2 and I-29 bypass	—	$9,077

	I-29N near MP 11	Damage to components of Fremont County scale	—	$30,872
	I-29 over Horse creek	Rip rap repair	—	$231,240
Fremont	I-29S MP 15.5 to 20	HMA delamination, erosion, damage to ramps, damage to culverts, replacement of fence	$2,522	$414,153
	I-29S between MP 20 and 25	Damage to ramps and shaping of ditches	—	$322,679
	I-29N between MP 0 and 25.5	Removal of debris, silt, and water scum on pavement and shoulders from receding flood waters	$173,197	—
	IA2E	Removal of debris, silt, and water scum on pavement and shoulders from receding flood waters	$35,513	—
	IA2E between MP 0.3 and 8	Pavement under water for about 5 months leaving behind saturated subgrade conditions, which resulted in pavement cracks, subsidence due to voids during spring/thaw in 2012	$30,360	—
	IA2W between MP 0 and 8	Debris removal, cleaning of pavement surface, reconstruction of roadway (partial), undermining of bridge appraoches, damage to pavement joint material, erosion of shoulders, delamination on pavement overlay, separated pipe joints, erosion to fore slopes and ditches, and pavement undermining	$3,071,184	$659,675
	IA2E at 2.4 miles and 6.1 miles East of Missouri River	Erosion of several drainage ditch levees	—	$148,645
	IA2E at 1 mile west of I-29	Emergency repair of revetment	$446,807	—
	IA333E near MP 0 to 1	Damaged pavement and shoulder, fore slope erosion, undermined bridge approaches due to erosion, and dead vegetation	$261,064	$22,100
Harrison	US30W between MP 0 and 4	Fore slope erosion	—	$322,743
	US30E between MP 1 and 3	Place and remove trap bags to avoid flooding on US30	$3,228,423	—
Mills	I-29S between MP 25 and 32.4	Reconstruction of eroded fore slopes	—	$246,253
	I-29S between MP 32.4 and 35.5	Culvert and apron separation, damage to fence, loss of slope vegetation	—	$102,076

	US34E between MP 0 and 3	Damage to ditches and vegetation	—	$51,090
Pottawattamie	Old Mormon bridge East	Damaged electronics	$48,385	—
Pottawattamie	I-29N between MP 43.6 and 46	Removal of debris, silt, and water scum on pavement	$188,270	—
	I-29N between MP 56 and 57	Pavement markings and seeding	$1,280	$49,500
	I-29S between MP 57 and 62	HMA delamination, eroded shoulder, lost paint markings, missing joint seal/backer rods, damaged guardrails, culvert and apron separation/damage, reshaping of slopes, railroad ballast in east ditch, damaged fencing, loss of vegetation	$663,670	$1,049,462
	I-29N between MP 62 to 66.4	Lost paint markings, HMA shoulder erosion, delamination, culvert joint separation, damaged fencing, and seeding	$48,320	$1,631,320
	I-29N between MP 66.4 and 71.6	Lost pavement markings, ditch shaping, seeding, and damage to fence	$49,320	$838,295
	I-29N and I-680	Placing trap bags, sand bags, and pipes with some grading to reduce amount of flooding and maintain traffic on ramps	$263,532	—
	I-680W between MP 0.0 to 3.1	Complete destruction of roadway	$21,387,000	—
	I-680E from MP 0.0 to 3.1	Removal of debris, silt, and water scrum on pavement and shoulders	$66,831	—
TOTAL (on Primary Roads in Iowa)			**$40,783,530 Emergency Costs**	**$9,925,005 Permanent Costs**

Table A2. Summary of damages, emergency operations, and damage costs on secondary roads in Iowa (Courtesy of Bonie Castillo, Iowa DOT)

County	Location	Brief Description of Damage and Emergency Operations	Emergency Costs	Permanent Costs
Fremont	220th St. (J34) West from 195th Ave. (L31) for about 0.59 miles	Damage to shoulder on both sides of seal coat pavement, damage to seal coat pavement, and some damage to base, and removal of debris and silt on pavement.	$43,068	—
	195th Ave. South from 230th St. to IA2 (2.13 miles)	Damage to entire roadway, base, and pavement	$20,950	$280,000
	310th St. (J64) from west of I-29 to 240th Ave. (4.03 miles)	Damage to entire roadway, base, shoulders, sealcoat, and concrete pavement.	$805,000	$790,000
	Waubonsie Ave. (J10) South from east of 200th Ave. (L31) for 1.9 miles	Damage to shoulder on both sides of pavement and removal of debris and chemical tanks.	$25,300	—
Pottawattamie	Old Mormon Bridge Road West (GPS West End N 502840.0 E 982255.0, East End N 504047.0 E 985825.0)	Damage to shoulders, PCC, and HMA pavements, and erosion of base material.	$131,486	—
	Joslin Ave North (GPS, West End N 487091.0 and E 988934.0, East End N 487112.0 and E 989311.0)	Damage to granular surfacing due to erosion, applied calcium chloride for dust control.	$49,451	—
	Sumac Road West (GPS, East End N 531196.2 E 990828.1, West End N 527439.1 and E 984678.0)	Damage to granular surfacing due to erosion, and removal of debris.	$32,089	—

	Old Mormon Bridge Rd W (GPS West End 41°21'23.5," 95°53'35.9," East End 41°21'24.5," 95°53'32.8")	HMA pavement undermined (erosion of underlying base material) and failed, replaced about 200 ft of HMA pavement with 2.5" to 3" HMA.	$15,487	—
	Old Mormon Bridge Rd W (GPS West End 41°21'20," 95°53'43," East End 41°21'21.6," 95°53'42")	PCC pavement undermined (erosion of base material) and failed, replaced about 200 ft of PCC pavement with 9" PCC.	$43,000	—
	Mynster Springs Road North (GPS East End 997931.9, 484422.9; West End 992681.5, 478780.7)	Damage to HMA pavement due to heavy construction loads (wheel track rutting, stress cracking, and failure). Agricultural traffic and heavy construction traffic used this roadway during I29 closures.	—	$322,000
	Old Lincoln Hwy North within Council Bluffs City Limits	Damage to HMA pavement due to heavy construction loads (wheel track rutting, stress cracking, and failure). Heavy construction traffic used this roadway during I29 closures, due to its proximity to the Crescent quarry.	—	$2,733,203
	Old Lincoln Hwy North within City of Crescent, Iowa		—	$189,637
TOTAL (on Secondary Roads in Iowa)			**$1,170,592 Emergency Costs**	**$4,310,080 Permanent Costs**

APPENDIX B. TIME-LAPSED GRAPHICAL DEPICTION OF FLOODWATER BOUNDARIES NEAR I-29 AND I-680

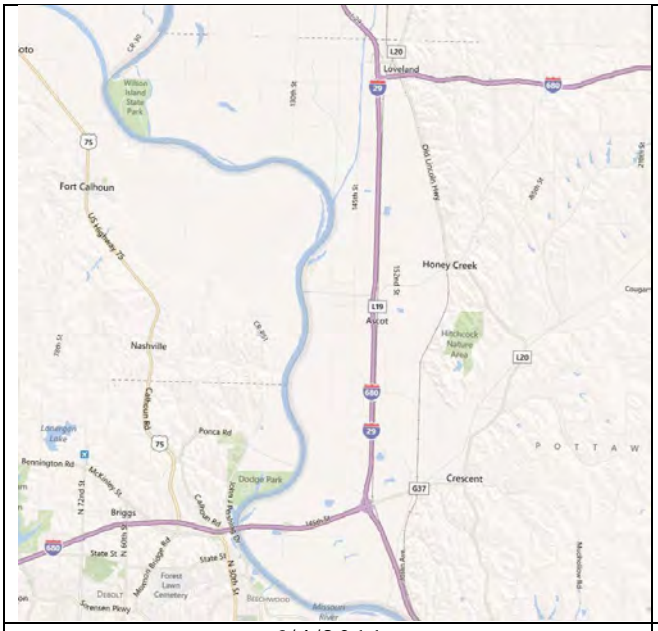

6/4/2011

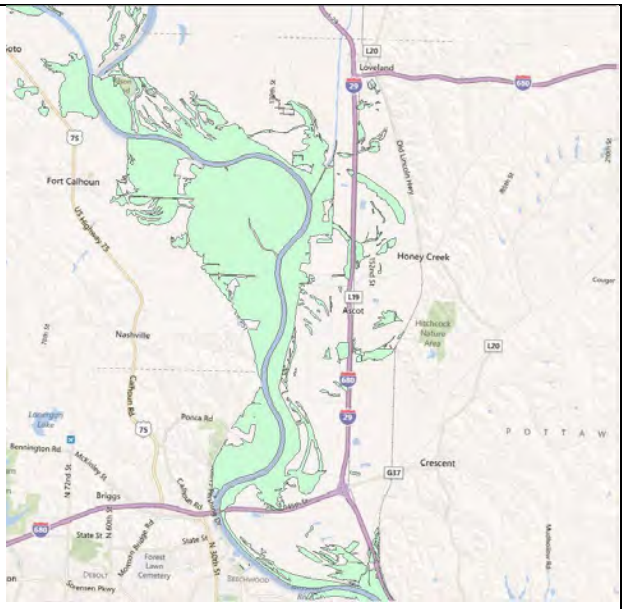

6/5/2011

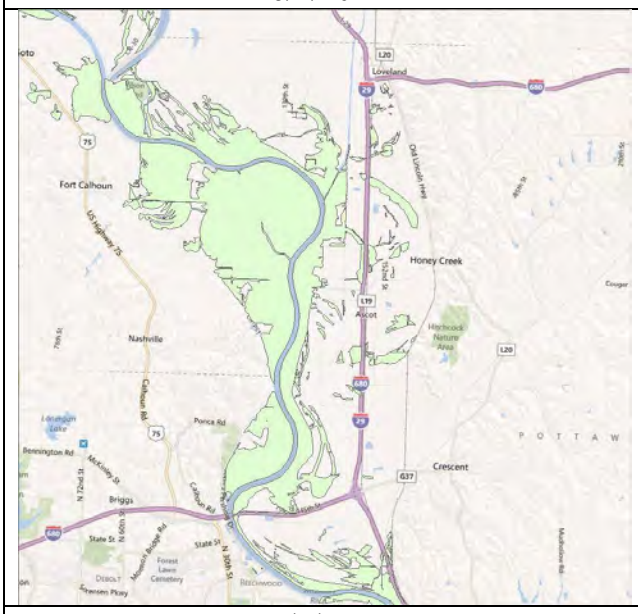

6/6/2011

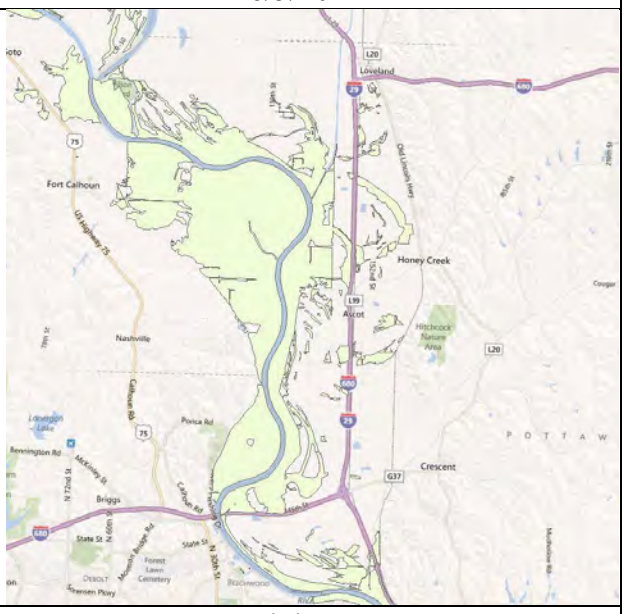

6/7/2011

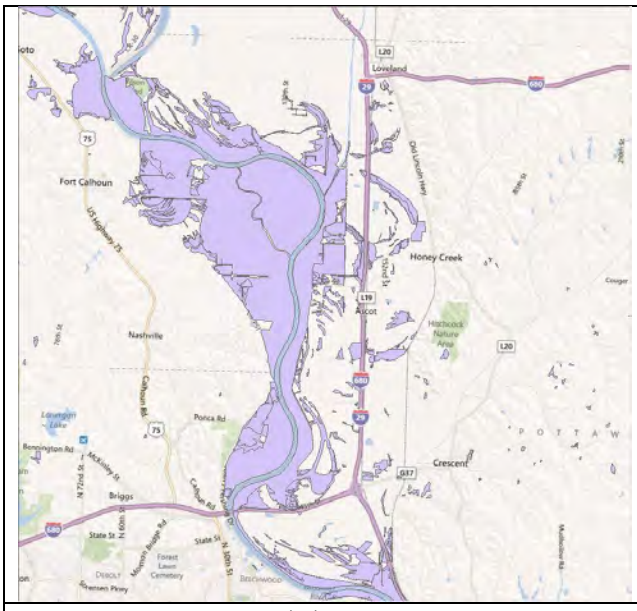

6/8/2011

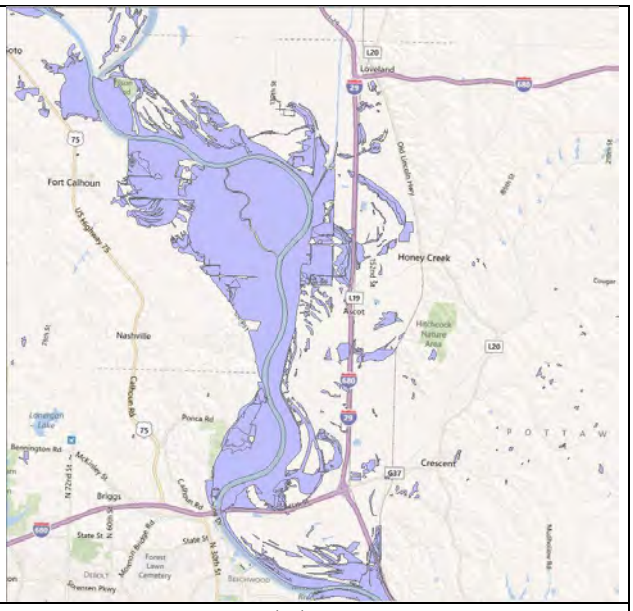

6/9/2011

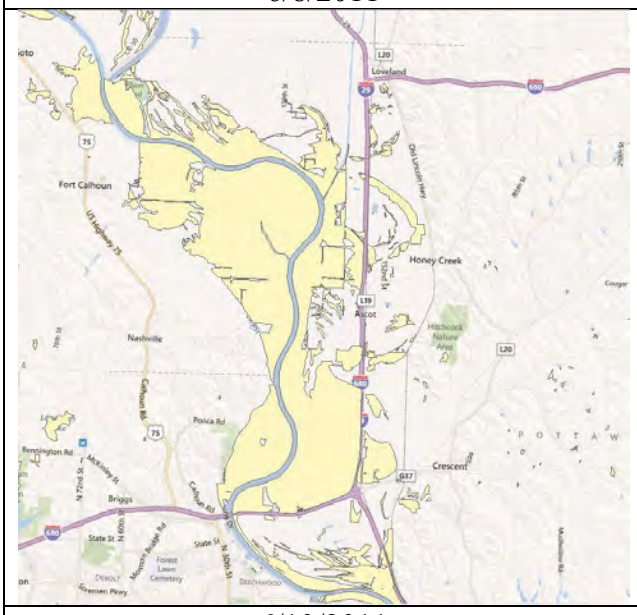

6/10/2011

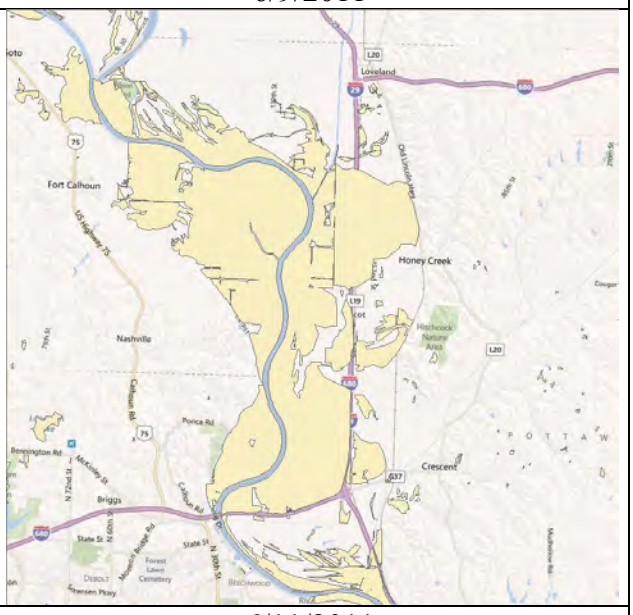

6/11/2011

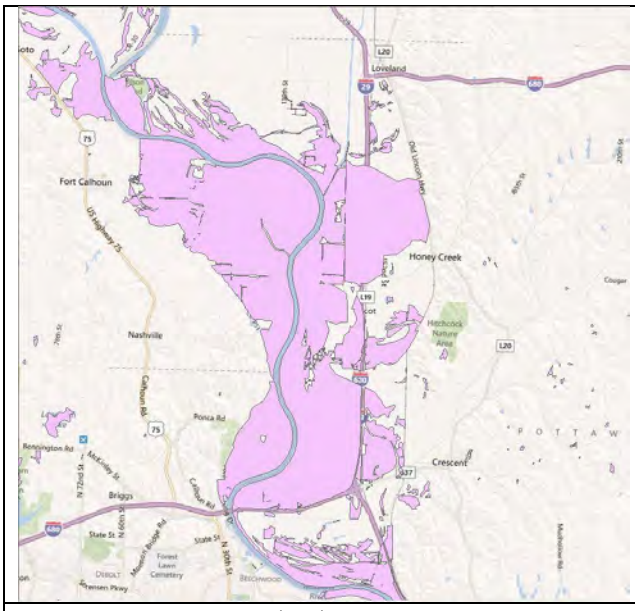	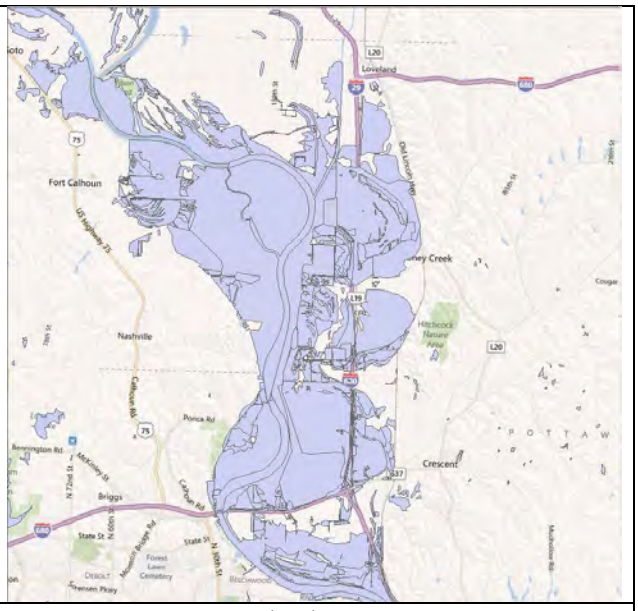
6/12/2011	6/13/2011
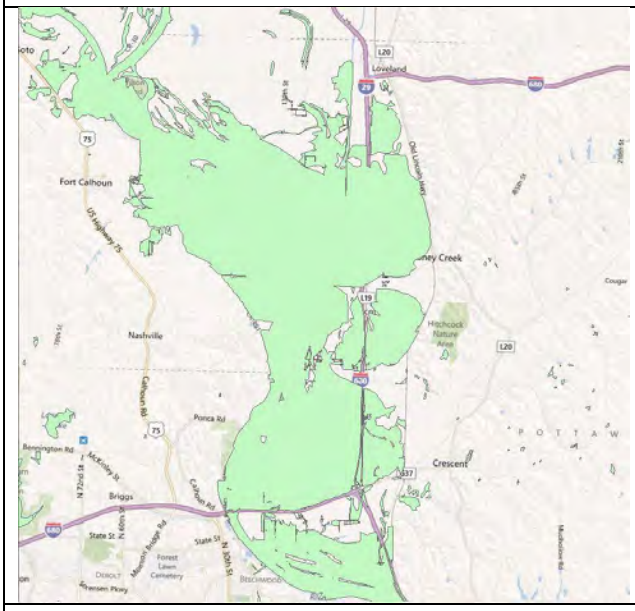	
6/14/2011	6/15/2011

6/16/2011

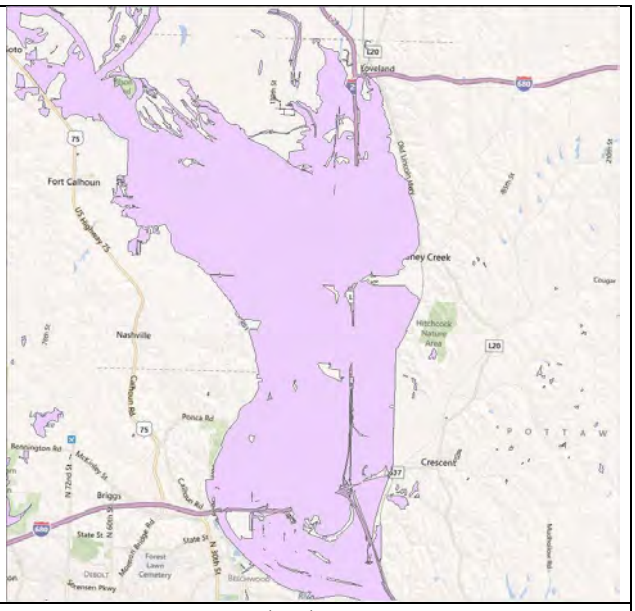

6/17/2011

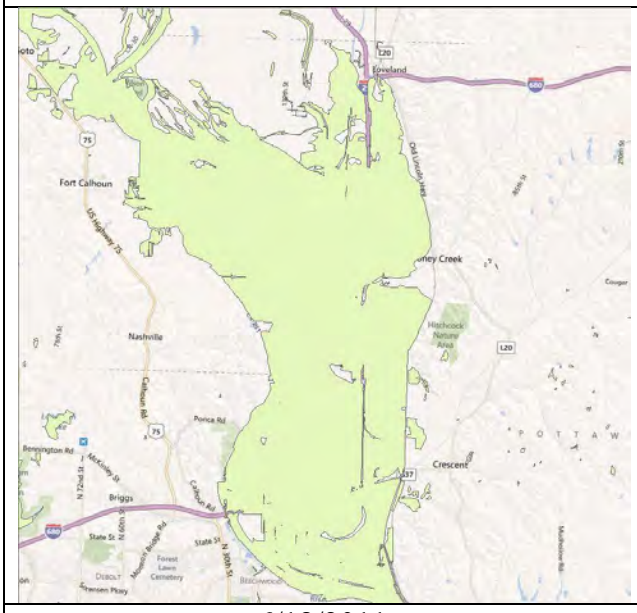

6/18/2011

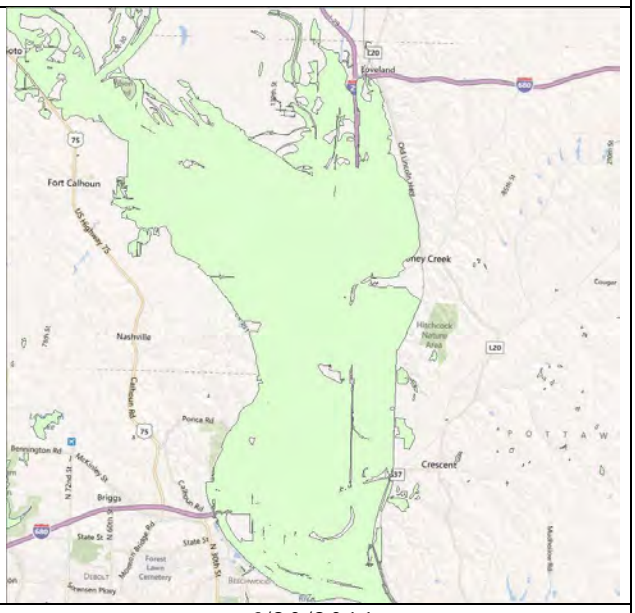

6/20/2011

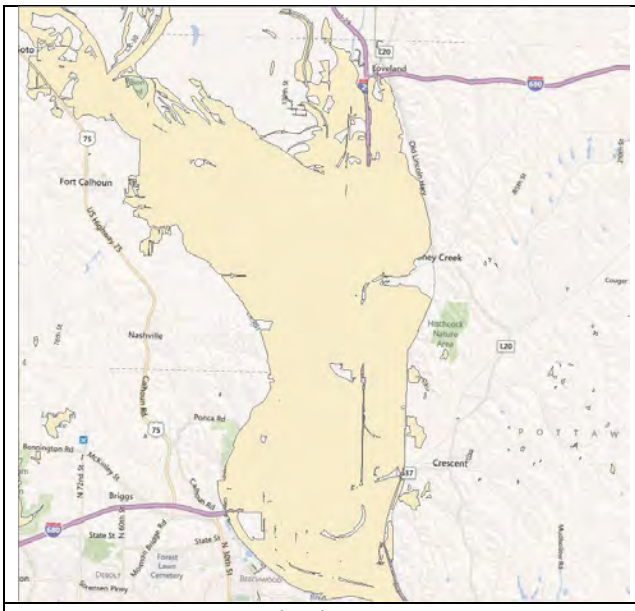

6/21/2011

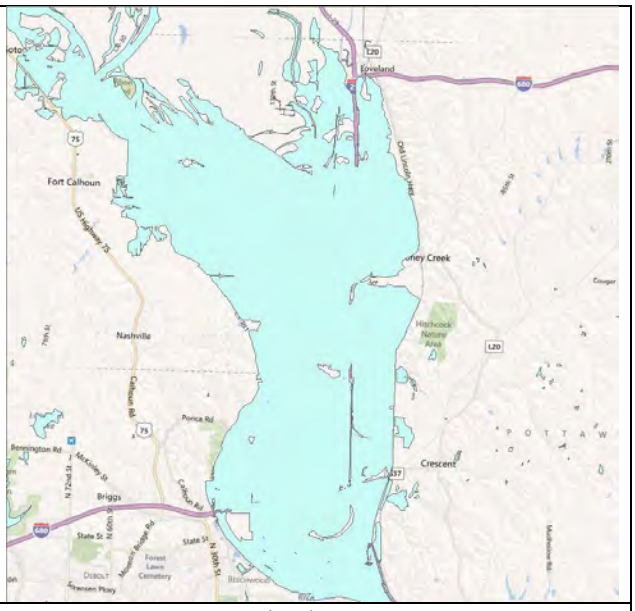

6/22/2011

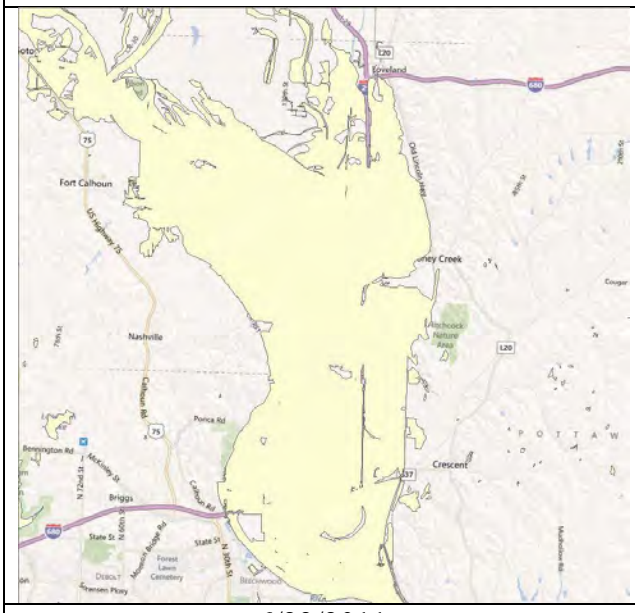

6/23/2011

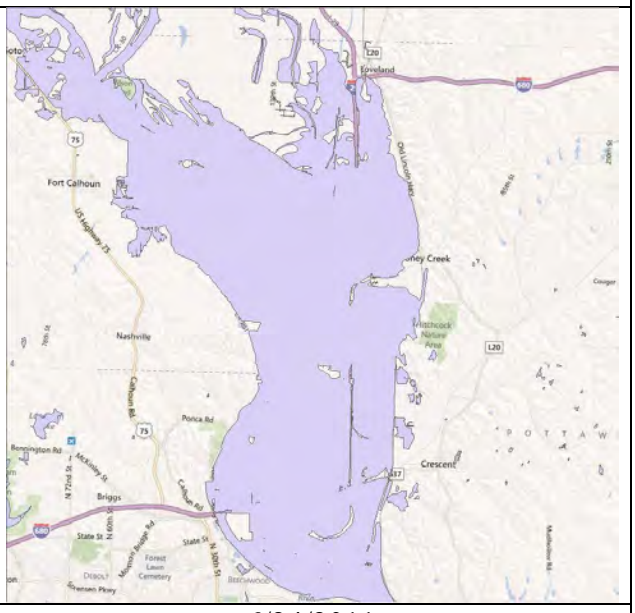

6/24/2011

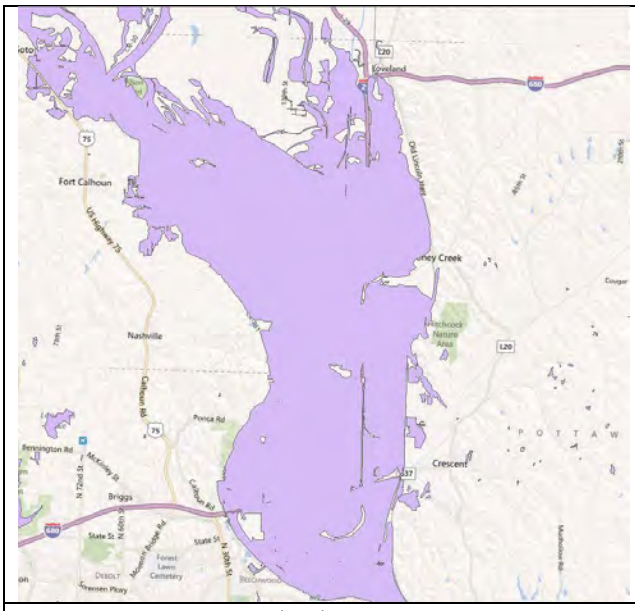	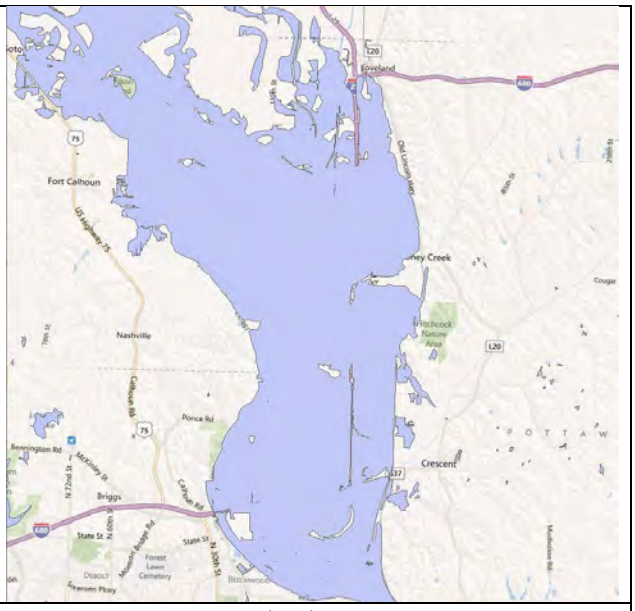
6/27/2011	6/29/2011
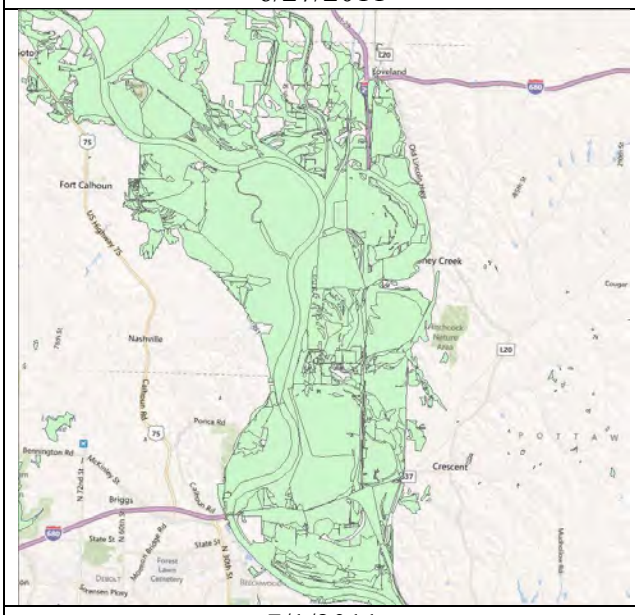	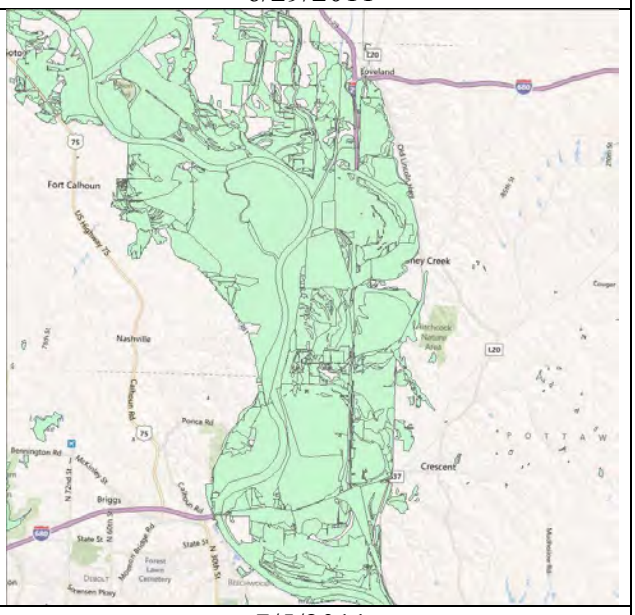
7/1/2011	7/5/2011

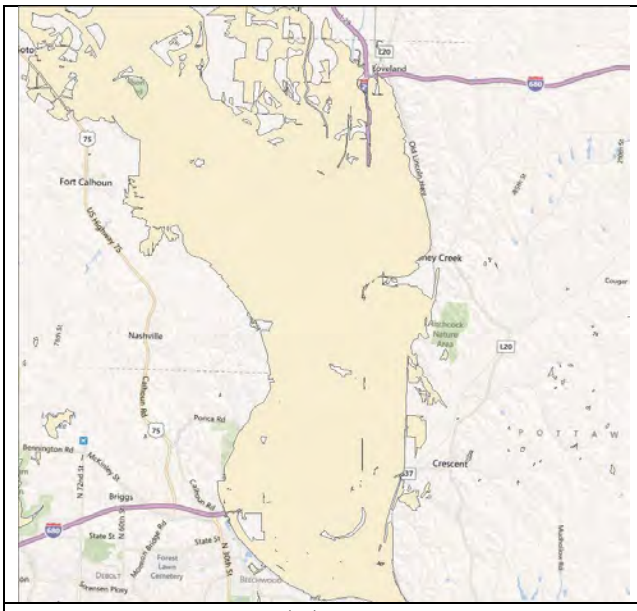	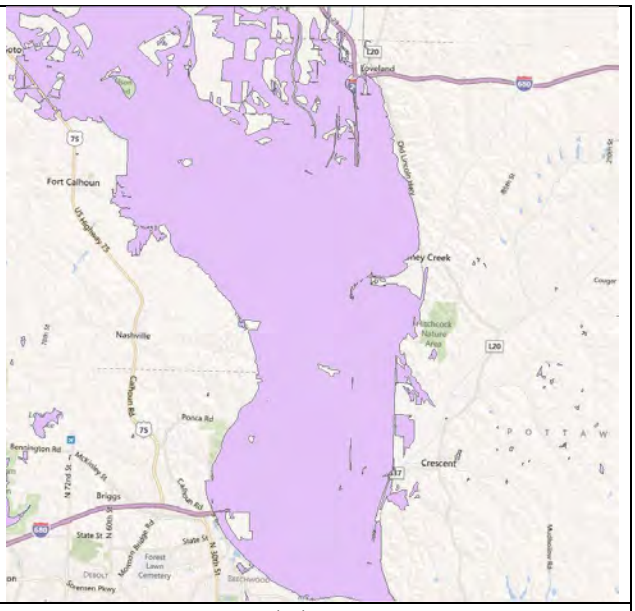
7/6/2011	7/8/2011
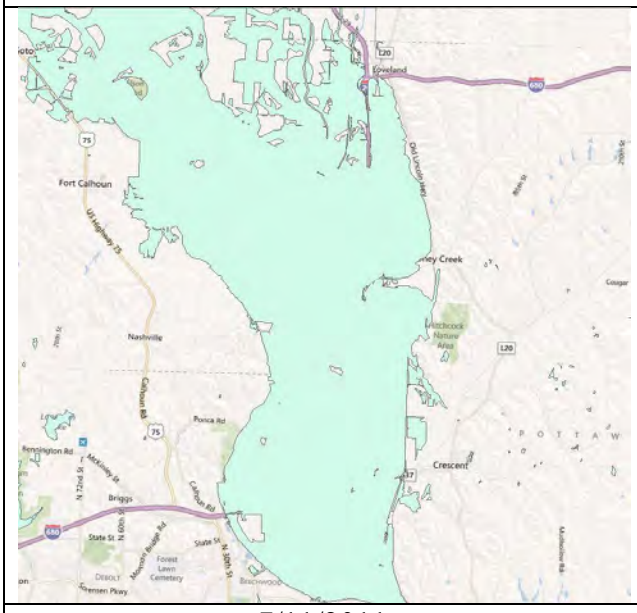	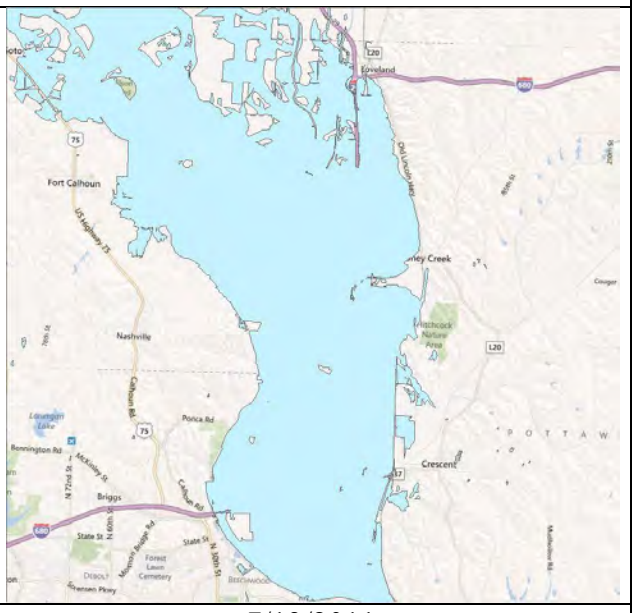
7/11/2011	7/13/2011

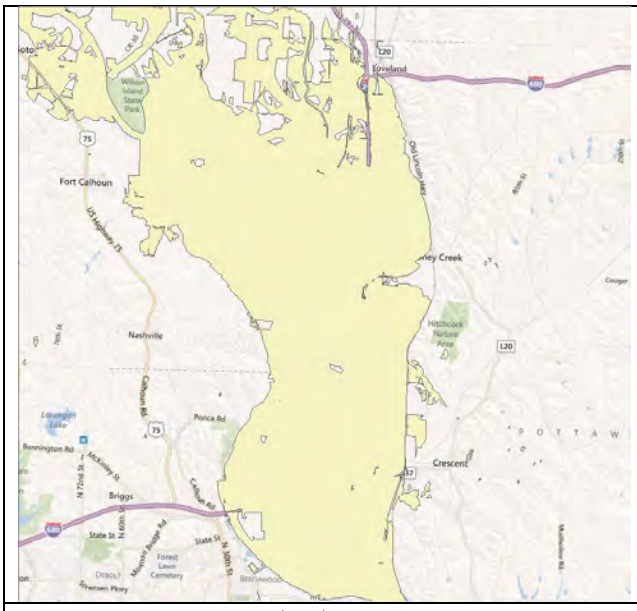	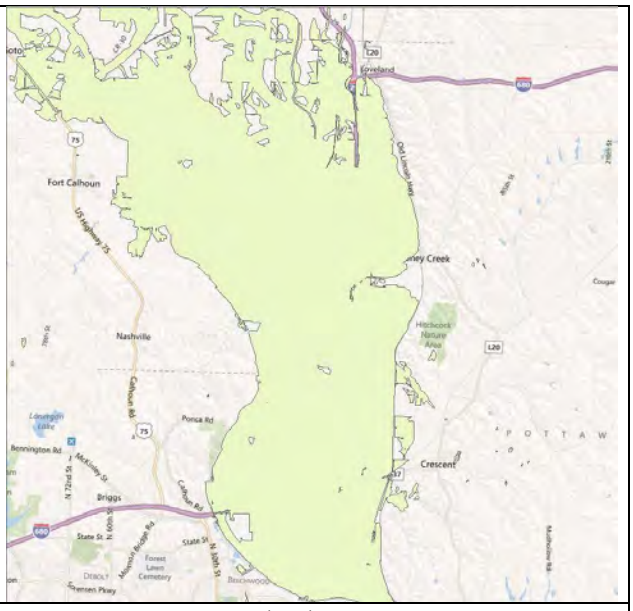
7/15/2011	7/18/2011
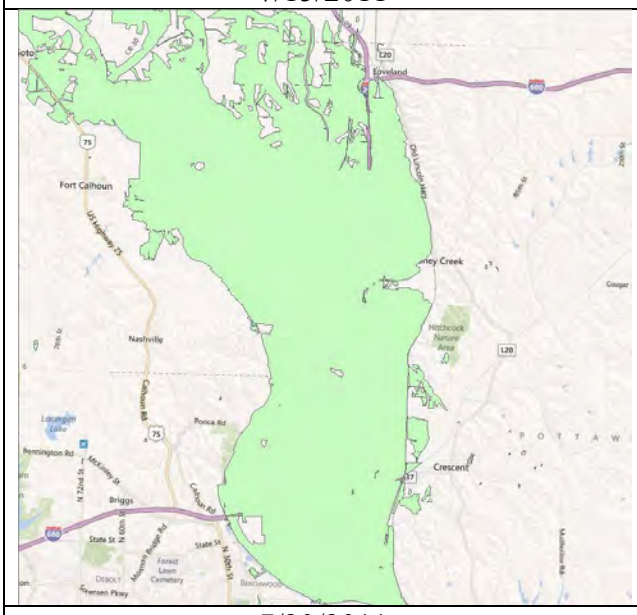	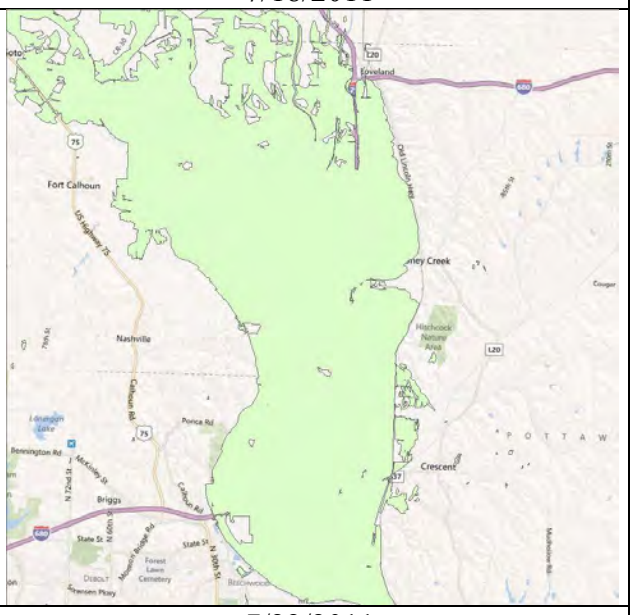
7/20/2011	7/22/2011

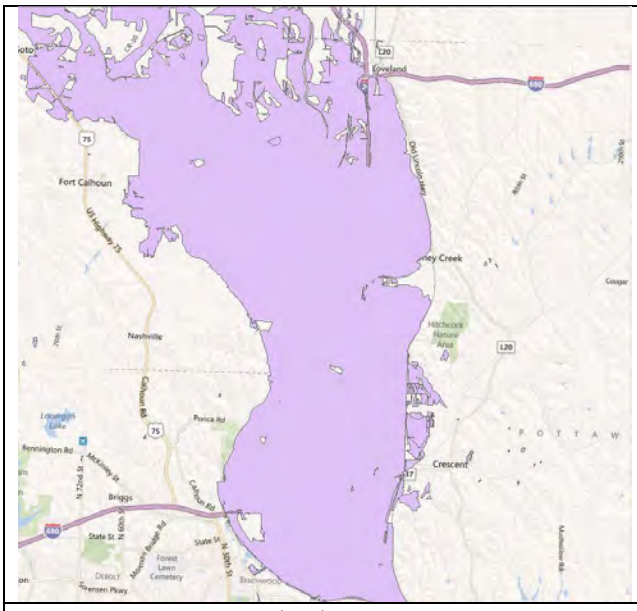	
7/29/2011	8/10/2011
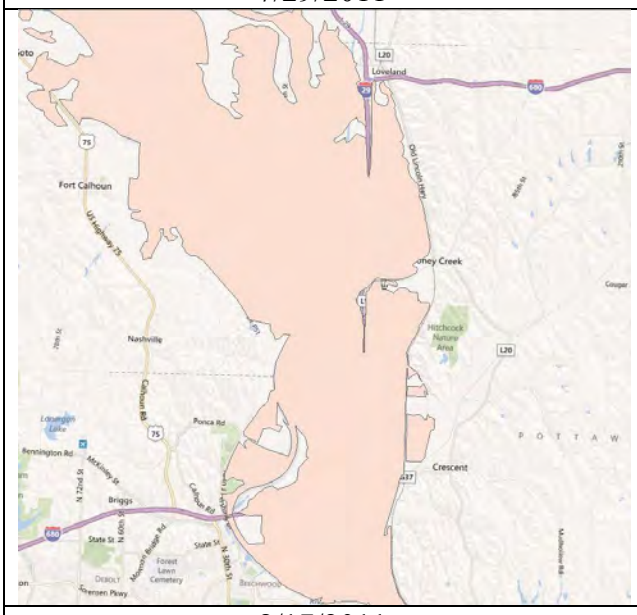	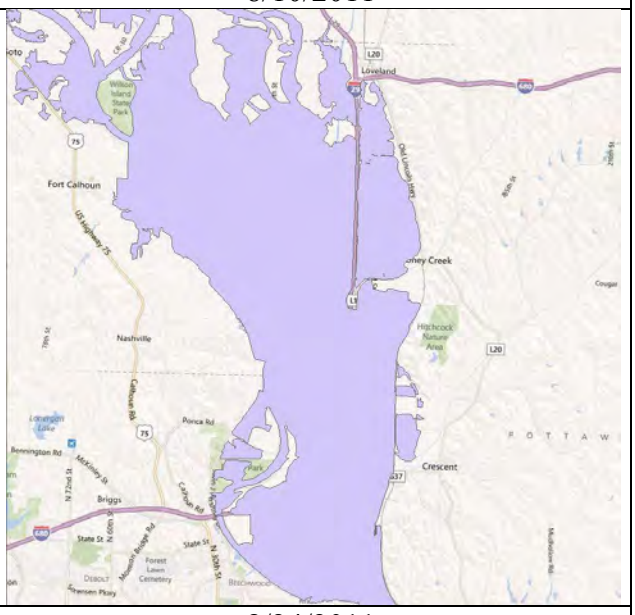
8/17/2011	8/24/2011

 L20 Loveland Fort Calhoun Nashville Hitchcock Nature Area Crescent Ponca Rd Pennington Rd Briggs State St Forest Lawn Cemetery Bascomwood	
8/31/2011	

APPENDIX C. GROUND TEMPERATURE DATA FROM MOVILLE, IOWA

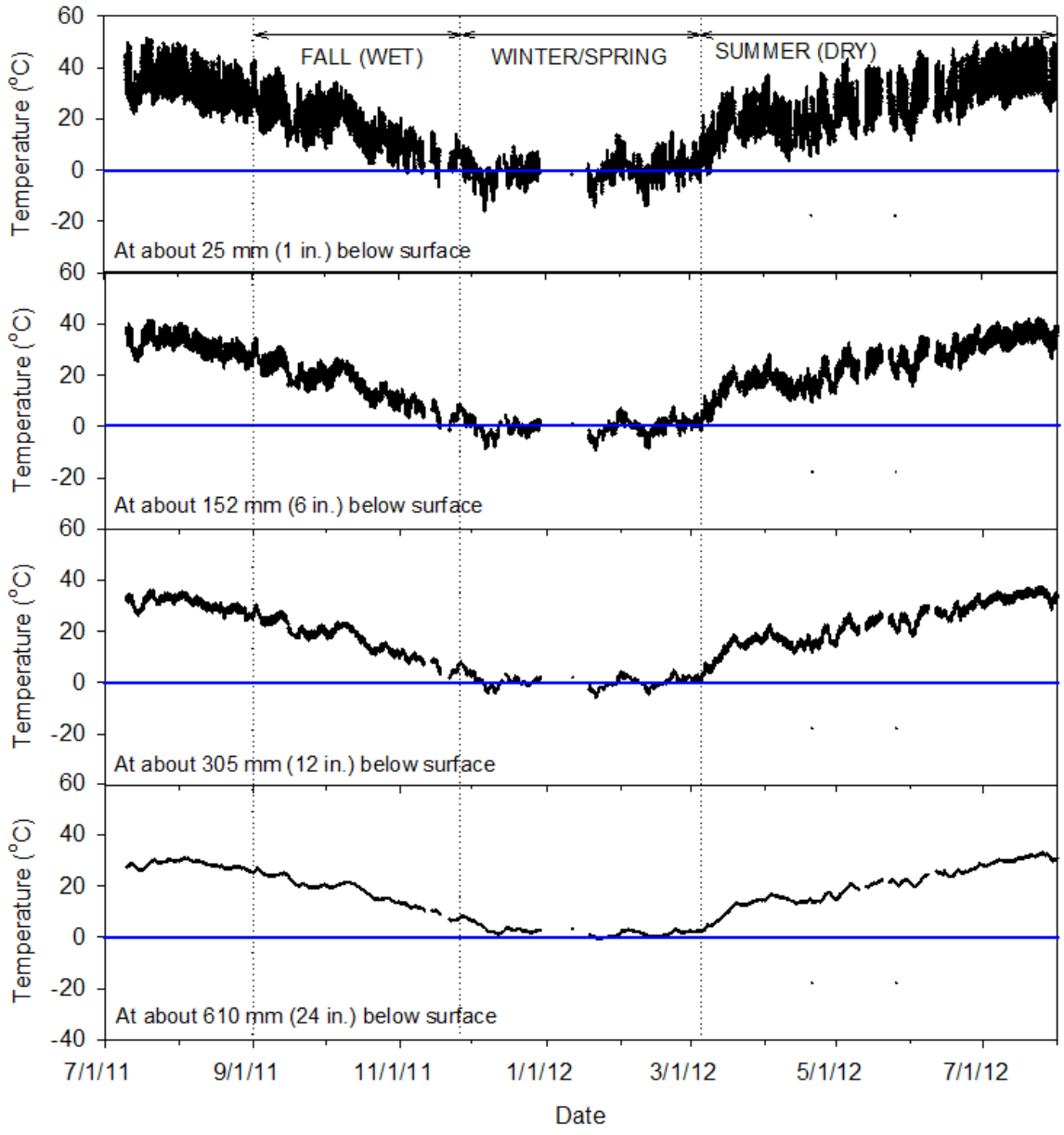

Figure C1. Temperature data at different depths from Moville, Iowa (Based on data collected from Iowa Environmental Mesonethttp://mesonet.agron.iastate.edu/request/rwis/soil.phtml**)**

APPENDIX D: DESCRIPTION OF DAMAGE ASSESSMENT TEQHNIQUES AND REAPAIR/MITIGATION SOLUTIONS

This appendix presents a catalog of options for flood damage assessment, and potential repair and mitigation solutions. A flow chart relating the damages, assessment techniques, and potential repair/mitigation solutions is provided. These options are discussed for paved/unpaved roads, culverts, and bridge abutments, and are applicable for both primary and secondary roadways.

The list below shows the various flood damage assessment techniques and a brief description of each of these technologies is provided in the following subsections of this appendix:

- Aerial and LiDAR imagery review
- Visual inspection
- Dynamic plate load tests (i.e., FWD, LWD, or Clegg Hammer)
- Penetration tests (Push T-bar or DCP tests)
- Roller-integrated compaction monitoring
- Ground penetrating radar (GPR)
- Surface Laser scanning
- Underwater sonar scanning
- Pipe Crawler for Culvert pipe inspection

The list below shows the various potential repair and mitigation solutions in alphabetical order, and a brief description of these solutions and key references are provided in the following subsections of this appendix:

A. Bio-Stabilization
B. Bulk-Infill (Cement) Grouting
C. Chemical Grouting
D. Chemical Stabilization of Subgrade/Base
E. Combined Soil Stabilization with Vertical Columns
F. Electro-Osmosis
G. Excavation and Replacement
H. Excavation and Replacement (using non-erodible fill)
I. Fiber Reinforcement of Subgrade/Base
J. Geosynthetic Reinforced Soil for Approach Backfill
K. Geosynthetics for Reinforcement/Separation/ Drainage
L. Geocell Confinement of Granular Materials
M. High Energy Impact Roller Compaction
N. Injected Light Weight Foam Fill
O. Mechanical Stabilization (Blending)
P. On-Site Recycling of Pavement Materials
Q. Partial Encapsulation
R. Rapid Impact Compaction
S. Sheet Pile Abutments
T. Rip-Rap for Erosion Protection

The list of technologies have been developed based on author's experience, field observations, ad literature review. It must be noted that a few of these technologies (i.e., A, B, C, E, F, N, and Q) warrant additional research with field trials to evaluate their effectiveness. Table D1 summarizes the assessment techniques and repair/mitigation solutions related to various damages observed in this study. A flow chart and associated notes are provided in Figure D1, to aid in selection of assessment techniques and potential repair/mitigation solutions for different damages observed.

Table D1. Summary of potential flood damage evaluation techniques and repair/mitigation solutions

Damage Description	Assessment Techniques	Repair/Mitigation* Solutions
A. Paved Roadways		
5. Isolated voids at shallow depths (< 0.5 ft)	Visual inspection, GPR, FWD, DCP	B, N
6. Isolated voids at deeper depths (> 0.5 ft)	GPR, DCP[3]	B, C, N
7. Partial to complete erosion of pavement and base	Visual inspection, Aerial survey, LiDAR	A, D*, F[1], G, I, K, L*, M[2], O, P, Q*, R[2]
8. Erosion of granular shoulders	Visual inspection, aerial survey, laser scan	A, D*, G, I, K, L*
B. Bridge Abutments		
3. Erosion of approach backfill	Visual inspection, GPR, DCP, laser scan	B, C, G[4], H*[4], J*, S[5], T
4. Embankment fore slope erosion	Visual inspection, laser scan	E*, H, T[6]
C. Culverts		
4. Erosion of culvert backfill	Visual inspection, GPR, DCP	B, G[4], H*[4], T*[6]
5. Culvert separation	Visual inspection, GPR	
6. Water outflow blockage	Visual inspection, pipe crawler, under water sonar	Clear debris, T*[6]
D. Unpaved Roadways		
4. Erosion of gravel surface	Visual inspection, laser scan, GPR	A, D*, G, I, K, L*
5. Rutting under traffic loading	Visual inspection, FWD[7], DCP[7]	A, D*, G, I, K, L*, M[8]
6. Full breach of roadway embankments	Visual inspection, aerial survey, laser scan, LiDAR	D[9], E, H*, G, K[9]

*Potential mitigation solution
[1]For dewatering in silts/clays only
[2]For rubbilizing concrete (only if voids are small enough for the equipment to safely drive over the concrete)
[3]At locations selected based on GPR scans for verification
[4]Control lift thickness as appropriate to compaction equipment
[5]On low-volume bridges
[6]Place rip-rap over geosynthetic placed over natural material
[7]Determine FWD modulus or CBR of subgrade to select appropriate treatment/stabilization option
[8]May not be a viable option if the subgrade layer is wet/saturated
[9]To serve as a construction working platform

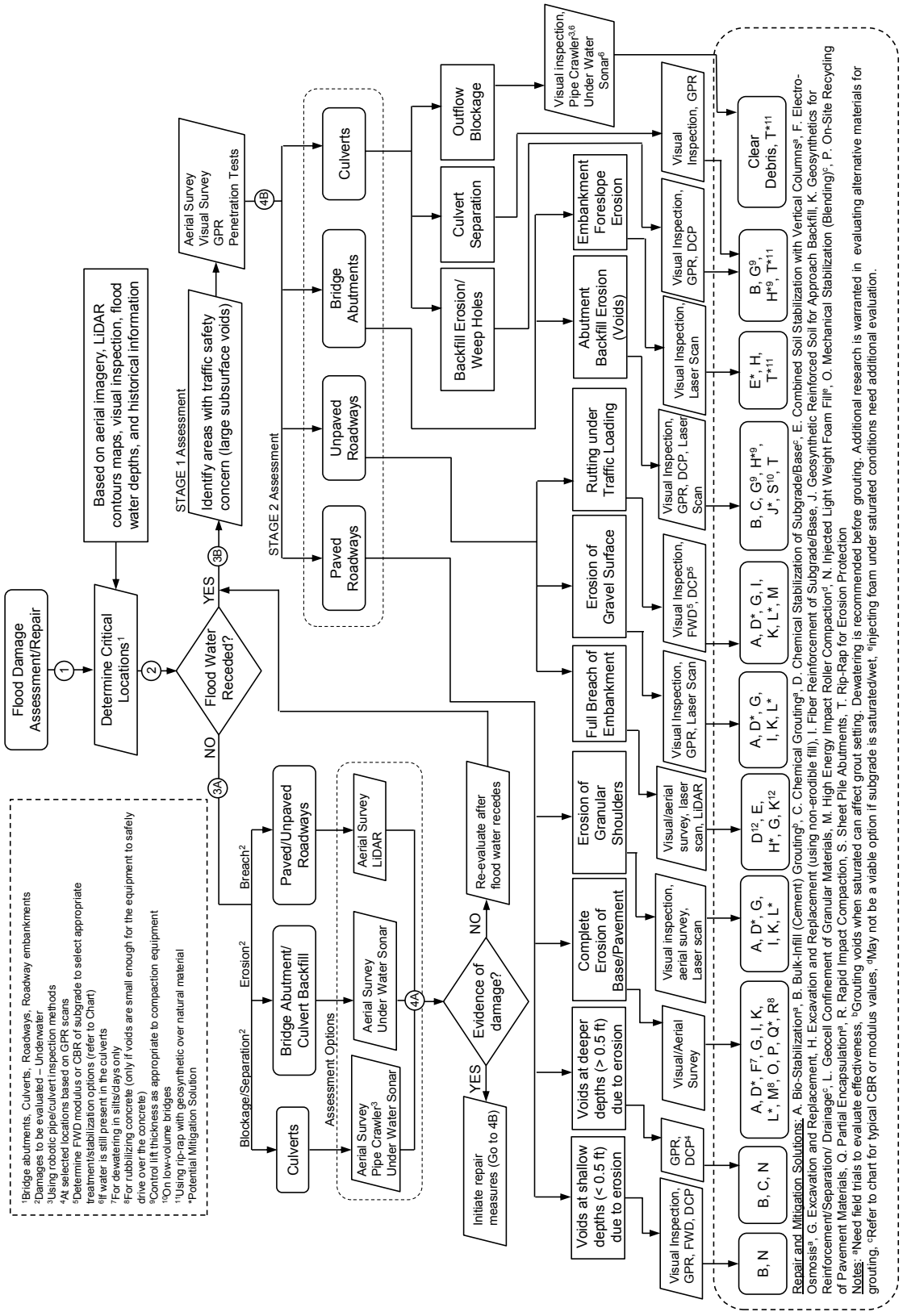

Figure D1. Flow chart to select assessment techniques and repair/mitigation solutions

Flood Damage Evaluation Procedures

The list below shows the various rapid flood damage evaluation techniques:

- Aerial and LiDAR imagery review
- Visual inspection
- Dynamic plate load tests
- Penetration tests
- Roller-integrated compaction monitoring
- Ground penetrating radar
- Surface Laser scanning
- Underwater sonar scanning
- Culvert pipe inspection

Aerial and LiDAR Imagery Review

Review of aerial imagery is recommended to select areas for potential testing when assessing damage on roadways. An example to illustrate this is shown in Figure D2. Light Detection and Ranging (LiDAR) based elevation data (in 0.6 m (2 ft) contours) is now available for all Iowa Counties though the Iowa Department of Natural Resources (DNR). According to Iowa DNR, the LiDAR elevation data has an accuracy of about 0.2 m (8 in.). The data is available as metadata and can be downloaded and visualized using ArcGIS. As an example, LiDAR data overlaid on Pottawattamie County map is shown in Figure D3.

Iowa HSEMD (2011) reported that during the 2011 Missouri River flooding, LiDAR data was used by the Iowa DOT to determine areas that are in potential danger for flooding and that areas are not, which can allow better utilization of resources and protection of the infrastructure. Area of higher ground elevations can be easily determined using simple query features within ArcGIS (see Figure D4). Based on the LiDAR ground elevation data and water level elevations obtained using Global Positioning System (GPS) measurements at several locations, Pottawattamie County department developed a flood water depth map during peak runoff release from Gavin's Point Dam in July 2011. This map is shown in Figure D5. Geo-referenced aerial photos can also be imported into ArcGIS for visualization. An example of such an application along with LiDAR elevation data in Fremont County, during the 2011 Missouri River flooding is shown in Figure D6. In addition, a database of critical locations in the flood plain such as culverts, bridges, and areas with "soft" subgrade conditions, etc. that can be imported into GIS, can assist the field engineers in selecting areas that require the most attention during a flood event. All these features can be helpful in making decisions for field assessment after a flood event.

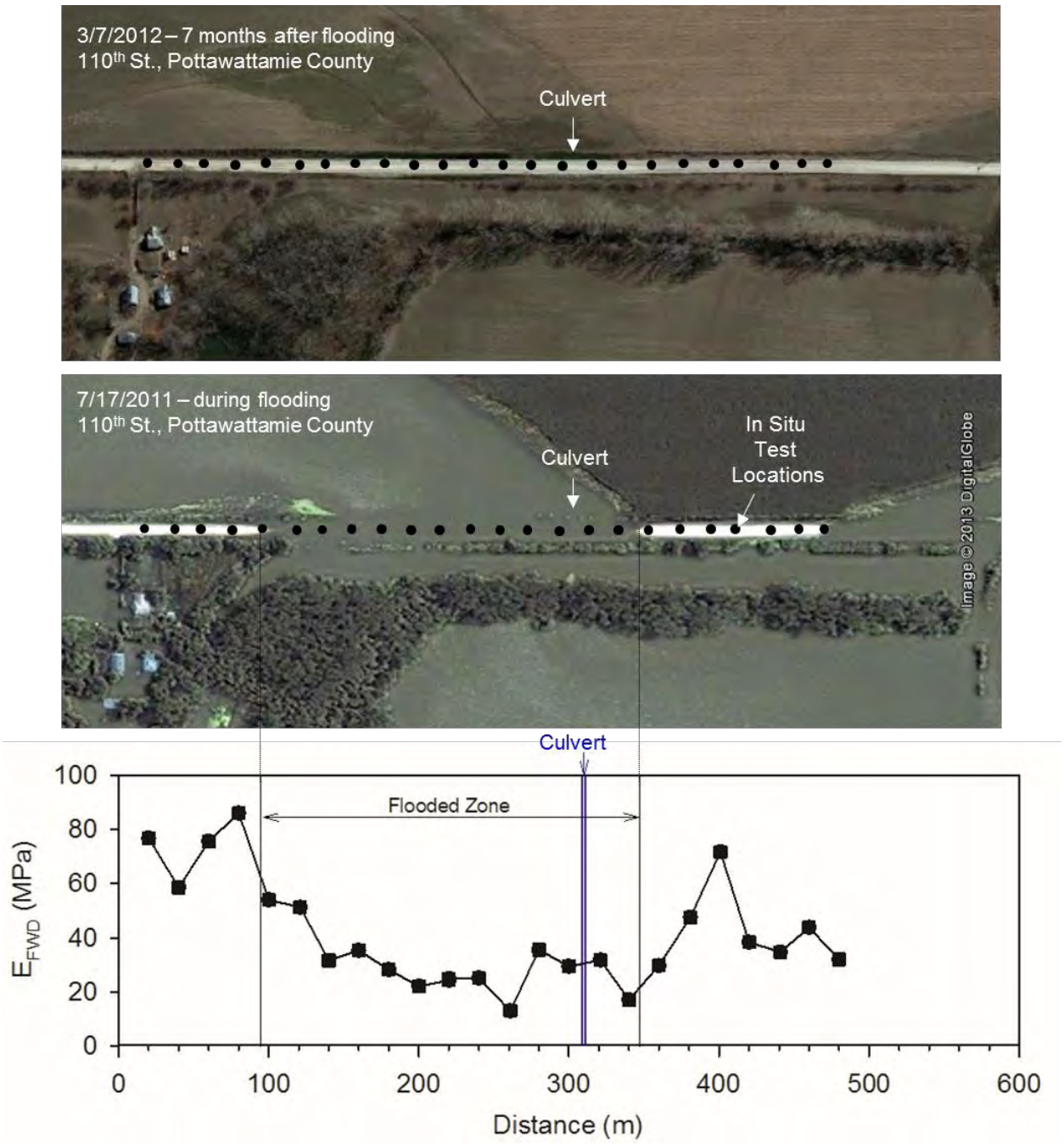

Figure D2. Aerial imagery showing during flood and after flood conditions, and FWD test results in flooded and non-flooded areas (imagery from Google Earth)

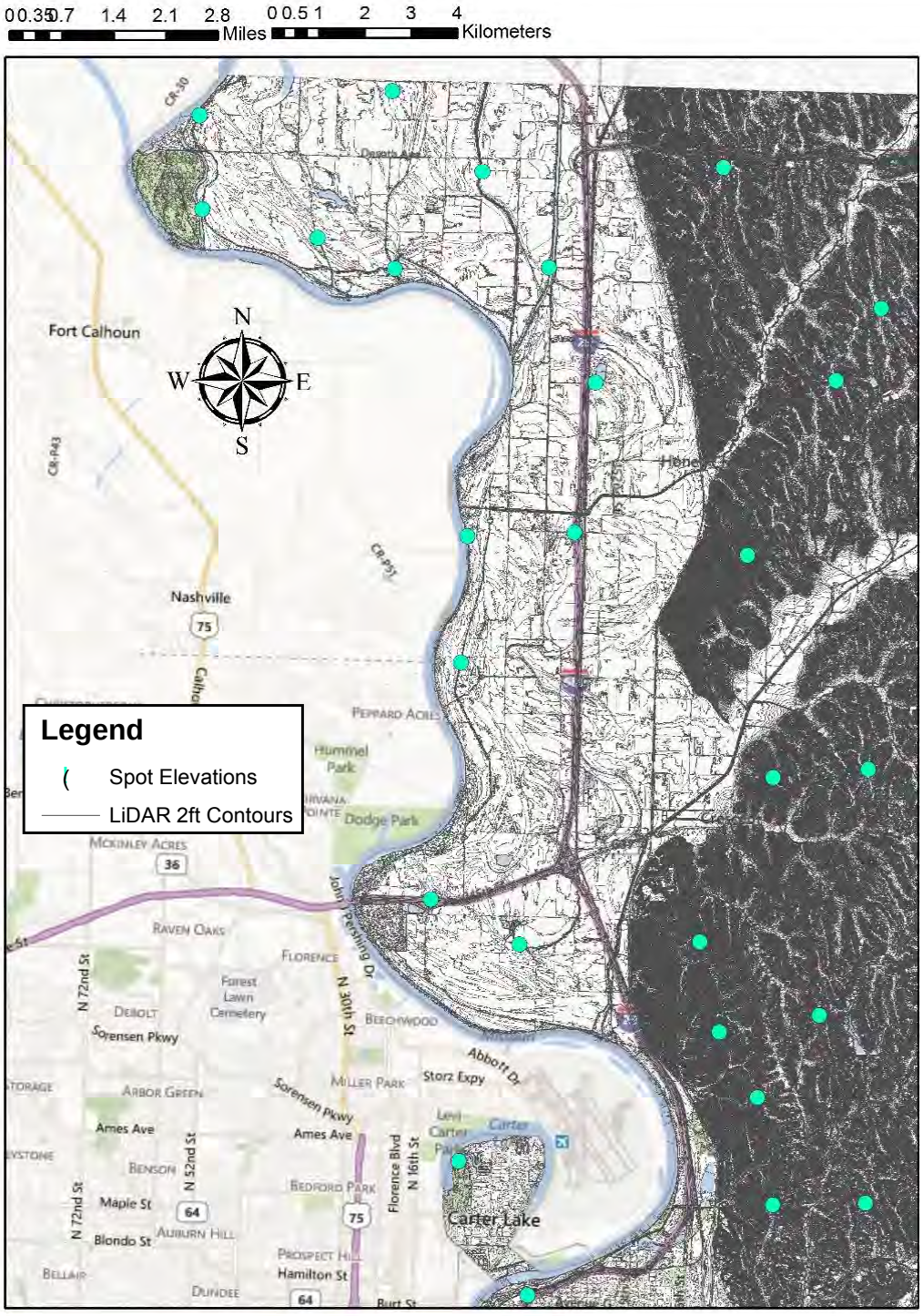

Figure D3. LiDAR 0.6 m (2 ft) contours from 2010 overlaid on Pottawattamie County map in ArcGIS

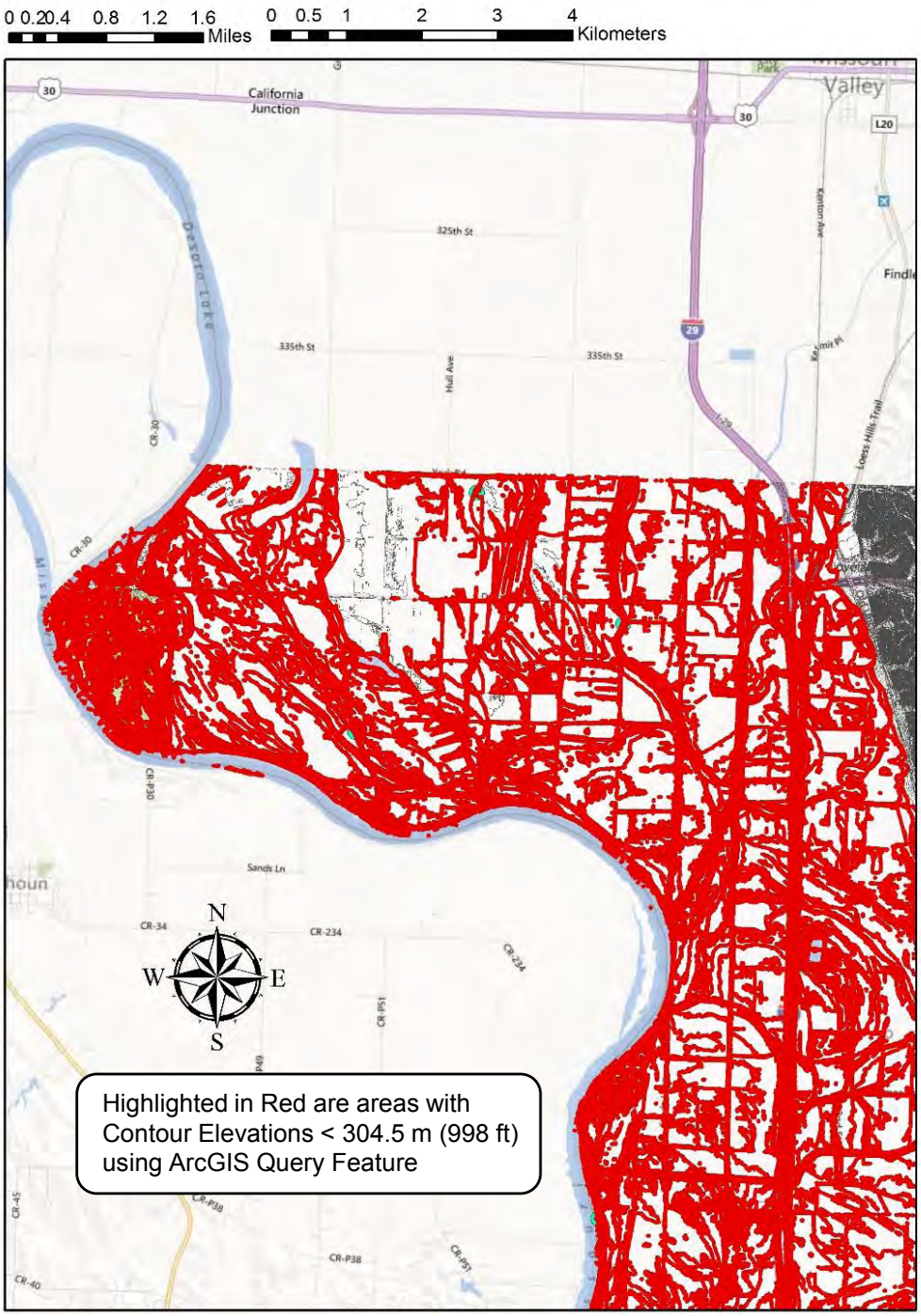

Figure D4. Demonstration of ArcGIS query feature to select areas with elevations higher than flood water levels using LiDAR data from 2010

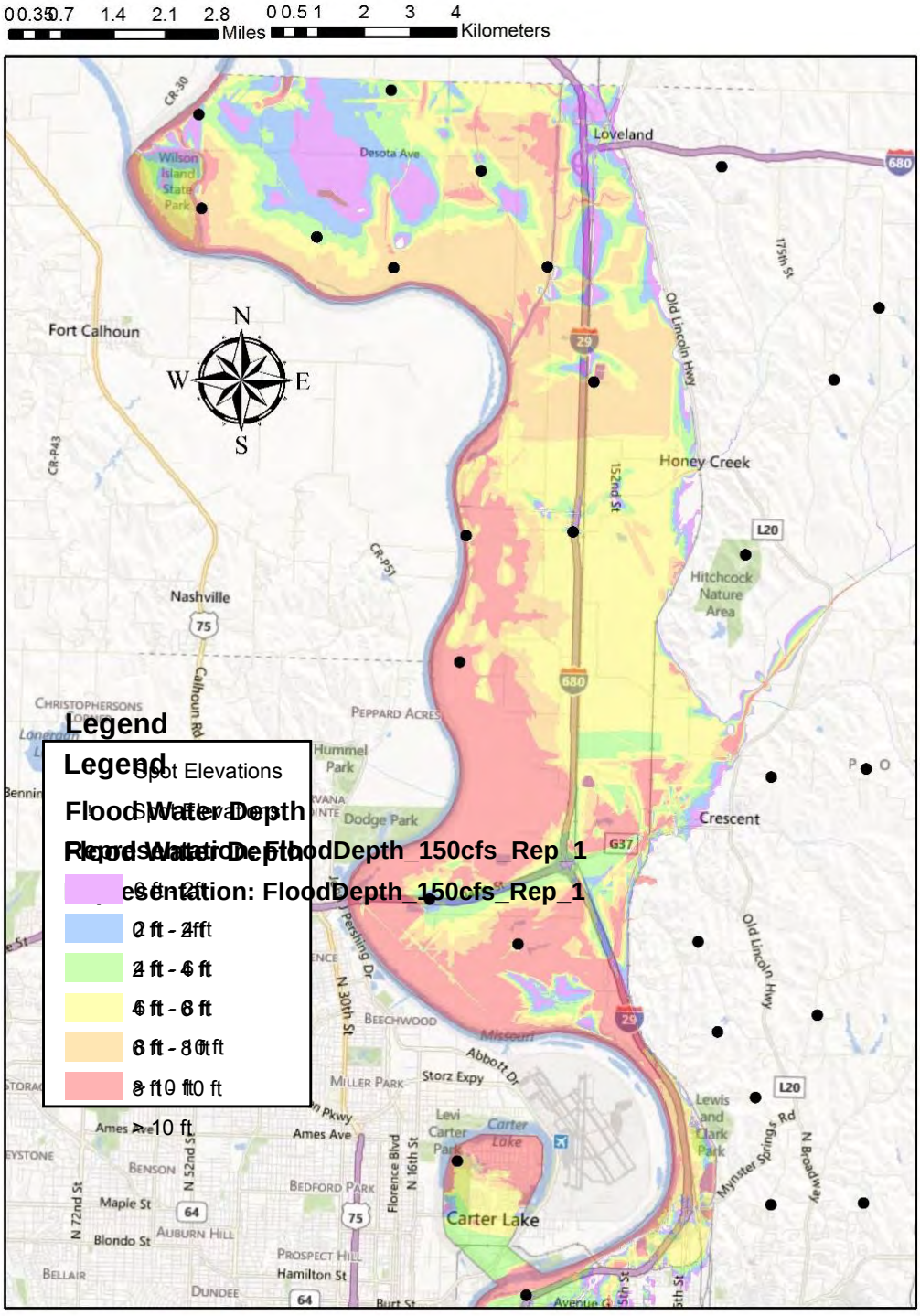

Figure D5. Flood water depth map overlaid on Pottawattamie County map in ArcGIS

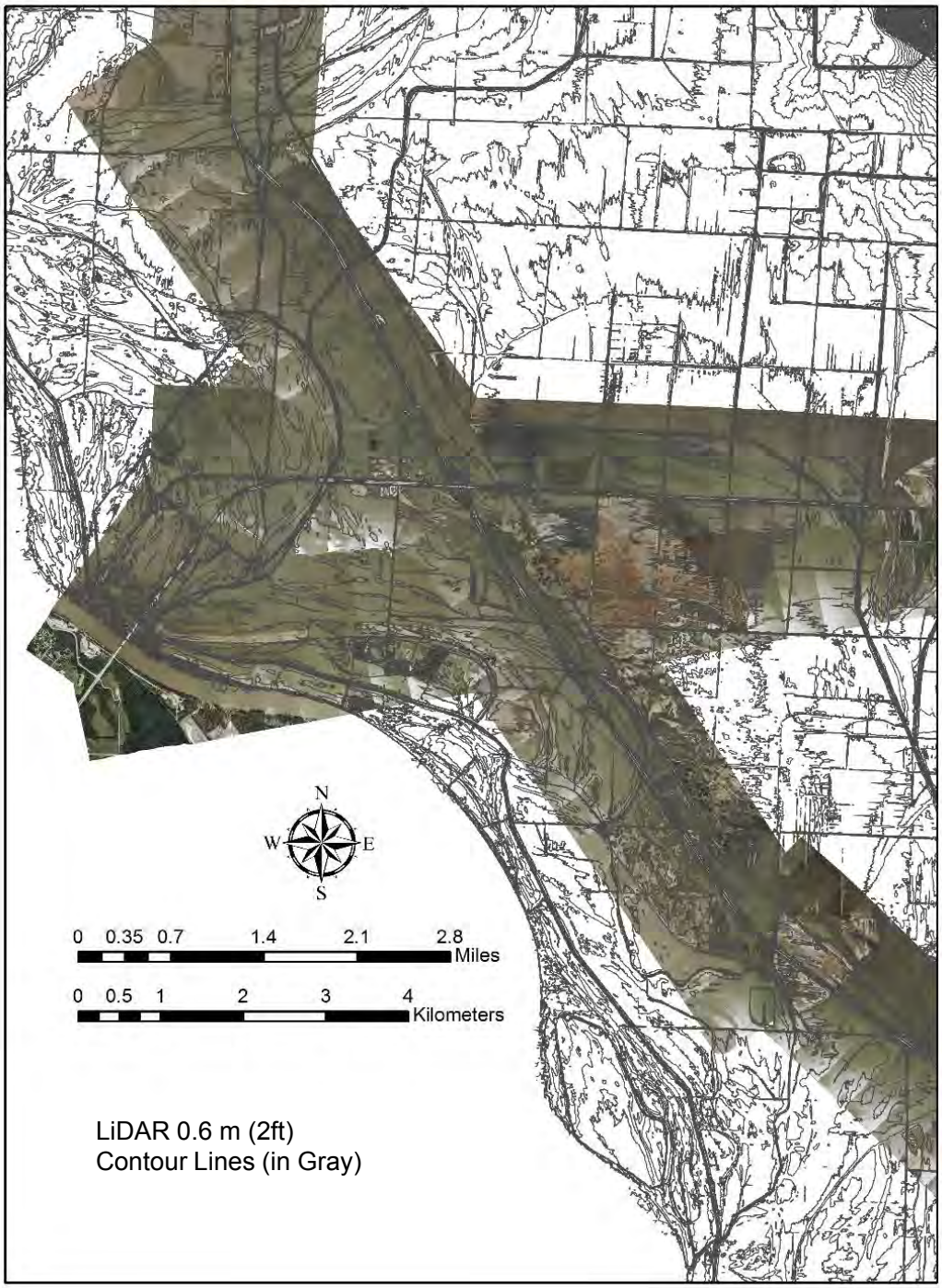

Figure D6. LiDAR contour lines from 2010 overlaid on aerial imagery for Fremont County in ArcGIS

Visual On-Ground Inspection

Visual inspection plays a vital role in evaluating the damage. Documenting the visual inspection by capturing photos and videos can contribute significantly in assessing the damage. Visual on-ground inspection is however possible only after the flood waters are receded. Conducting aerial surveys and reviewing the imagery can aid in selecting critical locations for on-ground inspection, as illustrated in the above section. Special attention is needed in inspecting roadways with culvert crossings. Severe erosion of backfill materials can lead to formation of deep potholes and voids under the roadway. Having updated maps with culvert crossings during on-ground inspection can aid in field inspection.

Dynamic Plate Load Tests

Dynamic plate load tests can be conducted to rapidly determine the ground stiffness/modulus. Light weight deflectometer (LWD), falling weight deflectometer (FWD), and Clegg hammer tests fall into this category. Both LWD and FWD tests involve applying a dynamic impulse loading and obtaining plate deflections. FWD tests are described in ASTM D4694. In addition to plate deflections, FWD tests are setup with an array of deflection sensors spaced away from the loading source to develop deflection basin data and determine the stiffness/modulus of the subsurface layers. Loads can be varied from about 22 kN (5,000 lbs) to 67 kN (15,000 lbs). LWD is a portable version of the FWD test and is described in ASTM E2835. LWD tests involve applying lower applied contact stresses (about 0.2 MPa or less) than FWD testing (up to 1.0 MPa). Clegg hammer test involves measuring hammer decelerations (g's) under impulse loading (ASTM D5874), and provides an index value called as Clegg impact value (CIV). CIV is correlated to CBR (ASTM D5874). Pictures of FWD, LWD, and Clegg hammer devices are shown in Figure D7.

FWD equipment is trailer-mounted and pulled with a suitable vehicle. LWD and Clegg hammer are portable devices which come in an enclosed box and can be carried in a truck. LWD and FWD are available commercially by several manufacturers. Although the methodology of the test is similar, different manufacturers use different type of measurement sensors to measure deflections (e.g., geophones, accelerometers, or seismometers). For LWD testing, some devices assume a constant load while some devices use a load cell to measure the applied load. These differences between device configurations affect the modulus value. LWDs are generally setup with 200 and 300 mm diameter plates, while FWDs are generally setup with 300 and 450 mm diameter plates. The modulus values are affected by the plate diameter and applied contact stresses. Additional information about factors affecting the dynamic modulus values is documented in Vennapusa and White (2009). Clegg hammer is available with a 10-kg drop hammer or a 20-kg drop hammer.

All three tests are relatively fast to perform – takes about 5 minutes per test. LWD and Clegg hammer tests have relatively shallow measurement depth (i.e., $\leq$ 0.5 m) compared to FWD tests (which provide information up to 2 m). Experience and special setup are necessary for FWD tests. Use of LWD and Clegg hammer generally require less training and are more economical than FWD. FWD can be used directly on paved or unpaved surfaces, while LWD and Clegg hammer can only be used on unpaved surfaces.

(a)

(b)

(c)

Figure D7. Dynamic plate load tests: (a) FWD, (b) LWD, and (c) Clegg hammer

Penetration Tests

Hand push T-bars and dynamic cone penetrometer (DCP) tests fall under this category. Hand push T-bars can be helpful to detect near surface voids or weep holes (Figure D8). DCP tests (Figure D9) can be used to determine California bearing ratio (CBR) of gravel base and subgrade layers, typically up to a depth of about 1 m. Extension rods can be used to measure soil properties up to a depth of about 2 m. An example plot showing DCP-CBR profiles in flooded and non-flooded areas is shown in Figure D9.

DCP test method is described in ASTM D6951. DCP test method involves driving a cone tip into the soil by lifting an 8 kg (17.6 lbs) sliding hammer to 575 mm (22.6 in.) drop height and then releasing it. The total penetration for a given number of blows is then measured and recorded as mm/blow. ASTM D6951 provides correlations between CBR and mm/blow for different soil types. A chart relating CBR of subgrade and gravel layers, estimated rut depths under 40 kN (18

kip) traffic loading, FWD and LWD modulus, and typical range of CBR values for various stabilized subgrade soils during spring-thaw (saturated state), is shown in Figure D10.

DCP tests are advantageous in assessing soil properties with depth, particularly in culvert or bridge backfill areas. It is common to see poor compaction in backfill materials around these structures, and DCP test can help detect these areas. DCP tests can be run by one or two persons and requires minimal training.

Figure D8. Hand push T-bar to inspect weep hole

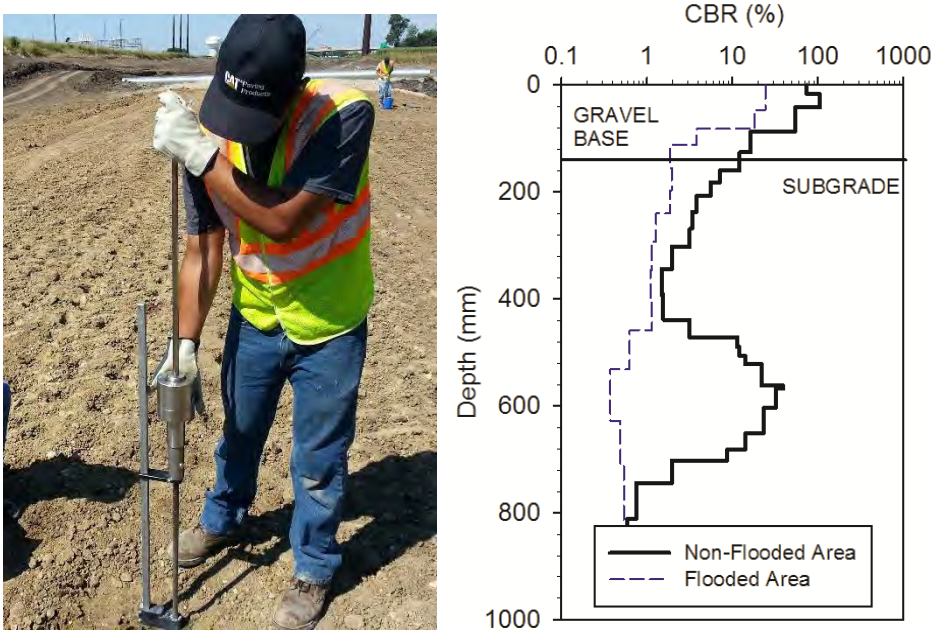

Figure D9. Dynamic cone penetrometer testing (left) and an example plot comparing DCP-CBR profiles in flooded and non-flooded areas

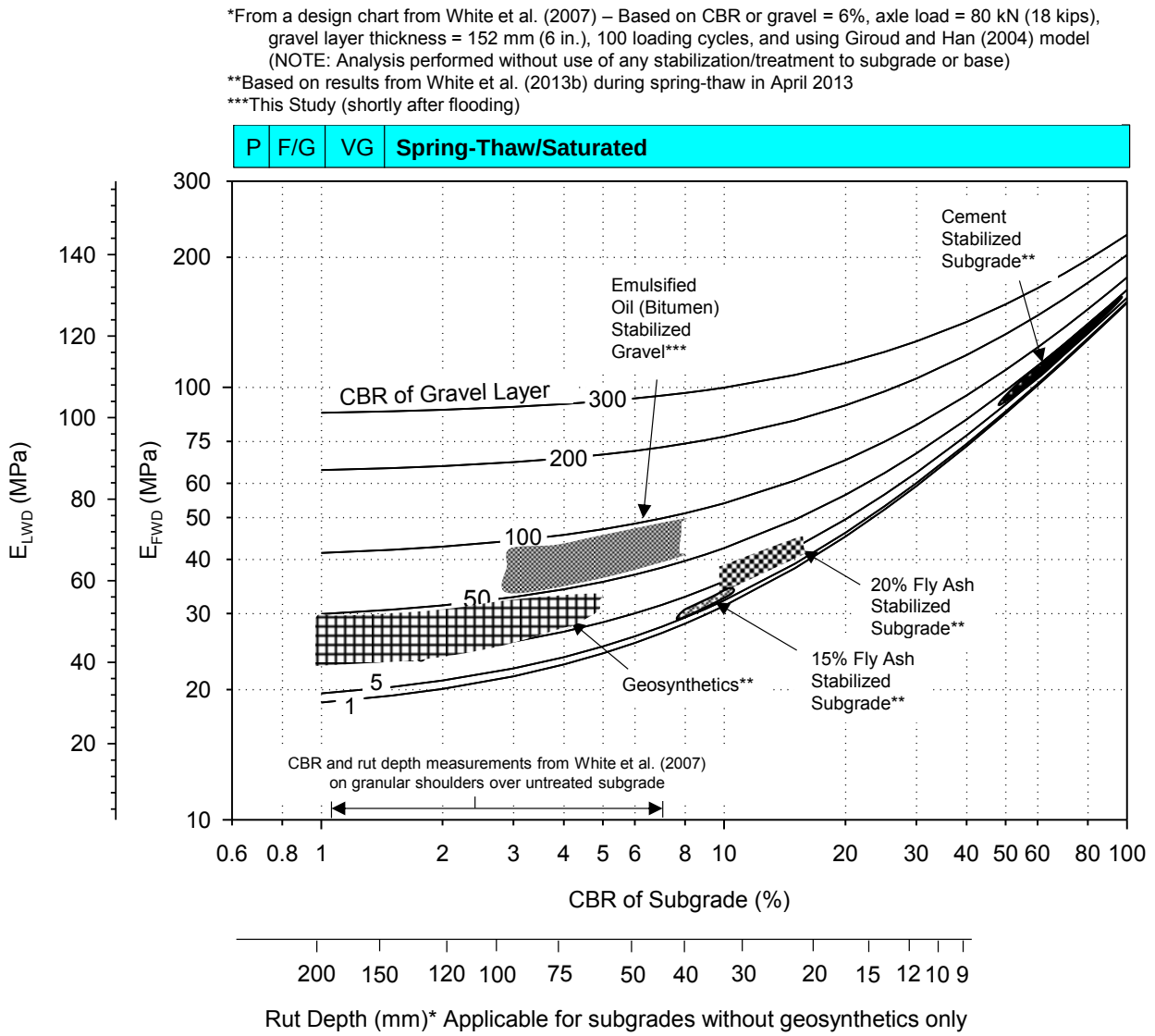

Figure D10. Chart showing relationship between CBR, rut depth, and FWD and LWD modulus, and typical range of CBR values observed after spring-thaw in Iowa (White et al. 2013b) for different stabilization methods

Roller-Integrated Compaction Monitoring

Roller-integrated compaction monitoring (RICM) (or also referred to as intelligent compaction or continuous compaction control) refer to sensor measurements integrated into compaction machines. This technology allows recording and color-coded real time display of integrated measurement parameter values on rollers over 100% of the compacted area, including roller operation parameters, position (based on GPS measurements), and roller-ground interaction parameter values. Several manufacturers currently offer RICM technologies on smooth drum vibratory roller configurations for compaction or mapping of granular materials and non-vibratory roller configurations for compaction or mapping of non-granular materials. Pictures of various roller configurations and computer display units are shown in Figure D11. An example

spatial map of compaction measurements obtained using a smooth drum vibratory roller from a project site in Boone, Iowa, on test sections constructed with different stabilization technologies after spring-thaw is shown in Figure D12.

Figure D11. Pictures of various roller manufacturers, roller configurations, and display software's with RICM technology (note that this does not represent a complete list)

The compaction measurement values (noted next to the manufacturer names in Figure D13) vary between the manufacturers and technologies. These current technologies calculate: (1) an index value based on a ratio of selected frequency harmonics for a set time interval for vibratory compaction, (2) ground stiffness or dynamic elastic modulus based on a drum-ground interaction model for vibratory compaction, or (3) a measurement of rolling resistance calculation from machine drive power for vibratory and non-vibratory compaction (White et al. 2011). Research over the past three decades on this technology indicated that these measurements generally

correlate well with modulus or stiffness based measurements (such as FWD or LWD modulus) than with dry density or CBR measurements (White et al. 2011). This technology can be used on gravel/base/subgrade layers to detect areas of concern to apply appropriate stabilization to improve the conditions. The data obtained using this technology is geo-referenced and can be easily imported into ArcGIS for data archiving and visualization.

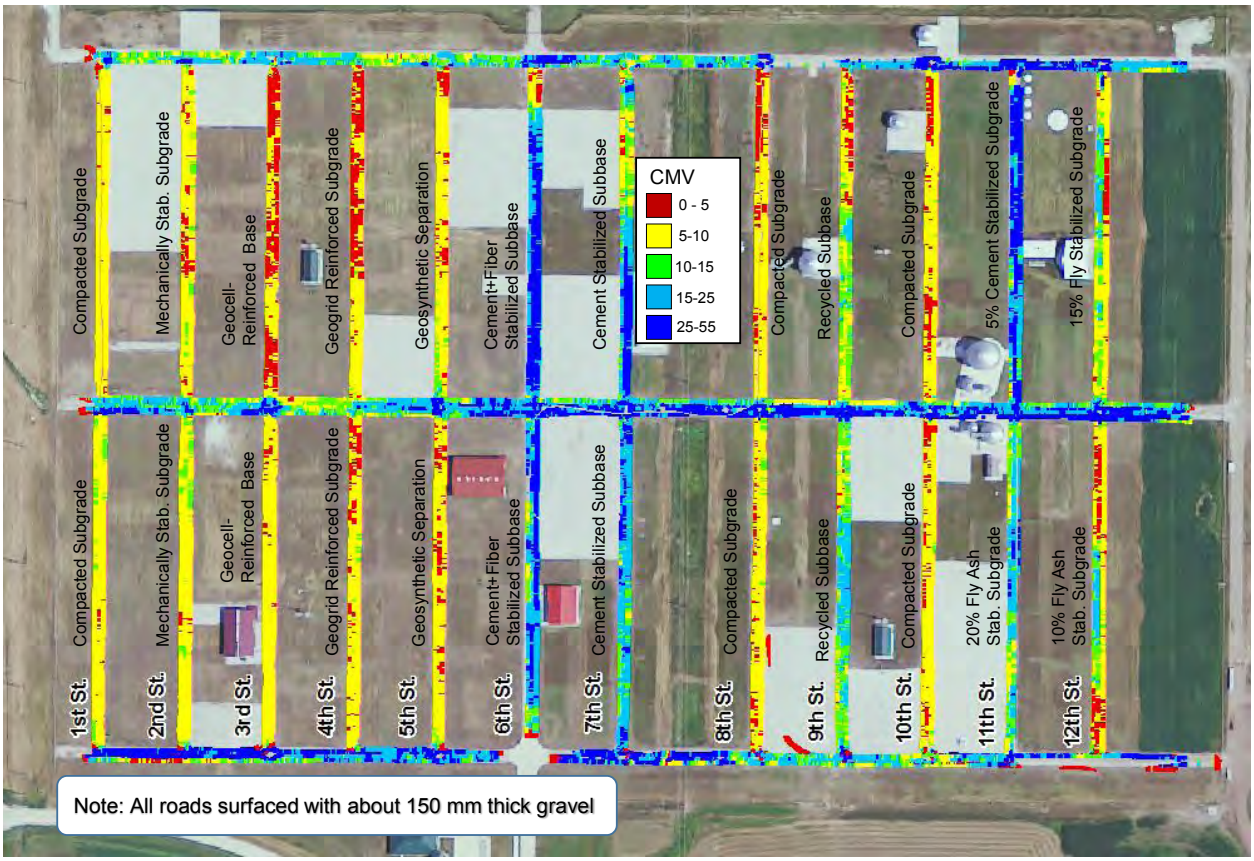

Figure D12. Example RICM spatial map of compaction measurements obtained using CS74 smooth drum vibratory roller after spring-thaw on test sections in Boone constructed using different stabilization methods (White et al. 2013b)

Ground Penetrating Radar (GPR)

Two main applications of GPR during post-flood evaluation include detecting: (a) voids or weep holes beneath surface (under paved or unpaved surface), (b) voids/erosion in bridge abutment backfill, and (c) depth to water table.

The GPR sends a pulse of energy into the ground and records the strength and time required for the return of any reflected signal. When a series of pulses are sent over a single area, then it is referred to as a scan. Signal reflections are produced when the energy pulse enters into materials with different electrical conductivities (i.e. dielectric permittivity), from the material it left. The strength or amplitude of the reflection is determined by the contrast in the dielectric constants of the two materials (Geophysical Survey Systems, Inc. 2009). For example, when a pulse moves

from dry sand (with a dielectric constant of about 5) to wet sand (with a dielectric constant of about 30), it will produce a strong reflection. On the other hand, when a pulse moves from dry sand to limestone (with a dielectric constant of about 7) it will not produce a strong reflection. While some of the transmitted energy is reflected back to the antenna, some energy keeps travelling through the material until it is dissipated (or attenuated) or until the control unit has closed its time window. The rate of signal attenuation is dependent on the dielectric properties and conductivity of the materials. If the materials are highly conductive (e.g., wet clays), the signal is attenuated rapidly (Geophysical Survey Systems, Inc. 2009).

The frequency of the antenna used is a major factor in the depth of penetration into the ground. The higher the frequency of the antenna, the shallower into the ground it will penetrate. Table D2 provides a summary of the appropriate depth ranges for difference frequency antennas and potential applications. It must be noted that the maximum depth of penetration values will be lower when high conductivity materials are encountered (e.g., wet clays).

Table D2. Summary of depth ranges for different frequency GPR antenna's (ground-coupled) and potential applications (Geophysical Survey Systems, Inc. 2009)

Depth Range (Approximate)	Primary Antenna Choice	Secondary Antenna Choice	Applications
0 to 0.5 m	1500 MHz	900 MHz	Structural concrete, roadways, bridge decks
0 to 1 m	900 MHz	400 MHz	Structural concrete, shallow soils, archeology
0 to 3 m	400 MHz	200 MHz	Shallow geology, utilities, underground storage tanks, archaeology
0 to 9 m	200 MHz	100 MHz	Geology, environmental, utilities, archaeology
0 to 30 m	100 MHz	Sub-Echo 40	Geologic profiling
> 30 m	80 to 16 MHz		Geologic profiling

GPR scanning can be performed using ground-coupled antennas (Figure D14) or air-borne antennas (Figure D15). GPR scanning using ground-coupled antennas can be performed by pulling the antenna on the ground using a wheel cart or a hand-held survey wheel on paved and unpaved roadways. These antennas can also be mounted to a truck, however, the scans can only be obtained at slow travel speeds (< 5 mph). Example GPR scans over bridge backfill materials are shown in Figure D16.

Air-borne antennas, commonly referred to as horn, are high frequency antennas (2600 MHz) and are suitable for pavement applications only (i.e., to scan rebars and thickness of pavements). The depth of signal penetration is shallow using the horn antennas (0 to 0.4 m), but scanning can be performed at driving speeds.

Air-borne step-frequency GPR (SF-GPR) is being currently evaluated by the FHWA (Figure D17). This technology uses 3D radar geoscope and uses multiple frequencies (150 MHz to 3000

MHz) in a single scan, which allows detection depth of up to 3 m (10 ft) over the full width of a lane. The technology also allows visualizing data in 2D (Figure D17) and 3D (Figure D18), and the data can be collected at driving speeds (5 to 50 mph).

Figure D13. GPR scanning using ground-coupled antennas

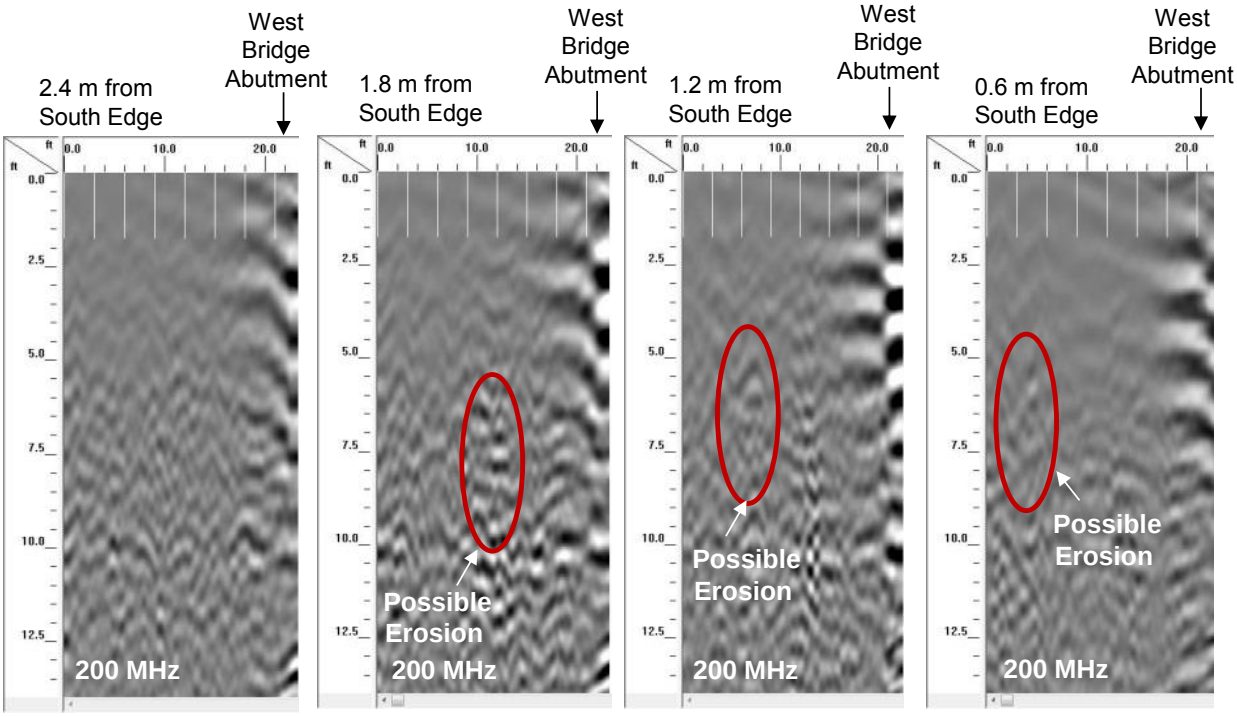

Figure D14. GPR scans using 200 MHz antenna on bridge approach backfill materials at several locations from the edge of the bridge identifying possible erosion/voids beneath surface

Figure D15. GPR scanning using air-borne (horn) antenna

Figure D16. FHWA step-frequency GPR (Courtesy of Jim Grove, FHWA)

Figure D17. GPR scan map showing voids under composite pavement (Yu 2012)

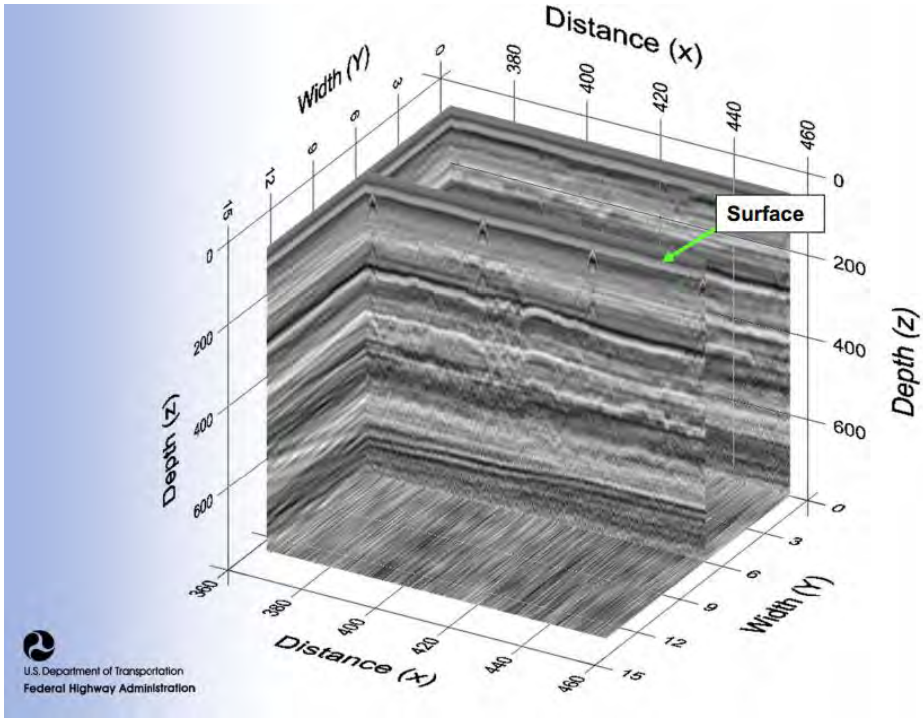

Figure D18. 3D visualization of SF-GPR data (Yu 2012)

Surface Laser Scanning

3D surface laser scanning using for e.g., Trimble CX 3D laser scanner (Figure D19), can be useful in rapidly calculate earthwork volumetrics in case of a road breach or eroded backfill behind bridge abutments, etc. The laser scanning technology allows overlaying photos and contour lines, and performing volumetric calculations in real-time. Example images after processing the laser scanning data are shown in Figure D20 to Figure D22.

Figure D19. Trimble CX 3D laser scanner

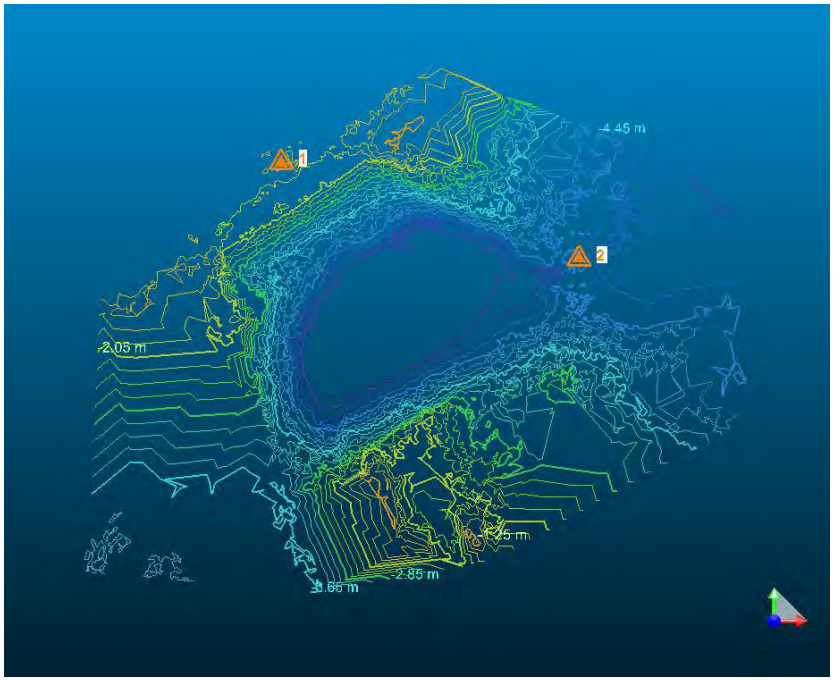

Figure D20. Contour map of site used for volumetric calculations

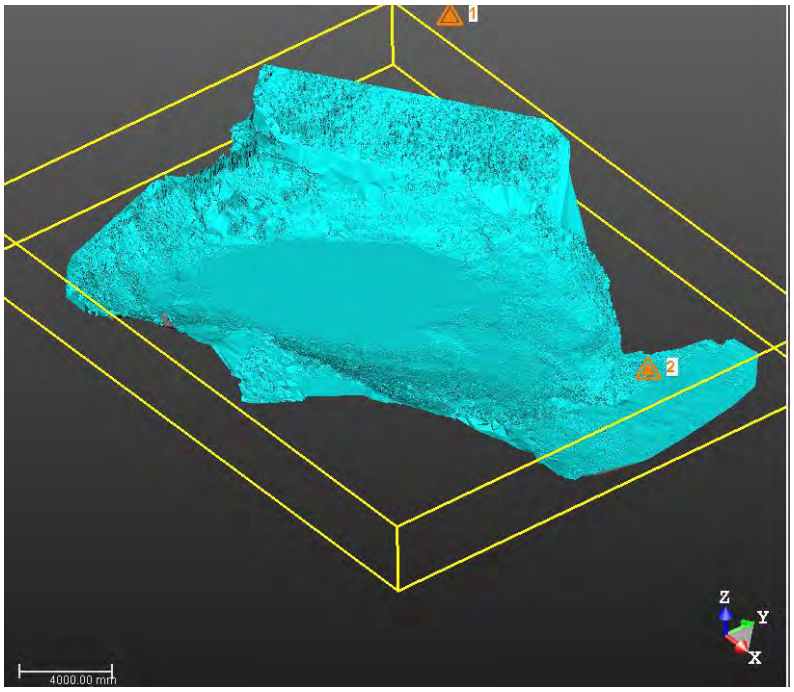

Figure D21. Meshed surface used for volumetric calculations

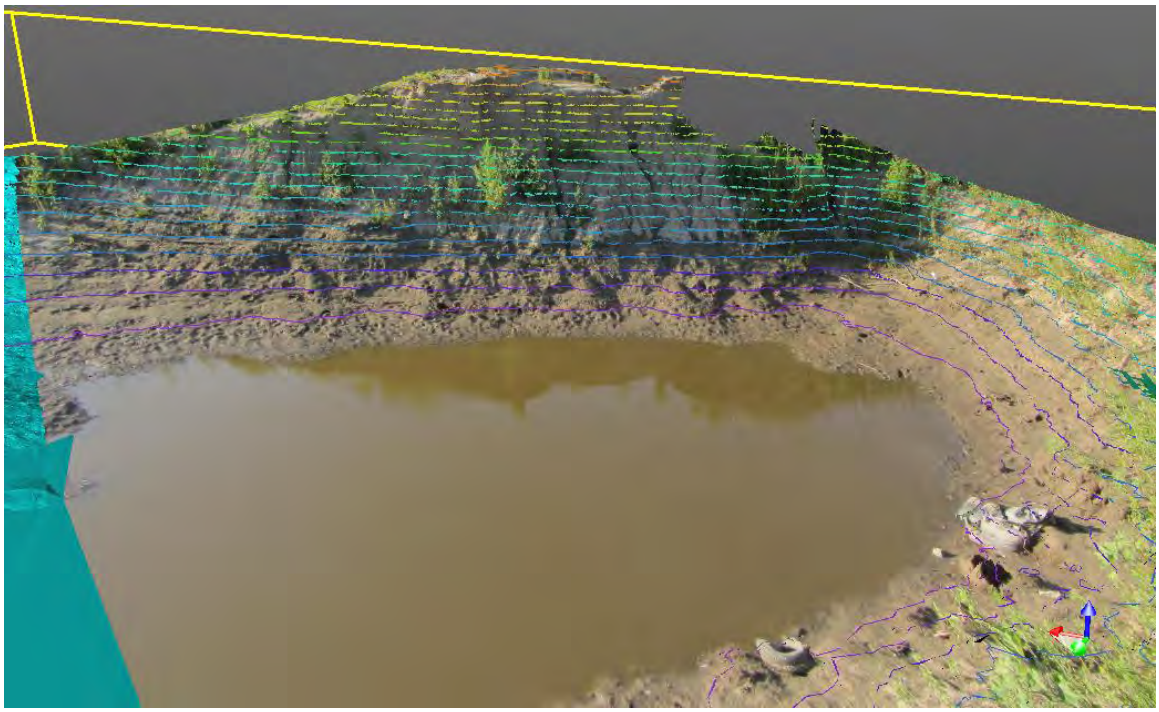

Figure D22. Colored mesh surface with 0.6 m (2 ft) contour lines

Underwater Sonar Scanning and Culvert Inspection

Underwater sonar scanning technologies are available commercially from many manufacturers. These technologies can provide 2D and 3D imagery underwater and in low visibility areas. Examples of 2D and 3D imagery captured from Blue View technologies imaging sonars are shown in Figure D23 and Figure D24 Another example acoustic sonar from Starfish is shown in Figure D25. These technologies would be useful in assessing damage underwater near critical bridge abutment and culvert locations, before the flood waters recede. Specifically, erosion behind backfill and debris blockage in culverts can be detected. The sonar scanning devices are portable and can be either purchased or rented from the manufacturers/ distributors. The devices must can be operated by lowering them down to a desired elevation into the water from a boat. The P900 series sonar can be attached to a robotic mobile crawler to conduct underwater inspections in culverts. Figure D26 shows an underwater pipe culvert crawler, which is also a robotic mobile device.

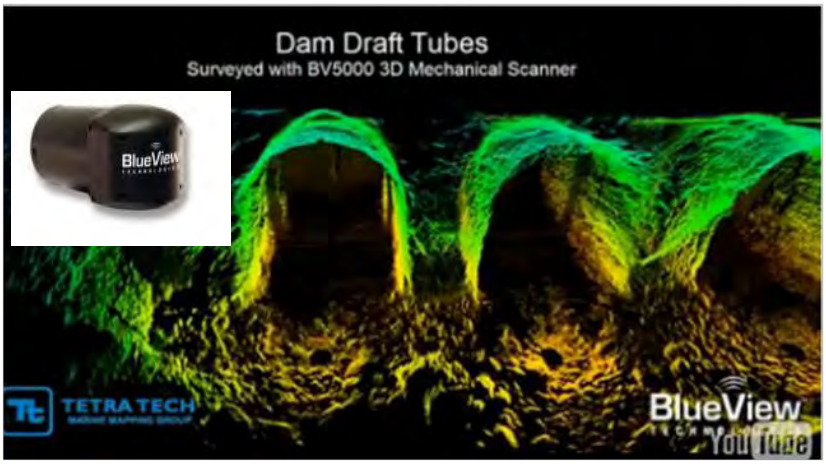

Figure D23. 3D imagery under water using BV5000 3D mechanical imaging sonar (sonar shown in insert) (Courtesy of Blue View Technologies, Inc., Seattle, Washington, USA)

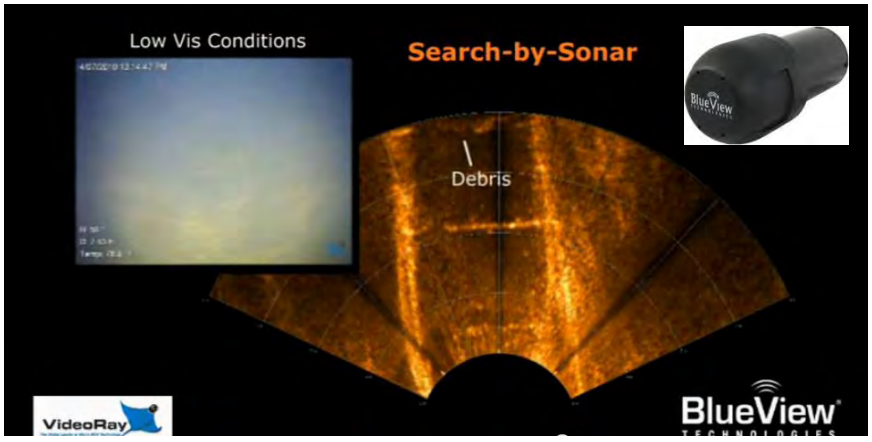

Figure D24. 2D imagery from sonar scanning in low visibility conditions in a culvert using P900 series sonar (sonar shown in insert) (Courtesy of Blue View Technologies, Inc., Seattle, Washington, USA)

Figure D25. Starfish 990F side scanning acoustic sonar (Courtesy of Starfish Seabed Imaging Systems, Aberdeen, UK)

Figure D26. Versatrax 100™ for pipe/culvert inspection (Courtesy of Inuktun Services Ltd., British Columbia, Canada)

Potential Damage Repair and Mitigation Solutions

A list of twenty potential damage repair and mitigation solutions are provided in Table D3 along with the applications where the solution can be used. Some of these solutions are described in the following subsections, while the remaining are referred to the Strategic Highway Research Program (SHRP2) web-based portal where a detailed description of these technologies are available.

Table D3. Summary of repair/mitigation solutions and their applications

Repair/Mitigation Solution	Applications	Notes
A. Bio-Stabilization	Roadways	See discussion in the following sections
B. Bulk-Infill (Cement) Grouting	Roadways, Culverts, Abutments	http://www.geotechtools.org/
C. Chemical Grouting	Roadways	http://www.geotechtools.org/
D. Chemical Stabilization of Subgrade/Base	Roadways	See discussion in the following sections http://www.geotechtools.org/
E. Combined Soil Stabilization with Vertical Columns	Embankment Fore slopes	http://www.geotechtools.org/
F. Electro-Osmosis	Roadways, Embankments	http://www.geotechtools.org/
G. Excavation and Replacement	Roadways, Culverts, Abutments, Embankments	http://www.geotechtools.org/
H. Excavation and Replacement (using non-erodible fill)	Roadways, Culverts, Abutments, Embankments	See discussion below for non-erodible fill
I. Fiber Reinforcement of Subgrade/Base	Roadways	http://www.geotechtools.org/
J. Geosynthetic Reinforced Soil for Approach Backfill	Abutments	See discussion in the following sections
K. Geosynthetics for Reinforcement/Separation/ Drainage	Roadways, Embankments	See discussion in the following sections http://www.geotechtools.org/
L. Geocell Confinement of Granular Materials	Roadways	http://www.geotechtools.org/
M. High Energy Impact Roller Compaction	Roadways	See discussion in the following sections http://www.geotechtools.org/
N. Injected Light Weight Foam Fill	Roadways	http://www.geotechtools.org/
O. Mechanical Stabilization (Blending)	Roadways	See discussion in the following sections http://www.geotechtools.org/
P. On-Site Recycling of Pavement Materials	Roadways	http://www.geotechtools.org/
Q. Partial Encapsulation	Roadways	http://www.geotechtools.org/
R. Rapid Impact Compaction	Roadways	http://www.geotechtools.org/
S. Sheet Pile Abutments	Abutments	See discussion in the following sections
T. Rip-Rap for Erosion Protection	Embankments, Culverts, Abutments	See discussion in the following sections

Roadways

Stabilizing aggregate base or subgrade layers can help improve strength/stiffness, resistance to rutting under wheel loading, and durability (freeze-thaw) characteristics. Selecting critical areas (for e.g., areas with subgrade CBR < 3) for stabilization, can help reduce maintenance costs and also serve as a good mitigation measure to avoid failure during flooding. Use of stabilized aggregate base layers can help reduce risk of erosion or undermining and pavements, as experienced under some roadways during the 2011 Missouri River flood event. The stabilization techniques described below are applicable for both unpaved and paved roadways.

Commonly used stabilization methods include: (a) chemical stabilization of subgrade/aggregate, (b) bio-stabilization of subgrade/aggregate, (c) mechanical stabilization (i.e., mixing gravel into soil), and (d) geosynthetic reinforcement at the subgrade/aggregate interface. High-energy impaction roller compaction is another in situ soil densification method that can potentially be used on unpaved roadways. Brief information and key references for each of these methods are provided below. A summary of cost information from a project conducted in Boone, Iowa (White et al. 2013b) and this research project, for different stabilization methods is provided in Table D4.

Table D4. Summary of cost information for different stabilization method

Method	Costs	Source
Portland cement stabilization of subgrade (5%)	Range: $3.33 to $6.95 per sq. yd. Median: $4.43 per sq. yd.	White et al. (2013b)*
Fly ash stabilization of subgrade (15%)	Range: $4.61 to $7.28 per sq. yd. Median: $5.91 per sq. yd.	
Fly ash stabilization of subgrade (20%)	Range: $5.83 to $8.39 per sq. yd. Median: $7.21 per sq. yd.	
Woven geotextile	Range: $3.00 to $4.60 per sq. yd. Median: $3.75 per sq. yd.	
Non-woven geotextile	Range: $1.50 to $3.90 per sq. yd. Median: $2.75 per sq. yd.	
Geogrid (biaxial and triaxial)	Range: $2.40 to $5.50 per sq. yd. Median: $3.96 per sq. yd.	
Emulsified oil (bitumen) stabilized gravel	$140,000 per mile**	This Report
Woven Geotextile	Range: $3.00 to $5.00 per sq. yd.	
Flowable mortar (Cement grout)	Range: $100 to 200 per cubic yd.	

*Project bid costs for material only (does not include construction related costs)
**Cost reported in DDIR on a low volume secondary roadway

Chemical Stabilization

Chemical admixtures commonly used for stabilization include portland cement, lime, and bitumen. Information published in the literature for selecting stabilizer based on soil grain-size characteristics and Atterberg limits are shown in Figure D27 to Figure D29 and Table D5. Chemical stabilization process involves application of stabilizer to loose soil, mixing the stabilizer with a soil reclaimer and moisture-conditioning the mixture, and compacting the mixture within a specified time (typically less than 1 to 2 hours). Compaction time is critical and is dependent on the chemical admixture set time and must be determined using laboratory testing.

ASTM class C self-cementing fly ash has been used (on a limited scale) in Iowa to treat unstable/wet subgrades. Some of the reported benefits of using self-cementing fly ash for soil stabilization include environmental incentives in terms of using a waste product, cost savings relative to other chemical stabilizers, and availability at several power plants across Iowa (White et al. 2005). The characteristics of fly ash can vary significantly between different plants due to

variations in the coal used and various operating conditions in the plant. Laboratory mix design is recommended when using fly ash for stabilization.

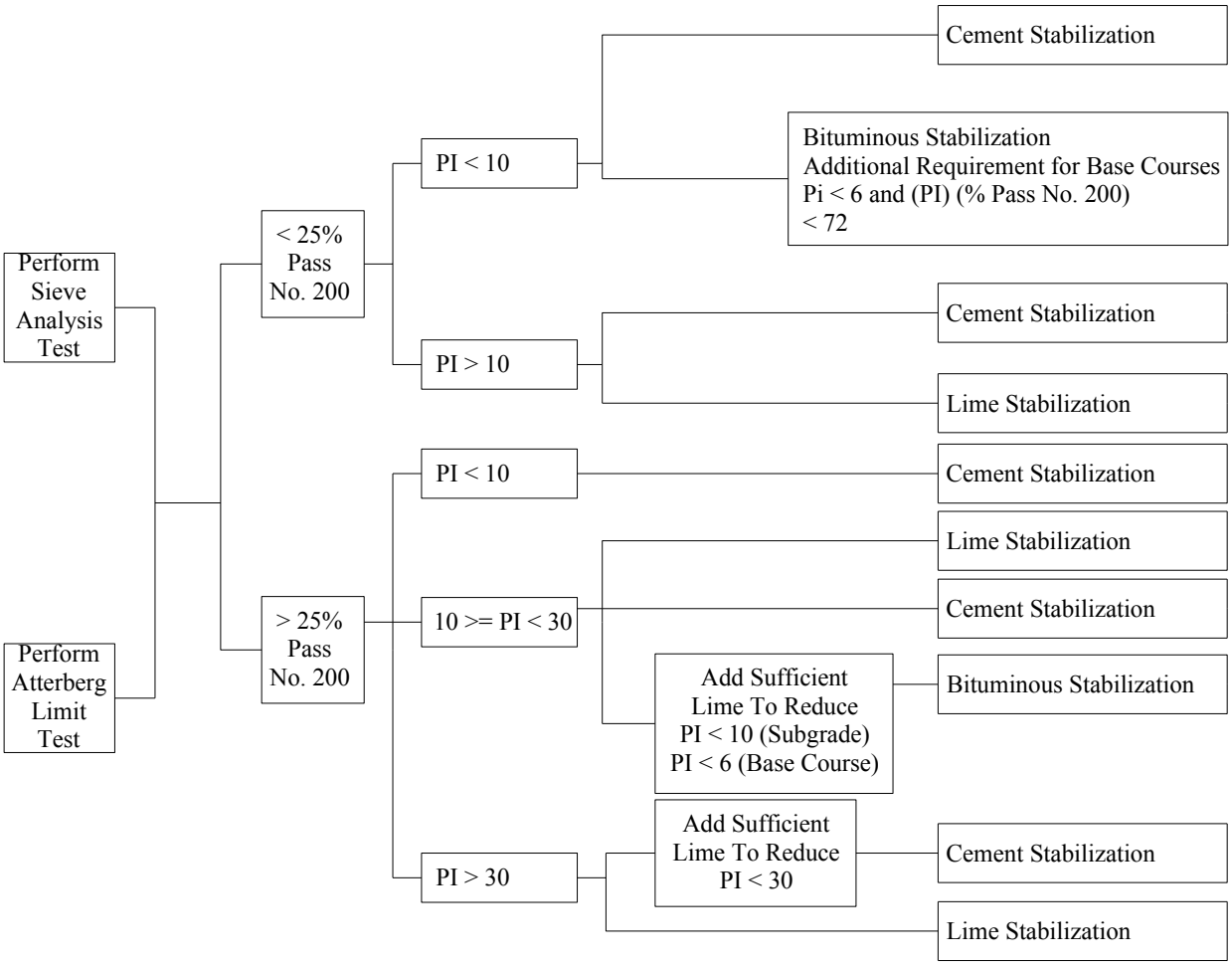

Figure D27. Chart for selection of stabilizer (Chu et al. 1955)

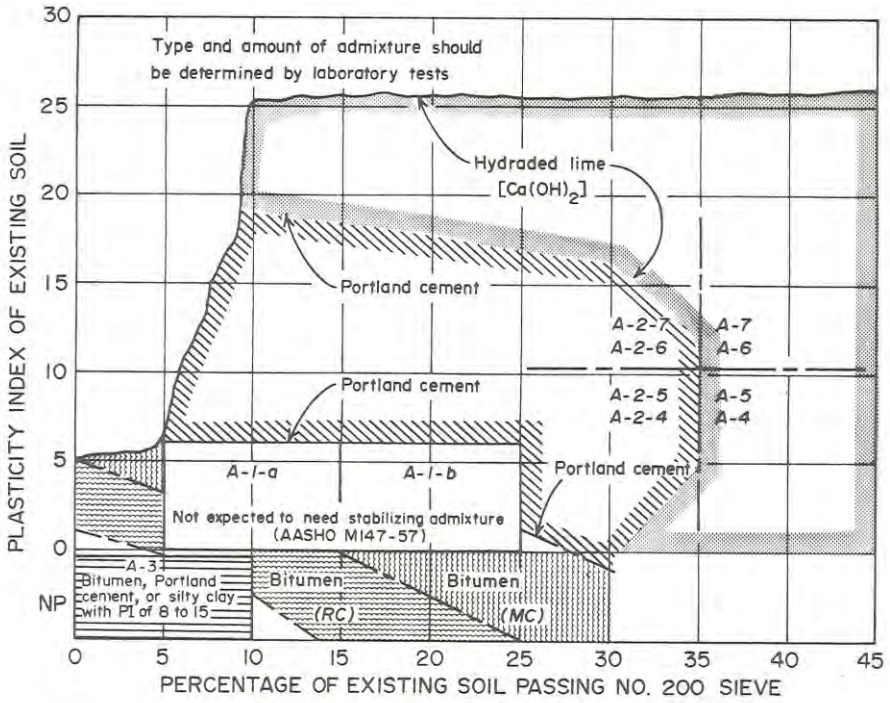

Figure D28. Chart for selection of stabilizer (Terrel et al. 1979)

	MORE THAN 25% PASSING 75μm			LESS THAN 25% PASSING 75μm		
Plasticity Index	PI ≤ 10	10 < PI <20	PI ≥ 20	PI ≤ 6 PI x % passing 75μm ≤ 60	PI ≤ 10	PI > 10
Form of Stabilisation						
Cement and Cementitious Blends						
Lime						
Bitumen						
Bitumen/ Cement Blends						
Granular						
Miscellaneous Chemicals*						

Key: Usually suitable; Doubtful; Usually not Suitable

* Should be taken as a broad guideline only. Refer to trade literature for further information.

Note: The above forms of stabilisation may be used in combination, e.g. lime stabilisation to dry out materials and reduce their plasticity, making them suitable for other methods of stabilisation.

Figure D29. Guide to selecting stabilization method (Austroads 1998)

Table D5. Recommended cement contents for different soil types (Portland Cement Association 1995, Fang 1990)

AASHTO soil classification	Unified soil classification	Normal range of cement requirements		Cement content for moisture-density test, % by weight	Cement contents for wet-dry and freeze-thaw tests, % by weight
		% by volume	% by weight		
A-1-a	GW, GP, GM, SW, SP, SM	5-7	3-5	5	3-5-7
A-1-b	GM, GP, SM, SP	7-9	5-8	6	6-4-8
A-2	GM, GC, SM, SC	7-10	5-9	7	5-7-9
A-3	SP	8-12	7-11	9	7-9-11
A-4	CL, ML	8-12	7-12	10	8-10-12
A-5	ML, MH, CH	8-12	8-13	10	8-10-12
A-6	CL, CH	10-14	9-15	12	10-12-14
A-7	MH, CH	10-14	10-16	13	11-13-15

Figure D30. Photos showing typical chemical stabilization process

Stabilization of aggregates, sand, and silt soils using foamed asphalt also showed good performance on unpaved roadways (Collings et al. 2004). The foamed asphalt is produced by a

process in which water is injected into the hot bitumen resulting in immediate foaming. The foam expands to approximately 15 times its original volume forming foam with high surface area and low viscosity, and is mixed with aggregate in its foamed state (Kendall et al. 2001 and Muthen 1998). Foamed asphalt can offer a cheaper means of mixing asphalt/bitumen into soils compared to emulsified asphalt.

Bio-Stabilization

A recent Iowa DOT research study (TR-582) by Gopalakrishnan et al. (2010) conducted a laboratory study investigating the use of bio-fuel (ethanol) co-products (BCPs) such as liquid type BCPs with high lignin content and BCPs with low lignin content. Their study results indicated that the BCPs are effective in stabilizing Iowa Class 10 soils (CL or A-6(8)) with excellent resistance to moisture degradation. BCPs with high lignin content performed better than BCPs with low lignin content (Figure D31). The authors of that study indicated that additional research is warranted to evaluate the freeze-thaw durability of the stabilized soils.

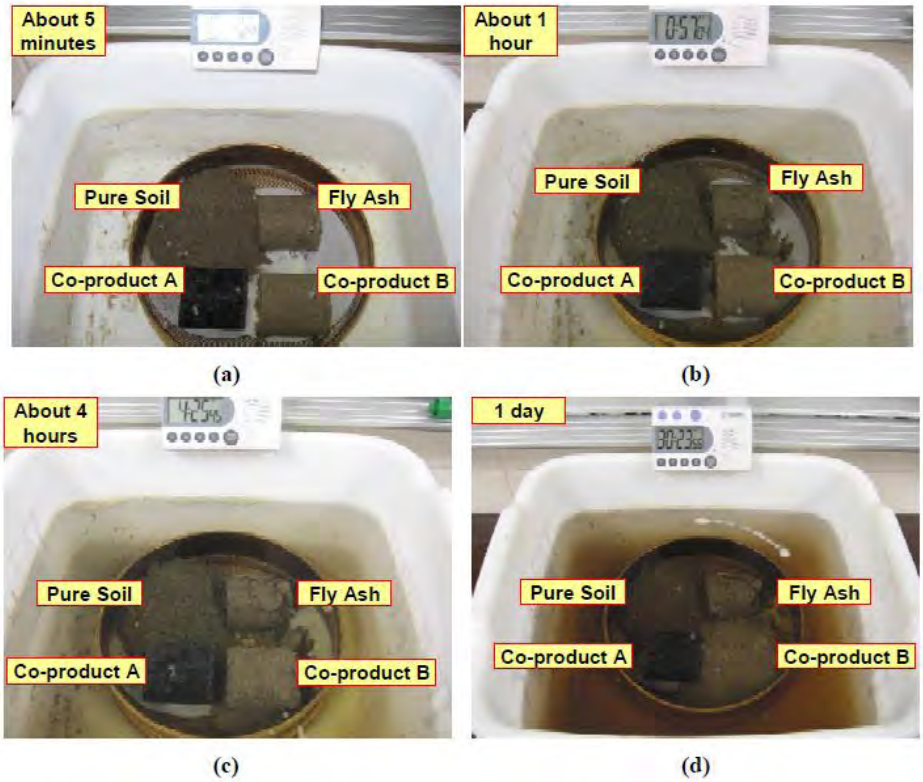

Figure D31. Pictures showing soaking test results of different specimens after: (a) five minutes, (b) one hour, (c) four hours, and (d) one day (Gopalakrishnan et al. 2010)

Use of lignosulfonates to treated unpaved gravel roads is documented in the literature (Cook 2002 and Bushman et al. 2004). Lignosulfonates are the glue found mainly in trees. During the pulping process, lignosulfonates are removed from the pulp and flushed into tanks or lagoons. The chemicals added during the pulping process determine whether it is a calcium, sodium, or

ammonium lignosulfonate. The liquid is typically sold in a 50% suspended solid solution (Cook 2002). Previous research documented mixed performance information on lignosulfonate stabilized granular materials. Cook (2002) reported good performance results based on studies conducted in New York on shoulder material with no signs of erosion or distress after two years. In contrary, Bolander (1999) reported that lignosulfonates have poor durability to wet-dry and freeze-thaw cycles.

Mechanical Stabilization (Mixing Gravel with Subgrade)

Mechanical stabilization by mixing/blending granular subbase materials with wet subgrade soils and compaction can provide a stable working platform and foundation layer under pavements (Christopher et al. 2005). The mechanically stabilized layer can exhibit lower plasticity, lower frost-heave potential, and higher drainage characteristics than the subgrade soils (Kettle and McCabe 1985, Rollings and Rollings 1996). Based on laboratory testing, Kettle and McCabe (1985) indicated that the magnitude of reduction in frost-heave is related to the coarse-aggregate content and the type of aggregate used in the mechanically stabilized layer. The support capacity of a mechanically stabilized layer is influenced by the degree of saturation and the percentage of clay-particles present in the mixture (Hopkins et al. 1995). Therefore, post-construction changes in saturation (due to freeze-thaw) must be considered in properly understanding the long-term performance of a mechanically stabilized layer. Hopkins et al. (1995) indicated that a soil-aggregate mixture must be designed to have a CBR $\geq$ 10 in soaked condition but cautioned that this limiting condition must be viewed as very approximate. A field study was recently conducted in Boone, Iowa (White et al. 2013b) where crushed limestone material with 7% fines (classified as GP-GM or A-1-a) was mixed with lean clay subgrade classified as CL or A-6(5) (Figure D32). At the time of this report, laboratory tests are underway as part of that project characterizing the durability of mechanically stabilized mixtures.

Figure D32. Blending granular material with subgrade using a soil pulverizer

Geosynthetics

Geosynthetics have been used in roadway foundation layers for separation, filtration, lateral drainage, and reinforcement purposes (Berg et al. 2000). The mechanisms by which geosynthetics provide reinforcement when placed at the subbase and subgrade interface include lateral restraint or confinement of aggregate material, and increase in bearing capacity. Previous research has documented the following benefits of using geosynthetics in roadways (Berg et al. 2000, Giroud and Han 2004, Powell et al. 1999):

- Reduction of the intensity of stress on the subgrade.
- Increase the bearing capacity of the subgrade.
- Preventing the subgrade fines from pumping into the base.
- Preventing contamination of the base materials allowing for more open graded, free-draining aggregates.
- Reducing the depth of excavation required for the removal of unsuitable subgrade materials.
- Reducing the thickness of the aggregate layer required to stabilize the subgrade.
- Minimize disturbance of the subgrade during construction.
- Minimize maintenance and extend the life of the pavement.
- Prevents development and growth of local shear zones and allows the subgrade to support stresses close to the plastic limit while acting as if it is still in the elastic limit.

Two types of geosynthetics are commonly used: geotextiles and geogrids. There are two types of geotextiles (woven and non-woven) and both act primarily as separation layers between strata to prevent the upward migration of fine-grained particles from the subgrade into aggregate layers. The non-woven geotextiles can also provide lateral drainage. Polymer geogrids act primarily as reinforcement by providing lateral restraint or confinement of aggregate layers above subgrade. Some pictures of geotextiles and geogrids are shown in Figure D33 and Figure D34 respectively.

Giroud and Han (2004) presented a theoretical method to predict rutting behavior of unpaved roadways by calibrating the method using experimental results. In this method, the subgrade is assumed as saturated, has low permeability, and behaves in an undrained manner. The following equation was developed for calculating gravel layer thickness:

$$h = \frac{0.868 + (0.661 - 1.006J^2)\left(\frac{r}{h}\right)^{1.5}}{f_E} \log N \; X\left[\sqrt{\frac{P/(\pi r^2)}{mN_c f_C CBR_{sg}}} - 1\right] r \qquad \text{(D1)}$$

where, h = required base course thickness (m); J = geogrid aperture stability modulus (mN/^{o}); N = number of axel passages; P = wheel load (kN); r = radius of equivalent tire contact area (m); *m* = bearing capacity mobilization coefficient; N_c = bearing capacity factor; f_c = factor equal to 30 kPa; and CBR_{sg} = CBR of subgrade soil. For unreinforced unpaved roads, J = 0 and N_c = 3.14. For geotextile-reinforced unpaved roads, J = 0 and N_c = 5.14. For geogrid-reinforced unpaved

roads, J > 0 and N_c = 5.71. The bearing capacity mobilization coefficient, *m*, is calculated using the following equation:

$$m = \left(\frac{s}{f_s}\right)\left\{1 - \xi \exp\left[-\omega\left(\frac{r}{h}\right)^n\right]\right\} \quad \text{(D2)}$$

where, s = rut depth (mm); and f_s = factor equal to 75 mm rut depth. ζ, ω, and n are parameters equal to 0.9, 1.0, and 2, respectively, based on the experimental data used for calibration. The bearing capacity mobilization coefficient, m, cannot be greater than unity. If m > 1, the base course thickness must be increased or a smaller allowable rut depth is selected.

To calculate the required base course thickness for specific site conditions, the second equation is first used to calculate m using an assumed base course thickness and then the base course thickness h is calculated using the first equation and is compared to the assumed h value. The process is repeated until the assumed base course thickness value in the first step equals the calculated value in the second step.

The limitations of this method are the following:

- The method was validated for Tensar biaxial geogrids and geotextiles products only.
- Only aperture stability modulus of less than or equal to 0.8 mN/^{o} can be used.
- Tensioned membrane effect is not taken into account.

A recent Iowa DOT study (TR-531) on granular shoulder material stabilization indicated that rut depths measured in field compared well with rut depths predicted using the Giroud and Han (2004) method (White et al. 2007).

Figure D33. Woven geotextile (left) and non-woven geotextile (right) placed at subgrade/aggregate layer interface

Figure D34. Triaxial (left) and biaxial (right) polymer geogrids placed on the subgrade

High Energy Impaction Compaction

Application of high-energy impact roller (IR) compaction technology to earthwork and stabilization projects in Iowa has been limited primarily to concrete pavement recycling projects, but is recently seeing increased interest. IR is essentially a non-circular-shaped, tow-behind solid steel compactor that typically varies in weight from about 9 to 15 tons (Figure D35). The dynamic impact compaction energy is transferred to the soil by means of the lifting and falling motion of the non-circular rotating mass. The rollers are pulled at relatively high speeds (typically about 9.8 to 12.9 km/h (6 to 8 mph)) to generate a high-impact force that reportedly can densify material to depths greater than 2 m (6 ft), which is significantly deeper than conventional static or vibratory rollers (Clegg and Berrangé 1971). Significant improvement of subgrade may not be possible if the subgrade is wet/saturated (White et al. 2013b).

Figure D35. High energy impact roller (equipment by Impact Roller Technology, Plattsmouth, Nebraska)

The range of applications of IR is broad and includes the following:

- In situ densification of existing fill, collapsible sands, landfill waste, chemically-stabilized soils, mine haul roads, and bulk earthwork
- Thick lift compaction
- Existing pavement rubblization to create a new subbase
- Construction of water storage and channel banks in the agricultural sector

One disadvantage of this technology is that the high-impact forces disturb (i.e., loosen) the top 0.1 to 0.5 m (0.25 to 1.5 ft) of the surface so the top layer needs additional compaction with conventional rollers. The vibrations caused by the impact rollers and their effect on nearby structures (e.g., underground utilities/pipe lines or nearby building structures) are important to consider with this technology. Some case studies indicated that the vibration effect is minimal beyond 9.1 to 13.7 m (30 to 45 ft) from the impact source (Bouazza and Avalle 2006).

Bridge Abutments

Common post-flood damages associated with bridge abutments include erosion of backfill materials and embankment fore slopes. Use of sheet pile abutments (TR-568 (Evans et al. 2012)) and use of geosynthetic reinforced soil (GRS) as backfill material (Iowa DOT TR-621 project; Vennapusa et al. 2012) can help mitigate these problems. Some details about these alternatives are provided below. Further, use of non-erodible fill material is recommended in the backfill material and their specifications are also provided in this section.

Sheet Pile Abutments

Using steel sheet piling as the primary bearing foundation component has several potential advantages. A sheet pile abutment system can retain abutment fill while simultaneously providing a foundation for the bridge abutment. In areas where materials such as concrete abutment systems are expensive or not available locally, steel sheet pile bridge abutment systems can be an effective alternative. When used for bridges over rivers or streams, sheet pile abutment systems can protect against scour. Along with the potential for accelerated construction, sheet pile bridge abutment systems facilitate installation and maintenance by county engineers and their construction crews (Carle and Whitaker 1989). When considering steel sheet piling for use as a bridge abutment system there are two main alternatives for design: (1) axially loaded sheet piling, or (2) backfill retaining structures. More details regarding these alternatives are provided in Evans et al. (2012). Evans et al. (2012) documented three case studies for bridges constructed with sheet pile abutments in Iowa. Cross-section of a bridge abutment constructed with sheet pile abutment system from a project site in Boone is shown in (Figure D36) and photos from the site are shown in Figure D37.

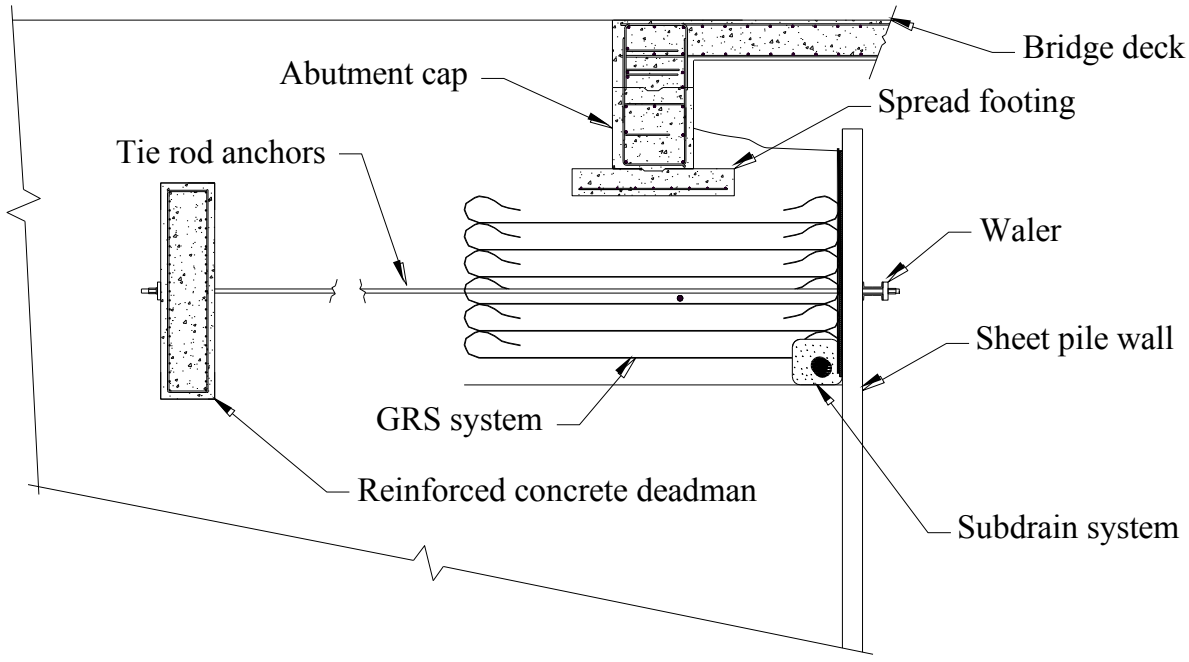

Figure D36. Cross-section of sheet pile abutment foundation system at a bridge site in Boone (Evans et al. 2012)

Figure D37. Pictures of a bridge site in Boone constructed with sheet pile abutments with geogrid-reinforced backfill material (Evans et al. 2012)

Geosynthetic Reinforced Soil (GRS)

GRS fill in bridge abutments involves constructing engineered granular backfill material with closely spaced alternating layers of geosynthetic reinforcement. GRS fill materials are relatively less expensive than conventional concrete bridge abutments, due to its rapid construction method and materials cost (Wu et al. 2006). Small scale to large scale test results on reinforced soil systems have been documented by researchers over the past several years demonstrating improvements in the soil bearing capacity, reduction in settlement under static and cyclic loading, and reduction in lateral stresses induced on the surrounding soil (Milligan and Love 1984, Huang and Tatsuoka 1990, Wu et al. 2006, Adams et al. 2007). Recently, the Federal Highway Administration developed guidelines regarding the design and construction of GRS abutments with flexible facing elements, i.e., with unreinforced concrete masonry as facing and with geosynthetic wrapped around each individual layer and anchored by the overburden of the overlying layer (Adams et al. 2011a, b). Recommendations are provided therein on requirements of the backfill material gradation, type of geosynthetic material, and minimum factors of safety for bearing capacity and global stability, hydraulic and drainage design considerations, and quality control/assurance requirements.

Recently, two case study projects are documented in Vennapusa et al. (2012) for bridges constructed in Buchanan County using GRS fill in bridge abutments. One of the bridge sites (Olympic Ave.) included GRS fill constructed with a slope and riprap capped with cement grout was used for erosion protection (Figure D38, Figure D39). Another bridge site (250th St.) included supporting the bridge on GRS fill using the existing bridge abutment and soil as facing (Figure D40). A summary of the 250th St. bridge construction costs are provided in Table D6. Both these bridges experienced flash flooding during summer of 2013 and flood waters overtopped during the flood event. At the Olympic Ave. bridge site, some of the rip rap facing was eroded (Figure D41) and at the 250th St. bridge site, some of the gravel surfacing was eroded into the ditches. Despite these, no other distresses were observed at the two sites (Figure D42).

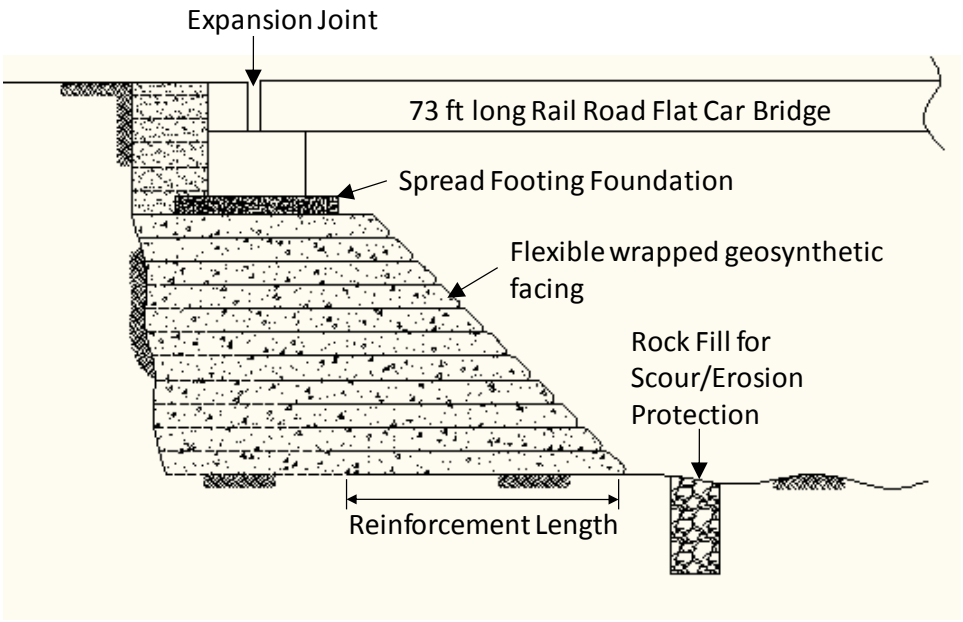

Figure D38. Schematic of GRS bridge abutment with geosynthetic wrapped sheets flexible facing at a bridge site in Buchanan County (Olympic Ave.) (Vennapusa et al. 2012)

Figure D39. Pictures of a bridge site in Buchanan County (Olympic Ave.) during construction of GRS fill in bridge abutments, placement of riprap and grout cover for erosion protection, and the finished bridge in 2011 (Vennapusa et al. 2012)

Figure D40. Pictures of a bridge site in Buchanan County (250th Street) during construction of GRS fill in bridge abutments, placement of rail road flat cars for superstructure, and after final placing the final gravel surface in 2011 (Vennapusa et al. 2012)

Figure D41. Pictures of a bridge site in Buchanan County (Olympic Ave.) after flash flooding occurred in May 2013

Figure D42. Pictures of a bridge site in Buchanan County (250th Street) after flash flooding occurred in May 2013

Table D6. Construction costs of a bridge constructed with GRS backfill and rail road flat cars in Buchanan County (Vennapusa et al. 2012)

Description	Unit Cost (USD)	Quantity	Total Cost (USD)
Geosynthetic Material	$0.70/yd^2	533.3 yd^2	$373.00
Crushed Rock (for excavation)	$7.00/ton	156 tons	$1,088.60
Labor (6 crew members)	$26/hr	16 hrs	$2,496.00
Railroad flat cars	$12,500/each	3	$37,500.00
Crushed Rock (for backfill + road surfacing)	$7.00/ton	160 tons	$1,120.00
		Total	**$42,577**

Backfill Gradation Selection

Using non-erodible backfill material can help avoid erosion of backfill during a flood event. Materials containing silt and fine sand material are more erodible than other soil types (Briaud et al. 1997). The range of most erodible soils (Briaud et al. 1997) in comparison with Iowa DOT granular backfill gradation requirement is presented in Figure D43.

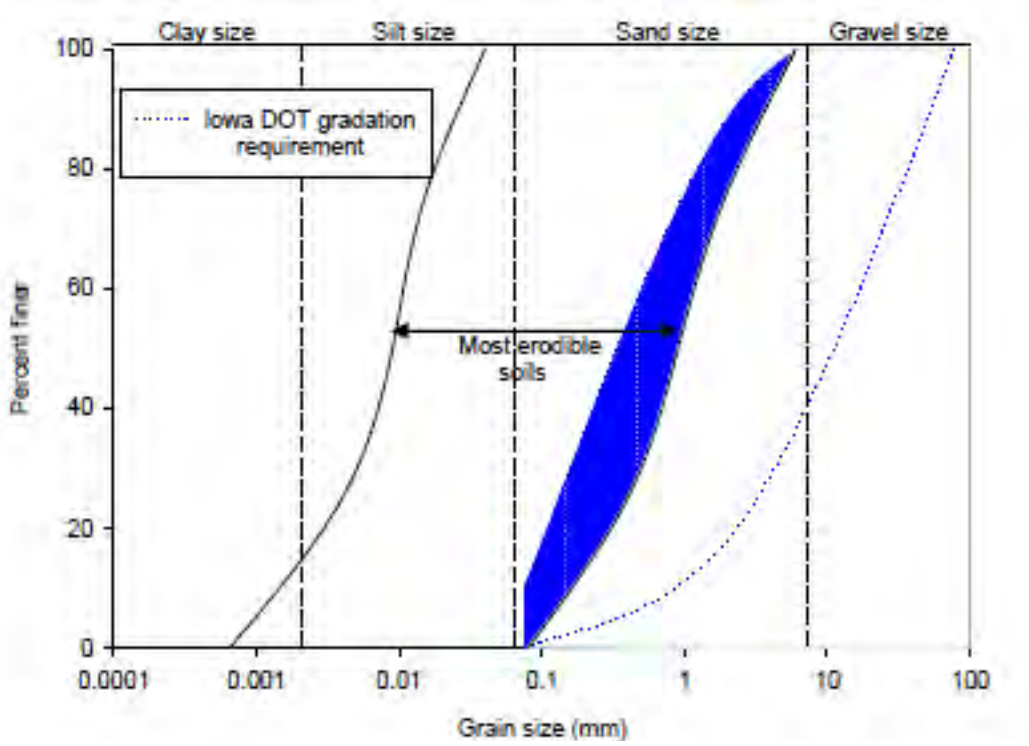

Figure D43. Iowa DOT granular backfill gradation requirement compared with the range of most erodible soils

Culverts

Common post-flood damages observed at culvert crossing include erosion of backfill materials and culvert washout or separation. Previous research (TR-503, Schaefer et al. 2005) indicated that backfill materials commonly used in Iowa under City roadways showed high collapse potential (9% to 36%). Use of non-erodible backfill materials (per Figure D43) or flowable mortar around the culvert can help mitigate the erosion problem. Also, geotextiles can be used to wrap around the backfill materials, which can help mitigate erosion.